Cross-shelf flow forced by daily variable winds in the presence of a cape

Doutoramento em Ciências Geofísicas e da Geoinformação
Especialidade de Oceanografia

Luísa Andrade e Sousa Lamas

Tese orientada por:
Professor Doutor Álvaro Peliz e Doutor Patrick Marchesiello

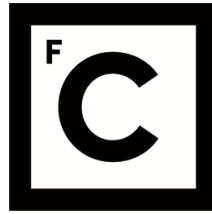Documento especialmente elaborado para a obtenção do grau de doutor

2018

UNIVERSIDADE DE LISBOA

FACULDADE DE CIÊNCIAS

Ciências
ULisboa

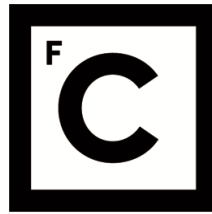# Cross-shelf flow forced by daily variable winds in the presence of a cape

Doutoramento em Ciências Geofísicas e da Geoinformação
Especialidade de Oceanografia

Luísa Andrade e Sousa Lamas

Tese orientada por:
Professor Doutor Álvaro Peliz e Doutor Patrick Marchesiello

Júri:
Presidente:
• Doutora Margarida Maria Telo da Gama, Professora Catedrática e Presidente do Departamento de Física da Faculdade de Ciências da Universidade de Lisboa
Vogais:
• Doutor Jesús Manuel Pedreira Dubert, Professor Auxiliar, Departamento de Física da Universidade de Aveiro;
• Doutor Paulo José Relvas de Almeida, Professor Auxiliar, Faculdade de Ciências e Tecnologia da Universidade do Algarve;
• Dr. António da Costa Neves dos Santos Martinho, Chefe de Divisão, Divisão de Oceanografia do Instituto Hidrográfico, na qualidade de especialista de reconhecido mérito;
• Doutor Joaquim Guilherme Henrique Dias, Professor Auxiliar, Faculdade de Ciências da Universidade de Lisboa;
• Doutor Álvaro Júdice Ribeiro Peliz, Professor Auxiliar, Faculdade de Ciências da Universidade de Lisboa.

Documento especialmente elaborado para a obtenção do grau de doutor

2018

Abstract

This thesis intends to contribute to the knowledge of the nearshore circulation in the vicinity of a cape under daily variable wind conditions. Throughout this study, several different tools were used to understand the diurnal variability of the circulation, with special emphasis on the cross-shelf transport in the leeside of the cape. In-situ data collected near Cape Sines, on the southwestern coast of Portugal, during three summers, indicated that the wind was consistently favourable to upwelling with recurrent sea breeze-like diurnal variability. Current data collected by an ADCP in the leeside of the cape during events of strong diurnal variability of the wind showed that the average day of the cross-shelf circulation consisted of three distinct periods: a morning period with a 3-layer structure with onshore velocities at mid-depth, a mid-day period where the flow is reversed and has a 2-layer structure with onshore velocities at the surface and offshore flow below, and, lastly, in the evening, a 2-layer flow with intensified offshore velocities at the surface and onshore flow at the bottom. A simplified 2D numerical model hinted at the fact that the cross-shelf flow reversal which occurred at mid-day was forced by the local acceleration of the along-shelf velocity. A numerical modelling experiment exclusively forced by winds simulated successfully most of the circulation at a location consistent with the ADCP, especially the mid-day reversal and the evening's upwelling-type structure. This supported the hypothesis that the observed cross-shelf circulation at diurnal timescales was dominantly wind-driven. Analysing a set of modelling experiments with simplified topography and wind forcing helped to clarify the dynamics behind the ocean circulation around the cape, indicating that the cross-shelf flow reversal resulted as a response to the rapid change of the wind magnitude at mid-day. The fact that the wind diurnally undergoes relaxation and intensification strongly affects the cross-shelf circulation, promoting surface onshore transport in the leeside of the cape.

Keywords:: Coastal Oceanography; Wind-driven Circulation; Upwelling; Diurnal Variability; Topography; Shelf Dynamics

Resumo

Esta tese tem como objectivo principal contribuir para o conhecimento da circulação costeira numa região próxima de um cabo, em condições de vento favorável ao afloramento costeiro (upwelling) e com acentuada variabiliade diurna. A área de estudo centra-se na costa sudoeste de Portugal, na região adjacente ao cabo de Sines. O processo de recrutamento de algumas espécies intertidais existentes nesta região (como cracas e percebes) tem sido investigado ao longo de vários anos no âmbito de diversos projetos (Cruz, 1999; Cruz et al., 2005; Jacinto and Cruz, 2008; Trindade et al., 2016), no entanto, não houve possibilidade de identificar de modo concludente quais os processos físicos que dominam a dinâmica local associada ao transporte de larvas para a costa. A existência de uma série de dados in-situ e a particularidade da região costeira em questão tornaram este local especialmente interessante para um estudo aprofundado do transporte transversal à costa. Para tal, para além do processamento e análise dos dados in-situ recolhidos durante três verões consecutivos (2006-2007), um conjunto de simulações numéricas do oceano, tanto realistas como de configuração idealizada, foi desenvolvido e os resultados analisados de forma a obter respostas sobre o forçamento do transporte transversal à costa, com especial enfâse na região a sul do cabo. A forte variabilidade diurna observada nos dados do vento motivaram o destaque deste estudo para a variabilidade diurna da circulação.

A circulação oceânica transversal à costa sobre a plataforma continental desempenha um papel essencial no transporte e distribuição de plâncton, nutrientes, calor e sedimentos. Devido à sua complexidade dinâmica e importância sócio-económica no que respeita a gestão e monitorizãçao de recursos marinhos, tem sido um tópico bastante estudado ao longo da última década (Fewings et al., 2008; Lentz et al., 2008; Hendrickson and MacMahan, 2009; Marchesiello and Estrade, 2010; Ganju et al., 2011; Lentz and Fewings, 2012; Liu and Gan, 2014; Brink, 2016). No entanto, existem grandes dificuldades em estudar o transporte transversal à costa e a sua dependência a diferentes condições de forçamento, batimetria e estratificação, em parte devido à escassez de longas e coerentes séries temporais de dados in-situ e em outra devido à dificuldade dos modelos numéricos resolverem concorrentemente diferentes escalas temporais e espaciais, que é essencial para um estudo aprofundado da circulação nas regiões costeiras. A resposta da circulação em regiões costeiras sem grande variabilidade topográfica é

já bastante conhecida. Situações de upwelling são particularmente interessantes pois nestas condições existe promoção de transporte transversal à costa, especialmente em regiões com elevada estratificação (Austin and Lentz, 2002). Nestas condições, ventos favoráveis ao upwelling forçam uma circulação transversal à costa que consiste em velocidades para o largo na camada de mistura superficial, e velocidades para a costa junto ao fundo. Este sistema de circulação ocorre para profundidades tipicamente superiores a 50 m, quando as camadas limites de superfície e fundo têm uma espessura relativamente reduzida quando comparada à profundidade total da coluna de água. Esta região é habitualmente referida como plataforma continental média (Lentz, 2001). Quando a estratificação da coluna de água é elevada, a espessura das camadas limite é menor devido à elevada estratificação, permitindo a circulação transversal à costa ser mais intensa a menor profundidade, relativamente a condições de fraca estratificação (Austin and Lentz, 2002; Horwitz and Lentz, 2014). Na zona entre a frente de upwelling e a costa, a estratificação é normalmente fraca e existe sobreposição entre as camadas limite de superfície e fundo, causando a redução do transporte transversal à costa (Lentz, 2001; Estrade et al., 2008). Esta região é normalmente referida como plataforma continental interna (Lentz, 2001; Austin and Lentz, 2002; Fewings et al., 2008).

Tipicamente, a dinâmica oceânica na plataforma continental média é dominada pelo vento, principalmente pela componente do vento paralela à costa. Na zona de surf, que é a região mais costeira da plataforma continental, as ondas são tradicionalmente dominantes. A plataforma continental interna situa-se no meio destas duas regiões, e por ser uma zona de transição, a dinâmica associada é bastante complexa, pois processos como vento, ondas e marés poderão ser igualmente importantes no forçamento da circulação (Lentz et al., 1999; Liu and Weisberg, 2005; Fewings and Lentz, 2010). Apesar de ser uma região em que tipicamente o transporte é fraco, a plataforma continental interna é uma região bastante atractiva para muitas espécies marinhas, em particular para as espécies que se encontram na plataforma média durante a sua fase larvar e que necessitam de atravessar esta região para chegar à costa, razão pela qual o transporte perpendicular à costa sobre a plataforma continental é de grande importância.

A circulação em regiões com variações topográficas apresenta ainda uma maior complexidade. Vários estudos sobre a interacção entre circulação e topografia

na presença de cabos (Gan and Allen, 2002; Roughan et al., 2005b; Kuebel Cervantes and Allen, 2006), promontórios (Barth et al., 2000; Castelao and Barth, 2006) ou canhões (Kämpf, 2012) verificaram que o termo de advecção não-linear contribui significativamente para o balanço de momento, resultando num sistema complexo com dinâmica tridimensional. Por exemplo, quando o vento é favorável ao upwelling, o jacto costeiro é destabilizado e desviado para o largo quando se aproxima de um cabo, com a possível formação de filamentos e turbilhões como consequência (Barth et al., 2000; Peliz et al., 2003; Meunier et al., 2010), modificando significativamente a circulação na região. Na zona a sul do cabo, alguns estudos verificaram que se forma uma região de sombra (Roughan et al., 2005b; Oliveira et al., 2009), onde as velocidades são significativamente mais fracas e a estratificação é fraca. A formação de uma região de sombra é particularmente importante para a promoção de transporte transversal à costa pois há diminuição do fluxo paralelo à costa, que é dominante em condições de upwelling.

A análise dos dados meteorológicos próximos do cabo de Sines demonstraram que o vento durante os três verões de 2006 a 2008 era predominantemente para sul, como acontece tipicamente na costa oeste portuguesa durante o verão (p. ex., Relvas et al. (2007)), com períodos recurrentes de forte variabilidade diurna, semelhante à brisa marítima. Dados de ADCP recolhidos a sul do cabo de Sines a uma profundidade de 12 m mostraram que em eventos de forte variabilidade diurna do vento a circulação transversal à costa apresentava um dia médio que pode ser dividido em três períodos: o período da manhã, em que a circulação está dividida em três camadas, com velocidades para o largo à superfície e junto ao fundo, e velocidades para a costa no interior; o período a meio do dia, em que a circulação apresenta duas camadas e há inversão do sentido da corrente à superfície, tendo agora velocidades para a costa à superfície e para o largo junto ao fundo; e, por último, o período da tarde, onde a circulação é de novo invertida mantendo as duas camadas, com velocidades para o largo à superfície e para a costa junto ao fundo, consistente com uma circulação de upwelling. Seguidamente utilizou-se um modelo da plataforma continental interna desenvolvida por Lentz et al. (2008) para analisar a resposta da circulação a determinadas condições de vento e agitação marítima, e assim conseguir discernir qual o papel de cada um destes mecanismos de forçamento. Através deste estudo foi possível concluir que a inversão do sentido da circulação transversal à costa que ocorre à superfície no período do meio dia deve-se à aceleração local da velocidade paralela à costa. Apesar disso,

não foi possível retirar mais conclusões pois o modelo simplificado não simulou correctamente a maior parte da circulação observada. Por essa razão, procedeu-se ao desenvolvimento e análise de uma simulação numérica semi-realista do oceano nesta região, utilizando o modelo ROMS, e forçada exclusivamente pelo vento. A grande semelhança entre o resultado da simulação e as observações demonstrou que o vento é o forçamento dominante da circulação observada. Por fim, através de um conjunto de simulações numéricas com topografia e forçamento atmosférico simplicado foi possível clarificar alguns mecanismos responsáveis pelas estruturas de circulação na zona adjacente ao cabo e identificar que a inversão da circulação transversal à costa a sul do cabo resulta da resposta inercial da corrente após o relaxamento do vento. Esta resposta é realçada a sul do cabo, pois há um efeito de sombra que diminui a velocidade da corrente naquela zona.

Os resultados principais deste trabalho são consistentes com outros estudos em regiões semelhantes (Barth et al., 2000; Roughan et al., 2005b; Castelao and Barth, 2006; Kuebel Cervantes and Allen, 2006; Gan et al., 2009; Ganju et al., 2011). No entanto, a maioria destes estudos concentra-se na interacção e ajustamento da circulação a variações topográficas em condições de upwelling estável ou com períodos de relaxamento de mais de um dia. Neste estudo, todavia, foi demonstrado que a circulação, principalmente a sul do cabo, é fortemente dominada pela variabilidade diurna do vento. O facto do vento ser variável a uma escala diurna e efectivamente ser zero a meio do dia faz com que a circulação tenha uma acentuada variabilidade diurna e haja promoção de transporte para a costa, especialmente na região de sombra, a sul do cabo.

Apesar da pequena escala do domínio, a circulação transversal à costa descrita e analisada neste estudo pode ser particularmente útil para o conhecimento de como se processa e em que condições é favorável o transporte e distribuição de material através da plataforma continental nesta região, e noutras regiões costeiras com semelhante topografia e regime de vento (p. ex., brisa marítima).

Esta tese está dividida em quatro capítulos. No primeiro capítulo é feita uma descrição do processamento dos dados in-situ e são discutidos os principais resultados relativamente à variabilidade diurna da circulação transversal à costa a sul do Cabo de Sines. No segundo capítulo são analisados e discutidos os resultados obtidos em várias simulações numéricas utilizando o modelo de Lentz et al. (2008) forçado pelas condições de vento e agitação marítima observadas na região. No

capítulo 3 os padrões de circulação costeira na região adjacente ao cabo de Sines são estudados recorrendo aos resultados de uma simulação numérica semi-realista obtida pelo ROMS. No quarto capítulo são analisadas 18 simulações numéricas da região de estudo, mas com topografia e forçamento simplificado, de forma a estudar a dinâmica associada ao transporte transversal à costa. Por fim, a tese termina com um resumo das principais conclusões e perspectivas de trabalho no futuro.

Palavras-chave: Oceanografia Costeira; Afloramento Costeiro, Variabilidade Diurna, Dinâmica na plataforma continental, Topografia

Acknowledgements

I would firstly like to express my deep gratitude to my advisors Álvaro Peliz and Patrick Marchesiello, for all their support, advice and friendship throughout this thesis. They allowed me to grow individually as a scientist and working with them was an enriching experience that I will forever value. Thanks especially to Álvaro for all the advices and discussions and most important to endure this journey with me, always encouraging me to continue forward. Many thanks to Patrick Marchesiello for welcoming me in Toulouse and for all the great advice, even from the other side of the world.

Many thanks to Paulo Oliveira for all the constructive discussions throughout this thesis and in particular for the help with in-situ data processing. My grateful thanks are also extended to Maria Manuel Angélico, João Castro, Teresa Cruz, Joana Fernandes and Ana Trindade for the useful inputs on the article, and to David Jacinto and Teresa Silva for help during field work. I would also wish to acknowledge the Port of Sines Authority for providing oceanographic and meteorological data. Special thanks must be given to Dr. Lentz for providing the model scripts and for promptly answering all my questions.

Many thanks to my friend Ana Machado, for reading this thesis and for giving me the LaTeX templates, which saved me a lot of time. Thanks also to Joaquim Dias, for looking after my lab computer, which allowed me to work on this thesis remotely from home while on parental leave, this meant a great deal to me and my family.

I would like to extend my thanks to my colleagues at Instituto Hidrográfico, for the good work environment and challenging projects which gave me renewed interest in oceanography. A special thanks to Sara Almeida and José Paulo Pinto for giving me extra time to finish this thesis, while working under their supervision on other projects.

Contents

List of Figures

List of Tables

List of Abbreviations

ADCP	Acoustic Doppler Current Profiler
EVP	Eddy Viscosity Profile
GEBCO	General Bathymetric Chart of the Oceans
KPP	K-Profile Parametrization
MODIS	Moderate Resolution Imaging Spectroradiometer
ROMS	Regional Ocean Modelling System
SSH	Sea Surface Height
SST	Sea Surface Temperature
WRF	Weather Research and Forecast Model

Introduction

The cross-shelf transport over the nearshore region plays a key role on the distribution of plankton, nutrients, heat, salt and sediments, and has been the subject of many recent studies (Fewings et al., 2008; Lentz et al., 2008; Hendrickson and MacMahan, 2009; Marchesiello and Estrade, 2010; Ganju et al., 2011; Lentz and Fewings, 2012; Liu and Gan, 2014; Brink, 2016). The zone between the mid-shelf and the coast is a transition zone in what concerns the role of dynamical processes on transport patterns. In mid and outer shelves, high frequency dynamics are usually neglected in circulation models since sub-inertial transports associated with wind-driven currents predominate. In shallow areas, however, tidal currents also become important and in the surf zone wave-driven littoral flows are dominant (Lentz et al., 1999). Finally, sea breeze (Woodson et al., 2007; Hendrickson and MacMahan, 2009), wind shadow zones and strong river outflows are all potentially important contributors to the nearshore circulation. Despite all these forcing factors, in some occasions the nearshore zone may act as a barrier to cross-shore transport. This may arise due to strong drag effects which cause horizontal dispersal in the nearshore zone to be strongly polarized alongshore. Consequently, nearshore circulation is a complex dynamical system with a variety of forcing which cannot be disregarded in transport models. Yet, the shallow part of the shelf is an attractive habitat for many coastal species. For example, intertidal species, having their planktonic larval phase in mid-shelf, must cross the nearshore zone for settlement. Cross-shore transport processes over the shelf are thus critical for the larvae supply to the shore, which then determines recruitment (Pineda et al., 2009). Understanding the physical processes behind the cross-shelf exchange over the continental shelf is of particular interest for this type of studies.

This thesis focuses on the cross-shelf flow response to diurnal winds over the continental shelf, in the particular case of a coast with a cape. The wind-driven shelf response over a straight coastline has been extensively studied. Upwelling-favourable winds drive cross-shelf exchange with an offshore flow at the surface

boundary layer and a compensating onshore flow near the bottom. This occurs for depths typically greater than 50 m, when the surface and bottom boundary layers are relatively thin when compared with total water depth (a region often called mid-shelf (Lentz and Fewings, 2012)). In the region onshore of the upwelling front, stratification is often weaker and the surface and bottom turbulent layers occupy the entire water column, causing the reduction or shut-down of the cross-shelf transport (Lentz, 2001; Estrade et al., 2008). With strongly stratified waters, the turbulent layers thin due to stronger stratification, allowing stronger cross-shelf circulation closer to the coast, when compared with unstratified conditions (Austin and Lentz, 2002; Horwitz and Lentz, 2014).

Less is known for systems with complex topography variations. In the inner-shelf and near-shore zones, the merging of surface and bottom boundary layers abruptly modifies the cross-shore circulation (Lentz, 2001). In this region, the circulation is mostly alongshore, manifested as strong coastal jets. However, interaction of these flows with complex coastline topography can drive substantial cross-shelf exchange (Barth et al., 2000; Gan and Allen, 2002; Kirincich et al., 2005; Sanay et al., 2008; Ganju et al., 2011). Gan and Allen (2002) showed that wind-driven circulation forced by upwelling-favourable winds interacting with the along-shelf variations of bottom topography that occur near a cape, can set up an along-shelf pressure gradient strong enough to force cross-shelf velocities over the inner-shelf. A cyclonic recirculation that may form in the presence of a cape (Meunier et al., 2010), can also be relevant since it enhances the onshore transport in the leeside of the cape (Barth et al., 2000; Doglioli et al., 2004; Liu and Gan, 2014).

Most inner-shelf studies, however, deal with steady upwelling conditions, or with relaxation periods of more than a day, but daily variable winds are a common feature in many coastal areas (Simpson et al., 2002; Woodson et al., 2007; Hendrickson and MacMahan, 2009; Sobarzo et al., 2010; Lucas et al., 2013; Aguiar-González et al., 2011). In previous studies, diurnal winds were found to generate local upwelling (Woodson et al., 2007), to enhance cross-shelf exchange through its influence on waves (Hendrickson and MacMahan, 2009) and also to force complex inertial currents, especially near the critical latitude ($30° \pm 10°$ N/S) where the inertial and diurnal periods are close to each other (Simpson et al., 2002; Sobarzo et al., 2010; Aguiar-González et al., 2011). These diurnal wind-driven features can also have a significant impact on the transport across the shelf.

In summary, the nearshore circulation is a complex multi-scale system that is very sensible to all mechanisms described above and the presence of a cape makes the study of the cross-shelf transport around this region particularly interesting, especially due to the fact that there are still few studies regarding this type of environment.

Area of Interest and Motivation

The study area lies within the meridional coast of Portugal around Cape Sines. The topography decays smoothly towards offshore almost everywhere and the shelf is relatively narrow (around 30 km) with the shelf break at approximately 150 m depth (Figure 1). South of the Cape, the shore is mostly rocky and crucial for many inter-tidal species, including barnacles (Cruz et al., 2005). The processes of barnacle recruitment at this site have been under investigation for many years now, in the frame of various projects (Cruz, 1999; Cruz et al., 2005; Jacinto and Cruz, 2008; Trindade et al., 2016). The existence of in-situ data and the particularity of the coastal zone make it especially appealing for studies of cross-shelf transport. Yet, previous studies in this region have failed to conclusively identify the physical forcing mechanisms connected to barnacle recruitment. This motivated the present research to focus on the dynamics involving the circulation around Cape Sines. To achieve this objective in-situ data was analysed and several modelling simulations were conducted, aimed at the study of the circulation around the Cape in one hand, and at the various contributions to cross-shelf transport in the other.

Emphasis was given to the daily variability during summertime, when in-situ data was collected. Summertime is the period when the larvae recruitment of several barnacle species is higher for the study region (Cruz, 1999; Cruz et al., 2005; Jacinto and Cruz, 2008), which can be particularly interesting since, during summer, the western Iberian coast is typically under upwelling-favourable winds (e.g., Relvas et al. (2007)), which intensify the along-shelf currents and promote the shut-down of cross-shelf transport in the region inshore of the upwelling front (Estrade et al., 2008). However, the presence of a cape and the diurnal relaxation of the wind may induce retention-favourable conditions, which can be beneficial
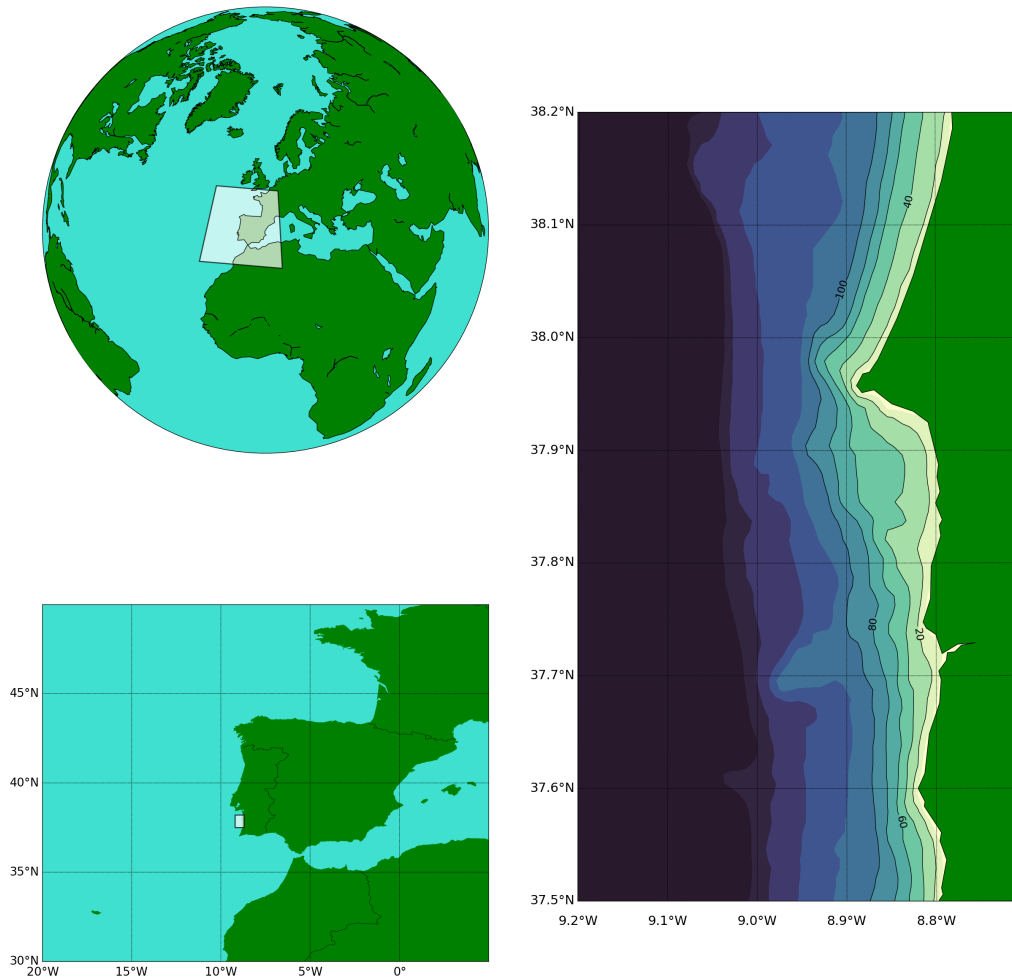
FIGURE 1: Map showing the study domain. *Bathymetry Source: GEBCO*

to larvae transport and recruitment in the leeside of the cape (Roughan et al., 2005b; Oliveira et al., 2009).

MODIS level-2 data of sea surface temperature (SST) and chlorophyll-a concentration from a few days of the summer of 2006 show the existence of intensified upwelling (colder temperatures) in the southward part of Cape Sines with increased chlorophyll-a concentration, which indicate that retention processes likely occurred during this summer (Figure 2). Other forcing elements, like tides and waves, are briefly discussed, but were discarded from the modelling studies, since the focus of this thesis shifted to the wind-driven circulation.
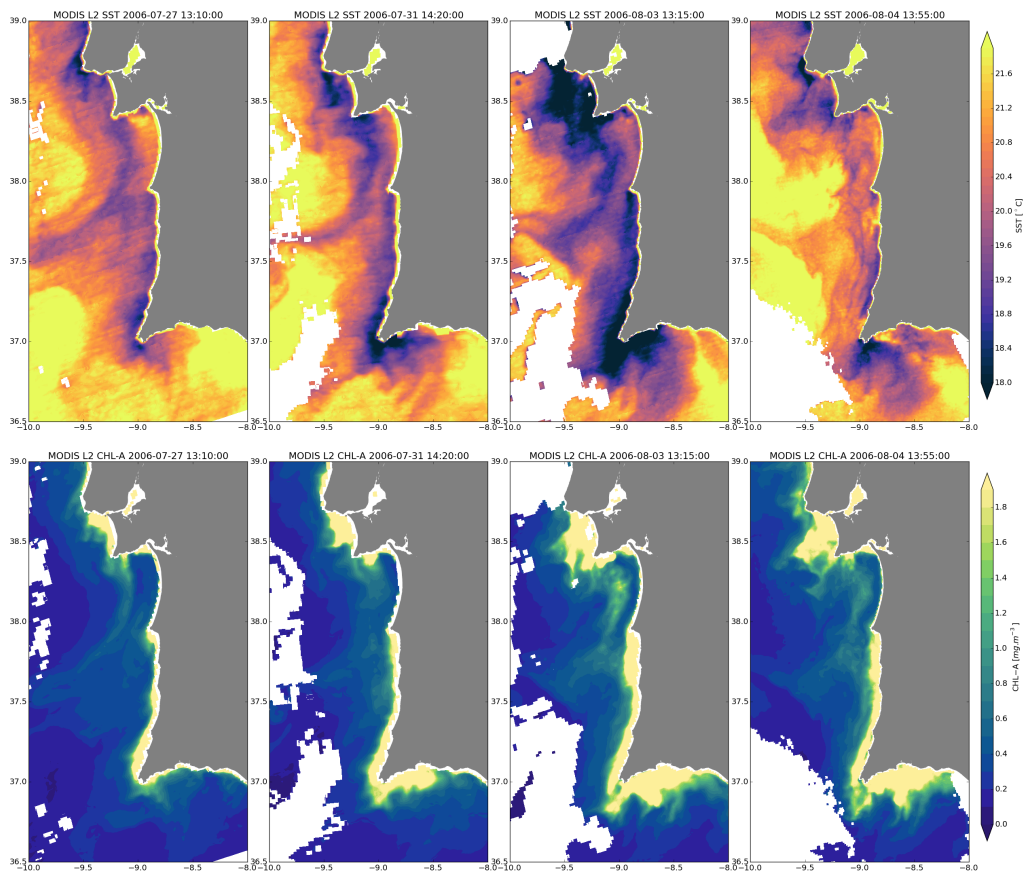
FIGURE 2: Top row: MODIS L2 SST [°C]; bottom row: MODIS L2 Chloropyll-a concentration [mg.m^{-3}]. MODIS Data available online: `http://oceandata.sci.gsfc.nasa.gov` .

Objectives and Thesis Outline

The main objective of this thesis is the analysis of the coastal circulation near a cape, under upwelling-favourable winds modulated by a diurnal cycle similar to sea breeze. Focus is given to the cross-shelf circulation and the investigation of what are the main processes that promote the transport of material across the shelf, under these conditions. This thesis is organized in the following way:

Chapter 1. Observed Inner-shelf Circulation in the Lee of Cape Sines.
This chapter describes the in-situ data collected and how it was processed. The main results are presented regarding both mean and diurnal timescales. The contribution of individual processes (tides, wind and waves) to the observed diurnal circulation and the depth-integrated momentum balances are analysed.

Chapter 2. Inner-shelf Response to Wind and Waves in an Idealized 2D Model.
This chapter presents a brief analysis of some simulations using a 2D model developed by Lentz et al. (2008) forced by the observed conditions. This model was used as a tool to understand the individual contributions of wind and wave to the circulation.

Chapter 3. A Modelling Study of the Wind-driven Circulation in the Vicinity of Cape Sines.
In Chapter 3, the wind-driven coastal circulation around Cape Sines is investigated using the results of a realistic numerical model simulation. Questions about the dynamics behind the diurnal variability of the cross-shelf circulation are addressed.

Chapter 4. Wind and topographic effects on the shelf circulation near a cape.
Chapter 4 provides a process-oriented, idealized modelling study applied to the continental shelf region, in the presence of a cape and forced by daily variable winds. The 18 experiments conducted with different topographies and forcing conditions are described and analysed. The analysis was focused on the dynamics behind the surface flow reversal observed at Cape Sines and the promotion of onshore transport in the leeside of the cape.

Finally, this thesis ends with a summary of the overall conclusions and future work perspectives.

Chapter 1

Observed Inner-shelf Circulation in the Lee of Cape Sines

A part of this chapter was included in an article published in *Continental Shelf Research*. The complete article was attached as Appendix A.

1.1 Introduction

In upwelling-favourable wind conditions, it is expected that the cross-shelf circulation over the continental shelf will be consistent with previous descriptions of coastal upwelling (Pedlosky, 1978; Allen et al., 1995), with an offshore flow at the surface boundary layer and a compensating onshore flow near the bottom. The region onshore of the upwelling front, where the surface and bottom layers overlap, is normally referred to as inner-shelf (Lentz, 2001; Austin and Lentz, 2002; Fewings et al., 2008). Being a transition region, the dynamics over the inner-shelf can be rather complex with many processes, like winds, surface gravity waves, tides, baroclinic circulation interplaying important roles over the circulation (Lentz et al., 1999; Gan and Allen, 2002; Kirincich et al., 2005; Liu and Weisberg, 2005; Fewings et al., 2008; Hendrickson and MacMahan, 2009; Ganju et al., 2011).

Several modelling studies (Austin and Lentz, 2002; Estrade et al., 2008; Marchesiello and Estrade, 2010; Tilburg, 2003) and observations (Lentz et al., 1999; Lentz, 2001; Kirincich et al., 2005; Fewings et al., 2008) found that along-shelf wind alone is not an efficient mechanism in driving cross-shelf exchange over

the inner-shelf. On the other hand, cross-shelf wind is found to be an efficient driver of cross-shelf exchange, with onshore winds promoting a two-layer flow with onshore transport near the sea surface and an equal and opposite (offshore) transport below (Tilburg, 2003; Kirincich et al., 2005; Fewings et al., 2008; Lentz et al., 2008; Hendrickson and MacMahan, 2009; Lentz and Fewings, 2012). The importance of surface gravity waves as a forcing element over the inner-shelf has been a subject of recent studies (Fewings et al., 2008; Lentz et al., 2008; Kirincich et al., 2009b). In the absence of wind, these studies have observed that Eulerian cross-shelf velocity profiles have the same vertical structure and opposite direction as the Stokes drift (Stokes, 1847), suggesting a wave-driven cross-shelf exchange.

This study was centred on the shelf circulation at a site with sharp along-shelf topography changes, and with a marked diurnal variability. Eulerian velocity measurements collected at 12-m water depth in the lee of a cape (Cape Sines, on the southwestern coast of Portugal) over 3 consecutive summers were used to study the inner-shelf circulation under upwelling conditions. The strong diurnal cycle of the wind motivated the focus on the daily variability of the circulation, since sea breeze events are found to be particularly important in promoting onshore transport across the inner-shelf, through its influence on both winds and waves (Woodson et al., 2007; Hendrickson and MacMahan, 2009; Lucas et al., 2013). The analysis was focused on a period between 20 July and 04 August 2006 when the wind showed a steady upwelling-favourable condition modulated by a diurnal cycle of the wind. This period offered optimal conditions to study the diurnal variability of the circulation as the main environmental conditions were maintained during this time.

1.2   Data and Methods

1.2.1   In-situ Data

Wind data for the summers of 2006, 2007 and 2008 were collected at the Meteorological station of the Port of Sines authority, at 37° 57' 25" N; 8° 52' 74"W which is about 10 km North of the ADCP location (Figure 1.1). Wave and tidal data for

the same period were collected at 37° 55' 14" N; 8° 55' 47"W , and 37° 56' 89" N; 8° 53' 27"W respectively (Figure 1.1).

Four thermistors (Stowaway TidBit, Onset Computer Corp.) were deployed from July 19, 2006 to September 15, 2006 and from 1 to 14 of August 2007, on a mooring next to the ADCP location. Temperature was measured at 4 different depths: 1 m, 3 m and 5 m above the sea floor, and at the surface. A fifth thermistor was deployed in 2006 at 2 m from the surface.

Velocity profiles were measured with a bottom-mounted upward looking Acoustic Doppler Current Profiler (WorkHorse Sentinel 1200kHz), with a bin size of 0.5 m, and a ping frequency between 0.83 and 1.67 Hz, deployed in approximately 12-m water depth at 37° 53' 11.52"N, 8° 48' 15.42"W, and about 600 m offshore (Figure 1.1). The data was collected in 2006, between July 19 and August 29; in 2007, between July 31 and August 14; and in 2008, between July 22 and September 9 (with a gap between August 05 and August 19). As bottom-mounted ADCPs do not sample the entire water column, the deepest bin corresponds to approximately 1.5 m above sea bed.

The upper bins of the ADCP correspond either to immersed or submersed depth cells depending on the height of the free surface, mainly due to tidal movements. Therefore it was first necessary to find the sea surface, and disregard all bins above that surface. To find the contaminated bins, and since the data was collected at a shallow location where the tidal amplitude ranges from 14 to 30% of the total depth, the 'tide-following method' was used (Kirincich et al., 2005). For each profile, the depth of maximum backscatter intensity was marked as the water surface and all bins above this surface were discarded, plus three bins immediately below it.

1.2.2   Time-averaging and Vertical Coordinate Transformation

The fact that the sea surface undergoes significant changes in shallow waters rises the question of how to compute the daily time averages of data along the same depth. If a bottom or surface reference coordinate system is used (Kirincich et al., 2005; Fewings et al., 2008; Lentz et al., 2008), an average along the same z-level will include data that are at very different relative distances to the surface
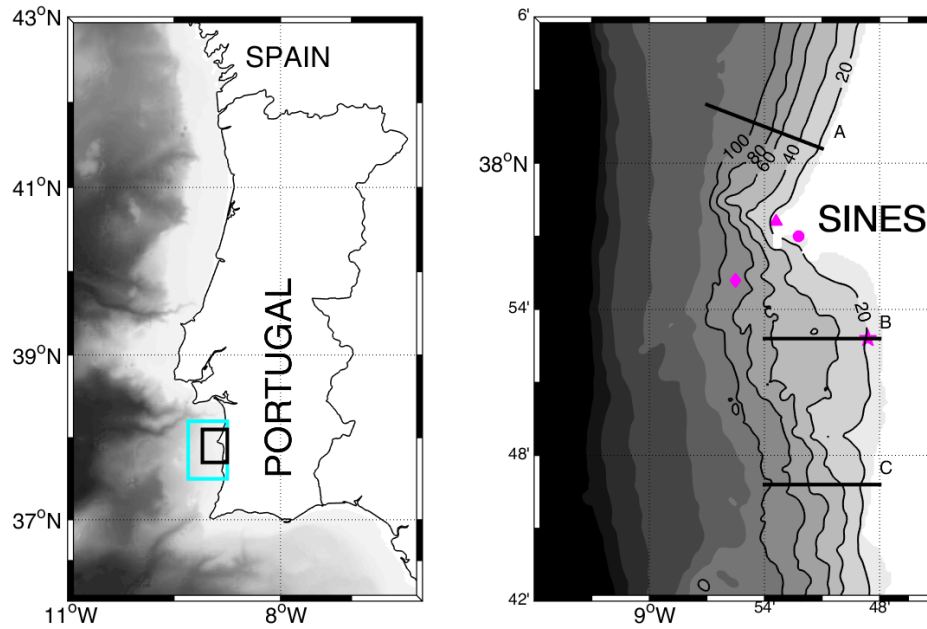
FIGURE 1.1: Left: Study area on the southwestern coast of Portugal. Right: zoom of the study area (black box) showing different sites of sampling: triangle - Meteorological Station, diamond - Wave-rider buoy, star - ADCP and Thermistors, and circle - Tide gauge.
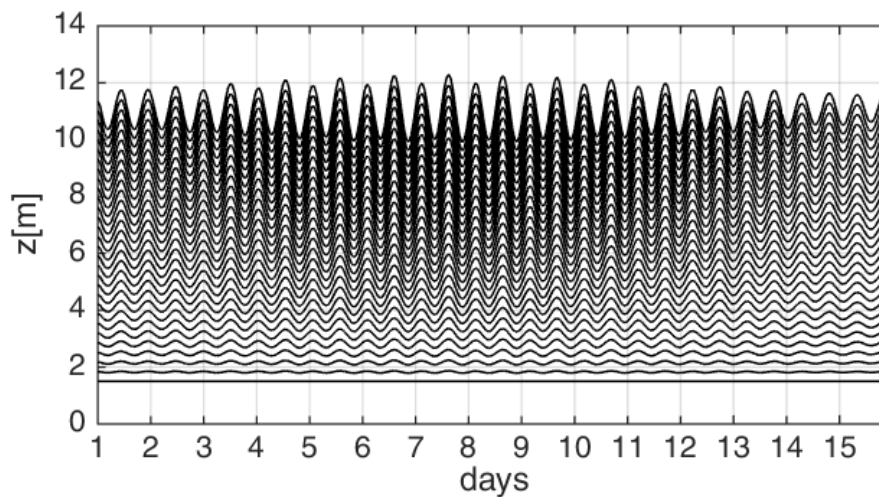
FIGURE 1.2: Z-levels of the dynamic vertical coordinate for 15 days of ADCP data during spring and neap tides.

(especially in spring tides and shallow waters) and this will produce an aliased mean. To overcome this problem, a dynamical (tide-following) vertical coordinate $z' = z/h$, where h is the total water column depth (changing with tides), was used. The total depth (or the sea surface height) was computed by adjusting the surface detected with the maximum of total backscatter intensity to the sea surface using the tidal height measured at the port of Sines (near the ADCP location, see Figure 1.1). Each ADCP profile was then interpolated into this new coordinate system. Time-averaging was then performed along each of the dynamical-surfaces, ensuring that the time-averaging of velocity values is done along levels that are at equal relative distances to the bottom and sea surface. The dynamical vertical coordinate conserves information of both bottom and surface bins and, therefore, it was the one chosen for this study.

The 15-day-averaged cross-shelf circulation was plotted to show the differences using the three approaches (Figure 1.3). For bottom and surface referred vertical coordinates, the time-averaged profile was only considered for bins without missing data. Overall there are no striking differences between these 3 methods, but using the vertical coordinate referred to the bottom, information at the surface will be lost, as it is shown in Figure 1.3. If instead the vertical coordinate referred to the surface is chosen, information at the bottom will be lost. The dynamical vertical coordinate conserves information of both bottom and surface layers and it was, therefore, the one chosen for this study.

The coordinate system was rotated based on the principal axis direction of the subtidal depth-averaged velocity. For most deployments, the major axis orientation was less than 2.4 ° clockwise from north, and it was roughly aligned with local bathymetry and coastline. The coordinate axis was rotated according to this angle and the velocity profiles are now considered to be in cross-shelf (x) and along-shelf (y) directions, with x negative offshore and y positive along-shelf northwards. All further analysis was performed with hourly averaged data.

1.2.3 Clock-hour Average Day

Throughout this study, it was given special attention to the diurnal variability of the circulation. A method defined by Hendrickson and MacMahan (2009) as the '24-h time-averaged' was used. The result consists of an average day (hereinafter
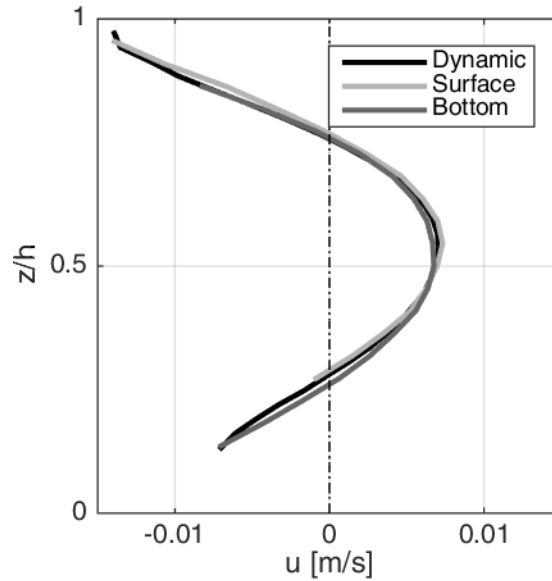
FIGURE 1.3: Time-averaged cross-shelf velocity for the three years,
in function of normalized depth z/h for the three different vertical
coordinate systems.

clock-hour average day) in which each hour corresponds to a mean of that same
hour throughout a chosen period (example: hour 1 is an average of every 1:00 am
for a chosen period).

Spectral wavelet analysis (Morlet) at diurnal timescales ($<$33 h with 95% of confidence level) of the observed wind stress showed that the highest energy was found in the diurnal period (Figure 1.4 c and d), and was consistent throughout the summers of 2006, 2007 and 2008. The stronger diurnal signals were found in the following periods: 20 July - 04 August 2006, 18-29 August 2006, 11-14 August 2007 (the strong diurnal signal remained until 23 of August but there is no ADCP data after day 14) and 18 - 27 August 2008. These periods are marked in Figure 1.4b and were the ones selected to compute the clock-hour average day of the current velocity and temperature profiles, wind parameters and wave height.

1.2.4   Partitioning the Role of Different Forcing Mechanisms

To understand the response of the inner-shelf circulation to each forcing mechanism (wind, waves and tides) separately, the datasets (for all 3 summers) were
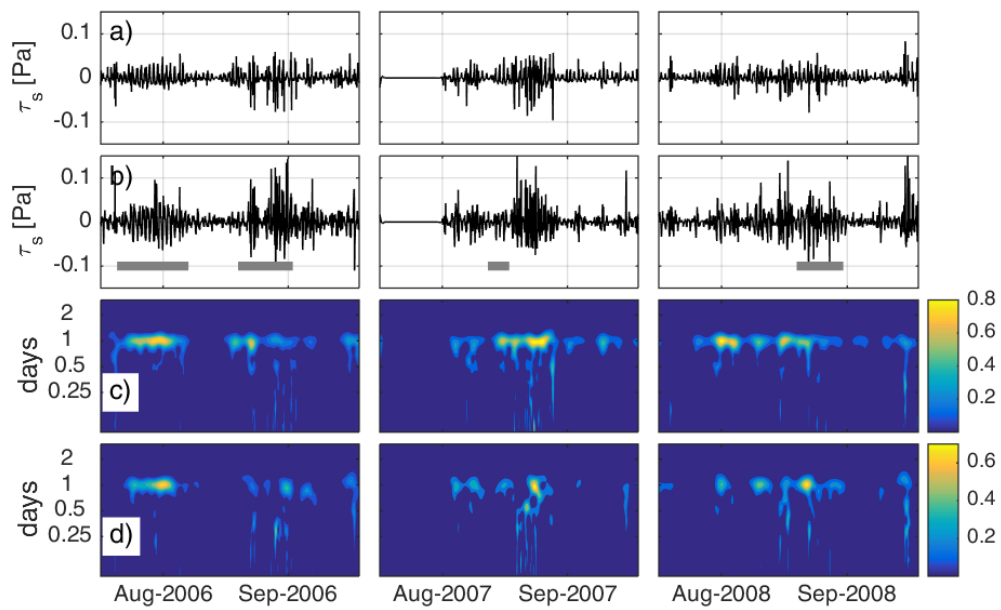
FIGURE 1.4: High passed ($<$ 33 h) cross-shelf wind stress (a) and along-shelf wind stress (b). Wavelet normalized power spectrum of the high passed ($<$ 33 h) cross-shelf (c) and along-shelf wind stress (d). Gray lines in b) represent the periods of strong diurnal cycle (considering the periods when ADCP data was collected).

divided into subsets according to different forcing conditions, in a way similar to Fewings et al. (2008), for periods when only one forcing was strong (above a given threshold value) while the others were weak.
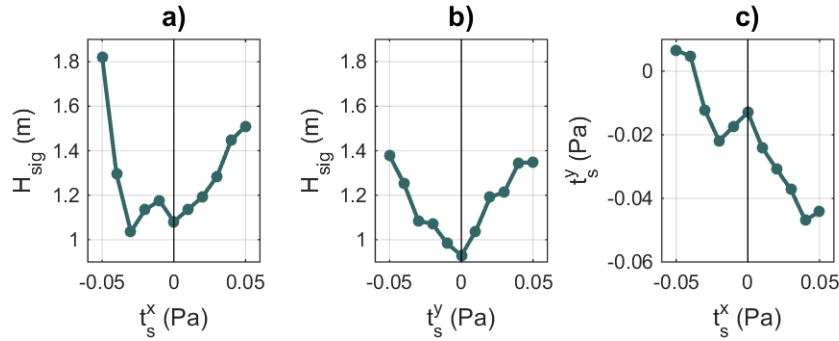
FIGURE 1.5: Significant wave height as a function of a) cross-shelf wind stress; and b) along-shelf wind stress; c) along-shelf wind stress as a function of cross-shelf wind stress.

Figures 1.5a and 1.5b show the mean values of H_{sig} for ranges of τ_s between - 0.05 and 0.05 Pa. The values were obtained by binning the $\tau_s^{x,y}$ data into intervals of 0.01 Pa and then averaging the corresponding H_{sig} values. The same strategy was adopted for the τ_s^x vs τ_s^y function (Figure 1.5c). Cross-shelf and along-shelf wind stresses of either direction were strongly correlated with wave height. H_{sig} changed with τ_s in a quasi-symmetrical way, although offshore winds were associated with slightly lower values of H_{sig}. Westerly winds (onshore: $\tau_s^x > 0$) were associated with northerly (upwelling-favourable: $\tau_s^y < 0$) winds and easterly winds were concurrent with weaker southerly winds (Figure 1.5c).

The high correlations between the forcing mechanisms make it hard to separate the influence of waves, cross- and along-shelf winds, since weak winds were associated with smaller waves and stronger wind stresses were associated with higher waves. Wind stress components were also highly correlated with each other. It is important to note that this analysis is limited, since the forcing mechanisms are all inter-correlated. The threshold values were chosen in order to have a maximum number of data points (at least 20 hours) for each group. The groups and respective thresholds are listed in table 1.1. Unfortunately, the representativeness of each group is not the same since the number of observations varied considerably, especially those with strong winds and small waves (strong winds rarely go with small waves). Weak wind stress was considered when $|\tau_s| < 0.01$ Pa and small waves when $H_{sig} < 1.1$ m. The subset of weak winds and small waves

TABLE 1.1: Threshold values considered for each subset. N represents the amount of hours for each subset. * represents absolute values of τ. Note that a single data point is exclusive to only one group and some data points are not included in any group.

	H_{sig} (m)	τ_s^y (Pa)	τ_s^x (Pa)	N (hours)
TIDE^{ebb}	< 1.1	< 0.01*	< 0.01*	384
TIDE^{flood}	< 1.1	< 0.01*	< 0.01*	362
WAVE	> 1.2	< 0.01*	< 0.01*	204
W_x$^+$	< 1.1	< 0.01	> 0.02	70
W_x$^-$	< 1.1	< 0.01	< -0.02	20
W_y$^+$	< 1.1	> 0.03	< 0.01	32
W_y$^-$	< 1.1	< -0.03	< 0.01	116

(**TIDE**), was considered in order to study the influence of tides on the cross-shelf exchange. For that purpose this subset was divided into flood and ebb tides. For wave forcing events (**WAVE**), the absolute value of wind stress in both directions had to be smaller than 0.01 Pa and waves higher than 1.2 m. For the cross-shelf wind forcing subset (**W_x**), along-shelf winds were weak ($|\tau_s^y| < 0.01$ Pa), waves were small ($H_{sig} < 1.1$ m) and the absolute value of cross-shelf wind stress had to be greater than 0.02 Pa. Also, the subset was divided for times of westerly (**W_x**$^+$: onshore) and easterly (**W_x**$^-$: offshore) winds. For along-shelf wind forcing subset, weak cross-shelf winds ($|\tau_s^x| < 0.01$ Pa), and small waves($H_{sig} < 1.1$ m) were considered, and $|\tau_s^y| > 0.03$ Pa. For this subset, the data was divided into northerly (**W_y**$^-$: upwelling-favourable) and southerly wind (**W_y**$^+$) events. Threshold values and number of hours for each subset are presented in Table 1.1.

1.2.5   Depth-integrated Momentum Balances

Depth-integrated momentum balances were analysed to gain some insight of the underlying mechanisms behind the cross- and along-shelf transport at this site.

The derivation of a depth-integrated momentum balance equation starts with the Boussinesq approximation of the horizontal momentum balances for the cross-shelf velocity, ignoring wave effects (since they were not possible to compute using the in-situ data and were not included in the model simulations) and assuming horizontal mixing is small compared with other terms:

$$\frac{\partial u}{\partial t} + \left(u\frac{\partial u}{\partial x} + v\frac{\partial u}{\partial y} + w\frac{\partial u}{\partial z} \right) - fv = -\frac{1}{\rho_0}\frac{\partial p}{\partial x} + A_v\frac{\partial^2 u}{\partial z^2} \tag{1.1}$$

where u and v are the cross-shelf and along-shelf velocities, respectively, $f = 2\Omega sin\phi$ is the Coriolis parameter, where Ω is the Earth's angular rotation frequency and ϕ is latitude; ρ_0 is the density of seawater, p is the dynamical pressure and A_v is the vertical eddy viscosity.

Vertically integrating over the water column, from bottom $(-h)$ to the free surface (η):

$$\int_{-h}^{\eta} \frac{\partial u}{\partial t}dz + \int_{-h}^{\eta} \left(u\frac{\partial u}{\partial x} + v\frac{\partial u}{\partial y} + w\frac{\partial u}{\partial z} \right)dz - \int_{-h}^{\eta} fvdz =$$
$$-\frac{1}{\rho_0}\int_{-h}^{\eta}\frac{\partial p}{\partial x}dz + \int_{-h}^{\eta}A_v\frac{\partial^2 u}{\partial z^2}dz \tag{1.2}$$

Considering the following boundary conditions: At the surface (z = η), the surface shear stress:

$$A_v\frac{\partial u}{\partial z}\bigg|_{z=\eta} = \tau_s^x \tag{1.3}$$

And at the bottom $(z = -h)$, the bottom shear stress:

$$A_v\frac{\partial u}{\partial z}\bigg|_{z=-h} = \tau_b^x \tag{1.4}$$

where τ_s and τ_b are the surface (wind) and bottom stress, respectively. And defining the depth-integrated velocity as:

$$\mathbf{u} = \int_{-h}^{\eta} udz \tag{1.5}$$

The cross-shelf momentum balance is:

$$\overbrace{\frac{\partial \mathbf{u}}{\partial t}}^{1} + \overbrace{\int_{-h}^{\eta} \left(u\frac{\partial u}{\partial x} + v\frac{\partial u}{\partial y} + w\frac{\partial u}{\partial z} \right) dz}^{2} - \overbrace{f\mathbf{v}}^{3} =$$

$$-\overbrace{\frac{1}{\rho_0} \int_{-h}^{\eta} \frac{\partial p}{\partial x} dz}^{4} + \frac{\overbrace{\tau_s^x}^{5} - \overbrace{\tau_b^x}^{6}}{\rho_0} \qquad (1.6)$$

and, correspondingly the along-shelf momentum balance:

$$\overbrace{\frac{\partial \mathbf{v}}{\partial t}}^{1} + \overbrace{\int_{-h}^{\eta} \left(u\frac{\partial v}{\partial x} + v\frac{\partial v}{\partial y} + w\frac{\partial v}{\partial z} \right) dz}^{2} + \overbrace{f\mathbf{u}}^{3} =$$

$$-\overbrace{\frac{1}{\rho_0} \int_{-h}^{\eta} \frac{\partial p}{\partial y} dz}^{4} + \frac{\overbrace{\tau_s^y}^{5} - \overbrace{\tau_b^y}^{6}}{\rho_0} \qquad (1.7)$$

Hereinafter, the momentum balance terms will be referred as follows: first term is acceleration, second term is advection, third term is Coriolis, fourth term is pressure gradient, fifth term is wind stress and the sixth term is bottom stress. Results are consistent with Fewings and Lentz (2010) and Lentz and Fewings (2012) although they used a depth-averaged approach instead of depth-integrated.

As was discussed above, the ADCP does not sample the entire water column, and in order to calculate depth-integrated velocities the velocity was set to linearly decay to zero from the lowest ADCP bin (1.5 m from sea bed) to the bottom. Since measurements were taken at a single point, pressure gradient and advection terms could not be estimated. We consider the sum of the computed terms as residual of the balance (R_x, R_y) which will balance the sum of the unaccounted terms:

$$R_x = -\int_{-h}^{\eta} \left(u\frac{\partial u}{\partial x} + v\frac{\partial u}{\partial y} + w\frac{\partial u}{\partial z} \right) dz - \frac{1}{\rho_0} \int_{-h}^{\eta} \frac{\partial p}{\partial x} dz \qquad (1.8)$$

and

$$R_y = - \int_{-h}^{\eta} \left(u\frac{\partial v}{\partial x} + v\frac{\partial v}{\partial y} + w\frac{\partial v}{\partial z} \right) dz - \frac{1}{\rho_0} \int_{-h}^{\eta} \frac{\partial p}{\partial y} dz \qquad (1.9)$$

For the computation of momentum balance terms using in-situ data, ρ_0 was considered to be equal to 1025 kg.m^{-3}. The acceleration term was estimated using backward differences with the depth-integrated velocity. Wind stress was estimated using (Smith, 1988) bulk formula ($\tau_s = \rho_{air}C_d|V_w| \cdot \mathbf{V_w}$), where the wind drag coefficient $C_d = 1.14 \times 10^{-3}$ is a function of the air density (ρ_{air}) and the wind speed (V_w) (Large and Pond, 1981). The bottom stress was estimated using the linear drag law: $\tau_b = \rho_0 r(u_b, v_b)$; with $r = 5 \times 10^{-4}$ m.s^{-1} and the near-bottom velocities (ub, vb) corresponding to the last ADCP bin (1.5 m above sea bed) (Lentz et al., 1999).

1.3   Results

1.3.1   Winds

Cross-shelf wind stress (τ_s^x) ranged, on average, between values of -0.05 Pa and 0.05 Pa (Figure 1.6a) and was mostly positive (onshore) with short periods of offshore winds. Along-shelf winds were dominantly from north (negative values of along-shelf wind stress), with episodic and weaker events of southerly winds (Figure 1.6b). Along-shelf wind stress (τ_s^y) was overall higher than cross-shelf wind stress, and ranged between -0.1 Pa and 0.05 Pa.

1.3.2   Waves and Tides

Throughout the 3 summers the waves had a mean significant wave height of 1.2 m (Figure 1.6c) and significant wave heights above 2.5 m were rare during this period. As seen in Lentz et al. (2008) and Fewings et al. (2008), wave-driven cross-shelf currents for waves with H_{sig} =1.2 m are in the order of 0.01 m.s^{-1}, and

directed offshore (wave-driven undertow). The tidal components were diagnosed using the tidal gauge data and the T_TIDE package (Pawlowicz et al., 2002). The dominant tidal component was the M2 (lunar semidiurnal tide, with period of 12.42 h) followed by S2, N2 (semidiurnal) and K1 (diurnal tide). The mean tidal amplitude at this site, during these 3 summers, was 1.7 m with maximum of 3.6 m (Figure 1.6d). Estimations of the barotropic tidal contribution of the M2 tide resulted in cross-shelf velocities around 2×10^{-3} m.s^{-1}.

1.3.3 Stratification

Throughout the period when water temperature was measured, the water column was stratified (Figure 1.6e). A mean difference between surface and bottom temperature of about 2 °C was observed, which is considered high stratification for a 12-m depth site (Lentz, 2001; Durski et al., 2004). Temperature changes are apparently connected with the variability of the along-shelf winds, with higher stratification periods occurring during relaxation of the northerly winds. However, periods of higher surface temperatures are also concurrent with spring tides, meaning that tidal effects on the stratification should not be neglected.
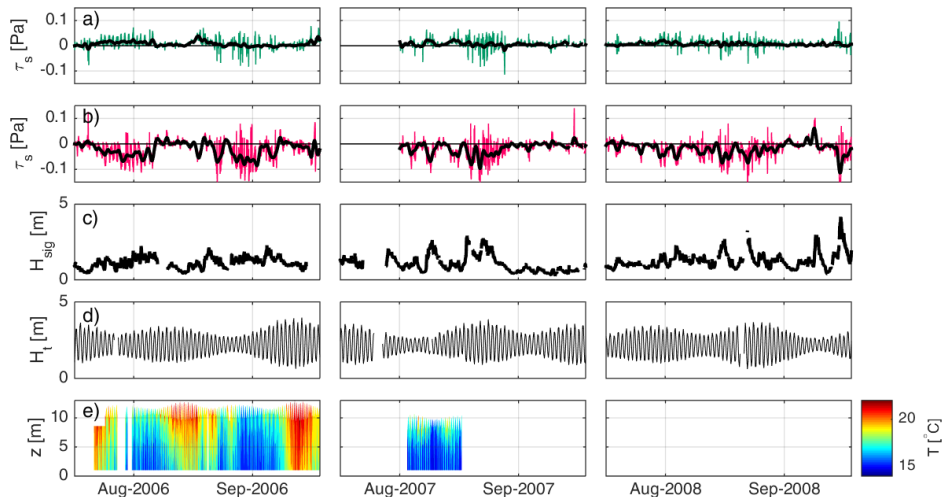
FIGURE 1.6: a) Hourly (green) and subtidal (black) cross-shelf wind stress [Pa]; b) Hourly (red) and subtidal (black) along-shelf wind stress [Pa]; c) Significant Wave Height [m]; d) Tidal Height [m] and e) Temperature [°C], between 15 July and 15 September. Each column indicates a different year, left to right - 2006; 2007 and 2008

1.3.4   Mean Circulation

During the summers of 2006, 2007 and 2008, the subtidal along-shelf velocity (Figure 1.7d) was southwards, consistent with a response to northerly, upwelling-favourable winds, which is a typical wind regime in the Western Iberian margin during summer (Relvas et al., 2007). There were a few events where the upwelling relaxed and the wind rotated northwards. During those events, the along-shelf velocity was northwards. The intensity of the along-shelf velocity was stronger at the surface and decayed with depth. The cross-shelf velocity (Figure 1.7c) had a persistent maximum onshore flow at mid-depth, with offshore velocities at surface and bottom. This parabolic profile did not change regarding northerly or southerly winds, except during strong upwelling-favourable wind conditions, when the cross-shelf velocity showed a two-layer vertical structure with offshore velocities at surface and an opposite flow in depth, as should be expected during upwelling conditions.
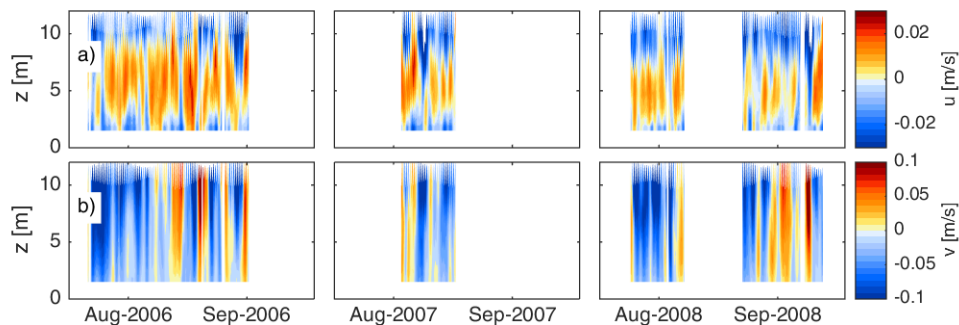
FIGURE 1.7: Subtidal time series of a) Cross-shelf velocity profiles [m.s^{-1}] and b) Along-shelf velocity profiles [m.s^{-1}]. Each column, left to right - 2006; 2007 and 2008. z=0 is the bottom.

1.3.5   Velocity Profiles for Different Forcing Conditions

The mean velocity profiles and corresponding standard deviations for each subset (Table 1.1) are shown in Figure 1.8. For most conditions, the cross-shelf velocity profile (top row in Figure 1.8) showed a consistent parabolic structure with maximum onshore flow at mid-depth for all forcing conditions, except when offshore wind forcing was strong. This indicates that the shape of cross-shelf flow profile is

not explained by any of the forcing mechanisms in isolation and probably results from a combination of several processes.

During weak wind and wave forcing (**TIDE** subset; Figure 1.8a; top row) there was a cross-shelf velocity different from zero. There are some differences between the cross-shelf velocity profiles during ebb and flood tides, especially near the bottom. Both profiles showed a parabolic structure, with maximum onshore velocity of 0.02 m.s^{-1} at mid-depth during flood tides, and with offshore velocities near the bottom, weaker for ebb tides.

The cross-shelf velocity profile, when waves were stronger (**WAVE** subset: Figure 1.8b, top row) had also a parabolic structure, as seen for the weak wind and wave forcing subset, but with weaker onshore velocities at mid-depth and stronger off-shore flow near the surface, reaching values of -0.02 m.s^{-1}. The cross-shelf velocity profile also showed an offshore flow just below the surface that resembles the wave-driven undertow predicted by (Lentz et al., 2008) and observed by (Fewings et al., 2008).

For both strong northerly and southerly winds (Figure 1.8c, top row), the cross-shelf profiles showed coincident structure and magnitude: a parabolic shape with maximum onshore flow at mid-depth.

The cross-shelf velocity profile for the onshore winds subset (**W_x**$^{+}$; Figure 1.8d, top row) had also a parabolic structure, with maximum onshore flow of $u = 0.02$ m.s^{-1} in the lower layer that decreased to near zero at the bottom, and an offshore flow in the surface layer, with maximum value exceeding -0.02 m.s^{-1}, and decreasing to zero near the surface. For the offshore winds subset (**W_x**$^{-}$) there was an offshore flow in the lower part of the water column, with maximum velocity near the bottom, and a weaker onshore flow near the surface.

1.3.6   Circulation at Diurnal Timescales

Emphasis was given to the period between 20 July to 04 August 2006 (hereinafter control period) when both wind and wave forcing maintained similar conditions (Figure 1.9) . The wind had a very stable pattern of northwesterly winds modulated by a diurnal oscillation of magnitude in both wind components (Figure 1.9a). Wave height increased on average throughout this period but had a daily
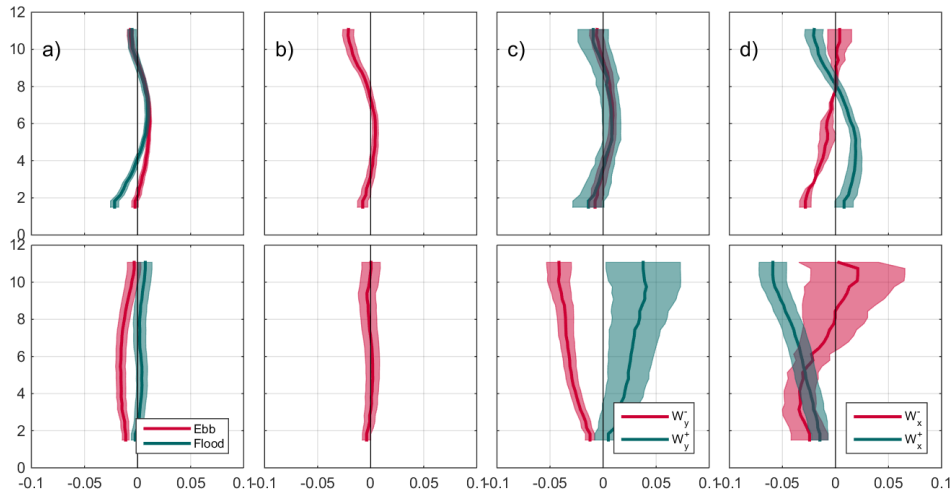
FIGURE 1.8: Mean cross-shelf (top) and along-shelf (bottom) velocity profiles for different subsets: a) **TIDE**; red: ebb tides, blue: flood tides; b) **WAVE**; c) **W_y**; red: northerly winds; blue: southerly winds; d) **W_x**; red: easterly winds, blue: westerly winds. Shaded areas correspond to variability of ± 1 standard deviation.

maximum concurrent with the maximum of wind magnitude (Figure 1.9b). During this period, the cross- and along-shelf velocity (Figure 1.9c and d, respectively) showed a repetitive circulation pattern. The flow in the along-shelf direction was southwards with a daily intensification in the afternoon. There was a daily flow reversal in the cross-shelf circulation at mid-day. Cross-shelf velocities ranged from 0.1 to -0.1 m.s^{-1} while the along-shelf circulation was stronger, reaching -0.3 m.s^{-1}. The water column remained stratified during this period, with a marked diurnal heating and an overall decrease in temperature towards the end of July and beginning of August (Figure 1.9e).

Results for the clock-hour average day over the control period are plotted in Figure 1.10. The diurnal sea-breeze cycle is clear in the wind stress plots (Figure 1.10a). Wind stress was weak in the morning period, but around 11 h there was an increase of both components of the wind stress, with cross-shelf wind stress peaking at 16 h and along-shelf wind stress at 18 h. There was a decrease in H$_{sig}$ throughout the morning and mid-day, with minimum height at 13 h. Afterwards, the significant wave height increased, peaking at 20 h (Figure 1.10b). A lag between wind and wave maximum was also described in Hendrickson and MacMahan (2009). The stratification (Figure 1.10c) was present throughout the day with
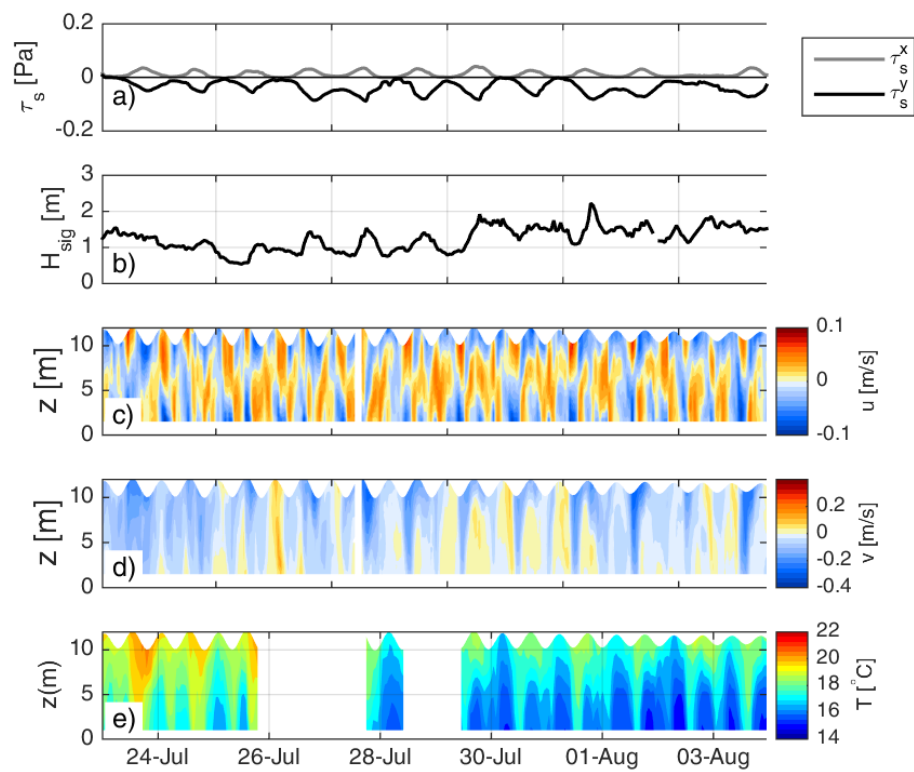
FIGURE 1.9: Time series, between 20 July and 04 August 2006, of a) Wind stress [Pa]; b) Significant wave height [m]; c) Cross-shelf velocity [m.s^{-1}]; d) Along-shelf velocity [m.s^{-1}]; and e) Temperature [°C]. z=0 is the bottom

a semi-diurnal peak and higher values late in the day, related to diurnal heating. In the cross-shelf flow (Figure 1.10d), 3 periods can be clearly identified. From 00 h to 11 h (morning period) the cross-shelf velocity had a 3-layer structure, with offshore velocities of approximately -0.01 m.s^{-1} at the surface and near the bottom, and an onshore flow at mid-depth. Between 12 h and 15 h (mid-day period), when wave height reached its minimum value and the wind increased in magnitude and rotated onshore, there was a reversal in the cross-shelf flow structure. The cross-shelf velocity profile had a 2-layer structure, with onshore flow in the surface layer, and offshore flow at the bottom (Figure 1.10d). After 15 h (evening period), the velocity profile was again reversed, with onshore flow near the bottom and offshore flow at the surface, much stronger than in the morning period. This period corresponds to maximum wave height and strongest wind magnitude with a clear cross-shelf component. Throughout the clock-hour average day the along-shelf velocity was always negative (Figure 1.10e) with maximum velocities between 16 h and 18 h, concurrent with the maximum of northerly wind. Overall, the cross-shelf circulation magnitude was around 0.01 m.s^{-1}, and the along-shelf circulation was much stronger, reaching up to 0.2 m.s^{-1}.

The diurnal variability of the circulation analysed before was noticeably consistent during other periods when diurnal cycle of wind in either component was also strong (shown as gray lines in Figure 1.4b). It can be seen in Figure 1.11 that the averaged diurnal variability for these periods was much similar to the clock-hour average day of the control period. The cross-shelf circulation (Figure 1.11d) also showed a daily three-period variability, although with weaker magnitudes than the clock-hour average day for the control period. The diurnal variability of the along-shelf velocity was also similar to the control period, with maximum (although slightly weaker) southwards flow near the surface in the evening, concurrent with maximum wind magnitude.

1.3.7   Dynamics

The depth-integrated cross-shelf and along-shelf momentum balances were computed using the clock-hour average day variables, over the control period. In the depth-integrated momentum balances three distinct periods can be identified, in which there are significant changes in the relative importance of each term of
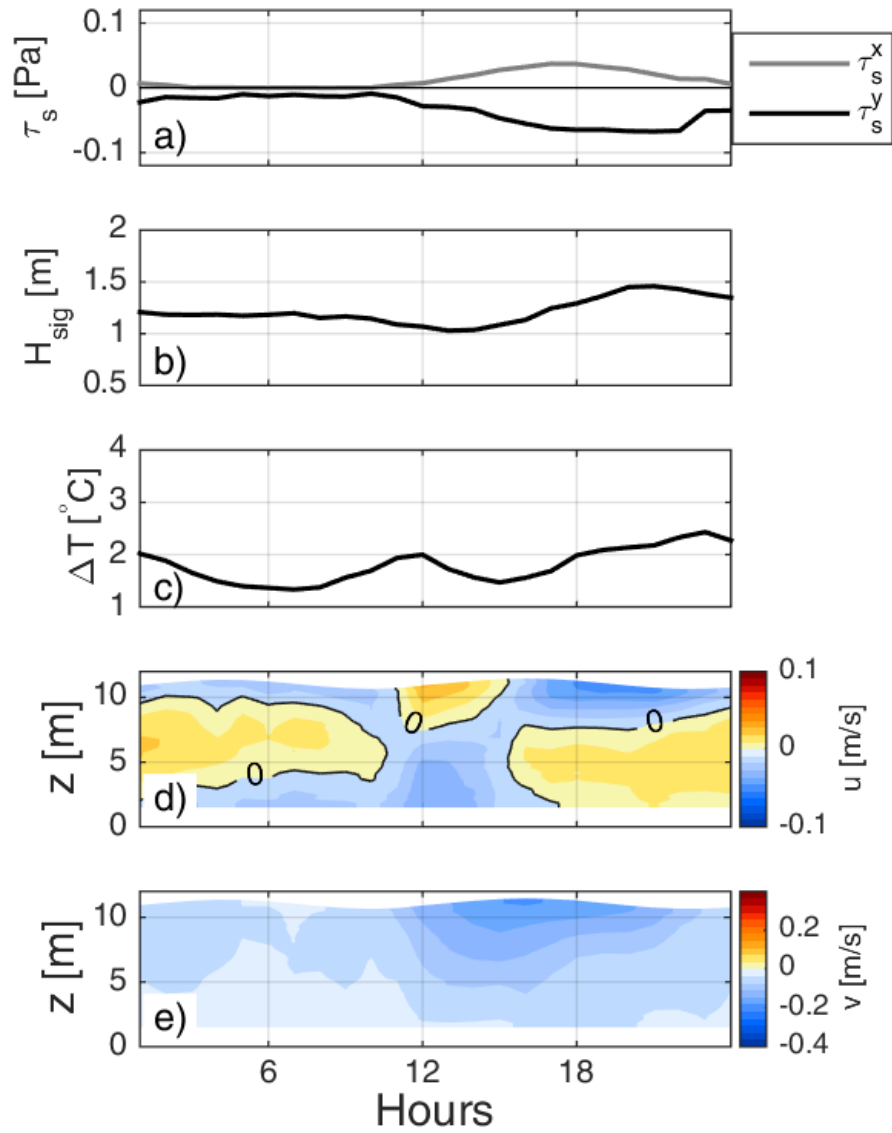
FIGURE 1.10: The clock-hour average day for the control period (July 20 to August 04 of 2006), of a) Wind stress [Pa]; b) Significant wave height [m]; c) Difference between temperature at the surface and at the bottom [°C]; d) Cross-shelf velocity [m.s^{-1}]; e) Along-shelf velocity [m.s^{-1}]. z=0 is the bottom. Thick black line marks zero and the contour interval is 0.01 m.s^{-1}.
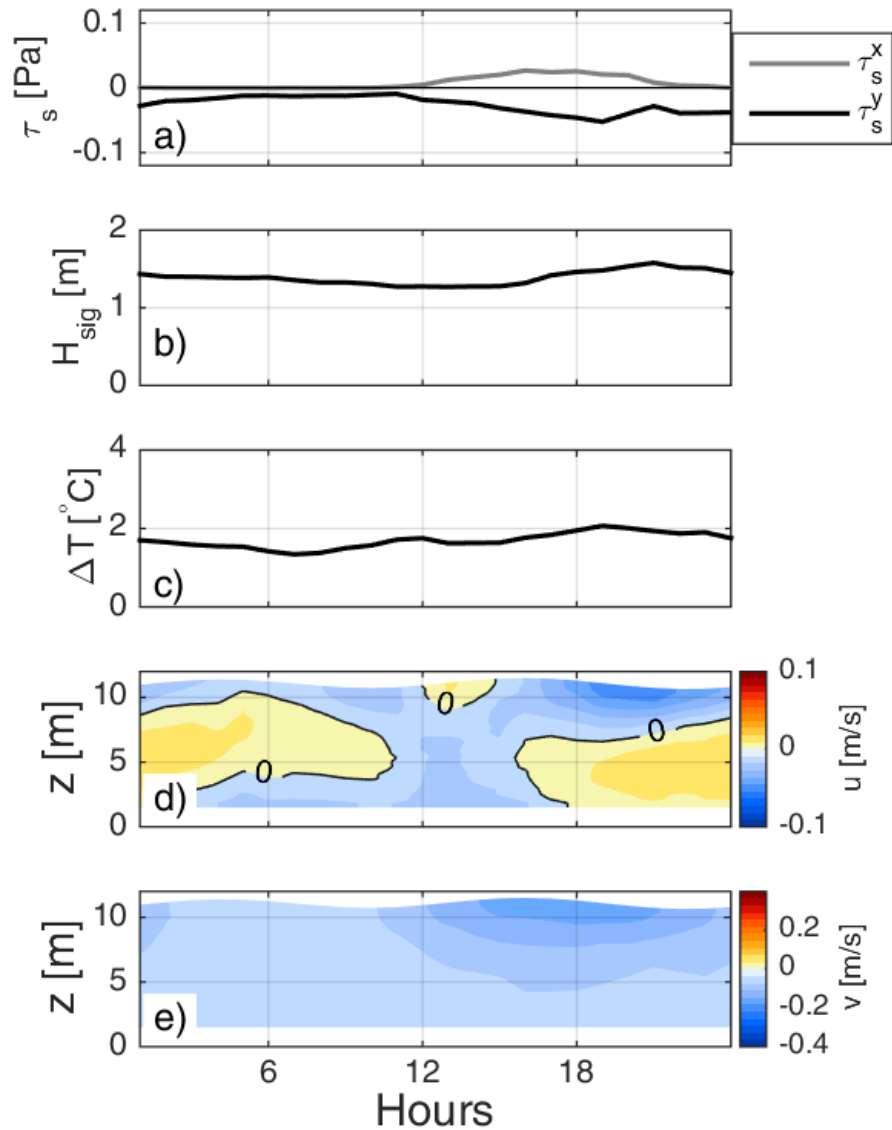
FIGURE 1.11: The clock-hour average day, for the four periods marked in Figure 1.4, of a) Wind stress [Pa]; b) Significant wave height [m]; c) Difference between temperature at the surface and at the bottom [°C]; d) Cross-shelf velocity [m.s^{-1}]; e) Along-shelf velocity [m.s^{-1}]. z=0 is the bottom.

the balance (Figure 1.12). In the morning period, all terms are relatively weak and near zero. For the along-shelf direction, the balance appears to be between the along-shelf wind stress and other terms that are part of R_y. In the cross-shelf direction, some part of R_x is balanced by the Coriolis term. Acceleration is a dominant term in the along-shelf direction, with stronger impact on the mid-day period. At this time, the acceleration is almost exclusively balanced by R_y. The relative importance of wind stress term in both balances, increases during the afternoon and evening.

In the cross-shelf momentum balance, Coriolis term is the stronger term, with a significant increase at mid-day, concurrent with the increase of the along-shelf velocities as a response to the wind intensification. This term is balanced by the wind stress term, which also increases in the afternoon, and with R_x, that fluctuates during the day, with higher intensity between 12 h and 16 h. Acceleration and bottom stress terms are considerably weaker than the other terms.

The balance is slightly more complicated in the along-shelf direction. The Coriolis and bottom stress terms are clearly the weakest terms of the balance. Wind stress and acceleration, together with R_y, are the dominant terms. However, until mid-day, acceleration is near-zero and wind stress is balanced by R_y. At mid-day, there is a sharp variation of the acceleration, which represents a strong increase of the southwards velocity at this time. This variation is followed by a sharp increase in R_y, and wind stress only accounts for a small part of the balance. Finally, in the afternoon, the wind stress increases in magnitude but the acceleration is weaker and positive, indicating a relaxation of the southwards current. The opposing signals of wind stress and acceleration at this time consequently increase the magnitude of R_y. It is clear that R in both directions represents a large amount of the balance.

1.4 Summary and Discussion

Nearshore circulation was analysed using ADCP data collected at 12-m in the lee of Cape Sines (Figure 1.1), during the summers of 2006, 2007 and 2008. The region is under persistent upwelling-favourable wind conditions modulated by a daily cycle similar to sea breeze. The analysis was focused on a 15-day period between
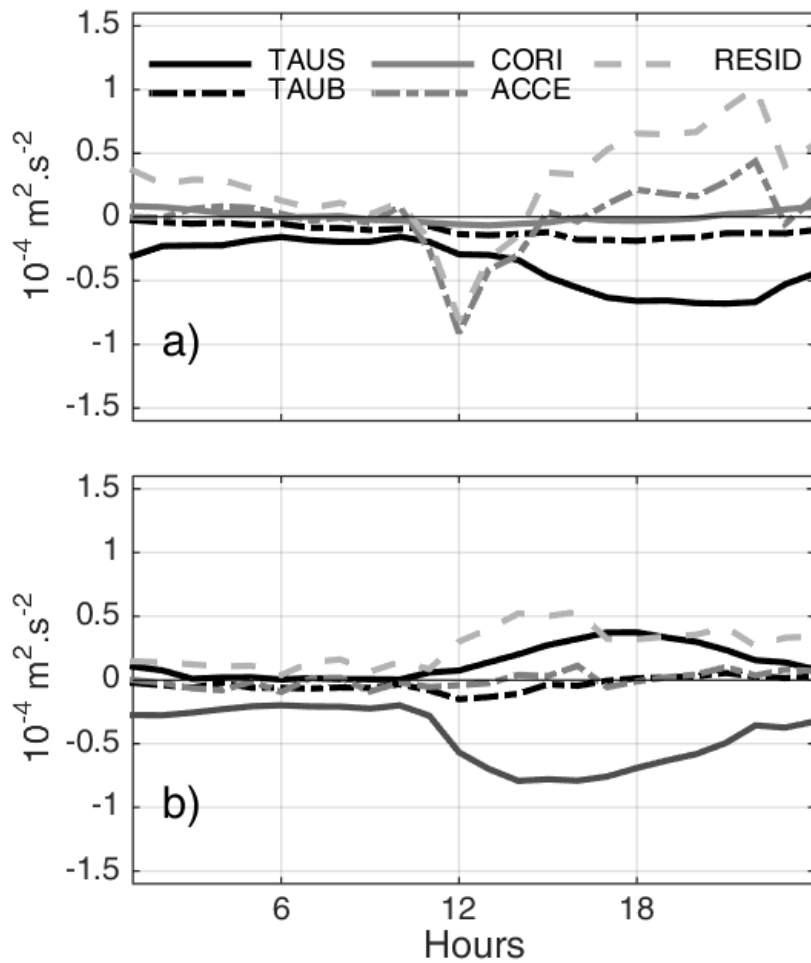
FIGURE 1.12: Depth-integrated along-shelf (a) and cross-shelf (b) momentum balance terms for the clock-hour average day. TAUS: wind stress; TAUB: bottom stress; ACCE: acceleration; CORI: Coriolis; RESID: Residual terms. Units are $m^2.s^{-2}$.

20 July to 04 August of 2006, when the wind maintained similar conditions, to study the diurnal variability of the cross-shelf circulation.

The observed cross-shelf circulation showed a vertical shape and diurnal variability different from several other systems described in literature (Tilburg, 2003; Kirincich et al., 2005; Fewings et al., 2008; Lentz et al., 2008; Hendrickson and MacMahan, 2009; Lentz and Fewings, 2012). The daily variability of the observed cross-shelf circulation consisted of three distinct periods. A morning period with a 3-layer structure with onshore velocities at mid-depth, a mid-day period where the flow is reversed and has a 2-layer structure with onshore velocities at surface and offshore flow at the bottom (downwelling), and, lastly, a 2-layer period, with strong offshore velocities at the surface and onshore flow at the bottom (upwelling). Most inner-shelf studies admit that cross-shelf wind stress may induce a circulation of similar magnitude as upwelling or downwelling, specifically over stratified waters. Cross-shelf wind stress is found to force a circulation of same direction as wind (onshore or offshore) in the surface layer and a compensating opposite flow underneath (Lentz and Fewings, 2012). Hendrickson and MacMahan (2009) described a diurnal circulation forced by sea breeze. In their study, the most clear feature was a wave-driven undertow forced by the sea breeze effect on wave height. They found that a wind stress threshold of 0.5 Pa was needed to modify the background circulation. We do not observe that type of circulation, probably due to lower H_{sig} and wind stress present at this location. Although previous works (Woodson et al., 2007; Hendrickson and MacMahan, 2009; Zhang et al., 2010) have found that the cross-shelf circulation is strongly modified by sea breeze events, the observed diurnal circulation did not show a simple wind- or wave-driven circulation coherent to previous inner-shelf studies.

A distinctive feature of the circulation at this site is the parabolic-shaped cross-shelf profile, with maximum onshore velocity at mid-depth, that appeared in most mean cross-shelf profiles, despite the different forcing conditions, and that is also present in the morning period of the clock-hour average-day. Lentz and Chapman (2004) showed that for strong stratification conditions, the onshore return flow (as response to upwelling) can be in the interior of the water column, as a response to increasing momentum flux divergence and small bottom stress in the momentum balance. Mid-shelf studies on the Middle Atlantic Bight (Lentz, 2008) and Oregon coast (McCabe et al., 2015) showed mean cross-shelf profiles with maximum

onshore flow at mid-depth which were explained by a combination between wind stress and local along-shelf pressure gradients. In a study around Point Conception, California, Fewings et al. (2015) consistently observed vertical profiles of the same form, which were associated with pressure gradients connected with local wind relaxations. These studies indicate that along-shelf pressure gradients are likely a key factor in the cross-shelf vertical profile form at this site.

Momentum balance analysis showed that the daily variability of the cross-shelf flow is associated with the evolution of the different terms and their relative importance in the balance. For instance, the along-shelf acceleration is dominant at mid-day, which may contribute for the flow reversal as a frictional response to the abrupt change of wind direction, as some studies indicate (Zhang et al., 2010; Kim et al., 2014). Since the net cross- and along-shelf momentum balances with the estimated terms are not zero, and the residual is a dominant term for most part of the day in both balances, it is clear that either pressure gradient or advection, or both, are an important forcing mechanism at this site.

Wave data collected at 98-m depth showed significant wave heights of less than 2 m for most part of the time (Figure 1.6). At this point it can only be assumed that waves are not energetic enough to modify the wind-driven circulation, since the mean H_{sig} is approximately 1.2 m, and the corresponding wave-driven cross-shelf velocities are expected to be below 0.01 m.s^{-1} (Fewings et al., 2008; Lentz et al., 2008; Hendrickson and MacMahan, 2009). Tidal forcing may have some significance in the circulation, especially in the morning period. However, the mean cross-shelf profiles for the **TIDE**^{ebb} and **TIDE**^{flood} subsets did not show significant differences and this may indicate that tides probably do not significantly affect the observed circulation, especially at the surface levels.

Taking all the points discussed above into consideration, it is clear that the in-situ data collected was not enough to study in detail the dynamics at the observations site. Simplified and more complex models are used in the next chapters to further analyse the diurnal circulation in the lee of cape Sines.

Chapter 2

Inner-shelf Response to Wind and Waves in an Idealized 2D Model

2.1 Introduction

As described in Chapter 1, the observed diurnal variability of the cross-shelf circulation in the leeside of Cape Sines showed a mid-day flow inversion not easily explained using in-situ data alone. To further analyse the forcing mechanisms responsible for this flow inversion, a 2-D (cross-shelf vs depth), steady model, developed by Lentz et al. (2008) was used.

This model has proven to be a helpful tool for successfully simulating the inner-shelf circulation over smoother shelves like Martha's Vineyard and North Carolina (Fewings et al., 2008; Lentz et al., 2008) and steeper slopes like the Oregon coast (Kirincich et al., 2009b) and Monterey Bay (Hendrickson and MacMahan, 2009).

The wave-driven undertow predicted by Lentz et al. (2008) has been found to significantly modify the vertical cross-shelf circulation, especially in the presence of weak wind forcing or wind relaxation periods, like sea breeze events (Hendrickson and MacMahan, 2009). As seen in the previous chapter, the in-situ datasite is under the influence of a daily relaxation of wind forcing, that may increase the importance of wave forcing during those periods.

To be noted that this numerical model will most likely not represent exactly the observed cross-shelf flow, since a number of simplifications are made. For example, it is expected that the vertical mixing, represented by the eddy viscosity

profiles (EVP), will not only be dependent on wind, waves and their role on bottom stress, but also on stratification, which is not included in the computation of the EVP (more details in Lentz (1995)). However, the main focus of this Chapter is to study separately the cross-shelf flow dependence on each forcing mechanism (wind and waves) and the use of a simplified numerical model that represents the cross-shelf flow driven by different conditions will be helpful to understand the individual contributions of wind and waves to the diurnal variability of the circulation.

2.2 2D Inner-shelf Model

The model developed by Lentz et al. (2008), assumes steady-state, linear dynamics, no along-shelf variations (except along-shelf pressure gradient), no cross-shelf transport at the coast and no stratification. This model resolves the numerical steady solution of the linear momentum equations:

$$-fv = fv_{st} - \frac{1}{\rho_0}\frac{\partial P}{\partial x} - F^{ws} + \frac{\tau_z^{wbx}}{\rho_0} + (Au_z)_z, \qquad (2.1)$$

$$fu = -fu_{st} - \frac{1}{\rho_0}\frac{\partial P}{\partial y} + \frac{\tau_z^{wby}}{\rho_0} + (Av_z)_z, \qquad (2.2)$$

where f is the Coriolis parameter, u, v are the cross-shelf and along-shelf velocities, v_{st} and u_{st} are Stokes velocities, z denotes vertical partial derivatives, y is the along-shelf direction and x is the cross-shelf direction, F^{ws} is the momentum flux due to shoaling waves, τ_{wb} is the wave stress due to bottom friction acting on waves, ρ_0 is the water density, P is pressure, and A is an eddy viscosity used to parametrize the Reynold stresses.

The cross-shelf wave-driven Eulerian velocity profile is predicted to be equal in magnitude and opposite in sign to the Lagrangian Stokes drift velocity profile u_{st}:

$$u_{st} = \frac{gkH_{sig}^2}{8c}\frac{cosh[2k(z+h)]}{sinh(2kh)}cos(\theta_w) \qquad (2.3)$$

where H_{sig} is the significant wave height, c is the phase speed of the waves, and θ_w is the wave direction to shore-normal (Longuet-Higgins and Stewart, 1964).

The model is forced by waves, wind stress and along-shelf pressure gradient, and different forms of eddy viscosity profiles are available. Except for the constant EVP, which has a constant value throughout the water column, all other EVPs linearly decay towards zero at the bottom and surface boundaries. The only difference is how they extend to the interior of the water column (more details in Lentz (1995)).

The numerical solution consists of a set of iterations to find the value of $\frac{\partial P}{\partial x}$ to minimize the cross-shelf transport.
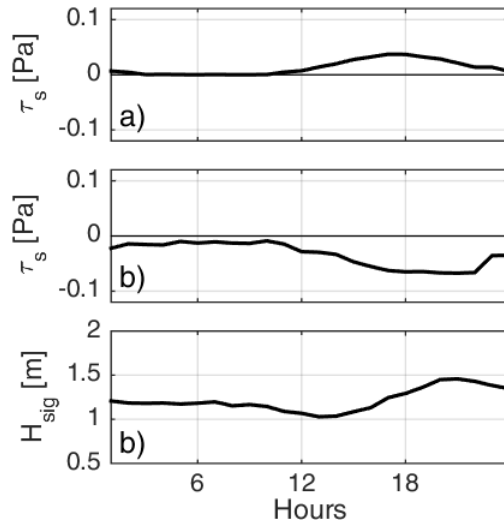
FIGURE 2.1: Clock-hour average day of the forcing parameters: a) cross- and b) along-shelf wind stress [Pa]; c) significant wave height [m].

2.3 Methods

To study the circulation's response to each forcing mechanism, the Lentz et al. (2008) model was forced separately with wind and wave data that resulted from the clock-hour average-day during the control period (July 20 to August 04 of 2006; Figure 2.1).

Analogous to the previous Chapter, each experiment was conducted by isolating one of the forcing mechanisms. For the **W_y** experiment, the main forcing mechanism was the along-shelf wind stress, and so the cross-shelf wind stress and wave parameters were set to zero. The **W_x** experiment was conducted to analyse the circulation's response to the cross-shelf wind stress, without wave forcing or along-shelf wind stress. Lastly, the **WAVE** experiment, where the model was exclusively forced with waves.

As a last exercise, the joint effect of wind and waves was analysed with the model forced by both wind and waves.

Sensitivity tests using the along-shelf circulation (since the model represented it fairly well; Figure 2.2) showed that the EVP profile that best fit the observations was the constant one, with $A_v = 2 \times 10^{-3}$ m.s^{-2}, and a bottom roughness of $z_o = 2 \times 10^{-3}$ m. These parameters were maintained for all experiments analysed in this chapter. Although we are under stratified conditions (see Chapter 1) and other EVPs are more adequate (Lentz, 2001), there are some inner-shelf studies where the use of a constant EVP obtained good results (Fewings et al., 2008).

2.4 Results

2.4.1 Model Response at Diurnal Timescales

The model results for the cross-shelf circulation based on either isolated or combined wind and wave forcing are very different from the observed profiles (Figures 2.3 and 2.4).

Forcing the model with along-shelf wind stress (Figure 2.3b), resulted in a cross-shelf circulation typical of upwelling, with a two-layer structure of offshore flow at the surface, and onshore flow in the bottom layer. Using cross-shelf wind stress as the only forcing mechanism (Figure 2.3c), the cross-shelf circulation obtained is also considerably different from the observations. Throughout the day, there is a two-layer structure with onshore flow at the surface, and an offshore flow in the deeper layer, similar to the wind-driven circulation reported in literature (Fewings et al., 2008; Lentz et al., 2008). The cross-shelf velocities are stronger after mid-day, as the wind magnitude also increases. When forced exclusively with
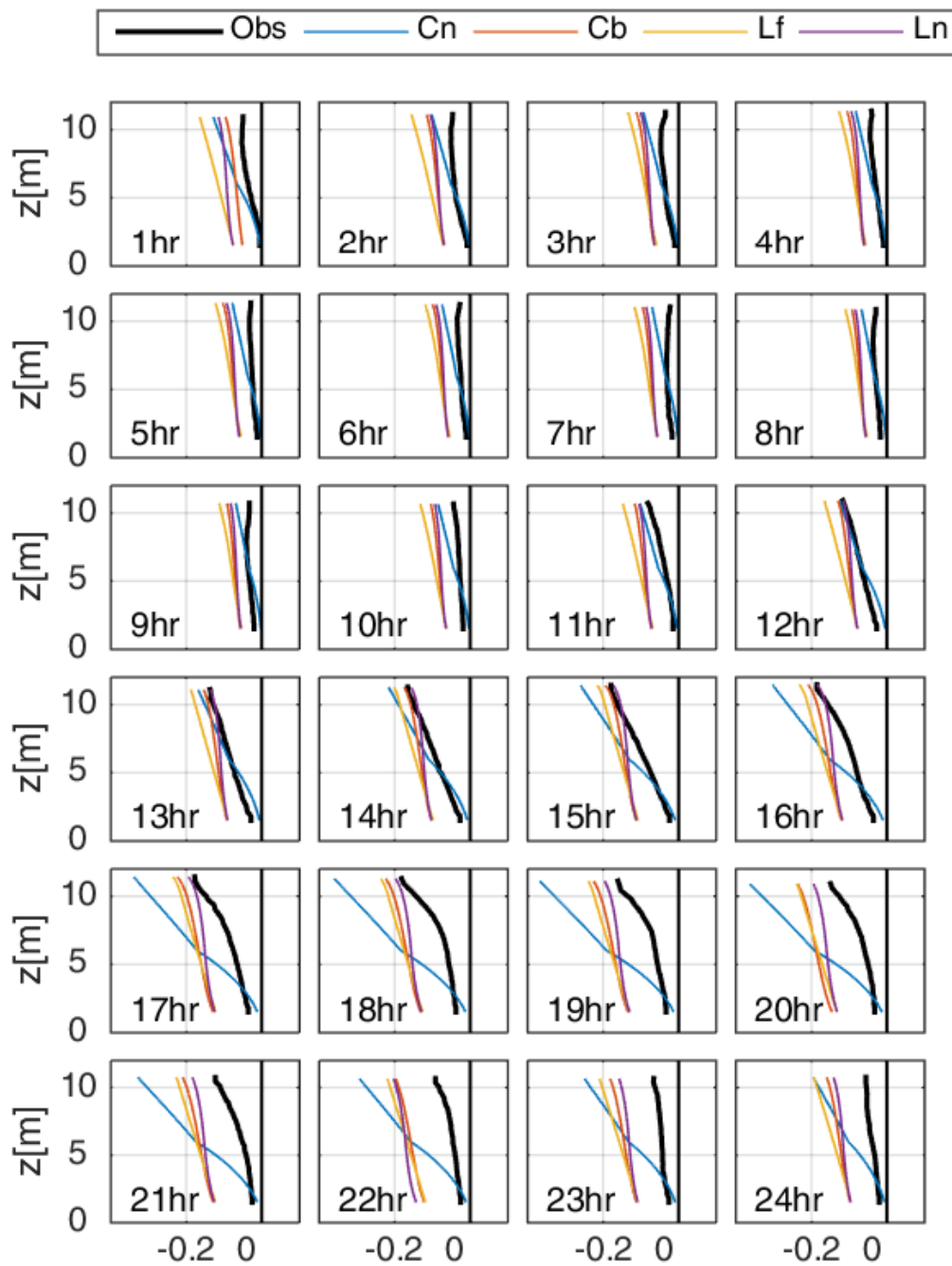
FIGURE 2.2: Observed Clock-hour average day of the along-shelf circulation (Obs); and modeled clock-hour average day of the along-shelf circulation obtained with different EVP: Constant (Cn); Cubic (Cb); Linear Cutoff (Lf); and Linear (Ln). Units are m.s^{-1}.

waves (Figure 2.3d), the model reproduced cross-shelf velocity profiles that are offshore (negative) throughout the water column except for a small layer at the surface, consistent with a wave-driven undertow profile described in Lentz et al. (2008). Since significant wave height was smaller around mid-day, the offshore velocity was also weakest at this time, and increased in the afternoon, concurrent with maximum H_{sig} values (Figure 2.1c). None of these simulations reproduced similar results to the observations, with the exception of the **W_y** experiment, which reproduced part of the observed cross-shelf circulation in the afternoon.

Forcing the model with both wind and waves (Figure 2.4), also resulted in a cross-shelf circulation dissimilar to the observations. The wind-driven model results, forced with both cross- and along-shelf winds (Figure 2.4b), did not differ much from the **W_y** experiment results, with only a slight oscillation of the interface between surface and bottom layers, that was not simulated by the **W_y** experiment. This indicates that, in these wind conditions, the along-shelf wind stress was dominant, and the cross-shelf wind stress was not strong enough to modify the circulation. When wave forcing was added to the **W_y** experiment (Figure 2.4c) the offshore flow at the surface layer was intensified and the layer thickened when compared with the **W_y** experiment, occupying the entire water column in the morning. The results from the model forced with a combination of cross-shelf winds and waves (Figure 2.4d), showed intensified onshore flow in a thin superficial layer and stronger offshore flow at the bottom, which was the expected outcome, since the wave-driven undertow (offshore flow throughout the water column) was added to the cross-shelf wind-driven circulation (onshore flow at the surface and offshore flow at the bottom). When the model was forced with wind and waves (Figure 2.4e), the circulation was offshore throughout the water column, for most part of the day. Except for the afternoon period simulated with **W_x**+**W_y**, the modelling experiments did not reproduce the observed cross-shelf circulation.

Nonetheless, the along-shelf circulation obtained by the model (Figures 2.3 and 2.4), showed great similarities with the observations, except when the along-shelf wind forcing is removed. The modelled circulation, always considering **W_y** experiment separately or combined with **W_x** and **WAVE**, was always offshore, with an increase of magnitude in the afternoon. This increase occurred later in the day, lasted longer and extended deeper for the model results when compared with the

observations. When the model was not forced with along-shelf winds, the along-shelf profiles were weaker and the increase of magnitude in the afternoon was hardly perceptible.
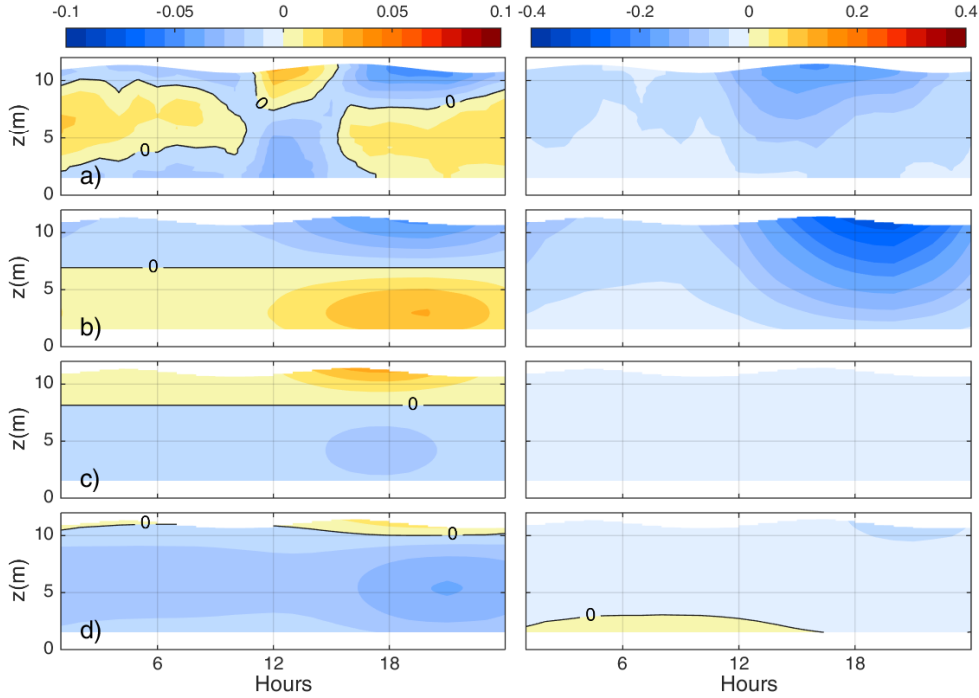
FIGURE 2.3: Clock-hour average day of the cross-shelf (left column) and along-shelf (right column) circulation obtained from in-situ data (a); and from the different modelling experiments: b) **W_y**; c) **W_x**; and d) **WAVE**. Units are in m.s^{-1}.

2.4.2 Inverse Model

Since the model forced with a combination of different parameters, did not reproduce the observed circulation, the next experiment consisted of using the model in an inverse way, fixing some of the known variables and varying a missing forcing term (hereinafter: *F*). For each hour of the clock-hour average-day, *F* was made to vary within a range of values (closer in magnitude based on the dominant terms in the momentum balances, described in Chapter 1) so that the resulting $u(z)$ would best-fit the hourly cross-shelf profiles of the observed clock-hour average day. The best-fit was done using the least squares method.
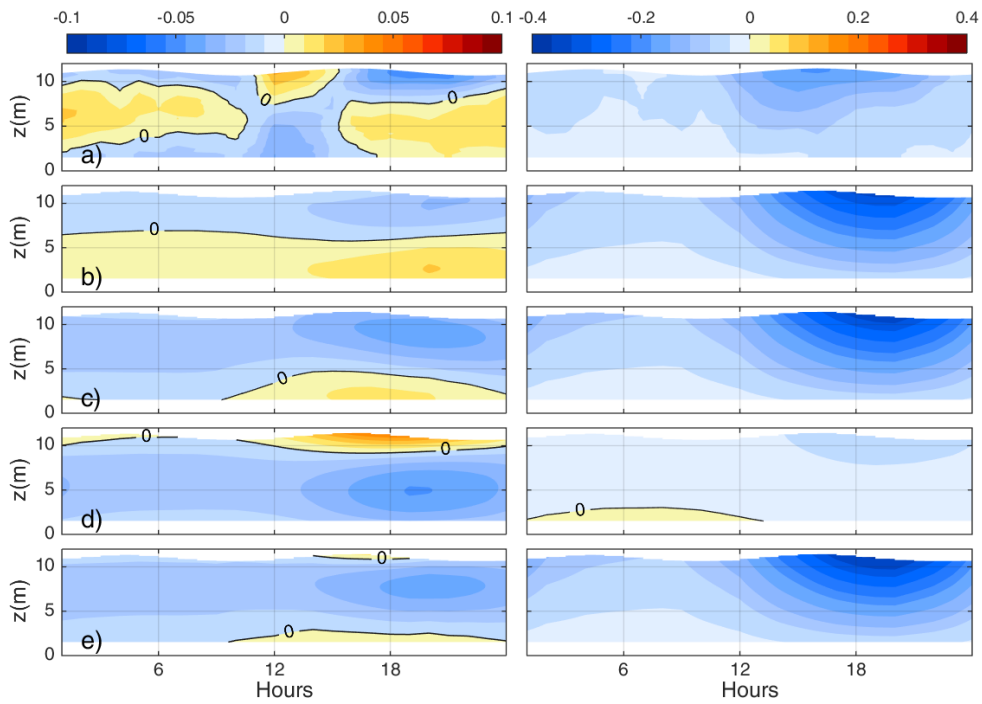
FIGURE 2.4: Clock-hour average day of the cross-shelf (left column) and along-shelf (right column) circulation obtained from in-situ data (a); and from the different modelling experiments: b) **W_y+W_x** c) **W_y+WAVE**; d) **W_x+WAVE**; e) **W_y+W_x+WAVE**. Units are m.s^{-1}.

Figure 2.5 shows the results obtained when the model was forced with the same hourly mean values of wind stress, wave parameters and the estimated *F* values (from the best-fit method described previously). In Figure 2.5a), the lines represent the diurnal variability of *F* for each experiment. The *F* obtained is very similar for all the different experiments. The variability and magnitude of *F* is similar for all the different experiments and compares reasonably well with the local acceleration term computed from in-situ data (Figure 1.12). By adding *F*, the modelled cross-shelf profiles started to become more similar to the observations, in several aspects (Figure 2.5). For all experiments with *F*, the surface flow inversion at mid-day was successfully simulated, indicating that the forcing term *F* was responsible for that inversion. The model also reproduced fairly well the observed circulation in the afternoon, but in the morning the circulation differed considerably from the observed cross-shelf profiles, which implies that adding *F* to the forcing was not enough to simulate the 3-layer vertical structure observed in the morning.

2.4.3   Mean Circulation

As mentioned in the previous section, the model computes the steady vertical profile of the cross-shelf velocity as a response to wave and wind forcing. However, the momentum balance analysis of in-situ data hinted to the fact that stationarity does not apply, during part of the day. In fact, at mid-day, the local acceleration term is dominant and seems to be balanced by the sum of the missing terms that make the residual R_y.

To reduce the effects of the local acceleration terms, focus is now given to the subtidal circulation (>33 h). Figure 2.6 shows the along-shelf momentum balance terms, computed from in-situ data, after a low-pass filter of 33h. The relative importance of the local acceleration term was significantly reduced, for each of the three summers. By reducing the local acceleration importance, it is possible to assess if the model inability to reproduce the observed circulation is due to the assumed stationarity of the model or if other processes are also contributing to the dynamics. As seen before, in this particular case, the waves do not add significant contribution to the modelled results and thus the next simulations were only forced by winds (Figure 2.7).
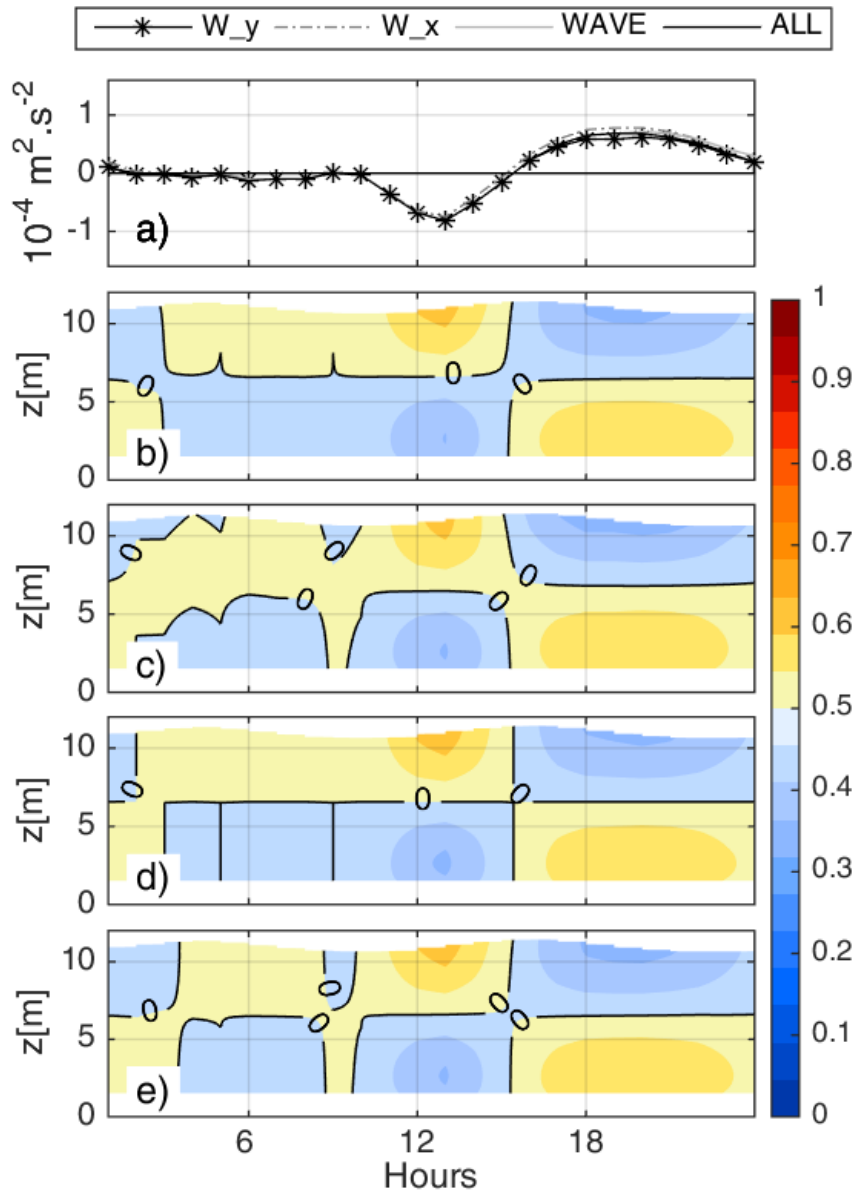
FIGURE 2.5: a) Hourly values of **F** obtained from **W_y**, **W_x**, **WAVE** and **W_y + W_x+ WAVE** experiments. Clock-hour average day of the cross-shelf circulation reproduced by the model for the experiments: b) **W_y + F**; c) **W_x + F**; d) **WAVE + F**; and e) **W_y + W_x + WAVE + F**.
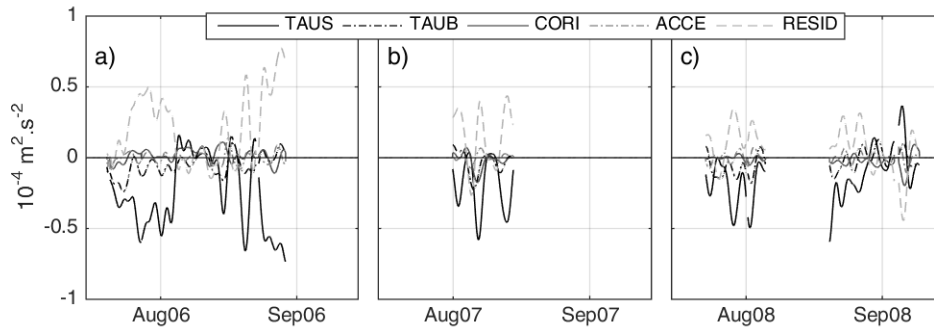
FIGURE 2.6: Subtidal (>33h) depth-integrated along-shelf momentum balance terms from in-situ data for: a) 2006; b) 2007; c) 2008. Units are in $m^2.s^{-2}$.
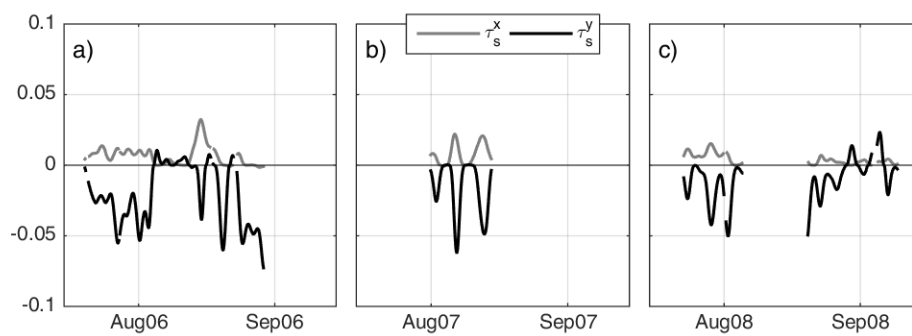
FIGURE 2.7: Subtidal (>33 h) wind stress for: a) 2006; b) 2007; c) 2008. Units are in Pa.

Throughout the three summers analysed, the subtidal cross-shelf circulation obtained from the model is considerably different from the observations (Figure 2.8). The modeled cross-shelf circulation is generally offshore throughout the water column with episodic onshore velocities at the surface, concurrent with episodes of stronger onshore winds. The observed cross-shelf circulation is quite different, with a mid-depth onshore flow that is rarely interrupted during the three summers and episodes of stronger offshore flows at the surface.

For the along-shelf circulation, the model represents fairly well the observations, although the negative values (southward currents) tend to be stronger and the positive values (northwards) weaker in the model results. Overall both positive and negative along-shelf velocities are surface intensified. The inversions of the along-shelf currents are present and concurrent in both model and observations, and are consistently connected with the inversions of the along-shelf winds. Applying the model in an inverse way, as described before, for the subtidal circulation, did not reproduce any improved results for and therefore it will not be discussed here.

2.5 Summary and Discussion

The along-shelf circulation was satisfactorily simulated using the model developed by Lentz et al. (2008) forced exclusively with winds, which implies that the dynamics for this component are mainly two-dimensional, with no strong dependence on other processes such as waves, tides, stratification effects and/or non-linear dynamics. The cross-shelf circulation, however, was not well represented by this model, not only for diurnal variability but also for subtidal timescales. For the diurnal circulation, the model failed to reproduce the 3-layer structure in the morning period, and the mid-day flow inversion was only present when a term comparable with the acceleration was added to the forcing. When the role of the local acceleration was reduced by analysing the circulation at longer timescales, the mid-day inversion was filtered out, but the modelled cross-shelf circulation was still not similar to the observations, since it did not reproduce the onshore flow at mid-depth, which is consistent throughout the observed period.
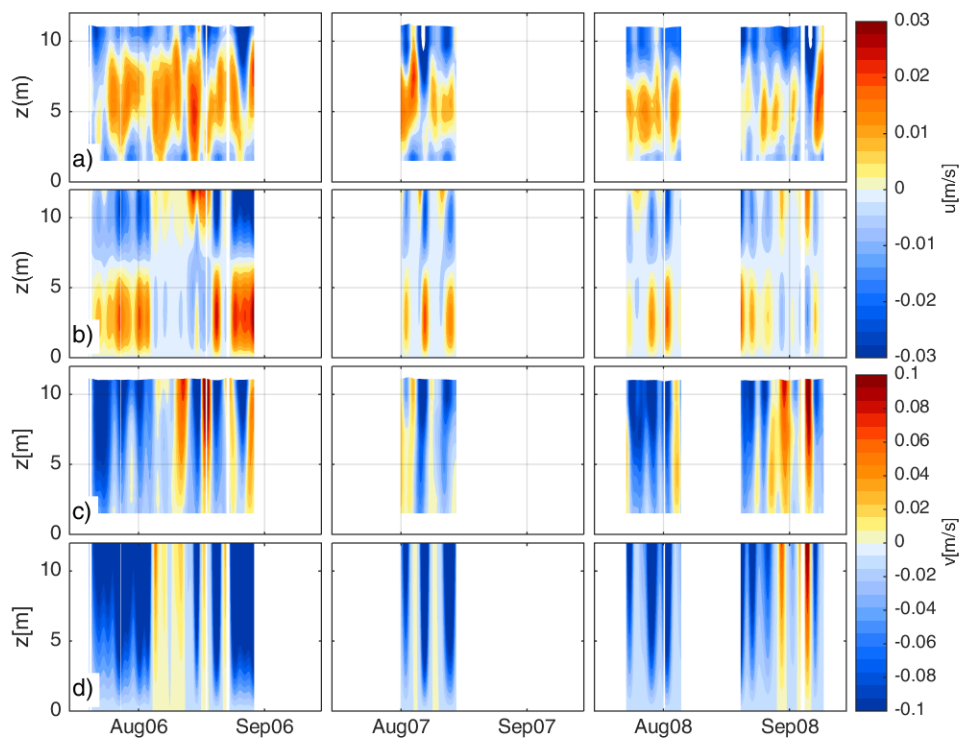
FIGURE 2.8: Subtidal (>33 h) results for 2006 (first column); 2007 (middle column) and 2008 (last column) for: a) In-situ cross-shelf profiles; b) Modeled cross-shelf profiles; c) In-situ along-shelf profiles; and d) Modeled along-shelf circulation. Units are in m.s^{-1}.

As described in Chapter 1, the water column at this site is continuously stratified, which may explain some divergences between the model results and the observations. Stratification affects the cross-shelf circulation since it influences the thickness of the boundary layers and inhibits vertical mixing, which therefore allows the wind-driven cross-shelf circulation to extend into shallower waters relative to an unstratified shelf. Lentz (2001) observed that the presence and absence of stratification influences the magnitude and vertical structure of the wind-driven cross-shelf velocity. Kirincich et al. (2005) observed that reduced cross-shelf transport occurred at times of decreased stratification (such as the shut-down of inner-shelf circulation process described by Lentz (2001) and modeled by Austin and Lentz (2002)).

Although this 2D model did not reproduce the observed cross-shelf circulation it was particularly helpful to understand that the acceleration has an important contribution in the establishment of the mid-day flow inversion of the cross-shelf circulation. It is clear that there are several other processes dynamically important, such as localized pressure gradients (Lentz, 2008; Gan et al., 2009; Fewings et al., 2015), nonlinear effects due to topographic variations (Sanay et al., 2008; Ganju et al., 2011), that contribute significantly to the vertical structure of the cross-shelf flow which are not accounted for in this model. The modelling study analysed in this Chapter showed that more realistic models are necessary to further investigate the dynamics of the observed circulation.

Chapter 3

A Modelling Study of the Wind-driven Circulation in the Vicinity of Cape Sines

A part of this chapter was included in an article published in *Continental Shelf Research*. The complete article was attached as Appendix A.

3.1   Introduction

As seen in the previous chapters, the inner-shelf circulation in the presence of a cape, specifically Cape Sines, on the southwestern coast of Portugal, can be particularly complex. The in-situ data collected and simplified 2D models were not enough to explain the diurnal flow inversion and onshore flow at mid-depth, present in both diurnal and subtidal timescales. Momentum balance analysis and the modelling study in Chapter 2 showed that the local acceleration term was an important factor in establishing the flow reversal seen at mid-day. Studies over different inner-shelves (Lentz et al., 1999; Liu and Weisberg, 2005; Fewings and Lentz, 2010) seem to agree that the along-shelf momentum balance is mainly between along-shelf pressure gradient (generated by local wind forcing) and wind stress, though other terms can also be important depending on water depth and wave regime, that can increase the relative influence of the bottom stress in the balance. A modelling study by Gan and Allen (2002) showed that strong along-shelf pressure gradients can form in the presence of a cape, when the upwelling

wind regime relaxes, with negative pressure gradient forming south of the cape and positive pressure gradient in the north. These pressure gradients are accompanied by the establishment of geostrophically balanced cross-shelf flows over the shelf, with the upwelling circulation being increased in the lee of the cape. A work by Sanay et al. (2008) over the inner-shelf showed that there is a 3-D circulation response to wind-driven circulation in the presence of a cape. Ganju et al. (2011) pointed out the importance of topographic features in the circulation over the inner-shelf by showing that the mean along-shelf momentum balance was dominated by the pressure gradient and horizontal advection terms, which vary with subtle bathymetric changes. Also important is the fact that the ADCP data was collected in the leeside of a cape, which can be located on the upwelling-shadow region (Roughan et al., 2005a; Woodson et al., 2007) and thus processes other than along-shelf winds, which are traditionally dominant (Lentz et al., 1999; Liu and Weisberg, 2005; Fewings and Lentz, 2010), may be relevant for the dynamics. Finally, several studies found that non-linear advection is particularly important in the vicinity of topographic features (Li and Weisberg, 1999b; Doglioli et al., 2004; Meunier et al., 2010; Liu and Gan, 2014). It is expected that Cape Sines will have a similar effect on the circulation, especially in the leeside, which will promote the generation of localized wind-forced pressure gradients and enhance the importance of non-linear advection terms. The use of a 3D realistic model seems to be required to further analyse the circulation at the observations site.

The objective of this chapter is to study the underlying dynamics of the shelf circulation induced by a daily variable upwelling-favourable wind condition in the presence of a cape. Focus was given to the circulation in the leeside of the cape at diurnal timescales. As seen in Trindade et al. (2016), different tidal conditions did not change significantly the circulation during the observed period and therefore were excluded from this modelling study.

3.2   Model Setup

The numerical simulation was conducted using the Regional Ocean Modeling System (ROMS) (Shchepetkin and McWilliams, 2005; Haidvogel et al., 2008), largely used for coastal applications (Marchesiello et al., 2003; Xu et al., 2013).

ROMS kernel is a split-explicit, free-surface and terrain-following vertical coordinate oceanic model. It employs a two-way time-averaging procedure for the fast mode, which satisfies the 3D continuity equation. A third-order, upstream-biased, dissipative advection scheme for momentum, implemented with a specially designed predictor-corrector time-step algorithm (Leapfrog-Adams-Moulton III), allows the generation of steep gradients, enhancing the effective resolution of the solution for a given grid size. A third-order, upstream advection scheme is also used for tracers with a correction to avoid spurious diapycnal mixing (Marchesiello et al., 2009). Robust open boundary conditions are also implemented (Marchesiello et al., 2001). A K-profile parametrization (KPP) boundary layer scheme (Large et al., 1994) for surface and bottom layers parametrizes the subgrid-scale vertical mixing processes.

The model configuration was developed to simulate the period between 20 July and 04 August 2006 in the region around Cape Sines, in the Southwestern coast of Portugal (following Trindade et al. (2016)).

The configuration consisted of a high resolution (220 m) grid in a 50×80 km domain around Cape Sines (blue square in Figure 1.1). 32-σ levels were used with enhanced vertical resolution at the surface. Topography data compiled in Peliz et al. (2013) was used with a minimum depth of 5 m. To avoid large differences of topography around the domain (in particular the canyons in the north), a low-level smoothing and a cut-off depth of 800m was imposed. Bottom drag parametrization was used with a variable coefficient $C_d = k/log(z_b/z_0)^2$ with $z_0 = 0.005$, where k is the von Kármán's constant and z_b is the height of the deepest level (Marta-Almeida and Dubert, 2006). The variable coefficient was empirically chosen, although tests with constant coefficients showed the model was not particularly sensitive to the bottom drag. Vertical mixing and diffusion is performed with the Large et al. (1994) KPP scheme. Radiation conditions were used along the open boundaries for momentum and tracers, together with a passive-active nudging open boundary forcing (Marchesiello et al., 2001). A sponge layer of 15 km and maximum horizontal viscosity of $A_h = 200$ m^2.s was placed near the open boundaries to reduce reflections that may be enhanced in a small size domain.

The model initially assumes a flat ocean with a vertical density distribution typical of summer time (a sharp thermocline and a linearly decaying salinity profile). The same salinity and temperature conditions are preserved near the open boundaries

using a relaxation time scale (Marchesiello et al., 2001). The model was forced with 15 days of winds downscaled from Era-Interim data using the Weather Research and Forecast (WRF) Model (Figure 3.1), with 9 km resolution, to allow for spatial inhomogeneity (Soares et al., 2012; Peliz et al., 2013). Since the WRF model seems to systematically overestimate the winds when compared with the observed time series, the WRF wind magnitude was reduced by the time-mean wind magnitude difference between data and model at the location of the meteorological station. The atmospheric forcing heat fluxes include shortwave radiation (a diurnal cycle peaking at 1100 W.m^{-2}), latent and sensible fluxes (using averaged data from the meteorological station, and the outgoing long-wave heat flux calculated based on the model SST). The surface heat fluxes are spatially homogeneous with a fixed daily variability during the 2-week experiment, only the long wave emission varies because of the internal SST dependence.

The focus of this study is to analyse the wind-driven circulation, and therefore tides were not included in the model forcing. A spin-up of 3 days was considered for the model to stabilize and the results from that period were disregarded. To avoid misinterpretations, the model description and analysis is based on the zonal (x) and meridional (y) oriented axes, bearing in mind that away from the cape (including the ADCP site) they are coincident with the along- and cross-shelf coordinate axes.

3.3 Results

3.3.1 Model-Data Comparison

Model results at the grid point consistent with the observations site are used for comparisons with in-situ data. Overall, the model simulated successfully most features of the circulation and temperature variability at the ADCP site (Figure 3.2). The wind underwent a diurnal cycle of both magnitude and direction, rotating onshore with increasing magnitude at the end of each day (Figure 3.2a). In the cross-shelf direction (Figure 3.2b), the circulation showed a permanent two-layer structure, with a repetitive daily cycle of flow reversal of the entire water column at mid-day. The along-shelf velocity (Figure 3.2c) was always southwards,
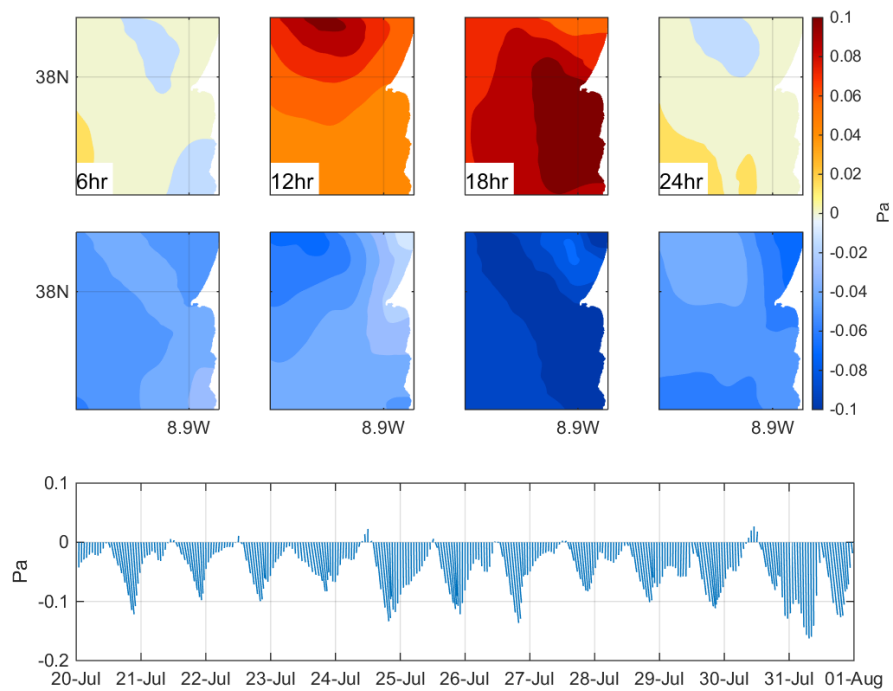
FIGURE 3.1: Wind field from the WRF model for the period between 20 July of 2006 and 04 August of 2006. First row: u-component of the wind stress [units: Pa] for different hours of the clock-hour average day; Second Row: v-component of the wind stress [units: Pa] for different hours of the clock-hour average day; Bottom Row: Wind vectors for the 15-day run at a grid point consistent with the ADCP site.

intensified at the surface, and with a daily increase of magnitude later in the day (concurrent with the daily maximum of wind magnitude). The water column was stratified at all times (Figure 3.2d), with stronger stratification in the first 5 days, and again in August 02. The 12-day average difference between surface and bottom temperature was 2.2 °C, which is consistent with the observations.
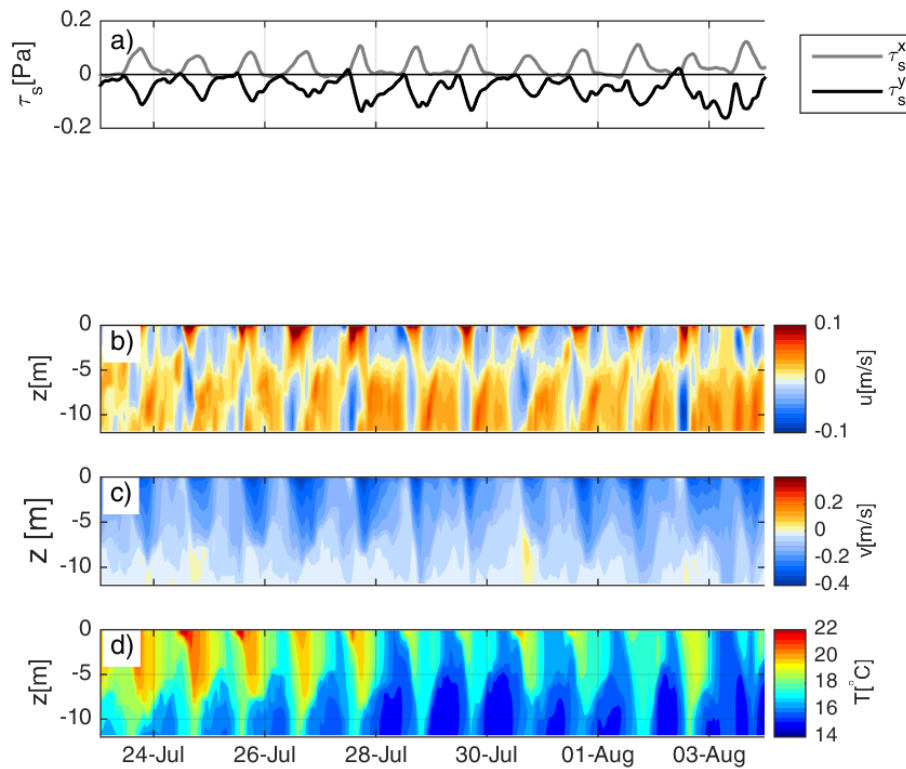
FIGURE 3.2: Modelled time series of a) Wind stress [Pa]; b) Cross-shelf velocity [m.s^{-1}]; c) Along-shelf velocity [m.s^{-1}]; d) Temperature [°C], at a grid point consistent with the ADCP site.

The results for the clock-hour average day of wind, cross- and along-shelf circulation and ΔT are shown in Figure 3.3. The model represents well the observed diurnal cycle of wind and stratification (Figure 3.3a and b, respectively) showing the wind variability and the temperature mean difference of around 2 °C between the surface and bottom layer. For the cross-shelf circulation (Figure 3.3c) the reversal at mid-day is present, with longer duration than in the observations, and the upwelling-type exchange in the evening was also reproduced. However, the

3-layer pattern with onshore flow at mid-depth that was observed in the morning period was not successfully simulated by the model. The modelled along-shelf velocity (Figure 3.3d) had the same structure and variability as the observations, with surface intensified southward velocities and an increase in magnitude in the afternoon. The model results are about 20 to 30% stronger than the observations for both velocity components, except for the offshore (cross-shelf negative) values which are about 10% weaker in the model results.

The depth-integrated along- and cross-shelf momentum balances were also computed, with an analogous method to what was described in Chapter 1. With the model results, pressure gradient and advection terms can be estimated; this was not possible using the data from the observations. There are straightforward differences between the momentum balance terms estimated with in-situ data and with the modelling results (Figures 1.12 and 3.4, respectively). As expected for both components, the wind stress term is more intense in the model results, and reaches its maximum earlier in the day, connected with the wind retrieved from the WRF model being slightly stronger than the wind measured at the meteorological station. The wind stress term in the along-shelf balance reaches near-zero values around 11 h, which is not the case in the observed wind. The modelled Coriolis term is also, on average, stronger than the term estimated from the observations. For example, considering the along-shelf balance, $f\mathbf{u}$ is nearly zero in the observations but not in the model results. This may be due to the missing ADCP data and the assumption of a linearly decaying velocity from the lowest ADCP bin towards the bottom. This is also an explanation for the stronger bottom stress term obtained from the observations. In the along-shelf component, the local acceleration term in the model does not show a variability as sharp as in the observations, but the variability throughout the day is similar, with a signal reversal at mid-day and an increase in magnitude in the afternoon.

The cumulative relative percentage of each momentum balance term was computed with the purpose of identifying the relative weight of each term throughout the day (Figure 3.5). In the morning period and late evening, the cross-shelf momentum balance is mostly geostrophic with a small contribution of the advection term. At mid-day, however, the Coriolis term is greatly balanced by the wind stress term in an Ekman-type balance, but the contribution of the advection term cannot be neglected. The balance in the along-shelf direction is slightly different.
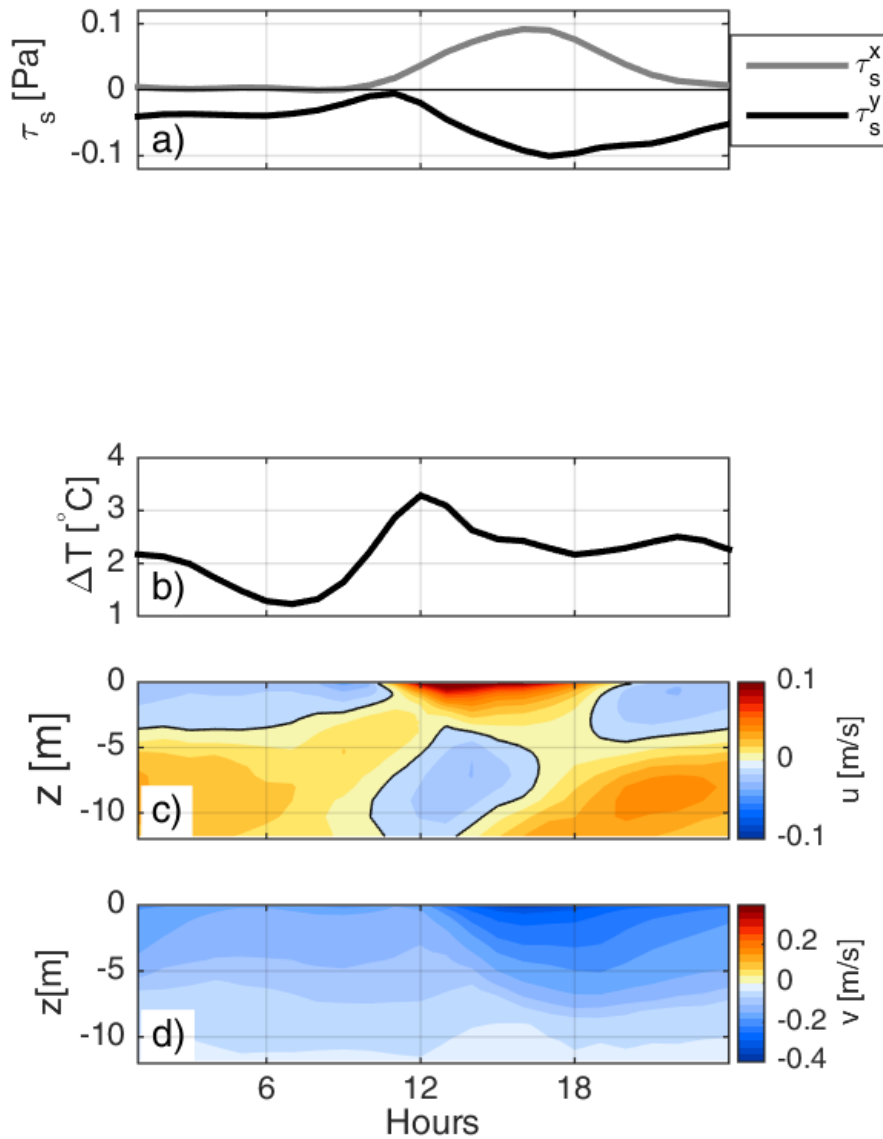
FIGURE 3.3: Modelled clock-hour average day of a) Wind stress [Pa]; b) Temperature difference between surface and bottom [°C]; c) Cross-shelf velocity [m.s^{-1}]; d) Along-shelf velocity [m.s^{-1}], at the ADCP site. Thick black line marks zero and the contour interval is 0.01 m/s.
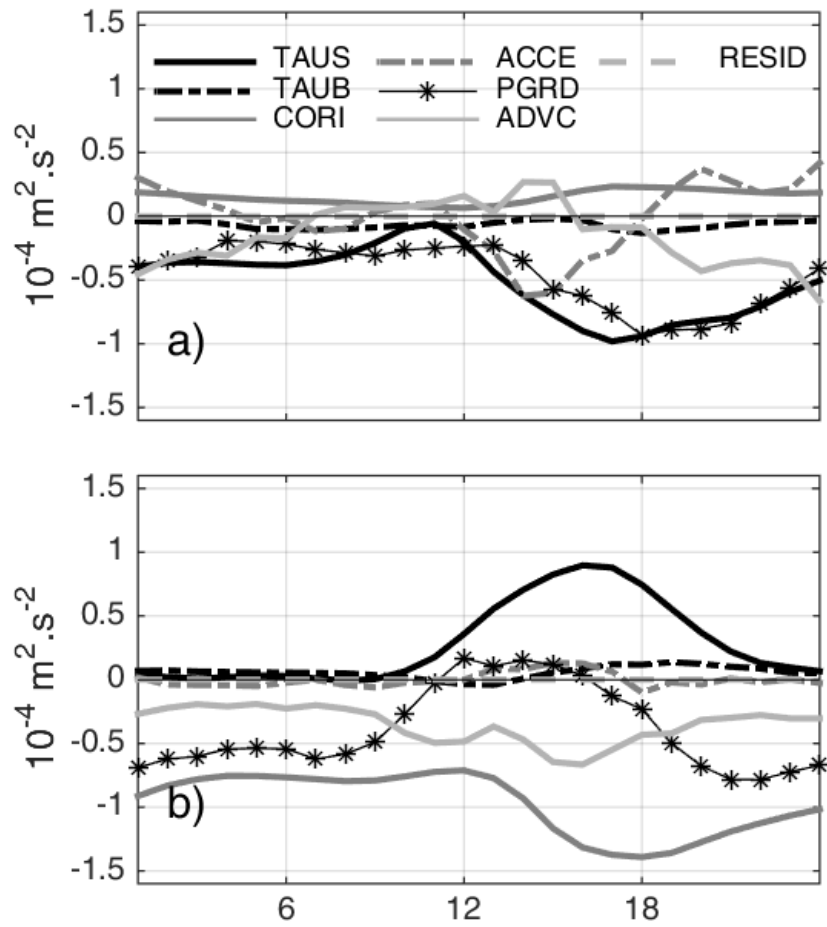
FIGURE 3.4: Depth-integrated along-shelf (a) and cross-shelf (b) momentum balance terms for the modelled clock-hour average day at the ADCP site. TAUS: wind stress; TAUB: bottom stress; ACCE: acceleration; CORI: Coriolis; PGRD: Pressure gradient; ADVC: Advection; RESID: Residual terms. Units are $m^2.s^{-2}$.

Throughout the day, wind stress and pressure gradient terms are the dominant contributors, and are mostly balanced by the advection term and by the acceleration at mid-day. The local acceleration relative percentage is higher in the mid-day period, consistent with the conclusion taken from Chapter 2, that the mid-day cross-shelf flow reversal was due to the local acceleration term.
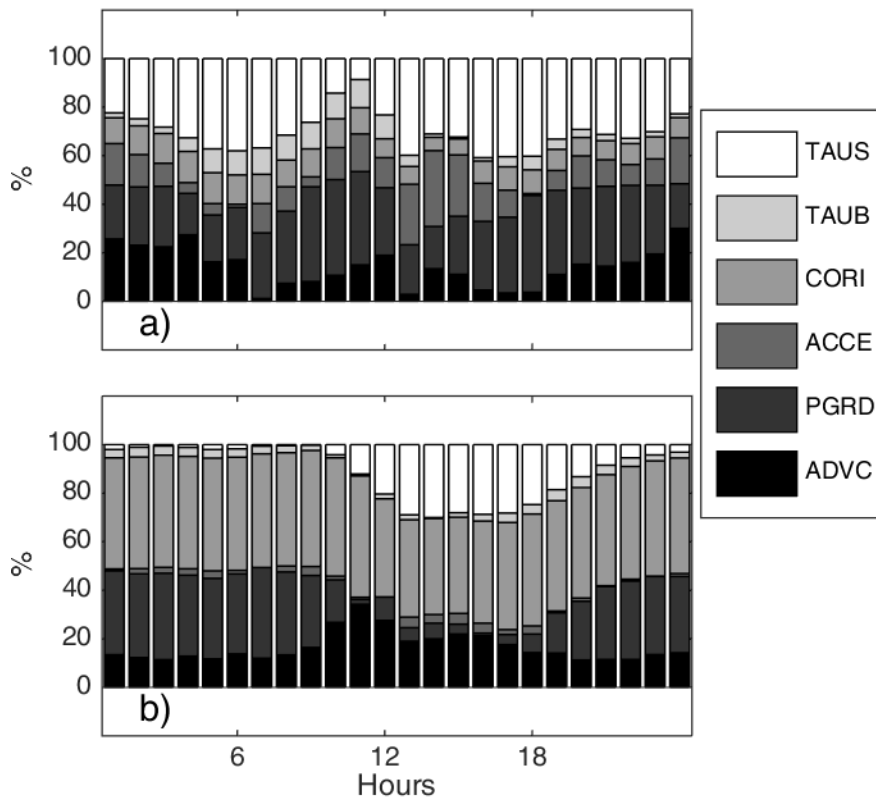
FIGURE 3.5: Cumulative percentage of the along-shelf (a) and cross-shelf (b) depth-integrated momentum balance terms for the modelled clock-hour average day at the ADCP site.

3.3.2 Regions with Similar Diurnal Variability

The distinct element identified in this study is the cross-shelf current reversal at mid-day. The question arises if this circulation pattern is particular to a specific location (e.g. the leeside of the cape) or is it a consistent feature in the study domain.

The multi-layer analysis of the model results was simplified by producing binary maps where the grid points with specific circulation characteristics were marked as one, and elsewhere was set to zero. These maps were based on the direction of the zonal flow (u) at the surface (top 5 m) and bottom (bottom 5 m) layers, and were constructed according to the following rules: i) For each grid point, the signal of u in both layers is compared; ii) The grid points of the binary map were set to one if, in the morning and evening, the surface velocity was negative (offshore at the ADCP site), and the bottom velocity was positive (onshore), and for the mid-day period the opposite, onshore flow in the upper layer and offshore flow in the bottom layer. iii) For any other situation the grid point value of the map is set to zero. Note that the 3-layer structure observed in the morning period was not reproduced by the model, and therefore, in the morning period, the circulation pattern considered was the same as the model simulated at the ADCP site (2-layer flow).

The binary maps for the set of hours: 8 h (morning), 12 h (mid-day) and 24 h (evening), for regions with depths less than 50 m, are shown in Figure 3.6, where gray represents 1 and white is 0. The binary maps representing the surface layer (top row), the bottom layer (middle row) and the interception of both (bottom row), are shown separately to facilitate the analysis. The top row of Figure 3.6 shows the regions where the surface zonal velocity is negative at 8 h (a), positive at 12 h (b) and again negative at 24 h (c). The middle row is analogous for the bottom layer but with opposite signal: positive u at 8 h, negative at 12 h and positive at 24 h. The right column in Figure 3.6 (d) shows the product of the previous three (a, b and c), showing in gray the grid points with the same circulation variability for each layer. The bottom row is the interception between the surface and bottom layer, representing in gray the regions where u in both layers has a similar vertical structure and variability as the model at the ADCP site.

In the surface layer, at 8 h (Figure 3.6a; top row), only a small region south of Cape Sines has negative velocities at the surface. This zone is limited to a small along-shelf band near the coast where the coast becomes meridionally aligned. On the other hand, at 12 h (Figure 3.6b, top row) a great part of the domain is marked in gray, showing that most of the domain (considering depths below 50 m) has positive zonal velocities. Lastly, at 24 h (Figure 3.6c, top row), most of the shallow

part of the domain has negative velocities at the surface, with the exception of a small region south of Cape Sines. It is clear that, at the surface, eastwards flow at mid-day and westwards flow in the evening are common in a large portion of the domain but only a small region has negative velocities in the morning period. It is visible in Figure 3.6 that the marked regions in the morning (a) and mid-day (b) hours on the bottom layer (middle row) are sparse and connected with small-scale topographic variations. However, at 24 h (c) most part of the domain show positive velocities. Combining the binary maps of both surface and bottom layers (bottom row of Figure 3.6) results in few regions with a behaviour synchronous with the observations, mainly due to the small scale variations in the bottom layer. The analysis of the last map indicates that only a few zones fit our criteria and, by definition, the ADCP site is included (marked as a star in Figure 3.6). The resulting map shows that these zones are mainly located in the shallow region south of Cape Sines, when the coast becomes meridionally aligned.

3.3.3   Circulation in the vicinity of the Cape

Figure 3.7 shows the horizontal fields of surface temperature (top row) and surface elevation (bottom row) with current velocity vectors superimposed (surface temperature and velocity correspond to the average of the first 5 m) for six different hours of the clock-hour average day: 4 h, 8 h, 12 h, 16 h, 20 h and 24 h. The blue vectors represent the wind at the ADCP site for the corresponding hour. Figure 3.7 clearly illustrates the influence of the cape on the temperature and surface elevation fields. The permanence of northerly wind maintains a background upwelling circulation throughout the domain. In the northside of the cape, the largest southward currents, associated with the upwelling-jet, are concentrated from the coast to the 50-m isobath. The presence of the cape causes the deflection of this jet to the west. The upwelling jet is then displaced offshore and follows the 100-m isobath after the cape. As the upwelling-jet is deflected by the cape, it rotates cyclonically. The deviation of the upwelling jet by the cape leads to lowering the sea surface elevation south of the cape. Similar to the surface elevation, lowest temperatures are seen south of the cape. In a region just below Cape Sines, the circulation is weaker and the cross-shelf component is slightly dominant.
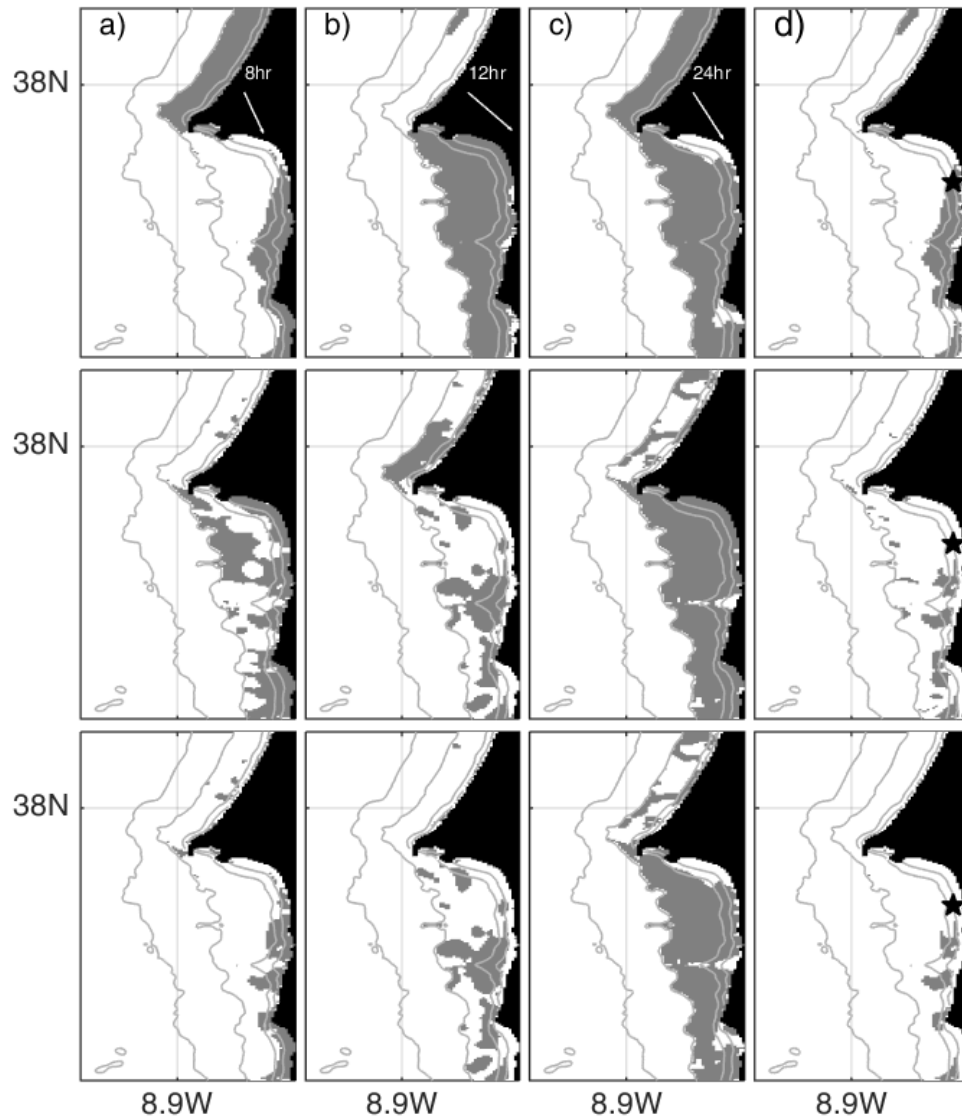
FIGURE 3.6: Binary maps representing the grid points where the modelled cross-shelf velocity had the same structure and evolution as in the ADCP site. Gray is 1, white is 0. Top row) Binary map for the surface layer; Middle row) Binary map for the bottom layer; Bottom row) Binary map combining both surface and bottom layers. a) 8 h; b) 12 h; and c) 24 h. d) The regions in gray represent the interception between a, b and c. The star represents the ADCP location.

Superimposed to the permanent upwelling-favourable wind regime there is also a daily oscillation of the wind magnitude and direction, which will have different impact on the circulation depending on the region of the domain. Overall, the circulation is dominantly to the south, with a weaker zonal component that rotates from west to east and again to west throughout the day. In the northside of the cape, the upwelling-jet is constrained by the presence of the coast. While most of the flow rotates to the east, the circulation aligns with the bathymetry near the coast, causing a circulation convergence (downwelling), which results in a region of warmer waters near the coast in the afternoon. In the leeside of the cape the flow becomes meridionally aligned, forming a secondary upwelling-jet within 5 km of the coast. This secondary upwelling flow is dominantly southwards but has a weak zonal component that alternates from westwards in the morning period, to eastwards at mid-day and finally to westwards later in the day. This is consistent with the surface flow reversal observed at the ADCP location (the red dot showing the ADCP location can be seen in Figure 3.7 over this secondary upwelling flow). The two upwelling jets are also responsible for the southwards advection of the colder, newly upwelled waters, from the south part of the cape (Figure 3.7 top).
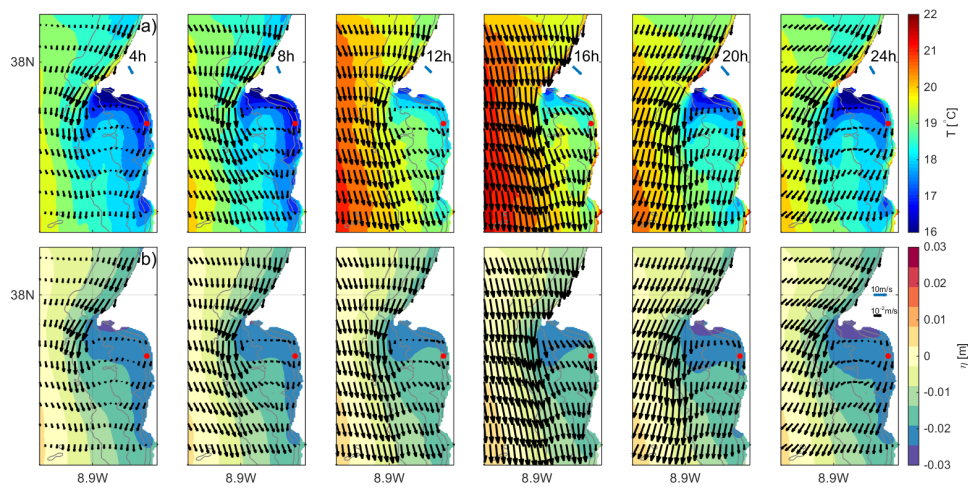
FIGURE 3.7: a) Sea surface temperature [°C] and b) Sea surface height [m], for different hours of the clock-hour average day (each column): 4 h, 8 h, 12 h, 16 h, 20 h and 24 h, with surface current velocity vectors superimposed. The blue arrow represents the wind vector at the ADCP site, for the respective hour. The red dot marks the ADCP location. Scale vectors are represented in the last subfigure.

3.3.4 Momentum Balances

To describe the dynamics behind the diurnal variability of the circulation, depth-integrated terms of the meridional momentum balance are analysed. The daily evolution of the dominant terms of the balance are displayed in Figure 3.8. Since the Coriolis (Figure 3.8c) and pressure gradient (Figure 3.8d) terms are considerably higher than the acceleration (Figure 3.8a) and advection (Figure 3.8b) terms in the deeper part of the domain, some saturation was introduced on the colour-scale in order to enable the analysis near the coast, where the magnitude of these terms is comparable. Although wind stress is dominant in magnitude, it has no spatial variability, and therefore, for simplicity, is not shown in Figure 3.8. Depth-integrated bottom stress term is weak throughout the domain, only showing a slight increase in magnitude around topographic features, showing small negative values on the north part of the perturbations. There is a dominance of Coriolis and pressure gradient terms for most part of the domain, but there are some regions where the local acceleration and advection play an important role. The spatial distribution of these terms remain fairly constant throughout the day, which indicates that although the pressure gradient is wind-driven, the daily oscillation of the wind stress is not enough to modify the pressure gradient, once it is set up. There are, however, small-scale pressure gradient variabilities in nearshore regions that are balanced by nonlinear advection. These regions are connected with small-scale along-shelf topographic perturbations. The local acceleration illustrates the deceleration of the deflected upwelling-jet in the morning and its acceleration after 16 h, concurrent with the increasing of the wind magnitude. This daily evolution is also visible for the secondary upwelling jet, where the ADCP site is located. Contrary to this diurnal variability, there is an overall background positive acceleration towards 16 h and deceleration afterwards. Strong positive nonlinear advection, located at the tip of Cape Sines and between isobaths 50-m and 100-m south of the cape, is associated with the deflection of the upwelling-jet.

To analyse in detail the along-shelf momentum balance terms in particular regions, the terms were spatially averaged across four areas around the Cape (Figure 3.9), where the most important circulation patterns are located: (**1**) the tip of the cape; (**2**) the region where the flow rotates cyclonically; (**3**) the shadow region just below the cape; and (**4**) the region over the secondary upwelling jet. The size of each area were chosen to be small enough to avoid averaging over different features of
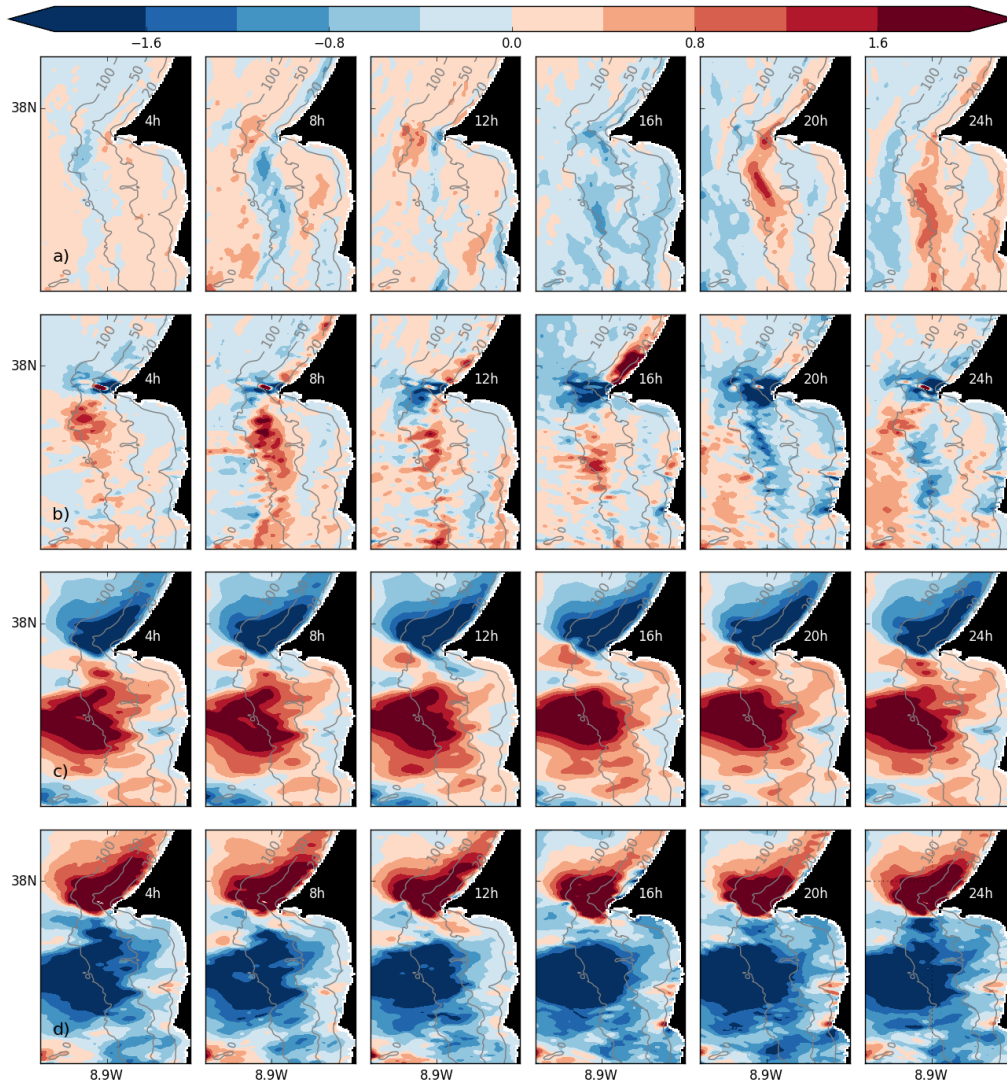
FIGURE 3.8: Horizontal fields of the depth-integrated meridional momentum balance terms for the clock-hour average day hours: 4h, 8h, 12h, 16h, 20h and 24h. From top to bottom row: Acceleration, Advection, Coriolis and Pressure gradient. Units are $m^2.s^{-2}$.

the region. Figure 3.10 shows that areas **3** and **4** have similar dynamics, but are rather different than the dynamics over areas **1** and **2**. In all four areas, the bottom stress term is small and does not contribute significantly to the balance. The wind stress term is equal in all areas since the wind forcing is spatially homogeneous, and, as described before, is small in the morning and increases in the afternoon.
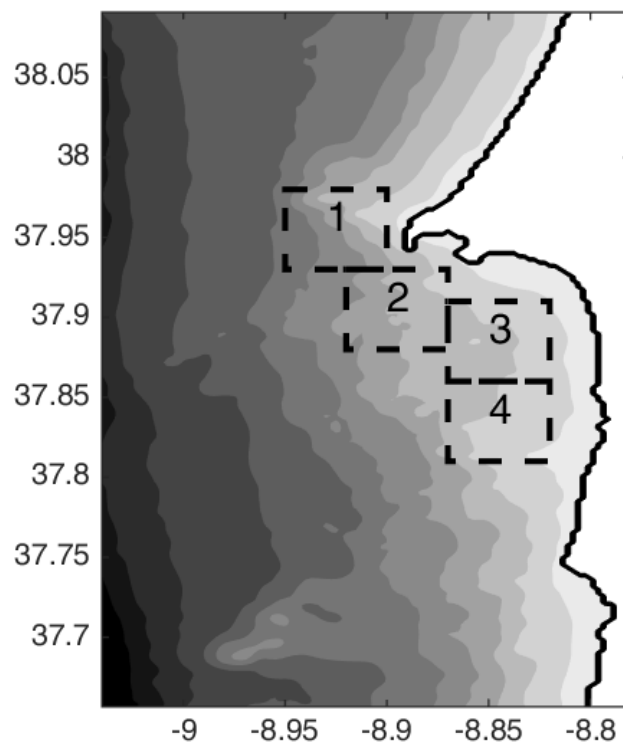
FIGURE 3.9: Map showing the 4 areas for the computation of the spatially averaged fields for the clock-hour average-day.

At the tip of the cape (area **1**) the pressure gradient term is positive and fairly constant throughout the day, with a small decrease at mid-day. On the other hand, the pressure gradient term in areas **2**, **3** and **4** is negative, and shows a sharper decrease at mid-day. In all balances the pressure gradient is mainly balanced by the Coriolis term in the morning, which is negative in **1**, but positive in **2**, **3** and **4**. In the afternoon, although the Coriolis term is still strong, the wind stress term also contributes to the balance. The advection term is small in areas **3** and **4** , but is an important part of the balance in areas **1** and **2**.
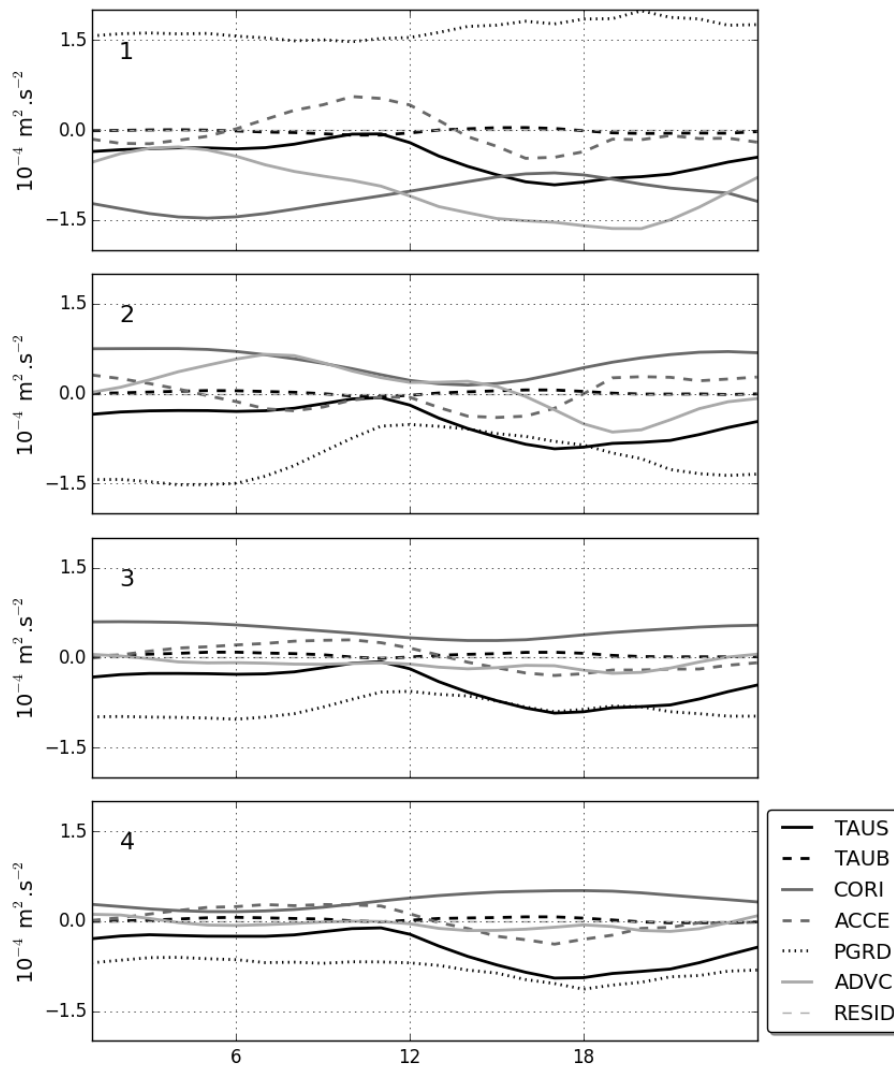
FIGURE 3.10: Clock-hour average-day of the momentum balance terms spatially averaged across areas 1 to 4. Units are 10^{-4} m^2.s^{-2}

In short, these four areas are mostly under geostrophic balance in the morning, with small contributions of advection and acceleration in areas **1** and **2**, connected with the jet acceleration, deflection and recirculation after encountering the cape. In the afternoon, the wind stress term also contributes to the balance. Although area **4** is located over the secondary upwelling jet, the Coriolis term does not show the flow reversal shown by the cross-shelf velocity profiles at the ADCP site, indicating that most part of the diurnal variability of the circulation is lost when the velocity is integrated over the entire water column.

3.3.5 Meridional Sections

Integrating the velocity over the entire water column seems to eliminate much of the diurnal variability of the cross-shelf circulation, due to its 2-layer nature (Figure 3.3), and therefore, more detailed analysis should be performed using depth-varying velocities. To investigate how the clock-hour average day circulation varies in depth, three meridional sections were chosen across the domain: section **A** located on the north side of the cape; section **B** in the south of the cape, at the same latitude as the ADCP site; and section **C** also in south of the cape, where the coast is again meridionally aligned (Figure 1.1).

The meridional and zonal velocities at each section are shown in Figure 3.11 and 3.12, respectively, for three averaged hours (8 h, 12 h and 24 h) that cover the different periods of the clock-hour average-day. In section **A** (Figure 3.11), in the morning period, the surface intensified southward flow (upwelling jet) is concentrated in the first 40 m of depth, within 10 km from the coast, and over the 40-m isobath. As the day evolves, the stronger southward flow extends farther offshore, but maintains its vertical extend and central location. The deflection of the upwelling jet and a northwards current corresponding to the cyclonic circulation can be seen in section **B** (Figure 3.11). The upwelling jet is now located 20 km offshore, at the 100-m isobath. Closer to the coast, the secondary jet described in the previous section can be observed. This jet is also intensified at the surface and is confined to the shallower part of the section, within 8 km from the coast. Between these two southward flows there is a cell of positive (northwards) velocities. The northward flow has an average of half of the magnitude of both southward flows and is more intense in the evening. In section **C**, both southward flows are still

present, but the northward flow has only a weak signal at 12 h in the bottom (Figure 3.11). This implies an horizontal extend of the cyclonic recirculation of less than 11 km (distance between section **B** and **C**). The horizontal scale of this cyclonic cell is in agreement with Crépon et al. (1984) that showed that the scale of a perturbation in the leeside of a cape is comparable to the offshore extend of the cape size itself (Cape Sines is approximately 10 km wide).
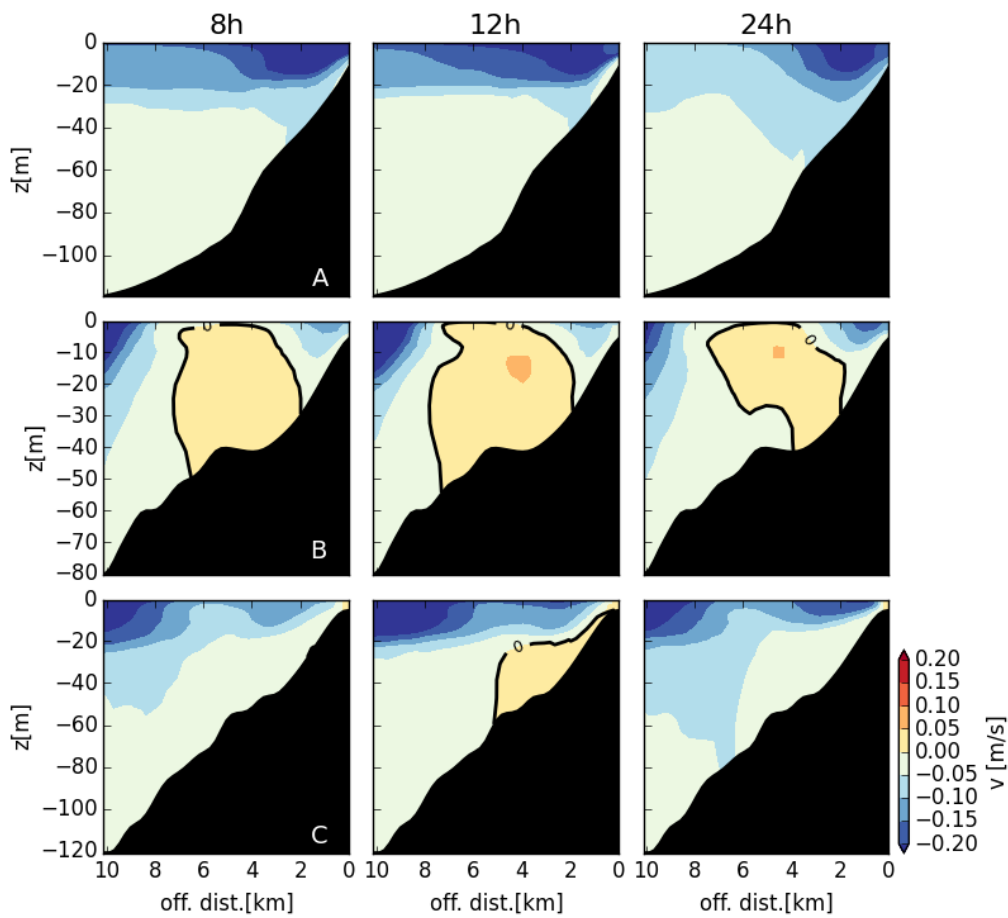
FIGURE 3.11: v fields for each section (**A**, **B** and **C**); at different hours of the clock-hour average-day (8h, 12h, and 24h). Units are m.s^{-1}.

Topography clearly influences the zonal circulation, especially between north and south of the cape. At 8h and 12h, the zonal circulation differs considerably across the three sections, implying that the topography has a stronger influence in the circulation during this period. As seen previously, north of the cape (section **A**), the surface flow is mostly to the west (offshore), connected with the offshore deflection of the upwelling jet. In the south side of the cape, zonal velocities
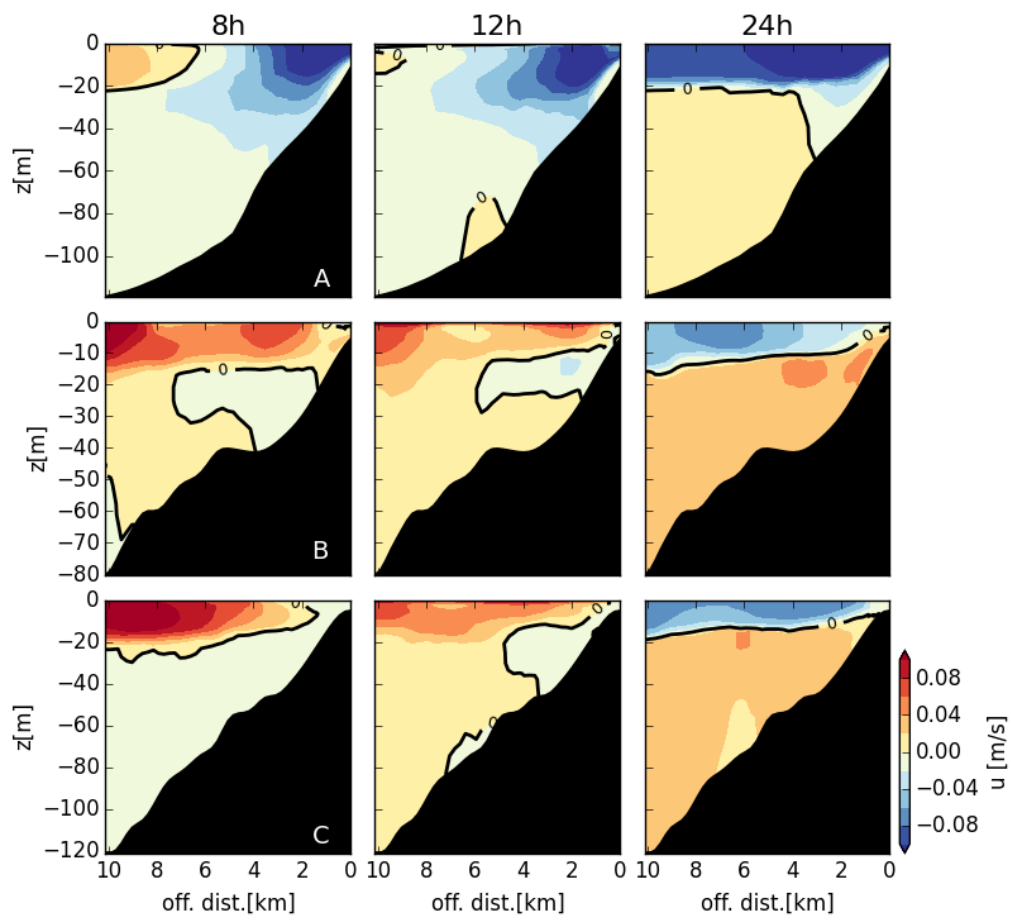
FIGURE 3.12: u fields for each section (**A**, **B** and **C**); at different hours of the clock-hour average-day (8h, 12h, and 24h). Units are m.s^{-1}..

show similar variability, with onshore velocities at the surface in most part of the section from 8h to 12h and offshore velocities at the surface for the rest of the day. There is a weak offshore flow near the coast in sections **B** and **C** at 8h and 12h, associated with the secondary upwelling jet. This region is consistent with the area south of the cape marked in Figure 3.6, where the circulation has the 3-period diurnal variability discussed before. At 24h, the main circulation features are consistent with previous studies regarding upwelling circulation (Allen et al., 1995; Austin and Lentz, 2002; Marchesiello and Estrade, 2010), with offshore flow in the surface and onshore flow at the bottom.

3.3.6 Transport in the Surface Layer
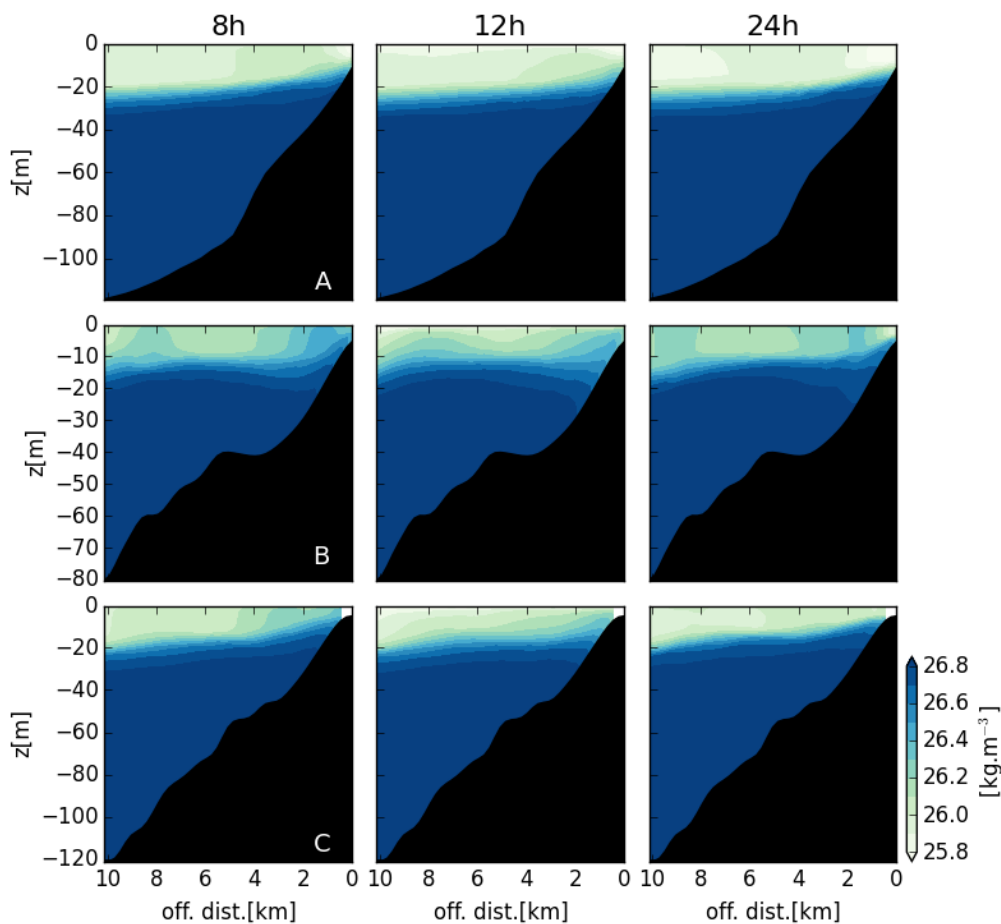
FIGURE 3.13: Density anomaly (σ) fields for each section (**A**, **B** and **C**); at different hours of the clock-hour average-day (8h, 12h, and 24h). Units are kg.m^{-3}.
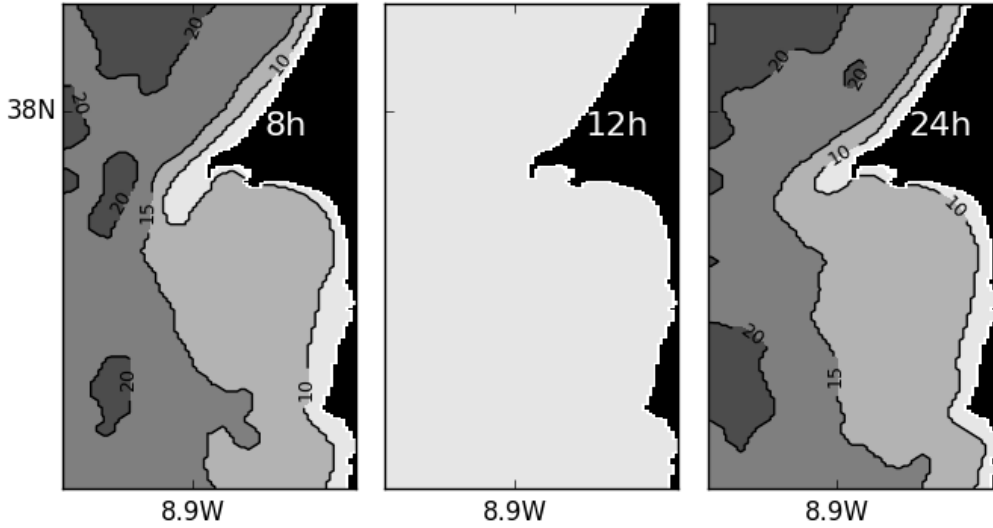
FIGURE 3.14: Mixed Layer Depth at different hours of the clock-hour average-day (8h, 12h, and 24h). Units are m.

The previous analysis showed that most of the cross-shelf variability is concentrated on the surface layer. The Ekman layer scale, $D_{Ek} = \left(\frac{2A_v}{f}\right)^{1/2}$, where A_v is the vertical eddy viscosity, with values ranging from 5×10^{-3} to 2×10^{-2} m^2.s$^-1$, is around 10 to 20 m. The mean mixed layer depth, roughly estimated using the temperature criterion of 0.2ºC absolute difference from surface (de Boyer Montégut et al., 2004), confirms that, except for the hours of strong diurnal heating, 15 m is a good approximation for a surface layer in most part of the domain (Figure 3.14). Density anomaly ($\sigma = \rho$ - 1000 $kg.m^{-3}$) profiles over the meridional sections described before (Figure 3.13), also show a layer interface (consistent with the pycnocline) at approximately 15 m. Finally, with the consideration that most Ekman transport occurs in the scale of the Ekman depth D_{Ek} (Marchesiello and Estrade, 2010), 15 m seems an appropriate thickness of the surface layer to study the transport and associated dynamics.

Depth-integrated velocity **v** in the surface layer does not change considerably throughout the day (Figure 3.15a), showing a strong southwards flow in most part of the domain, with the exception of the region in the leeside of the cape, where **v** is near-zero. As expected, the depth-integrated flow is intensified in the location of the upwelling jet and near the coast in the region south of the cape, consistent with the secondary upwelling jet. Overall **v** is more intense at mid-day, consistent with the intensification of the northerly wind stress in the afternoon. On the other

hand, **u** (Figure 3.15b) shows a strong diurnal variability, with strong eastwards (onshore) flow in the leeside of the cape at 8h and 12h and opposite at 24h. The onshore flow at 8h does not reach the shallower part of the domain (with the zero isoline clearly demarking the shallow waters), but at 12h and 24h onshore and offshore **u**, respectively, are still present near the coast, although weaker than over the deeper part of the domain. In the northside of the cape a strong westwards **u** is consistent with the deflection of the flow as it encounters the cape. On average, **v** is three times more intense than **u**, which indicates that the dominant surface transport should be directed southwards. However, in the lee of the cape, material may be transported eastwards or westwards across the shelf, depending on the hour of the day, since the meridional transport is weak in this region.
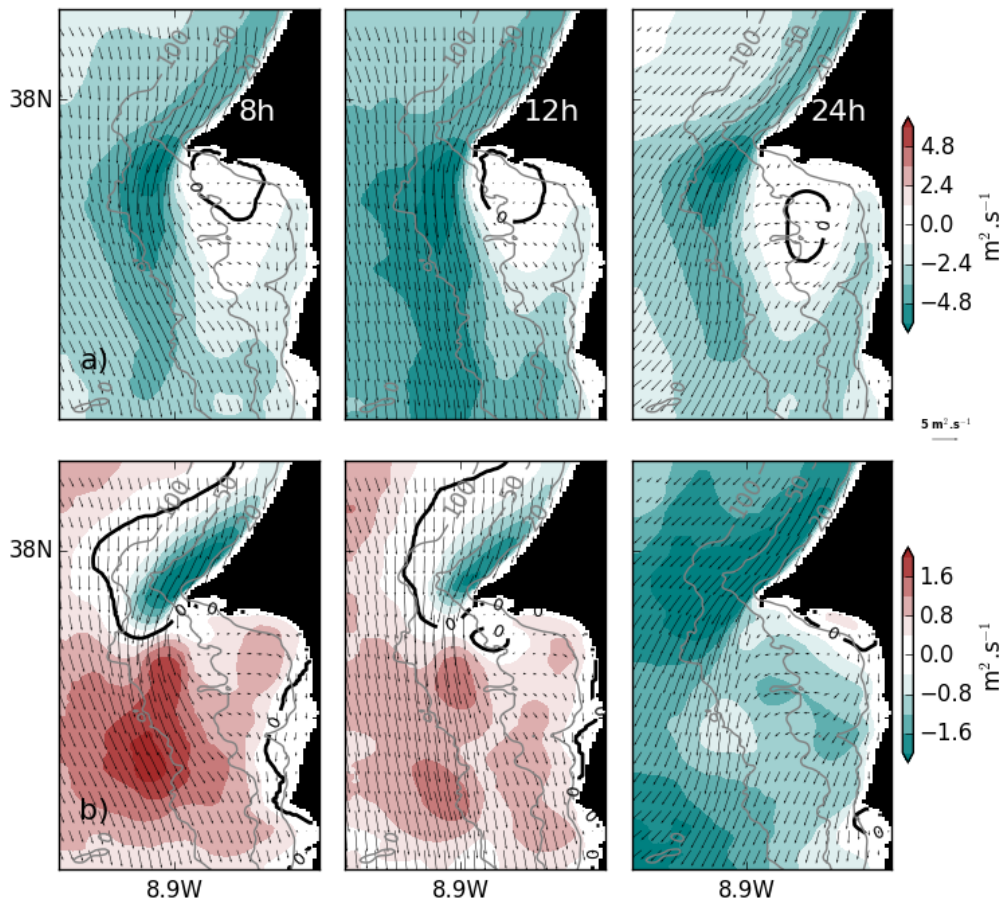
FIGURE 3.15: Depth-integrated velocity **v** (a) and **u** (b) in the surface layer (15 m) with depth-integrated velocity vectors superimposed, for three different hours of the clock-hour average day: 8h, 12h and 24h. Units are $m^2.s^{-1}$.

3.3.7   Vorticity and Divergence

As suggested before, the presence of the cape induces the deflection of the up-welling jet. After crossing the cape, the southward flow steers cyclonically as it crosses isobaths in order to conserve the vorticity. This can create regions of divergence in the south of the cape, which will consequently induce upwelling. Therefore, the mechanisms behind the surface transport around the Cape can be investigated using the horizontal divergence and vorticity fields, obtained from the modeled velocity fields (in a way similar to Roughan et al. (2005b)). The horizontal fields of relative vorticity (ξ_{rel}) and divergence (Div_h) were computed using:

$$\xi_{rel} = \frac{\partial \mathbf{v}}{\partial x} - \frac{\partial \mathbf{u}}{\partial y}, \tag{3.1}$$

and

$$Div_h = \frac{\partial \mathbf{v}}{\partial y} + \frac{\partial \mathbf{u}}{\partial x} \tag{3.2}$$

Where **u** and **v** are the depth-integrated velocity components for the surface layer (15 m). The clock-hour average day method was applied to analyse the diurnal variability of the vorticity and divergence fields, and Figure 3.16 shows the results for three averaged hours (8 h, 12 h and 24 h).

Divergence and relative vorticity fields remain fairly unchanged from 8 h to 12 h, with negative vorticity at the northside of the cape which is directly connected with the offshore deflection of the cape, and a region of convergence (negative divergence) near the coast. At the tip of the cape, strong divergence indicates enhanced localized topography-driven upwelling in this location. At the leeside of the cape, a region of maximum positive vorticity is present as the jet rotates cyclonically around the cape. Inshore of this high vorticity patch there is a strong positive divergence region, which confirms the enhancement of the upwelling in this location (Figures 2 and 3.7). In the morning and mid-day hours, there is strong convergence in the nearshore region, consistent with the location of the
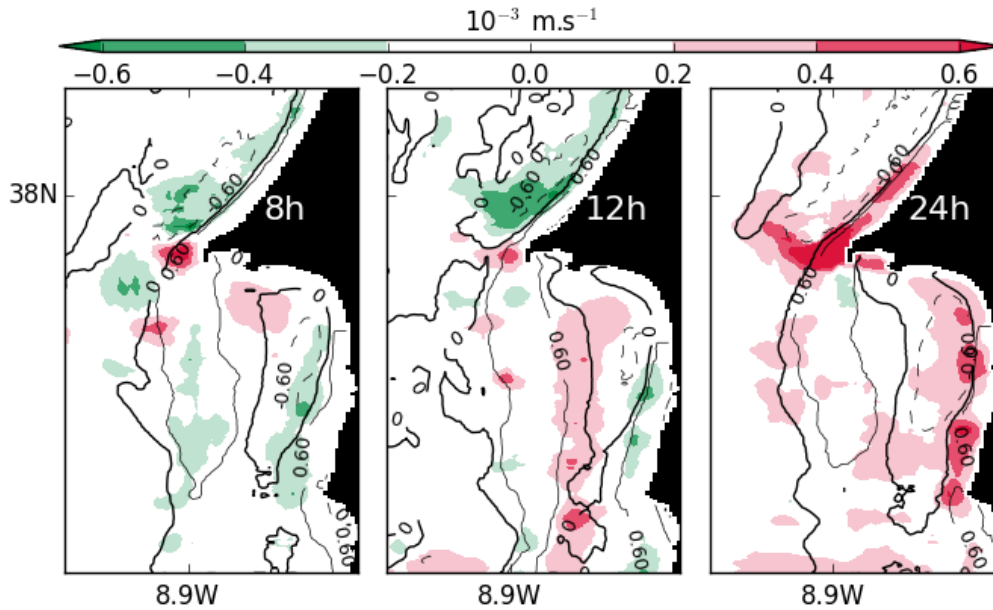
FIGURE 3.16: Coloured contour maps of Div_h superimposed with iso-lines of ξ_{rel}, for hours 8 h, 12 h and 24 h of the clock-hour average-day. Units are in m.s^{-1}.

secondary upwelling jet. In the south part of the domain, most regions of divergence and convergence are present in the boundaries between positive and negative relative vorticity patches, with higher values of divergence coincident with $\xi_{rel} = 0$ iso-line. This hints to the fact that the upwelling in this location is not directly connected with vorticity, but rather results from the divergence of the linear flows. Except for the strong divergence at the tip of the cape, the divergence field at 24 h is overall weak and positive.

The horizontal fields of divergence and vorticity were spatially averaged across the four areas around the Cape (Figure 3.9), to analyse the diurnal variability present in these specific areas, since they cover the main regions in the domain with different dynamics. The plots for each area are shown in Figure 3.17. The vorticity field changes substantially between area 2 and the other areas. Area 2 shows strong positive vorticity of one order of magnitude stronger than the other regions, connected with the deflection of the upwelling-jet as it reaches the cape. In this area, the vorticity also shows a daily cycle, with a magnitude peak at mid-day, related with the cyclonic rotation of the upwelling jet, which is stronger just after the wind stress is minimum (Figure 3.7). Regions 1, 3 and 4

show a similar magnitude and diurnal variability of relative vorticity, even though region 1 is located at the tip of the cape, whilst regions 3 and 4 are in the south side of the cape. These 3 areas show negative vorticity values, that increase in magnitude towards evening and decrease again during the night. In region 3 and 4 the vorticity reaches positive values around 16h, connected with the eastwards rotation (cyclonic) of the secondary upwelling jet (Figure 3.7).

The divergence across the four areas, in spite of showing similar magnitude for all regions, represent the complexity of the diurnal and spatial variability of this domain. Area 1 shows convergence in the morning and divergence in the afternoon, suggesting a localized topography-driven upwelling at the tip of cape Sines, similar to Roughan et al. (2005b). As expected, area 3 shows the stronger positive divergence agreeing with previous evidence of intensified upwelling in the lee of Cape Sines. Areas 2, 3 and 4 show a double peak in the diurnal cycle, although not exactly at the same hour, and with weaker magnitude. The timing of stronger divergence in these 3 areas suggests that enhanced upwelling happens when the wind stress is minimum (at 12 h) and after the maximum wind stress (at 18 h). This is in agreement with the surface flow adjustment to the diurnal variability of the wind, which is different across the domain (Figure 3.6), resulting in zones of convergence or divergence that will vary during the day.

3.4 Summary and Discussion

In this chapter the analysis was focused on the topographic influence on the wind-driven circulation in the vicinity of Cape Sines. The realistic model was forced exclusively with local winds and simulated most of the current variability seen at the ADCP site, including the mid-day flow reversal and the upwelling-type circulation in the evening, supporting the hypothesis that the observed cross-shelf circulation pattern at diurnal timescales is mostly wind-driven. The observed two-layer pattern in the evening (after 19 h) is typical of an upwelling circulation (Allen et al., 1995; Austin and Lentz, 2002). Although in shallow waters the circulation tends to align barotropically with the wind (Lentz, 2001; Kirincich et al., 2005), the presence of stratification enables the cross-shelf exchange to penetrate into shallower waters, as suggested in several studies (Lentz, 2001; Austin and
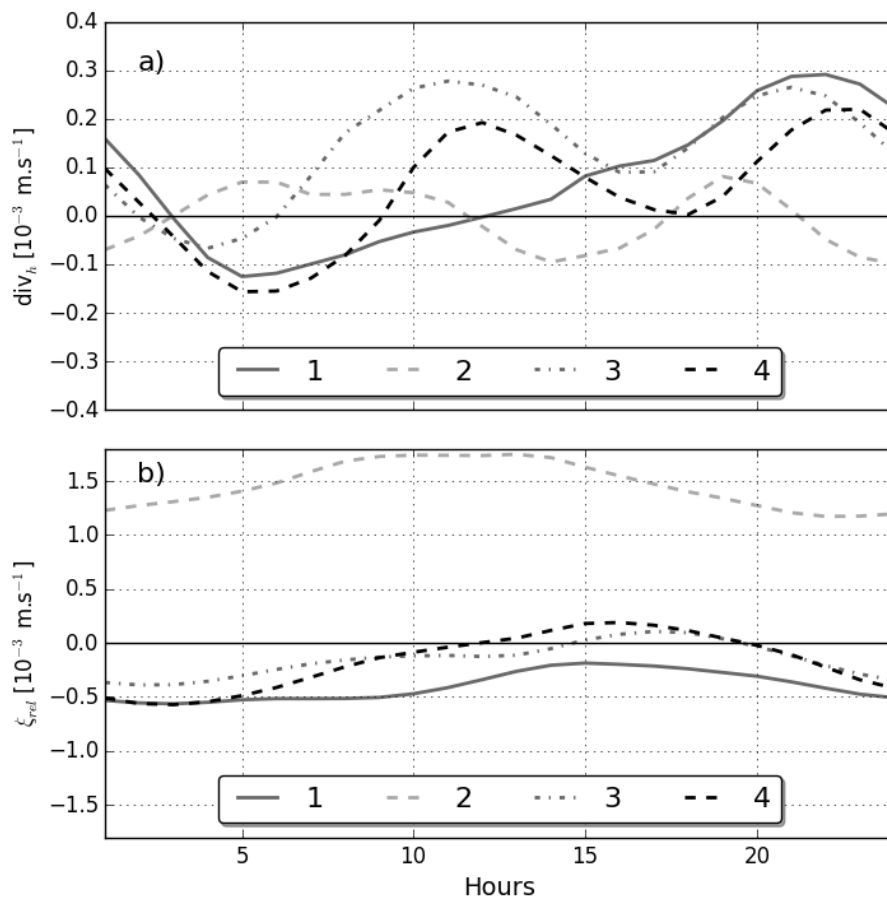
FIGURE 3.17: Clock-hour average-day of a) Div_h; and b) ξ_{rel}, spatially averaged across areas 1 to 4. Units are in m.s^{-1}.

Lentz, 2002; Durski et al., 2004; Kirincich et al., 2005). However, the model fails to reproduce the 3-layer structure seen in the morning. This can be due to the fact that other forcing elements may have a stronger impact in this period (like tides and or waves) or larger scale processes described before (Lentz, 2008; McCabe et al., 2015; Fewings et al., 2015) that are not reproduced in the model due to the small domain.

Although previous studies concluded that the depth-averaged momentum balance over the inner-shelf is primarily between wind stress, along-shelf pressure gradient and bottom stress (Lentz et al., 1999; Liu and Weisberg, 2005; Fewings and Lentz, 2010), in this study other terms of the balance are equally important. Momentum balance analysis showed that the daily variability of the cross-shelf flow at the observations location is associated with the evolution and relative importance of different terms in the momentum balances throughout the day. Advection and local acceleration are found to have a stronger impact in both balances, likely connected with the topography and diurnal wind forcing, consistent with previous studies (Allen, 1996; Gan and Allen, 2002; Sanay et al., 2008; Gan et al., 2009; Ganju et al., 2011). The diurnal variability of the along-shelf pressure gradient follows closely with the variability of the along-shelf wind stress term suggesting that the pressure gradient is wind-induced.

As seen in Gan and Allen (2002) and Kuebel Cervantes and Allen (2006), the interaction between the wind-driven flow and the variations in topography is responsible for the setting up of an along-shelf pressure gradient as a response to decreased surface elevation in the leeside of a cape, which results from the intensification of the along-shelf velocity around the cape. Near the coast, small-scale pressure gradients are established around coastline perturbations, which are balanced primarily by nonlinear advection. The primary jet has a strong geostrophic component but over the secondary jet all four terms have similar magnitude (pressure gradient and coriolis terms are not as strong for water depth below 50 m in the leeside of cape Sines), increasing the relative importance of acceleration and advection terms over shallower waters.

The upwelling jet deflection and corresponding cyclonic circulation due to the presence of a cape and the intensified upwelling in the leeside of the cape is consistent with several studies (Barth et al., 2000; Gan and Allen, 2002; Doglioli et al., 2004; Kuebel Cervantes and Allen, 2006; Meunier et al., 2010; Perlin et al., 2011;

Liu and Gan, 2014). However, most of these studies deal with steady upwelling regimes or with relaxation periods of more than one day, and do not describe the diurnal variability caused by a daily oscillating upwelling regime. In the present study, the diurnal variability of the wind is felt differently across the domain and the small-scale spatial alternation of upwelling/downwelling regions can effectively drive cross-shelf exchange, especially in the leeside of Cape Sines. The fact that the wind decreases until mid-day allows for the upwelling to relax, inducing surface onshore transport in the leeside of Cape Sines (as seen in Figure 3.15) which would not occur in persistent upwelling conditions. However, upwelling (divergence) in the lee of the cape is driven in the afternoon as the northerly wind increases in magnitude, which will bring nutrients and colder waters to the south side of the cape, promoting primary production, essential for biological development. The diurnal combination of these two regimes indicate that the study region has effective mechanisms to larvae development and posterior cross-shelf transport.

In summary, these modelling results helped to characterize the nearshore circulation in the vicinity of Cape Sines. The presence of the cape is responsible for the observed cross-shelf circulation pattern but only very few regions show a similar flow evolution as the observations. The persistence of upwelling-favourable winds promoted retention of cold and newly upwelled waters in the leeside of Cape Sines which is significantly relevant for pythoplankton blooms and larvae development (Roughan et al., 2005a, 2006; Peliz et al., 2007; Oliveira et al., 2009). The fact that the wind diurnally undergoes relaxation and intensification strongly modifies the cross-shelf circulation, promoting superficial onshore flows at mid-day, in the leeside of Cape Sines, that overpower the strong along-shelf currents. The combination of these two wind regimes indicates that the study region has effective mechanisms of onshore transport during this period, as seen in Trindade et al. (2016). The efficiency of different wind scenarios and topography on cross-shelf transport will be addressed in the following chapter.

Chapter 4

Wind and topographic effects on the shelf circulation near a cape

4.1 Introduction

Wind-driven circulation over a straight coastline is already well documented. In case of straight western coastlines in the northern hemisphere, northerly winds drive an offshore flow in the surface layer and a compensating onshore flow in the bottom layer, resulting in superficial offshore transport of cold, nutrient-rich water from below. The dynamics are relatively two-dimensional with a primary balance between Coriolis force and pressure gradient. In the presence of topographic variations, however, the flow response is more complex. Several studies of flow-topography interactions in the presence of headlands (Gan and Allen, 2002; Roughan et al., 2005b; Kuebel Cervantes and Allen, 2006), promontories (Barth et al., 2000; Castelao and Barth, 2006) or canyons (Kämpf, 2012) have found that nonlinear advection can significantly contribute to the momentum balance, resulting in three-dimensional dynamics and requiring more complex modelling studies to correctly simulate the circulation around these regions.

Literature describes that, in the vicinity of a perturbation, the wind-driven jet destabilizes and deflects off the coast with consequent development of filaments, squirts and eddies. The offshore displacement of the upwelling jet will consequently advect the upwelling front, which can cause a strong biological impact as the offshore extent of the ecosystem is modified. In the particular case of a headland or cape, an upwelling-shadow region can form in the leeside (Roughan

et al., 2005b; Oliveira et al., 2009), where velocities are weak and mixing is enhanced. This can affect the cross-shelf transport in this region, which is essential for the displacement and distribution of biological material across the continental shelf. In addiction, the fact that the wind has a marked diurnal variability can strongly impact the coastal circulation, and especially the cross-shelf transport. Previous studies have found that daily variable winds, such as the sea breeze, can generate local upwelling (Woodson et al., 2007), can enhance cross-shelf exchange through its influence on waves (Hendrickson and MacMahan, 2009) and can also force complex inertial currents, especially near the critical latitude ($30°$ $\pm\ 10°$ N/S) where the inertial and diurnal periods are close to each other (Simpson et al., 2002; Sobarzo et al., 2010; Aguiar-González et al., 2011). Thus, the study of the circulation associated with the diurnal variability of the wind seems crucial to understand the transport and distribution of biological material across the shelf. Yet, inner-shelf studies over coastal regions with topographic variations are still scarce due to sparse in-situ observations and the difficulty of resolving multiple spatial and temporal scales required to investigate nearshore dynamics.

As seen in previous chapters, the upwelling circulation is strongly modified in the presence of a cape, with the deflection and offshore displacement of the upwelling jet as the flow interacts with the coastline perturbation. The fact that the wind diurnally relaxes also contributes to the complex pattern of surface cross-shelf transport in the leeside of the cape. The main focus throughout this study is the consistent surface cross-shelf flow reversal at mid-day observed by the ADCP. By analysing the clock-hour average-day of the circulation and wind stress, we have observed that the surface circulation was offshore during minimum wind stress hours (morning), rotated onshore a few hours after minimum wind stress (mid-day) and reversed back offshore when the wind stress increased in magnitude. Results from the realistic modelling study presented in Chapter 3, showed that the circulation's diurnal variability, at a grid point that represented the ADCP location, was reproduced using wind forcing alone, suggesting that the major circulation features at this location are wind-driven.

This chapter intends to address some questions regarding the establishment of the surface onshore transport with daily-varying upwelling-favourable wind conditions (with variability within timescales of one inertial period). On one hand to analyse if there is indeed promotion of onshore transport in the leeside of the

cape and on the other how the topography and wind variability affect the cross-shelf exchange near the cape. To address these questions a process oriented study was conducted, using a set of modelling experiments of simplified geometry and stratification. In order to isolate the effects of topography and wind forcing, some assumptions and simplifications were considered:

- The stratification during these months will not change much near the coast and consequently the stratification will not constitute a varying parameter of the study.

- The wind forcing in the area and in summer is composed of almost stable northerlies with daily events of intensification/relaxation which were simulated with simplified analytical functions with a diurnal fluctuation to simulate sea breeze.

- Although waves and tides can be important drivers, especially in the shallow part of the shelf, previous chapters have shown that the main circulation features observed near Cape Sines were fairly well reproduced with a wind-forced model, and therefore waves and tides were not included in the modelling experiments.

The idealized topography with an asymmetric cape was chosen to fit the continental shelf region in the vicinity of Cape Sines, and the oscillatory wind forcing was developed to simulate the diurnal variability of the wind observed during the summer of 2006.

4.2   Model Setup

The model configuration was developed to simulate the circulation in the vicinity of Cape Sines, during summer. The numerical runs were conducted using ROMS, which was described in detail in Chapter 3. All experiments were run on a 400×200 grid for an extention of 200 km in the along-shelf direction and 100 km in the cross-shelf direction, which results in a 500 m horizontal resolution in both directions. 20 vertical σ-levels were used with enhanced surface resolution, to resolve the surface boundary layer. A linear bottom drag coefficient $r = 10^{-3}$ m.s^{-1} was chosen. The simulations were conducted in a N-S periodic channel

with an Orlanski-type radiation boundary condition (Marchesiello et al., 2001) in the West and a free-slip wall in the East. A sponge layer of 20 km was placed in the open boundary and vertical mixing and diffusion were parametrized using the Large et al. (1994) K-Profile Parametrization scheme. The initial density field is horizontally uniform with a constant salinity of 35 psu and a vertically decaying temperature ranging from 12 to 20 °C, to represent typical stratification during summer around Cape Sines. Coriolis parameter is constant and set to f = 1 x 10^{-4} s^{-1} which is approximately the value for the desired latitude range (37-40°N). A total of 18 experiments were performed, with different topographic features and wind forcing (Table 4.1).

TABLE 4.1: Table with various parameters used in the different experiments

Experiment	Topography	Wind Forcing
SLOPE_SN	Symmetric Cape with Slope	Steady N
SLOPE_SNW	Symmetric Cape with Slope	Steady NW
TOPO_SN	Symmetric Cape with Promontory	Steady N
TOPO_SNW	Symmetric Cape with Promontory	Steady NW
ATOPO_SN	Asymmetric Cape with Promontory	Steady N
ATOPO_SNW	Asymmetric Cape with Promontory	Steady NW
SLOPE_ON	Symmetric Cape with Slope	Oscillatory N
SLOPE_ONW	Symmetric Cape with Slope	Oscillatory NW
TOPO_ON	Symmetric Cape with Promontory	Oscillatory N
TOPO_ONW	Symmetric Cape with Promontory	Oscillatory NW
ATOPO_ON	Asymmetric Cape with Promontory	Oscillatory N
ATOPO_ONW	Asymmetric Cape with Promontory	Oscillatory NW
SLOPE_PN	Symmetric Cape with Slope	Oscillatory step N
SLOPE_PNW	Symmetric Cape with Slope	Oscillatory step NW
TOPO_PN	Symmetric Cape with Promontory	Oscillatory step N
TOPO_PNW	Symmetric Cape with Promontory	Oscillatory step NW
ATOPO_PN	Asymmetric Cape with Promontory	Oscillatory step N
ATOPO_PNW	Asymmetric Cape with Promontory	Oscillatory step NW

4.2.1   Topography

Three idealized bottom topographies were developed (Figure 4.1) to test the circulation's sensitivity to topographic features. All topographies consist of a North-South oriented channel and a coast that extends to all the eastern boundary and is

disrupted by a small cape in the middle. In all experiments the minimum depth is 5 m and a cut-off depth of 200 m was applied. For most part of the domain, the x-axis is coincident with the cross-shelf direction, and the y-axis with the along-shelf direction, and the only exception is the region over the cape. To avoid misinter-pretations, the model description and analysis will be based on the zonal (x) and meridional (y) oriented axis, with the consideration that away from the cape it is coincident with the along- and cross-shelf coordinate axis.

The first topography is a smoothly decaying slope with no variation in the meridional direction. This slope can be analytically described as a hyperbolic tangent function:

$$h(x, y) = Ht\left[1 + tanh(s(Ht - x))\right] - depth_{max} \tag{4.1}$$

where x, y are the zonal and meridional directions, respectively, $Ht = 200$, which is the middle point of the slope, $depth_{max}$ is the maximum depth; and $s = 0.05$ is a slope parameter, which was empirically retrieved to represent a smoothly decaying continental slope, consistent with the slope around Cape Sines. A triangular headland of 10 km wide and 20 km long was added to the slope, intending to simulate a cape with dimensions similar to Cape Sines. This configuration will further on be referred as **SLOPE**. We conducted this experiment to illustrate the effects of a headland on the shelf circulation.

The second topography consists of the same slope with an added perturbation in the form of a promontory:

$$h(x, y) = Ht\left[1 + tanh(s(Ht - x - cf(x, y))\right] - depth_{max} \tag{4.2}$$

with

$$cf(x, y) = Acos\left(\frac{\pi}{360}(y + Hc)\right)^B \tag{4.3}$$

where $A = 20$ and $B = 150$ are promontory shape parameters and $Hc = 100$ is a location factor of the promontory. To obtain a smoother cape, instead of a triangular headland, we considered land to be all $h(x, y) < 5m$, which satisfactorily

resulted in a cape with similar dimensions to Cape Sines. This configuration will be referred to as **TOPO**. This configuration is more realistic than **SLOPE** since the bottom topography accompanies the cape.

Both previous topography configurations simulate a symmetric cape; i.e. the topography on the north part of the cape is the same as the topography on the leeside. This is often not the case in the ocean and one example is Cape Sines, which is characterized by a slowly widening shelf in the northside and a sharper transition toward a narrow shelf in the leeside. To investigate the importance of the cape geometry in the flow response, an asymmetric topography was computed, which was obtained by using 4.2 with a modified $cf(x, y)$:

$$cf(x, y) = \frac{A e^{-2[\log(y')]^2}}{y'} \tag{4.4}$$

where y' is:

$$y' = s(y - Ht') \tag{4.5}$$

This results in a slowly varying topography in the north part of the cape, and an abrupt variation in the south side. This configuration will be referred as **ATOPO** and is the idealized topography that closely represents the vicinity of Cape Sines.

Results will be analysed in a zoomed region closer to the cape, shown in Figure 4.2.

4.2.2   Wind Forcing

The model was forced with a spatially uniform wind stress and no heat fluxes were added to the atmospheric forcing. The observations and the WRF model have shown that the wind around Cape Sines during the summer of 2006 had a diurnal variability much similar to a sea breeze cycle, with an increase of both wind components' magnitude in the afternoon. A total of six wind forcing conditions were developed in order to simulate this wind condition (Figure 1.9). All experiments start from rest and a 2-day ramping was added to decrease numerical instabilities. Afterwards, three different temporal patterns of the wind forcing
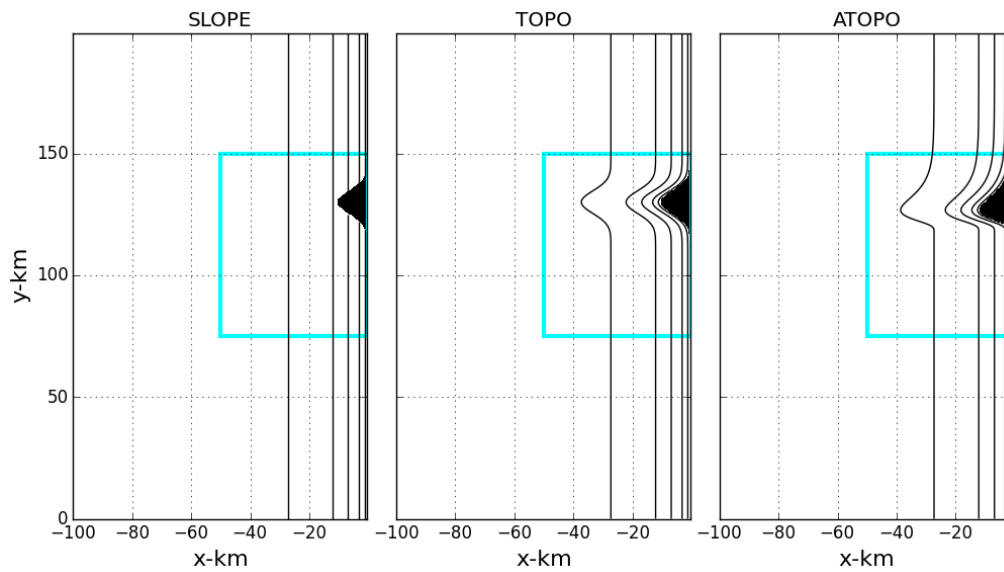
FIGURE 4.1: Bottom topography for the different experiments. 20-m, 50-m, 100-m and 200-m isobath shown in black. The blue box shows the region of the analysis.
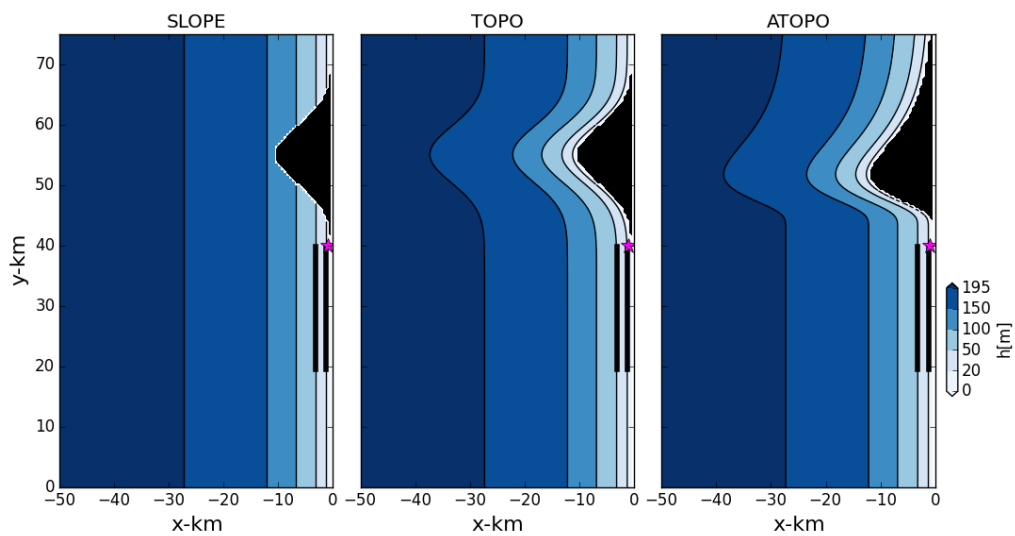
FIGURE 4.2: Zoom of the model domain (blue box in Figure 4.1) for the different experiments. 20-m, 50-m, 100-m and 200-m isobaths are shown in black. The black thick lines represent the zonal sections where cross-shelf transport and momentum balances are analysed.

were implemented during 13 days: Steady, Oscillatory and Oscillatory Step (Figure 4.3). The different wind stresses were considered in order to explore the circulation's response to different temporal patterns of the wind.

To analyse the response to a steady upwelling-favourable wind regime, two constant wind conditions were considered: one to represent northerly winds (hereinafter **SN**) with τ_s^y = -0.1 Pa (which corresponds approximately to 10 m.s^{-1}) and τ_s^x = 0; and other for northwesterly wind conditions (**SNW**) with the same τ_s^y as **SN** and τ_s^x = 0.05 Pa. For both experiments, the wind stress remained constant after the 2-day ramping.

Four different daily varying wind conditions were developed to study the circulation at diurnal timescales. The oscillatory wind stress consists of a simple sinusoidal function with a daily fluctuation between 0 and the maximum wind stress value. To simulate oscillating northerly (**ON**) and northwesterly wind conditions (**ONW**):

$$\tau_s^y(t) = A_y \left(0.5 - cos \left(\frac{\pi t}{T_o} \right) \right) \tag{4.6}$$

The τ_s^x is zero for **ON** but for **ONW** is represented by:

$$\tau_s^x(t) = A_x \left(0.5 + cos \left(\frac{\pi t}{T_o} + \varphi \right) \right) \tag{4.7}$$

where $A_y = -0.1$ and $A_x = 0.05$ are the wind stress amplitudes, period $T_o =$ 12 hours and phase $\varphi = 12$ hours.

To simulate the daily abrupt change of wind magnitude, much similar to the observations (Figure 1.10), the model was forced with an oscillatory wind stress with different temporal rates of increase and decrease of magnitude, which were called the Oscillatory Step experiments. The wind stress can be analytically described as a smooth sawtooth function, where, for northerly (**PN**) and northwesterly wind

conditions (**PNW**):

$$\tau_s^y(t) = A_y' \left[t' - \left(\frac{tanh(sk((-t'+0.5) - |-t'+0.5| - 0.5))}{2tanh(0.5sk)} + |-t'+0.5| - 0.33 \right) \right]$$
(4.8)

And, as before, the τ_s^x is zero for **PN** but for **PNW** is represented by:

$$\tau_s^x(t) = A_x' \left[t' - \left(\frac{tanh(sk((t'+0.5) - |t'+0.5| - 0.5))}{2tanh(0.5sk)} + |t'+0.5| - 0.33 \right) \right]$$
(4.9)

with

$$t' = \frac{t}{T_o}$$
(4.10)

where $sk = 12$ is a skewness factor; $A_x' = 0.075$ and $A_y' = -0.15$ are amplitudes.

The model is initialized with zero velocity and a flat ocean. All experiments ran for a 15-day period, with a barotropic and baroclinic timestep of 60 s. Results for the first 5 days (2-day ramping + 3-day spin up) were disregarded and therefore all further analysis were based on the last 10 days of the simulation. For the steady wind experiments (**SN** and **SNW**) results are shown regarding the average of the last 10 days of the simulation, and the model results for the daily varying wind experiments were focused on the daily evolution of the circulation based on the clock-hour average day computed for the last 10 days of the simulation (similar to what was described in Chapter 1). Since the maximum wind stress in the oscillatory and step wind experiments do not occur at the same hour of the day, the analysis was based on the hour of the highest (t_{max}) or lowest (t_{min}) wind stress, regardless of what hour of the day it occurs. The results were also analysed at the mid-point hour between the minimum and maximum wind stress (t_{1mm}) and at the mid-hour between the maximum and minimum wind stress (t_{2mm}) (Figure 4.3).
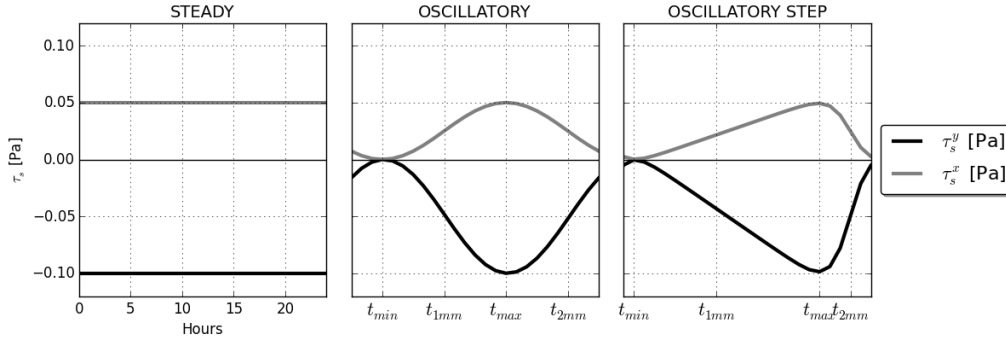
FIGURE 4.3: 24 hours of the Steady, Oscillatory and Oscillatory Step
wind stresses τ_s^y (black) and τ_s^x (gray) after the ramping period.

4.3 Results

4.3.1 Application to Cape Sines case study

The idealized topography with an asymmetric cape was chosen to fit the continental shelf region in the vicinity of Cape Sines (Figure 1), and the **PNW** wind condition is closest to the wind's diurnal variability observed during the summer of 2006 (Chapter 1). Analysis of the clock-hour average-day of the observed circulation and wind stress, have shown that the surface circulation was offshore during minimum wind stress hours (morning), rotated onshore a few hours after minimum wind stress (mid-day) and reversed back offshore when the wind stress increased in magnitude (Figure 1.10). To check if the idealized experiments with daily varying wind forcing reproduced the observed diurnal variability of the circulation, the vertical velocity profiles at a grid point consistent with the ADCP site (magenta star in Figure 4.2) are discussed. Results are shown in Figures 4.4 through 4.6. Despite the highly idealized nature of the modelling configuration and forcing, the observed circulation pattern is well reproduced in all daily varying wind experiments. There is a diurnal variability with a flow reversal between t_{min} and t_{1mm} that is accentuated in the experiments with τ_s^x different from zero, similar to the observations presented in Chapter 1. The cross-shelf circulation shows a consistent 2-layer structure throughout the day. For most part of the day, there is offshore flow at the surface layer and onshore flow near the bottom, except between t_{min} and t_{1mm} when the circulation is reversed and there is onshore flow at the surface and offshore flow below. The results also show that overall

the cross-shelf circulation is similar between different topography experiments, implying that the flow adjustment to the bottom topography does not contribute significantly to the circulation variability, at least in this location.
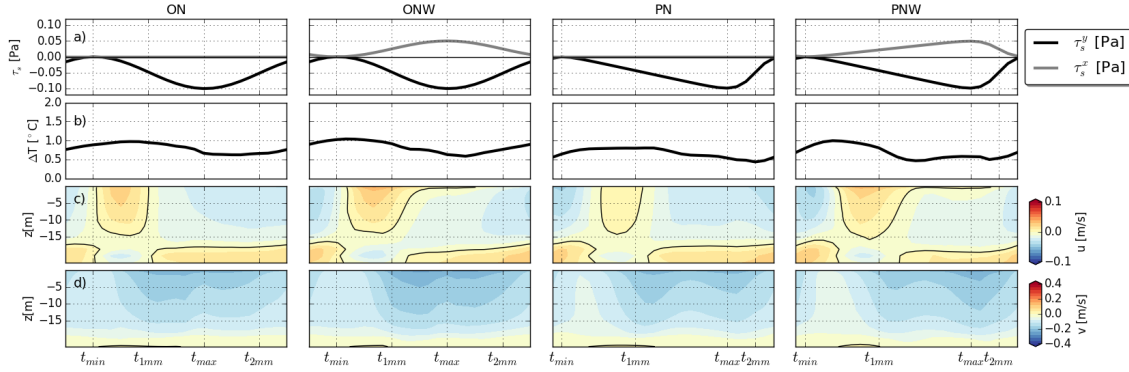
FIGURE 4.4: Modelled clock-hour average day, for the **SLOPE** experiment, of: a) Wind stresses $[Pa]$; b) Temperature difference between surface and bottom [°C]. c) cross-shelf velocity profiles [m.s^{-1}]; and d) along-shelf velocity profiles [m.s^{-1}]; at the grid point corresponding to the ADCP site (magenta star in Figure 4.2).
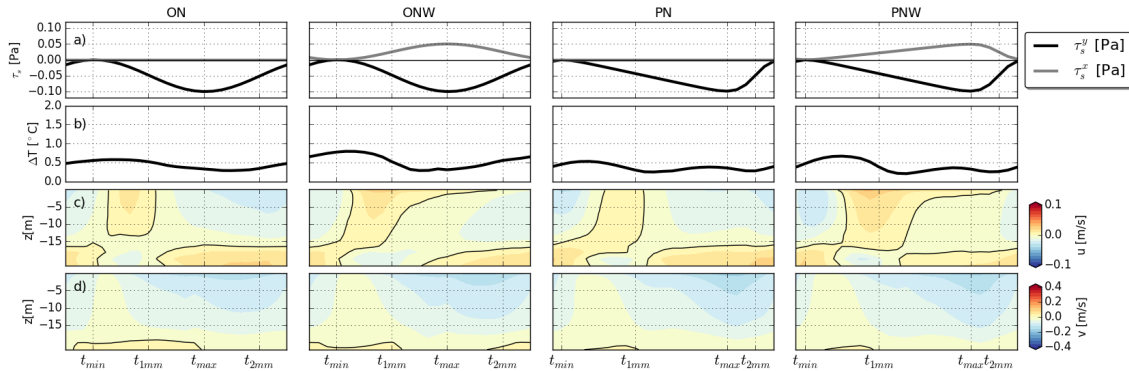
FIGURE 4.5: Same as Figure 4.4 for the **TOPO** experiment.

As in previous chapters, depth-integrated meridional momentum balances were computed to analyse the forcing mechanisms behind the flow reversal after t_{min}, directly comparable through the Coriolis term $f\mathbf{u}$. The depth-integrated along-shelf momentum balance terms for the clock-hour average day, at the grid point corresponding to the ADCP site (magenta star in Figure 4.2), were computed using the method described in Chapter 3, and the results are shown in Figure 4.7. As in the observations and the realistic modelling experiment, the momentum balance is not a straightforward two- or three-term balance that can easily connect
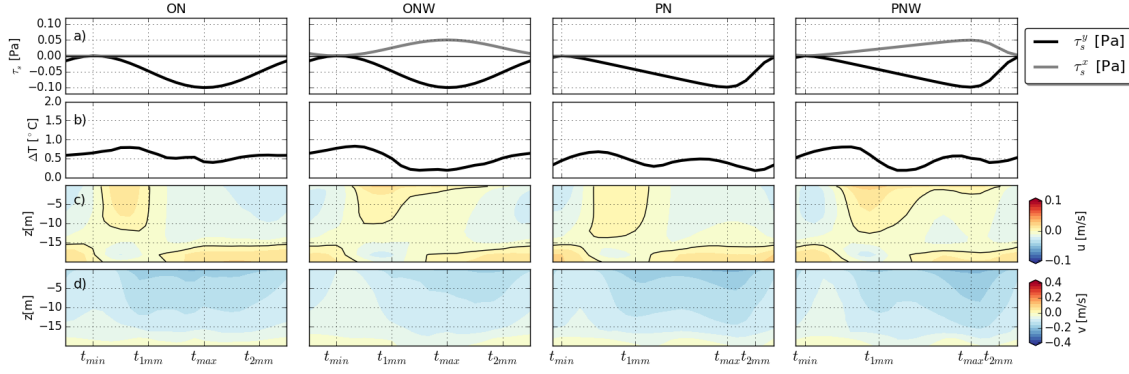
FIGURE 4.6: Same as Figure 4.6 for the **ATOPO** experiment.

forcing *vs* response, as all terms show significant relative importance that vary throughout the day. Wind stress term is dominant at t_{max} and is balanced by a combination of advection, acceleration and bottom stress in **ATOPO** and **SLOPE** and with a stronger contribution of the pressure gradient term in **TOPO** experiments. In fact, despite of what should be expected (Gan and Allen, 2002), except for the **TOPO** experiments, the pressure gradient term does not contribute significantly to the balance. The Coriolis term is the smallest term in all experiments, due to the cross-shelf flow being bidirectional in depth, which results in near zero depth-integrated velocities. During the time of the onshore flow at the surface, between t_{min} and t_{1mm}, there is a peak of the advection and acceleration terms, more accentuated in **ATOPO** and **SLOPE**. The term that shows more differences between all experiments is the bottom stress, showing the high sensitivity of the vertical mixing to topography and wind variability. The two-layer nature of the cross-shore flow enables the direct comparison between forcing *vs* response using the depth-integrated momentum balance terms, since **u** is close to zero. For that reason, further analysis will be focused on the surface layer, in order to study the underlying dynamics of the flow reversal that occurs after the wind stress is minimum.

4.3.2   Circulation in the Vicinity of the Cape

Results of the sea surface elevation, temperature and current velocity fields (first σ-level) for the daily varying wind conditions for the different hours of the clock-hour average day (t_{min}, t_{1mm}, t_{max}, t_{2mm}) can be seen in Figures 4.8 through 4.11.
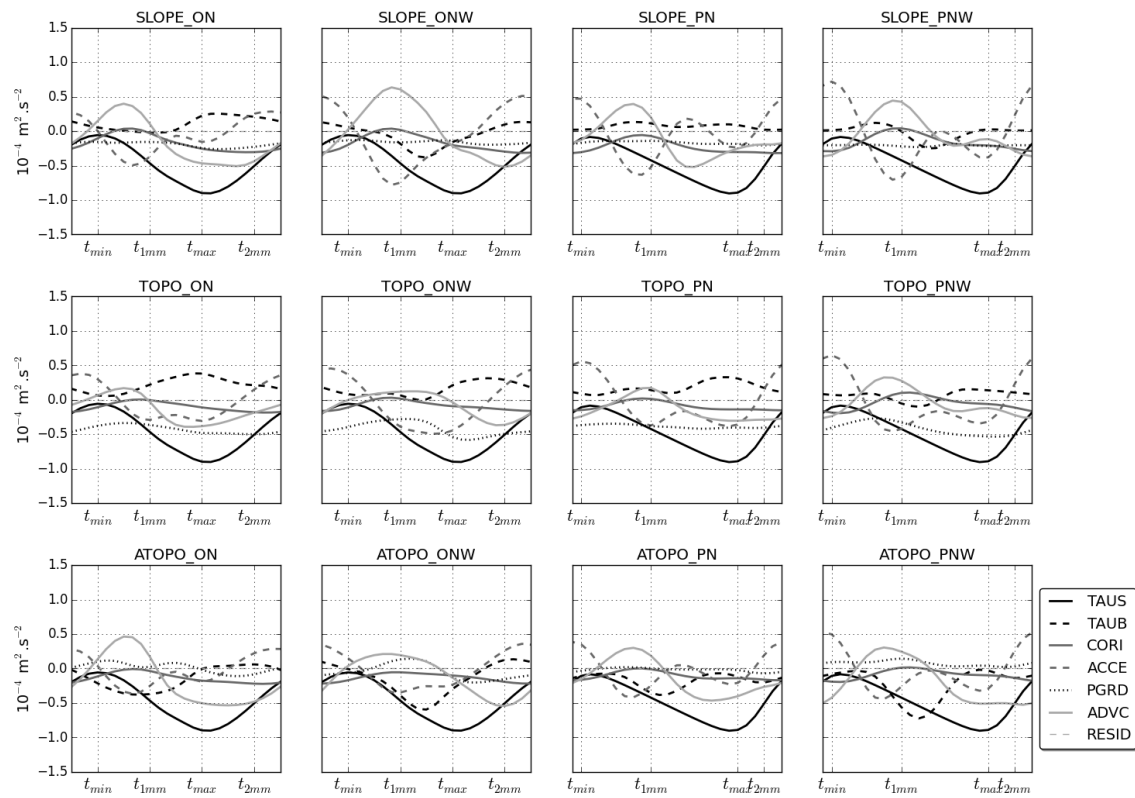
FIGURE 4.7: Depth-integrated along-shelf momentum balance terms for the modelled clock-hour average day at the grid point corresponding to the ADCP site.

The overall differences between experiments are small. In all wind conditions and away from the cape, the results are consistent with coastal upwelling systems, with an offshore flow at the surface that promotes the colder water from the bottom to be advected onshore, resulting in a decrease of sea surface temperature close to the coast. For all experiments the flow is consistently southwards and strongly polarized in the along-shelf direction. There is a strong coastal jet that is forced to accelerate and deviate offshore once it encounters the cape. This flow then recirculates cyclonically towards the coast and becomes aligned with the bathymetry after 20 to 30 km from the tip the cape. In the leeside of the cape, lower sea surface elevation and temperature indicate the intensification of the upwelling in this region. The diurnal variability of the wind, however, limits the upwelling intensity in the leeside of the cape, since the wind decreases in magnitude diurnally resulting in a relaxation of the circulation response and the upwelling not being continuously forced, as in the steady wind experiments. Colder water is advected to the south in two major veins, one following the tip of the cape, and one closer to the coast, indicating the presence of two major flows, with weaker surface velocities between them.

In the leeside of the cape, the westerly wind component weakens the upwelling intensity by decreasing the westwards component of the flow. This results in stronger upwelling for the **ON** and **PN** experiments, with consequently a stronger southwards advection of colder waters in the south part of the cape. The circulation and the magnitude of the upwelling (analysed as the offshore advection of colder waters) is more intense at t_{max} for the **PN** and **PNW** experiments, but for the **ON** and **ONW**, the upwelling is more intense at t_{2mm}, 6 hours after the maximum wind stress, which implies that the circulation does not respond so rapidly as the wind stress decreases more slowly than in the **PN** and **PNW** experiments. Differences between **TOPO** and **ATOPO** are more visible in the leeside of the cape, suggesting that the magnitude of the jet deflection is influenced by the topography in the north part of the cape (which is similar for all experiments), while the cyclonic flow rotation after the cape is mainly modified by the bottom topography in the leeside of the cape, which is significantly different between these experiments. The nearshore southwards advection of cold waters is higher for the **SLOPE** experiments, whereas the advection vein at the tip of the cape is stronger in the **TOPO** and **ATOPO** (experiments with meridional variations of the bottom topography).
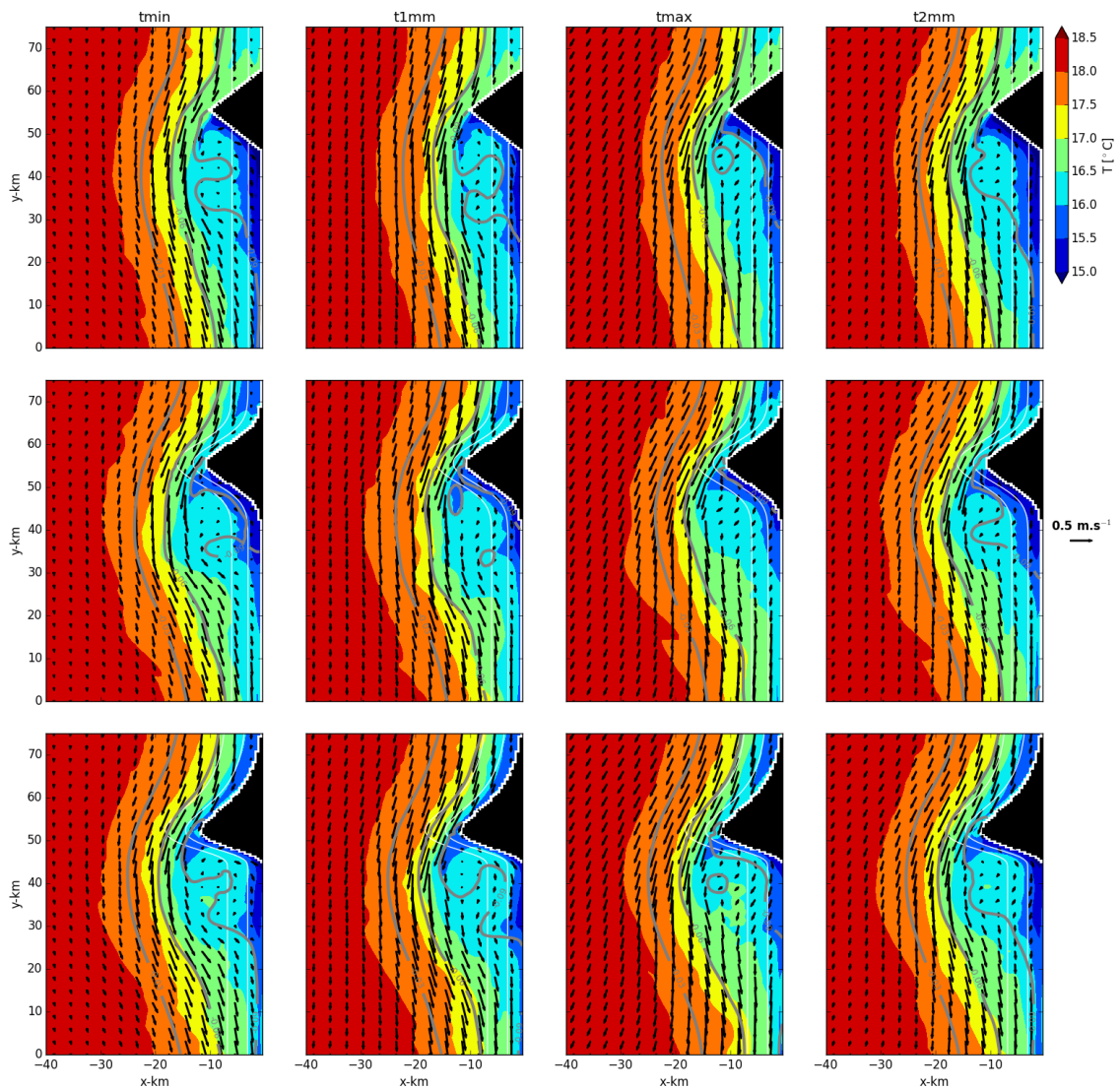
FIGURE 4.8: Sea surface temperature [°C] with sea surface elevation as gray contours (-0.09 m, -0.05 m and -0.01 m) and surface current vectors superimposed [m.s^{-1}], for the **ON** experiments at t_{min}, t_{1mm}, t_{max} and t_{2mm}. Top row: **SLOPE**; Middle row: **TOPO**; Bottom row: **ATOPO**.
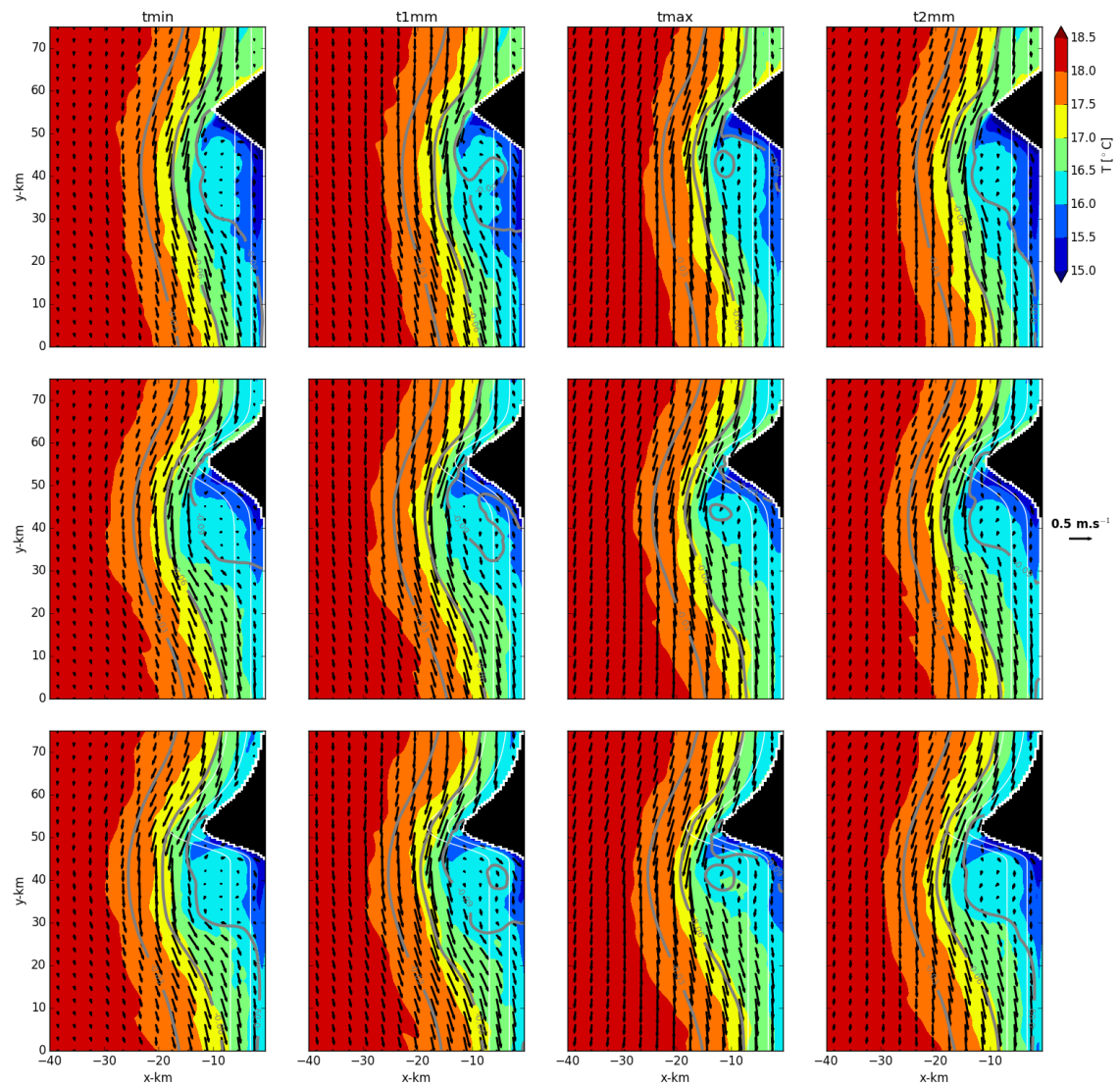
FIGURE 4.9: Same as Figure 4.8 for the **ONW** experiment.
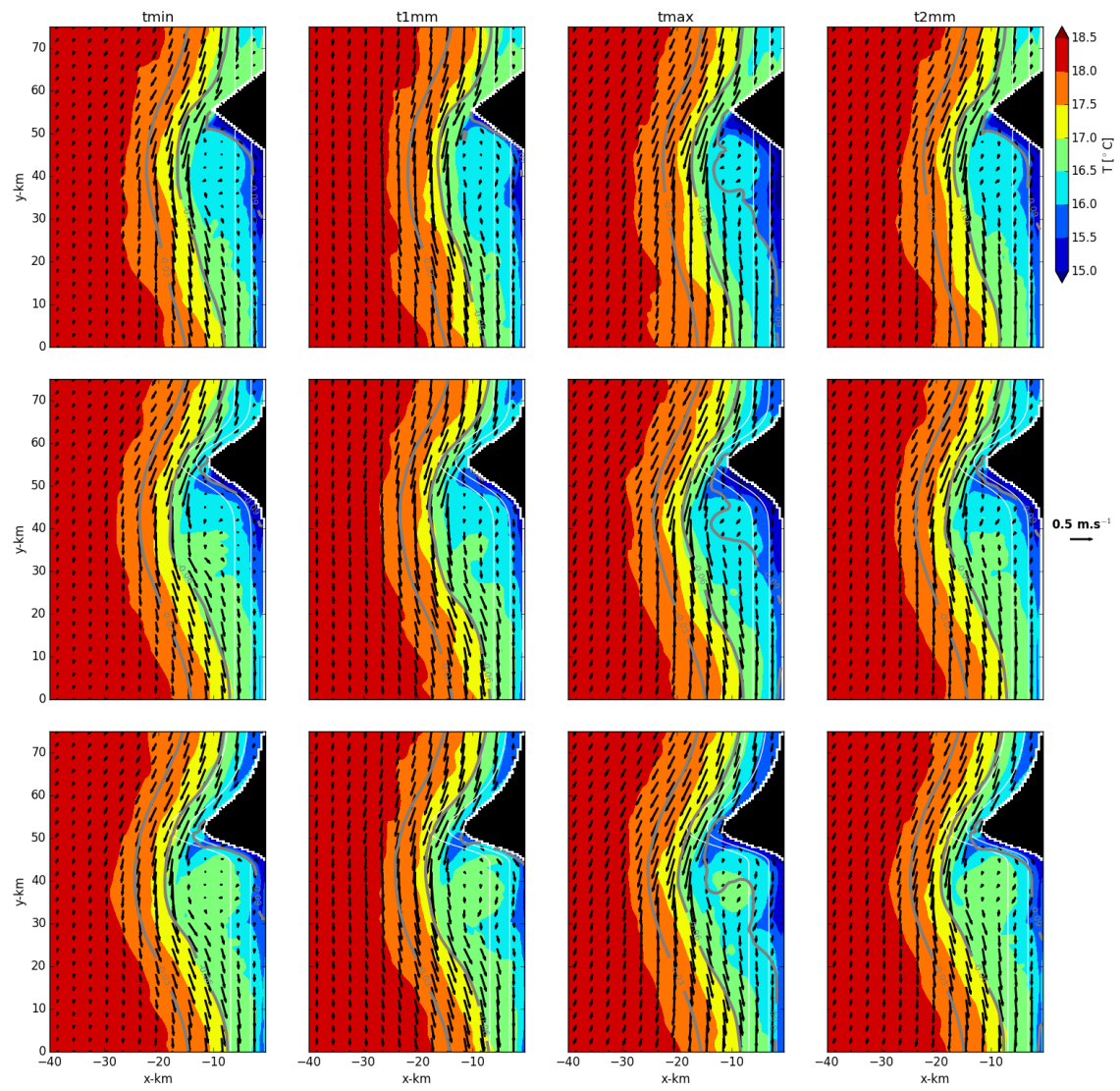
FIGURE 4.10: Same as Figure 4.8 for the **PN** experiment.
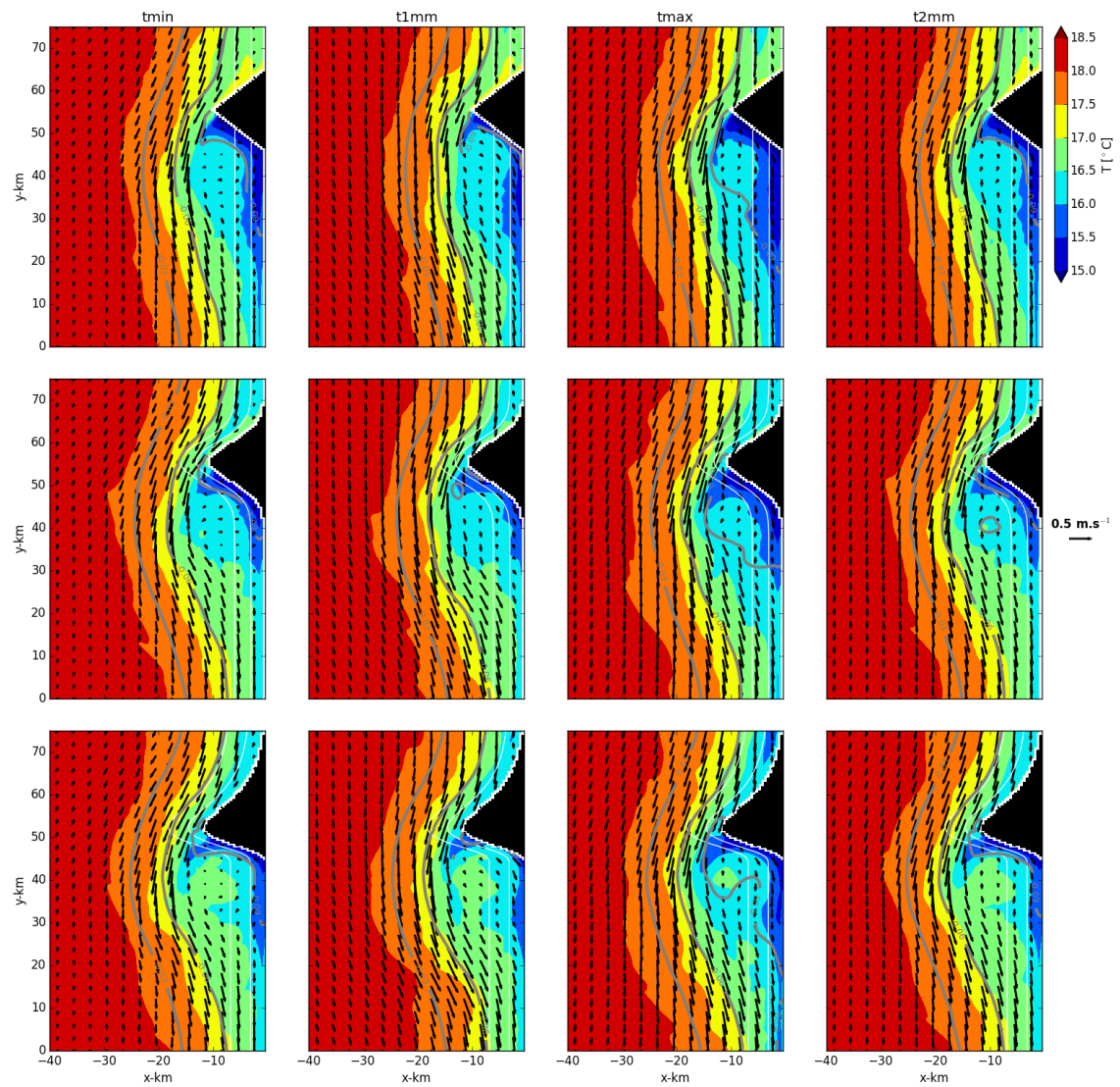
FIGURE 4.11: Same as Figure 4.8 for the **PNW** experiment.

4.3.3 Surface Transport Across the Shelf

The mixed layer depth, computed with the same criterion as in Chapter 3 (Figure 4.12) shows that a good approximation for the depth of the surface layer is 15 m, for most part of the domain between the 20- and 50-m isobath. This is consistent with the Ekman layer scale $D_{Ek} = \left(\frac{2A_v}{f}\right)^{1/2}$ estimated with A_v ranging from 5×10^{-3} to 2×10^{-2} m^2.s^{-1}.

It is clear by looking at Figures 4.13 through 4.15 that there are two main regions regarding the direction of the integrated zonal flow (**u**) in the surface layer (15 m). Overall, **u** is negative (offshore) in the northside of the cape and positive (onshore) in the leeside of the cape. These patch of negative zonal flow in the northside of the cape peaks at t_{max}, while the onshore flow is stronger after the wind relaxation, at t_{1mm}. Generally, the flow structure and magnitude does not vary considerably with different topographies or wind forcing. However, there are some small scale spatial variability between experiments, indicating that the topography and wind can have a significant impact in the cross-shelf exchange in particular locations, especially in shallow waters.

Although onshore (positive) **u** is common in the south side of the cape, due to the flow adjustment to the topography, the circulation is still strongly polarized along-shelf. In the area just south of the cape, however, the magnitude of **u** and **v** is similar, and the cross-shelf exchange may be dominant. Although this part of the domain is rather small, it is coincident with the location where the flow reversal was observed and so, henceforth, the analysis will be centred on this region. To investigate the conditions that will promote superficial transport towards the coast, analysis will be based on the flow between the mid-shelf (50-m isobath) and the 20-m isobath, which is inshore of the coastal upwelling jet, and can be considered as the inner-shelf where, as defined by Lentz (2001), where the surface and bottom boundary layers interact, velocities are small and there is a tendency for the cross-shelf transport to be suppressed.

The daily variability of the transport U at the south of the cape is analysed by computing the volume transport for the top 15 m, at the 50-m and 20-m isobath, for a section 20 km wide in the south part of the cape (black thick lines marked in Figure 4.2). These sections were chosen to represent the transition from the mid-shelf (at 50-m) to the inner-shelf (at 20-m), in the leeside of the cape after the
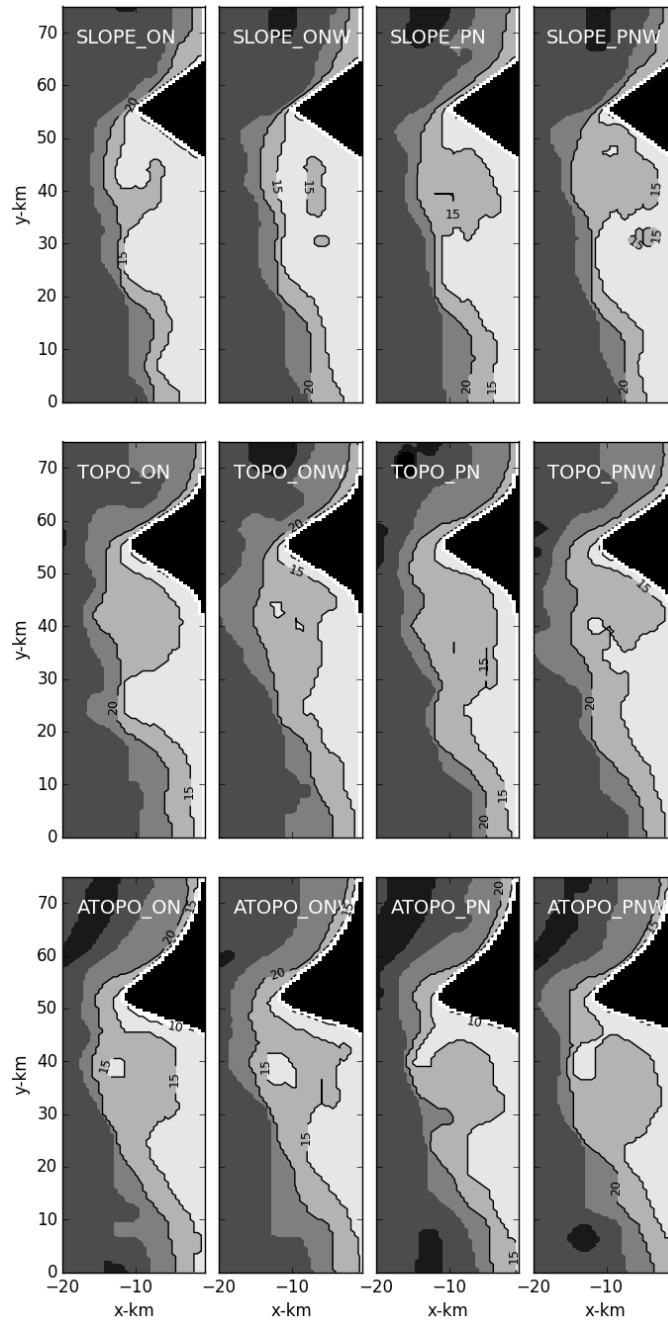
FIGURE 4.12: Mixed Layer Depth at t_{max}, for all experiments. Units
are m.
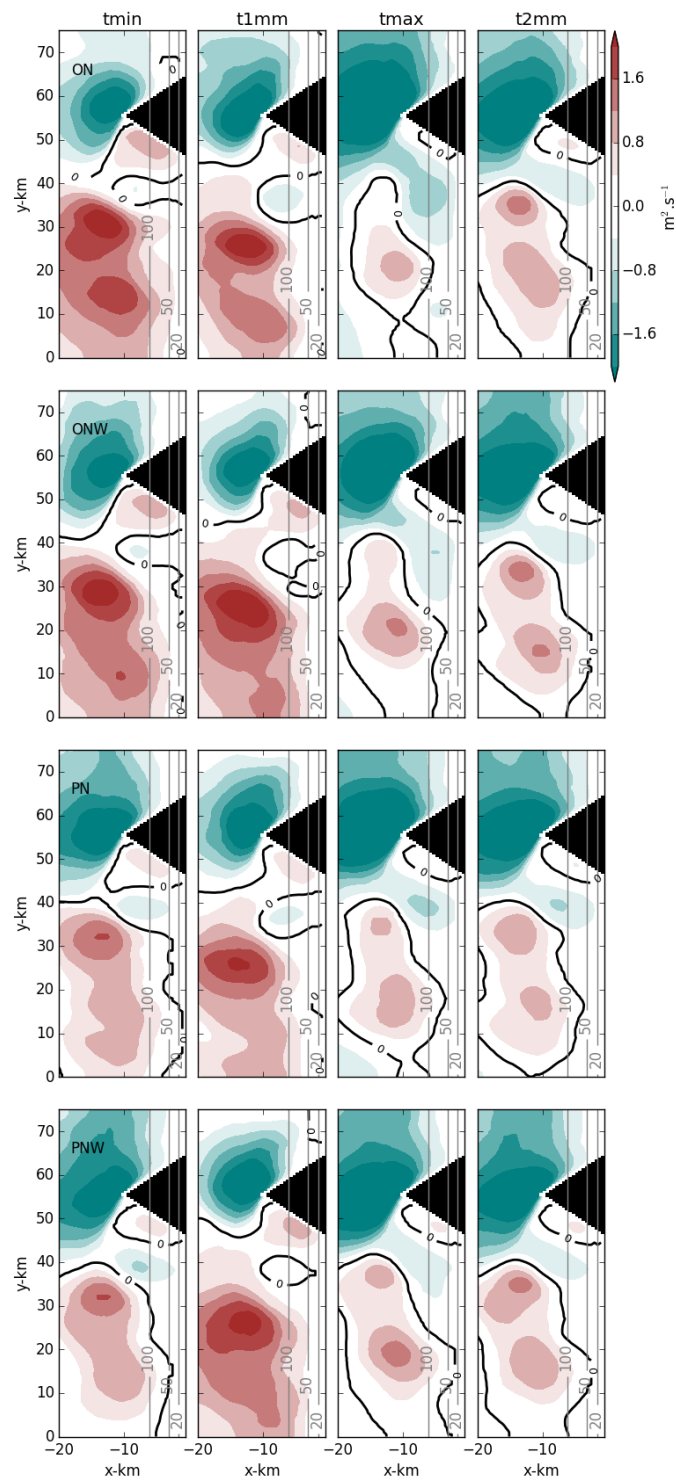
FIGURE 4.13: Depth-integrated zonal velocity (**u**) in the surface layer (first 15 m) for different hours of the daily varying wind experiments, for the **SLOPE** topography. Units are $m^2.s^{-1}$.
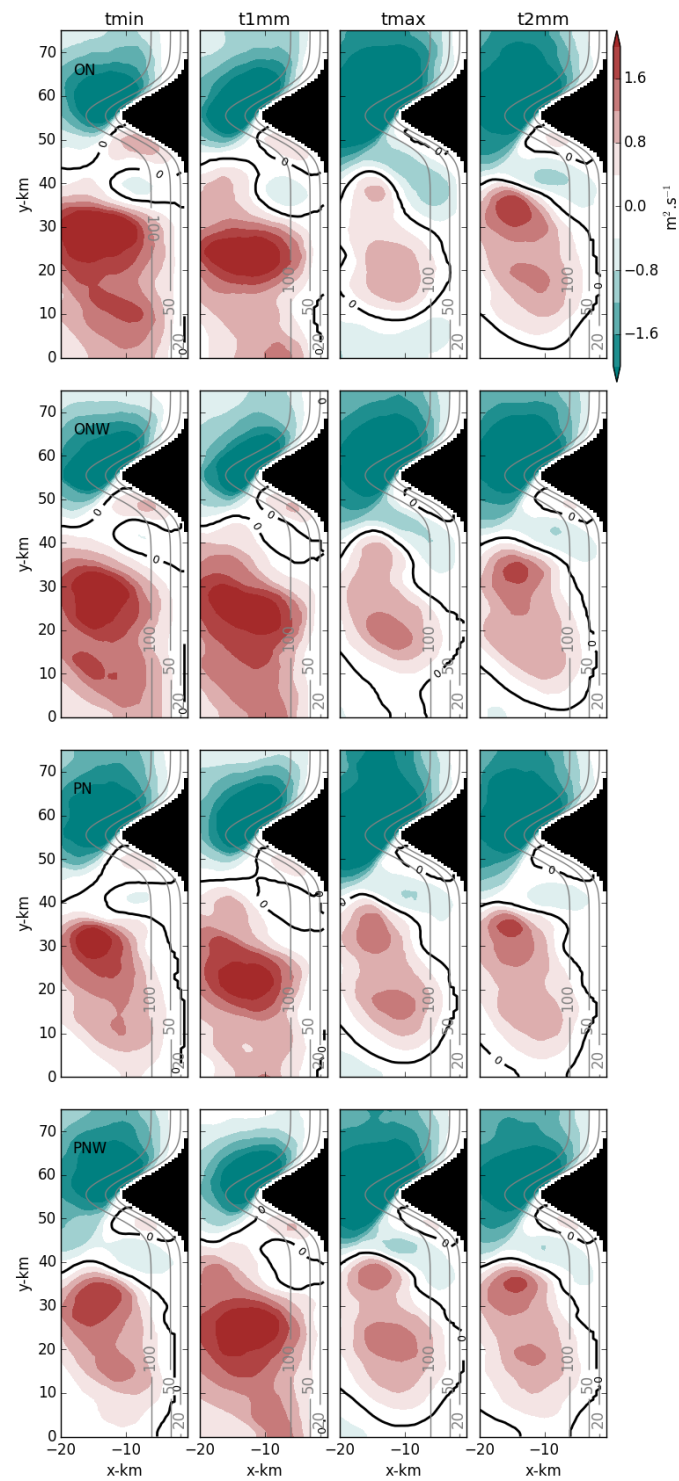
FIGURE 4.14: Same as Figure 4.13 for the **TOPO** topography.
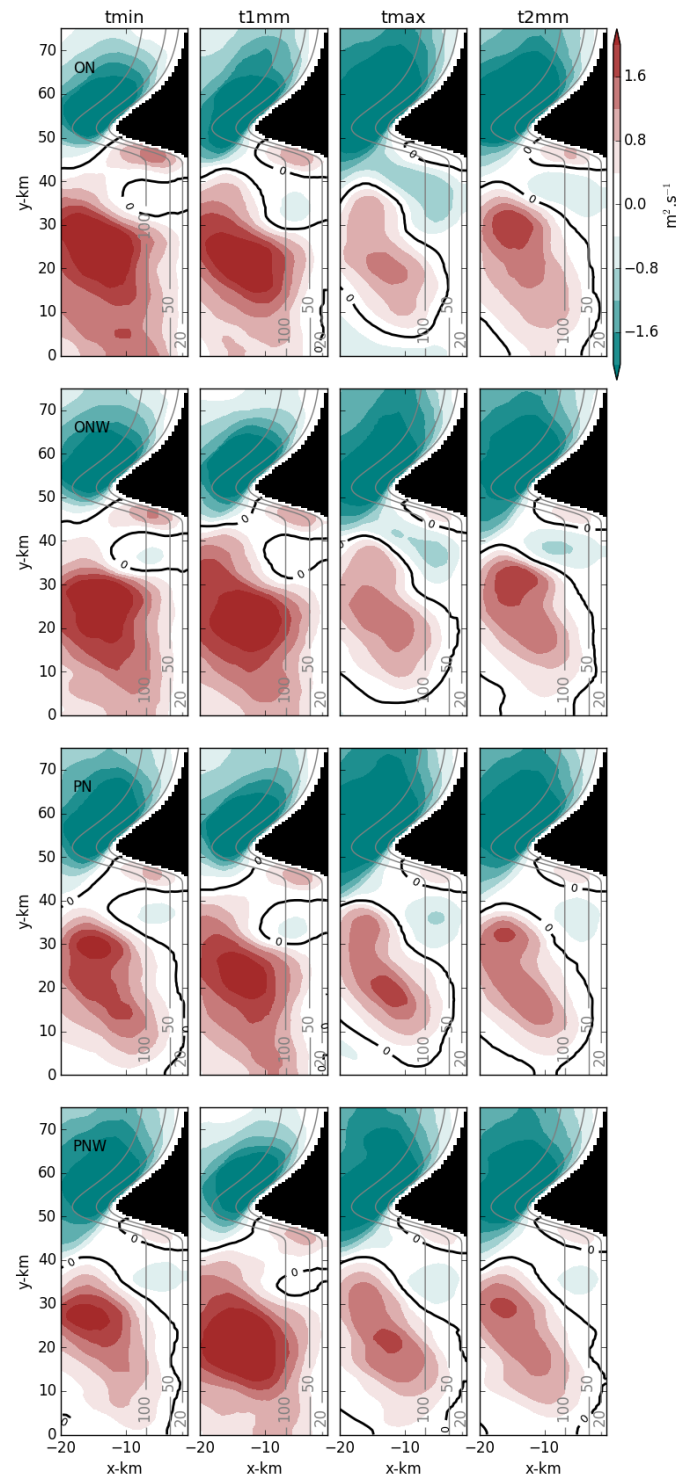
FIGURE 4.15: Same as Figure 4.13 for the **ATOPO** topography.

coast becomes meridionally aligned (consistent with the ADCP site). For reference, we also computed the steady Ekman transport in the zonal direction, which is estimated as $U_{Ek} = \frac{\tau_s^y(t_{max})}{\rho_0 f}$; where $\rho_0 = 1025$ kg.m^{-3} is the reference density and $\tau_s^y(t_{max})$ is the maximum wind stress. The clock-hour average day of the cross-shelf volume transport for the 50-m (U_{50}) and 20-m (U_{20}) isobath, is shown in Figure 4.16.

The theoretical Ekman transport, U_{Ek}, with $\tau_s^y(t_{max})$ = -0.1 Pa, integrated over a section 20 km wide is equal to -1.9×10^4 m^3.s^{-1} and as expected is directed west-wards (offshore). The modelled cross-shelf transport for all experiments and in both sections is weaker than the theoretical Ekman transport, although, U_{50} tends to U_{Ek} between t_{1mm} and t_{max}, especially for **ON** and **PN** experiments. At the 20-m section, it is clear that the cross-shelf transport is significantly suppressed, with all experiments showing U_{20} weaker than U_{Ek} and U_{50}. Onshore transport (positive U) is seemingly connected with the relaxation of the wind stress, as maximum values are found between t_{min} and t_{1mm}, concurrent with the time when wind stress is minimum. For the **SLOPE** experiment, the onshore transport is stronger for **ON** and **PN** forcing, as opposed to **TOPO** and **ATOPO** experiments, that show higher values of positive U for **ONW** and **PNW**. After t_{1mm}, transport is mostly offshore (negative U) and similar in magnitude between all experiments, with smaller magnitude with **ONW** and **PNW** forcing. For both sites and all topographies, there is a short time lag between maximum onshore transport between **N** and **NW** experiments, with the maximum onshore transport for the **NW** runs being shifted a few hours later.

4.3.4 Dynamics

Figures 4.17 and 4.18 represent the depth-integrated meridional momentum balance terms at the surface layer (first 15 m), for the 50-m and 20-m isobath sections, respectively, integrated over the same 20-km section described before, at four different hours of the clock-hour average-day. Since all terms of the balance are significant at some time during the day, it is extremely difficult to establish a simple forcing vs response relationship. However, each term's relative weight changes throughout the day, and therefore some points can be discussed. At the mid-shelf section (Figure 4.17), the advection term is relatively small and does
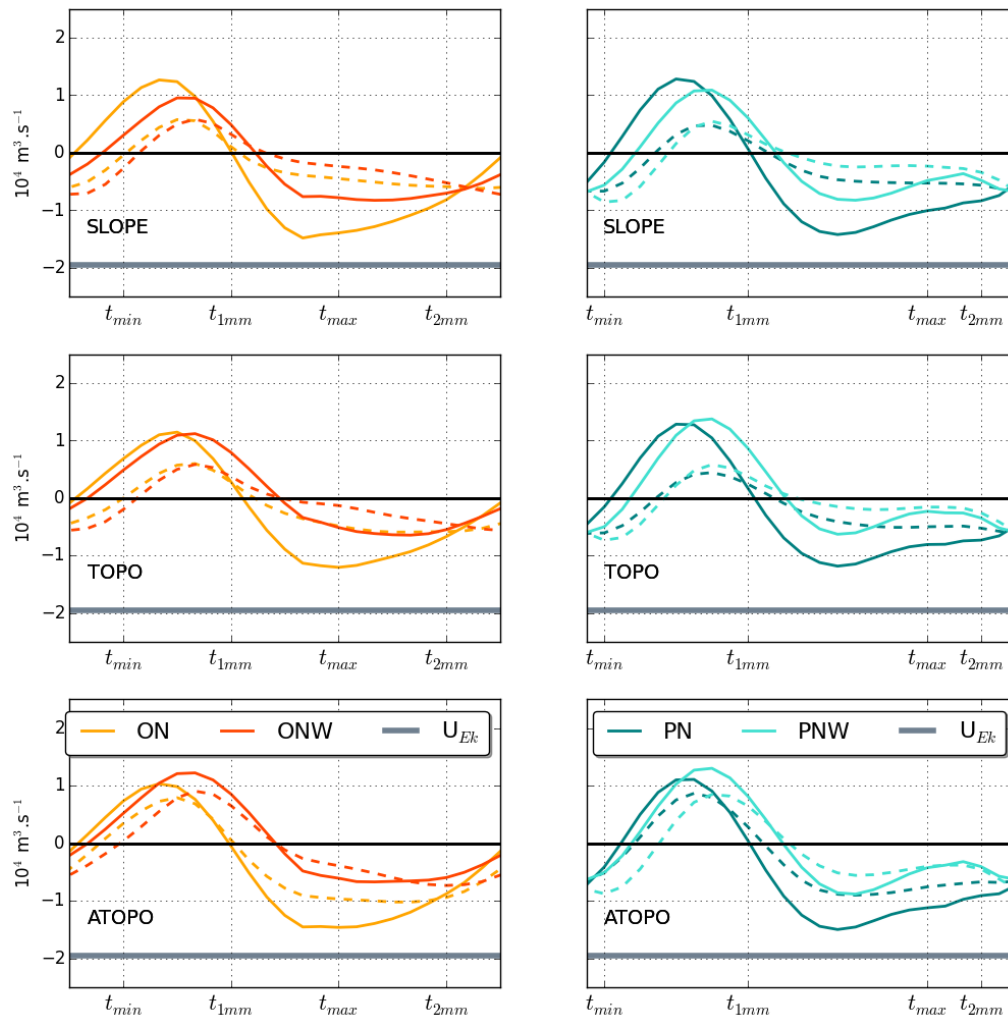
FIGURE 4.16: Clock-hour average day of the cross-shelf volume transport in the surface layer (first 15 m) for a section between 20 and 40 y-km (south of the cape) over the 50-m isobath (thick lines) and the 20-m isobath (dashed lines), for the daily varying wind experiments. The thick gray line represents the theoretical Ekman Transport U_{Ek} integrated over 20 km (the width of each section). Units are $m^3.s^{-1}$.

not contribute significantly to the balance. During the hours where wind stress is minimum, the balance is mostly between Coriolis and local acceleration terms, suggesting that inertia dominates the dynamics and that the onshore flow is most likely forced by the abrupt variation of the acceleration after the wind stops (at t_{min}). After t_{1mm}, the acceleration term is negligible and the Coriolis term is balanced by the vertical mixing term, consistent with an Ekman balance. The pressure gradient term is consistent in magnitude in all experiments and between mid- and inner-shelf, which implies that the setting up of a negative pressure gradient in the south side of the cape is a robust feature that does not change with the different topographies considered here or with the addition of a westerly component of the wind. Throughout the day the pressure gradient term is significant in magnitude but remains constant, implying that it is not a strong contributor to the diurnal variability of the circulation. Overall, the described diurnal variability of the momentum balance is consistent for all experiments, indicating that topography and different wind patterns only account for small variations of the momentum balance terms. There is, however, a small difference in the acceleration term between **ON**/**ONW** and **PN**/**PNW** runs, with the experiments forced by the oscillatory wind step showing two local minima, one at t_{1mm} and another at t_{max}, which contributes to a slight similar variability in the Coriolis term as well, especially in the **PNW** runs.

At the 20-m section, the dynamics are slightly more complex (Figure 4.18), with the advection term gaining relative importance, especially at mid-day. Although acceleration and vertical mixing terms are of the same order as in the deeper section, the Coriolis term is overall considerably smaller, probably linked with the increase of the advection term at this site. Stronger negative acceleration continues to be connected with the positive Coriolis term at t_{min}, but the advection term follows closely the Coriolis term, contributing to the decrease of onshore transport at 20 m, since pressure gradient is mostly constant throughout the day and similar in magnitude between both mid- and inner-shelf sections. There are stronger differences between experiments in the inner-shelf balance's terms, especially for the acceleration term, suggesting that the circulation response is strongly influenced by topography and wind forcing over shallower waters.
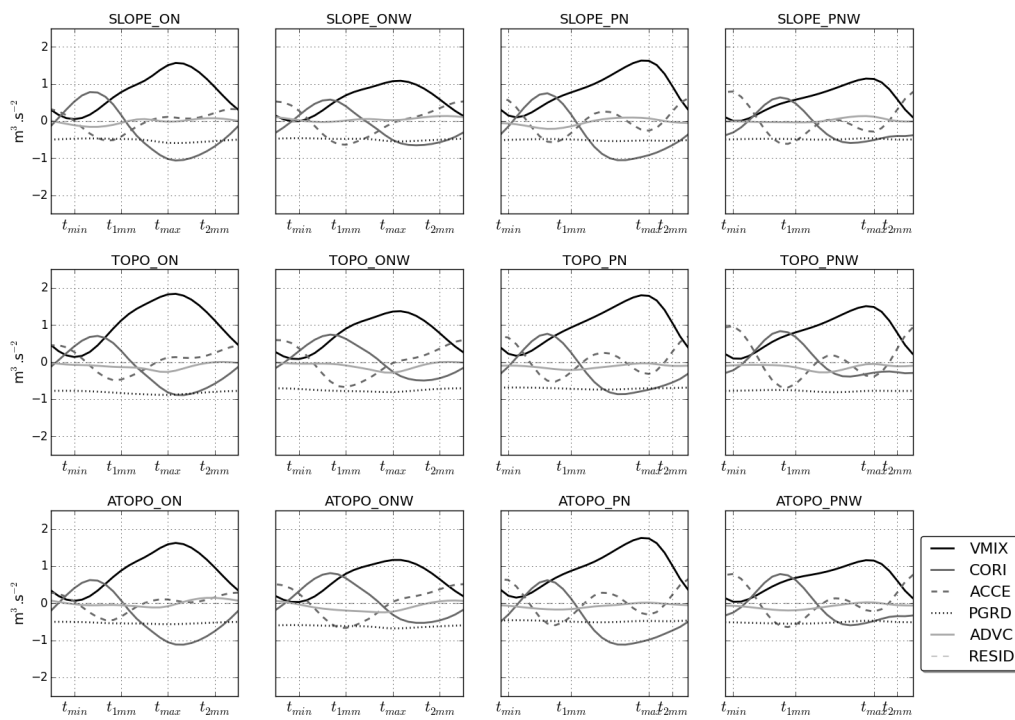
FIGURE 4.17: Depth-integrated along-shelf momentum balance terms [$m^3.s^{-2}$] in the surface layer (first 15m) for a section between 20 and 40 y-km, at the 50-m isobath, for the daily varying wind experiments.
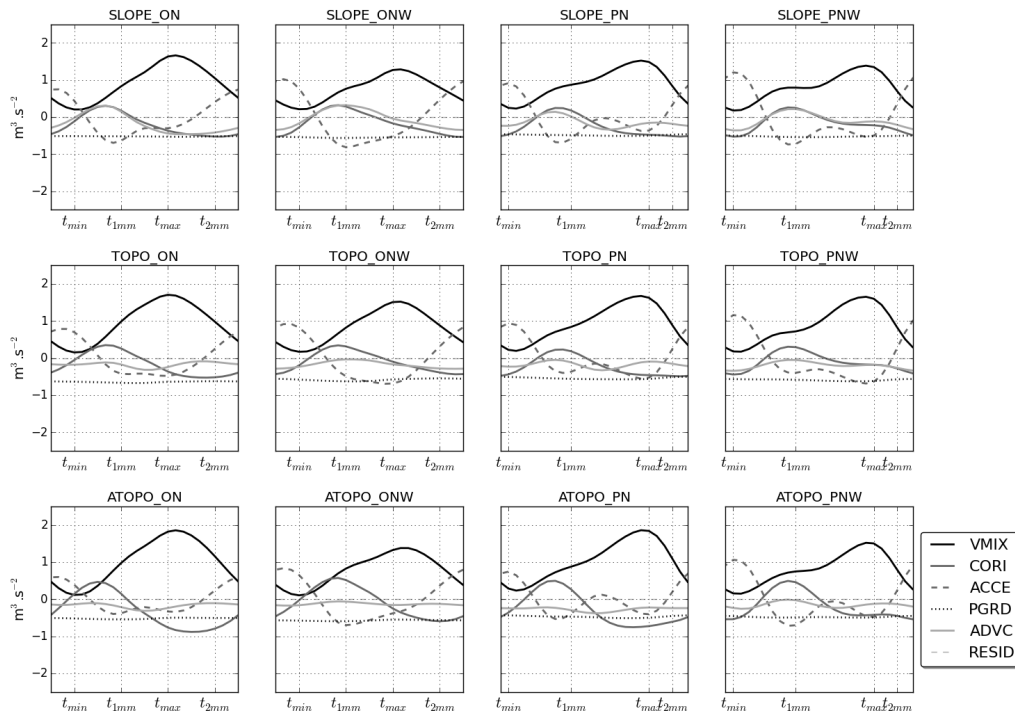
FIGURE 4.18: Same as Figure 4.17 at the 20-m isobath.

4.3.5 Steady Wind Forcing

Steady wind forcing experiments were included in this study to understand the topographic effects on a mature upwelling circulation. In steady wind forcing conditions, the circulation near the cape is similar to the daily varying wind experiments described before, but without the diurnal relaxation of the wind, the upwelling in **SN** and **SNW** experiments is substantially more intense (Figure 4.19).

However, the average cross-shelf volume transport at the mid- and inner-shelf sections is much weaker than the daily varying wind experiments (Figure 4.16) and the Ekman Transport (-1.9×10^4 m^3.s^{-1}) and varies considerably between different topographies and wind forcing (Table 4.2). At the mid-shelf section, U_{50} is onshore with the **SNW** wind forcing, showing higher values and close in magnitude in the **TOPO** and **ATOPO** results. Without the westerly wind component, U_{50} is offshore for all topographies, stronger in the **ATOPO** and near zero in the **TOPO** experiment. As in the daily varying wind experiments, the transport towards the coast is suppressed at the inner-shelf section. With the exception of **ATOPO_SNW**, U_{20} is offshore and stronger with the **SN** forcing.
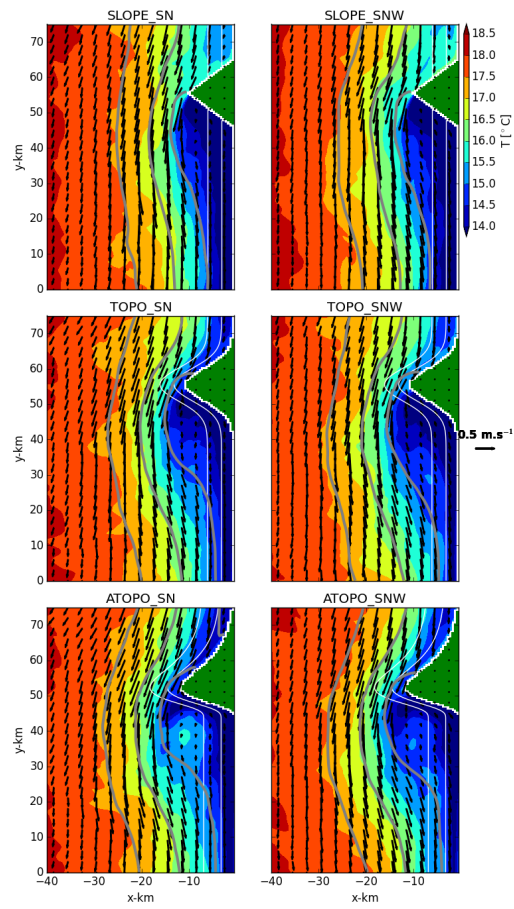
FIGURE 4.19: Sea Surface Temperature [°C] with sea surface height contours and surface current vectors superimposed [m.s^{-1}], for steady wind experiments, averaged for the last 10 days of the simulation.

The average values of the along-shelf momentum balance presented in tables 4.3 and 4.4, show that, even under steady wind conditions, the dynamics are complex at both sections, with multiple terms being comparable in magnitude. The vertical mixing is the highest term in the balance at both sections, the pressure gradient is also relatively high but only accounts for half of the vertical mixing term. The other contributor is the advection term, which is higher at the mid-shelf section, most likely connected with the deflection of the primary upwelling jet. Contrary to the daily varying wind experiments, the acceleration term is the smallest term of the balance for the steady wind experiments.

TABLE 4.2: Daily cross-shelf volume transport [10^4 m^3.s^{-1}] in the surface layer (first 15 m) for a section between 20 and 40 y-km (south of the cape) over the 50-m isobath (U_{50}) and the 20-m isobath (U_{20}), for the steady wind experiments, averaged for the last 10 days of the simulation.

		U_{50}	U_{20}
SLOPE	SN	-0.11	-0.32
	SNW	0.32	-0.16
TOPO	SN	-0.01	-0.28
	SNW	0.59	-0.07
ATOPO	SN	-0.20	-0.34
	SNW	0.56	0.08

TABLE 4.3: Depth-integrated along-shelf momentum balance terms [m^3.s^{-2}] in the surface layer (first 15m) for a section between 20 and 40 y-km, over the 50-m isobath, for the steady wind experiments, averaged for the last 10 days of the simulation.

		ACCE	ADVC	CORI	PGRD	VMIX
SLOPE	SN	0.02	**-0.83**	-0.11	-0.69	**1.61**
	SNW	-0.05	**-0.77**	0.32	-0.62	**1.12**
TOPO	SN	0.06	**-1.09**	-0.01	-0.94	**1.98**
	SNW	0.05	**-1.12**	0.59	-0.99	**1.47**
ATOPO	SN	0.04	**-0.96**	-0.20	-0.81	**1.93**
	SNW	0.05	-0.99	0.56	**-1.01**	**1.39**

TABLE 4.4: Depth-integrated along-shelf momentum balance terms $[m^3.s^{-2}]$ in the surface layer (first 15m) for a section between 20 and 40 y-km, over the 20-m isobath, for the steady wind experiments, averaged for the last 10 days of the simulation.

		ACCE	ADVC	CORI	PGRD	VMIX
SLOPE	**SN**	0.01	**-0.55**	-0.32	-0.38	**1.24**
	SNW	0.01	-0.22	-0.16	**-0.35**	**0.72**
TOPO	**SN**	0.02	-0.29	-0.28	**-0.49**	**1.04**
	SNW	0.02	-0.05	-0.07	**-0.49**	**0.59**
ATOPO	**SN**	0.03	**-0.64**	-0.34	-0.46	**1.41**
	SNW	0.04	-0.44	0.08	**-0.59**	**0.91**

4.4 Summary and Discussion

A process-oriented modelling study was conducted to clarify the complex dynamics involving flow-topography interactions in a daily varying wind regime over a shelf near a cape. In spite of the highly idealized nature of the wind forcing and bottom topographies, all results compared well to observational studies around capes (Gan and Allen, 2002; Barth et al., 2000; Trindade et al., 2016; Lamas et al., 2017). Surface velocity fields, temperature and sea surface elevation show that the upwelling is enhanced in the leeside of the cape, in the same way as described by Gan and Allen (2002) and Kuebel Cervantes and Allen (2006). As shown by Castelao and Barth (2006), magnitude and spatial variability of the circulation do not seem directly connected with the different wind conditions considered here, but rather depends primarily on the topography, with the upstream part of the cape being responsible for the deflection of the upwelling jet, and the downstream geometry affecting the jet recirculation back to the shore. The modelling results also compare considerably well with the observations in the vicinity of Cape Sines (Chapter 1), thus indicating that this model configuration is adequate to study the processes described before, in particular the diurnal variability of the circulation at the leeside of the cape.

It was shown that the wind forcing variability plays an important role in the cross-shelf surface circulation, since the offshore-onshore-offshore average day cycle at a location consistent with the ADCP site is only successfully simulated in the experiments with a daily variable wind forcing. The bottom topography, however, did not have much influence on the circulation at this location, as experiments with

different bottom topography but with same wind forcing showed similar results.

The zonal velocity integrated over the surface layer showed that the surface flow reversal is a feature that only occurs in the leeside of the cape. The flow reversal between t_{min} and t_{1mm} appeared in all daily varying wind conditions, indicating that it is not dependent on the addition of a westerly wind component. However, as seen in Figures 4.4 through 4.6, there is a surface onshore flow that lasts until t_{max} for the simulations with a westerly wind component, suggesting that, after t_{1mm}, the superficial circulation responds directly to the wind, with northwesterly winds forcing southeastwards currents.

Analysis of the volume cross-shelf transport at two sections, one over the mid-shelf and other over the inner-shelf, in the leeside of the cape, showed that onshore transport is strongly promoted in the daily varying wind experiments between t_{min} and t_{1mm}, even at 20 m depth. However, contrary to what was expected, adding a westerly wind component did not increase the magnitude of the onshore transport in the leeside of the cape, though it decreased the offshore transport at t_{max}. There is a time lag between the peaks of the onshore transport between the **N** and **NW** runs, which might be explained by the existence of onshore surface velocities until t_{tmax} in the simulations with a westerly wind component. The continuously forcing of northerly or northwesterly wind, as in the steady wind experiments, strongly suppressed the onshore transport, especially at the 20-m section. This is consistent with the upwelling shut-down described by Estrade et al. (2008).

As in previous chapters, momentum balance results suggest that the flow reversal is directly connected with the local acceleration of the along-shelf velocity, which is consistent in all runs with daily varying wind forcing, contrary to the steady wind experiments, where the acceleration is near-zero and there is no flow reversal. The similarity between different topographies is indicative that the set-up of a negative pressure gradient is a robust feature within this type of environment but the variability of the cross-shelf transport is not directly related with the variability of the along-shelf pressure gradient, as this term is mostly constant throughout the day. At the end of the day, after t_{max}, the wind stress is the dominant term in the balance and the circulation is offshore due to the Coriolis effect (Ekman balance).

The results of this study are interpreted in the following way: For all experiments with different topographies and with daily variable wind, there is a region south

of the Cape where the cross-shelf circulation shows significant diurnal variability. The surface onshore transport after t_{min} results from the inertial motion of the circulation after the wind stops, which causes the current to rotate anticyclonically. As the wind increases, the ocean adjusts to the wind and the cross-shelf flow is offshore. This finding is in agreement with previous studies (Simpson et al., 2002; Sobarzo et al., 2010; Aguiar-González et al., 2011), that have observed similar diurnal variability of the circulation, and explain the daily flow reversals as a result from the inertial motions that occur as a response to a regular diurnal wind forcing in regions near the critical latitude ($30° \pm 10°$ N/S), where the inertial and daily periods are close to each other. The fact that the flow reversal is present only in the south side of the cape seems to be connected with the sheltering effect of the cape, since the circulation is much weaker. At regions with stronger velocities (over the primary jet, for example), the diurnal variability is not significant, as the circulation remains locked to the steady state.

In short, the cross-shelf variability analysed here is a very localized, but robust, feature that occurs as a direct response to an oscillating upwelling-favourable daily variable wind in the leeside of a cape. Despite the small-scale nature of this study, onshore flows as the ones described here can be particularly helpful to explain the transport and settlement of larvae in regions with similar topography and wind characteristics.

Conclusions

The main objective of this thesis was to contribute to the knowledge about the nearshore circulation in the vicinity of a cape. Focus was given to the diurnal variability of the circulation and the cross-shelf transport over the continental shelf.

In-situ data collected at the inner-shelf south of Cape Sines showed that the average day of the cross-shelf circulation consisted of three distinct periods, not commonly seen in previous inner-shelf studies. The morning period had a 3-layer structure with onshore velocities at mid-depth and offshore velocities at the surface and bottom, followed by a mid-day period where the surface flow is reversed and has a 2-layer structure with onshore velocities at the surface and offshore flow below, and, lastly, in the evening, a 2-layer flow with intensified offshore velocities at the surface and onshore flow at the bottom. Momentum balance analysis showed that the along-shelf acceleration was dominant at mid-day, which may explain the flow reversal as a frictional response to the abrupt change of wind direction. However, the residual of both balances was not zero, and it was clear that the in-situ data collected was not enough to study in detail the dynamics at this site.

A simple modelling study using the 2D model developed by Lentz et al. (2008) forced by the observed conditions, was used to understand the individual contributions of wind and wave forcing to the circulation. Although the steady model, forced exclusively with winds, reproduced satisfactorily the along-shelf circulation, the cross-shelf circulation was not successfully simulated, not only for diurnal but also for subtidal timescales. The model only reproduced the mid-day cross-shelf flow reversal when a term comparable with $\frac{\partial \mathbf{v}}{\partial t}$ was added to the forcing, further indicating that the local acceleration of the along-shelf velocity had an important role in the establishment of the mid-day cross-shelf flow inversion.

The coastal circulation around Cape Sines was investigated using the results of a realistic numerical model simulation forced exclusively with winds. The model

reproduced satisfactorily the average day circulation, except the 3-layer structure in the morning period. The results showed that the cross-shelf circulation pattern observed by the ADCP only occurred in very few regions across the domain, mostly in the south side of the cape. Momentum balance analysis confirmed that the local acceleration was an important term at mid-day, reinforcing the previous hypothesis that the cross-shelf flow reversal was connected with the local acceleration of the along-shelf circulation. It was also shown that the wind's sharp diurnal cycle with daily periods of intensification and relaxation, enhanced the cross-shelf circulation, especially at the leeside of the cape, where the along-shelf currents are weaker.

The role of different wind conditions and topographic variations was analysed using a set of idealized modelling simulations. The modelling results compared well to observational studies around capes (Gan and Allen, 2002; Barth et al., 2000; Trindade et al., 2016) and the observations at Cape Sines, presented in Chapter 1. The flow reversal observed at mid-day in the leeside of the cape was simulated successfully in all daily variable wind experiments. Results also showed that, contrary to the steady wind simulation, onshore transport is promoted in the leeside of the cape with daily variable wind conditions, but adding a westerly wind component did not increase the onshore transport. Momentum balance results suggest that the cross-shelf flow reversal results from an inertial response of the circulation after the wind stops, which occurs in the leeside of the cape due to the sheltering effect that causes the background velocity of the circulation to be much weaker. Everywhere else, the diurnal variability is not significant and the circulation remains locked to the steady state.

It was shown that the offshore-onshore-offshore daily variability of the cross-shelf circulation at the surface is a specific feature to the leeside of the cape, but is present in all simulations with an oscillating upwelling-favourable daily variable wind. Studies like this can be very helpful to understand larvae transport, distribution and recruitment in coastal regions with similar topography and wind conditions. The persistence of upwelling-favourable winds promote retention of cold and nutrient-rich waters in the leeside of capes, which is significantly relevant for phytoplankton blooms and larvae development. The fact that the wind diurnally undergoes relaxation and intensification strongly modifies the cross-shelf circulation, promoting surface onshore flows, in the leeside of the cape, that overpower

the strong along-shelf currents.

Although some questions were answered throughout this thesis, other issues remain to be explored, such as the contribution of waves and tides to the observed circulation. Larger scale processes described before (Lentz, 2008; Fewings et al., 2015; McCabe et al., 2015), can be responsible for the vertical parabolic shape observed on the cross-shelf circulation, feature that was not simulated in the modelling studies presented here. This variety of forcing elements can bring relevant modifications to the cross-shelf circulation and should be addressed in the future. Lastly, this study showed that onshore transport can be promoted in the leeside of the cape with a daily variable wind regime similar to sea breeze, however it was not investigated in detail the horizontal spatial scales and patterns of the transport. This could be of particular interest to the investigation of larvae distribution and recruitment. Future work should include Lagrangian transport experiments using passively drifting particles to distinguish transport features around this region.

Appendix A

Diurnal variability of inner-shelf circulation in the lee of a cape under upwelling conditions

This Appendix is an article published in *Continental Shelf Research*. The authors are Luisa Lamas, Álvaro Peliz, Joaquim Dias, Paulo Oliveira, João Castro, Joana Fernandes, Ana Trindade and Teresa Cruz.

Diurnal variability of inner-shelf circulation in the lee of a cape under upwelling conditions

L. Lamas[a,b,*], A. Peliz[b], J. Dias[a], P.B. Oliveira[c], M.M. Angélico[c], J.J. Castro[d], J.N. Fernandes[d], A. Trindade[e], T. Cruz[d]

[a] MARE – Marine and Environmental Sciences Centre, Faculdade de Ciências da Universidade de Lisboa, Campo Grande 1749-016, Lisboa, Portugal
[b] Instituto Dom Luiz, Faculdade de Ciências da Universidade de Lisboa, Campo Grande 1749-016, Lisboa, Portugal
[c] Instituto Português do Mar e Atmosfera, 1449-006 Lisboa, Portugal
[d] MARE – Marine and Environmental Sciences Centre, Laboratório de Ciências do Mar, Universidade de Évora, 7520-903 Sines, Portugal
[e] Institut de Ciències del Mar, Departament Oceanografia Física i Tecnològica, 37-4908003 Barcelona, Spain

ARTICLE INFO

ABSTRACT

The nearshore circulation in the lee of a cape under upwelling conditions was studied using in-situ data from 3 consecutive summers (2006–2008). Focus was given to a period between 20 July and 04 August 2006 to study the diurnal variability of the cross-shelf circulation. This period was chosen because it had a steady upwelling-favourable wind condition modulated by a diurnal cycle much similar to sea breeze.

The daily variability of the observed cross-shelf circulation consisted of three distinct periods: a morning period with a 3-layer vertical structure with onshore velocities at mid-depth, a mid-day period where the flow is reversed and has a 2-layer structure with onshore velocities at the surface and offshore flow below, and, lastly, in the evening, a 2-layer period with intensified offshore velocities at the surface and onshore flow at the bottom. The observed cross-shelf circulation showed a peculiar vertical shape and diurnal variability different from several other systems described in literature. We hypothesize that the flow reversal of the cross-shelf circulation results as a response to the rapid change of the wind magnitude and direction at mid-day with the presence of the cape north of the mooring site influencing this response.

A numerical modelling experiment exclusively forced by winds simulated successfully most of the circulation at the ADCP site, especially the mid-day reversal and the evening's upwelling-type structure. This supports the hypothesis that the cross-shelf circulation at diurnal timescales is mostly wind-driven. By analysing the 3D circulation in the vicinity of Cape Sines we came to the conclusion that the diurnal variability of the wind and the flow interaction with topography are responsible for the circulation variability at the ADCP site, though only a small region in the south of the cape showed a similar diurnal variability.

The fact that the wind diurnally undergoes relaxation and intensification strongly affects the circulation, promoting superficial onshore flows in the leeside of Cape Sines. Despite the small-scale nature of the observed cross-shelf circulation, onshore flows as the ones described in this study can be particularly helpful to understand the transport and settlement of larvae in this region and in other regions with similar topography and wind characteristics.

1. Introduction

The cross-shelf circulation over the nearshore region plays a key role on the distribution of plankton, nutrients, heat, salt and sediments, and has been the subject of many recent studies (Fewings et al., 2008; Lentz et al., 2008; Hendrickson and MacMahan, 2009; Marchesiello and Estrade, 2010; Ganju et al., 2011; Lentz and Fewings, 2012; Liu and Gan, 2014). Wind-driven upwelling and downwelling systems are particularly important because of the cross-shelf exchange that is forced in these wind conditions, which promotes transport of material across the shelf, especially over stratified shelves (Austin and Lentz, 2002). In the region onshore of the upwelling front, stratification is often weaker and the surface and bottom turbulent layers overlap, causing the reduction or shut-down of the cross-shelf transport (Estrade et al., 2008). This region is normally referred to as inner-shelf (Lentz, 2001; Austin and Lentz, 2002; Fewings et al., 2008). In

---

spite of weaker cross-shelf transport conditions, this shallow part of the shelf is an attractive habitat for many coastal species. For example, inter-tidal species, having their planktonic larval phase over the shelf, must cross the nearshore zone for settlement. Cross-shelf transport processes over the shelf are thus critical for the larvae supply to the shore, which then determines recruitment (Pineda et al., 2009). Understanding the physical processes behind the cross-shelf exchange over the inner-shelf is of particular interest for this type of studies.

The wind-driven shelf response over a straight coastline has been extensively studied. Upwelling-favourable winds drive cross-shelf exchange with an offshore flow at the surface boundary layer and a compensating onshore flow near the bottom. This occurs for depths typically greater than 50 m, when the surface and bottom boundary layers are relatively thin when compared with total water depth (a region often called mid-shelf (Lentz and Fewings, 2012)). With strongly stratified waters, this region moves inshore as the turbulent layers thin due to stronger stratification, extending the cross-shelf circulation farther inshore when compared with unstratified conditions (Austin and Lentz, 2002; Horwitz and Lentz, 2014). Less is known for systems with complex topography variations. Divergences in the along-shelf and cross-shelf flows may occur with the presence of complex coastline topography and subtle bathymetric features, that can drive substantial cross-shelf exchange (Barth et al., 2000; Gan and Allen, 2002; Kirincich et al., 2005; Sanay et al., 2008; Ganju et al., 2011). As seen in several studies (Gan and Allen, 2002; Gutierrez et al., 2006; Kuebel Cervantes and Allen, 2006; Maza et al., 2006), strong along-shore pressure gradients can form in the presence of a cape, when the upwelling wind regime relaxes. These pressure gradients are accompanied by geostrophically balanced cross-shelf flows over the inner-shelf, resulting in the intensification of the upwelling in the lee of the cape. A cyclonic recirculation that may form in the presence of a cape, can also be relevant since it enhances the onshore transport in the leeside of the cape (Barth et al., 2000; Doglioli et al., 2004; Meunier et al., 2010; Liu and Gan, 2014).

here we conduct a study of the shelf circulation at a site with sharp along-shelf topography changes, and with a marked diurnal variability. the strong diurnal cycle of the wind motivated the focus on the daily variability of the circulation, since sea breeze events are found to be particularly important in promoting onshore transport across the inner-shelf, through its influence on both winds and waves (Woodson et al., 2007; Hendrickson and MacMahan, 2009; Lucas et al., 2013).

The study area lies within the meridional coast of Portugal around Cape Sines (Fig. 1). The shelf is relatively narrow (around 30 km) with the shelf break at approximately 150 m depth. South of the Cape, the shore is mostly rocky and crucial for many inter-tidal species including barnacles (Cruz et al., 2005). The processes of barnacle recruitment at this site have been under investigation for many years now, in the frame of various projects (Cruz, 1999; Cruz et al., 2005; Jacinto and Cruz, 2008; Cruz et al., 2009; Trindade et al., 2016). We used Eulerian velocity measurements collected at 12-m water depth in the lee of Cape Sines, over 3 consecutive summers (2006–2008). Summertime is the period when the larvae recruitment of several barnacle species is higher for the study region (Cruz, 1999; Cruz et al., 2005; Jacinto and Cruz, 2008), which can be particularly interesting since, during summer, the western Iberian coast is typically under upwelling-favourable winds (Relvas et al., 2007), which intensify the along-shelf currents and promote the shut-down of cross-shelf transport in the region inshore of the upwelling front (Estrade et al., 2008). However, in the presence of a cape, diurnal relaxation periods may induce retention-favourable conditions, which can be beneficial to larvae recruitment in the leeside of the cape (Roughan et al., 2005a, 2005b; Peliz et al., 2007; Woodson et al., 2007; Oliveira et al., 2009; Lucas et al., 2013).

We chose a period between 20 July and 04 August 2006 when the wind showed a steady upwelling-favourable condition modulated by a diurnal cycle of the wind. The use of a period with such stable wind forcing enabled us to minimize other forcing effects and to focus on the

wind-driven part of the circulation. A numerical model simulation was also conducted to study the wind-driven circulation in the vicinity of Cape Sines during this period. This study adds new insights about the spatial patterns of the circulation at diurnal timescales in the leeside of Cape Sines and how transport across the shelf may be promoted.

2. Data and methods

2.1. In-situ data

Wind data for the summers of 2006, 2007 and 2008 were collected at the Meteorological station of the Port of Sines authority, at 37° 57′ 25″ N; 8° 52′ 74″W which is about 10 km North of the ADCP location (Fig. 1). Wave and tidal data for the same period were collected at 37° 55′ 14″ N; 8° 55′ 47″W, and 37° 56′ 89″ N; 8° 53′ 27″W respectively (Fig. 1).

Four thermistors (Stowaway TidBit, Onset Computer Corp.) were deployed from July 19, 2006 to September 15, 2006 and from 1 to 14 of August 2007, on a mooring next to the ADCP location. Temperature was measured at 4 different depths: 1 m, 3 m and 5 m above the sea floor, and at the surface. A fifth thermistor was deployed in 2006 at 2 m from the surface.

Velocity profiles were measured with a bottom-mounted upward looking Acoustic Doppler Current Profiler (WorkHorse Sentinel 1200 kHz), with a bin size of 0.5 m, and a ping frequency between 0.83 and 1.67 Hz, deployed in approximately 12-m water depth at 37° 53′ 11.52″N, 8° 48′ 15.42″W, and about 600 m offshore (Fig. 1). The data was collected in 2006, between July 19 and August 29; in 2007, between July 31 and August 14; and in 2008, between July 22 and September 9 (with a gap between August 05 and August 19). As bottom-mounted ADCPs do not sample the entire water column, the deepest bin corresponds to approximately 1.5 m above sea bed.

The upper bins of the ADCP correspond either to emersed or submersed depth cells depending on the height of the free surface, mainly due to tidal movements. Therefore it was first necessary to find the sea surface, and disregard all bins above that surface. To find the contaminated bins, and since the data was collected at a shallow location where the tidal amplitude ranges from 14% to 30% of the total depth, the 'tide-following method' was used (Kirincich et al., 2005). For each profile, the depth of maximum backscatter intensity was marked as the water surface and all bins above this surface were discarded, plus three bins immediately below it.

2.2. Time-averaging and vertical coordinate transformation

The fact that the sea surface undergoes significant changes in shallow waters rises the question of how to compute the daily time averages of data along the same depth. If a bottom or surface reference coordinate system is used (Kirincich et al., 2005; Fewings et al., 2008; Lentz et al., 2008), an average along the same z-level will include data that are at very different relative distances to the surface (especially in spring tides and shallow waters) and this will produce an aliased mean. To overcome this problem, a dynamical (tide-following) vertical coordinate $z' = z/h$, where h is the total water column depth (changing with tides), was used. The total depth (or the sea surface height) was computed by adjusting the surface detected with the maximum of total backscatter intensity to the sea surface using the tidal height measured at the port of Sines (near the ADCP location, see Fig. 1). Each ADCP profile was then interpolated into this new coordinate system. Time-averaging was then performed along each of the dynamical-surfaces, ensuring that the time-averaging of velocity values is done along levels that are at equal relative distances to the bottom and sea surface. The dynamical vertical coordinate conserves information of both bottom and surface bins and it was, therefore, the one chosen for this study.

The coordinate system was rotated based on the principal axis direction of the subtidal depth-averaged velocity. For most deploy-
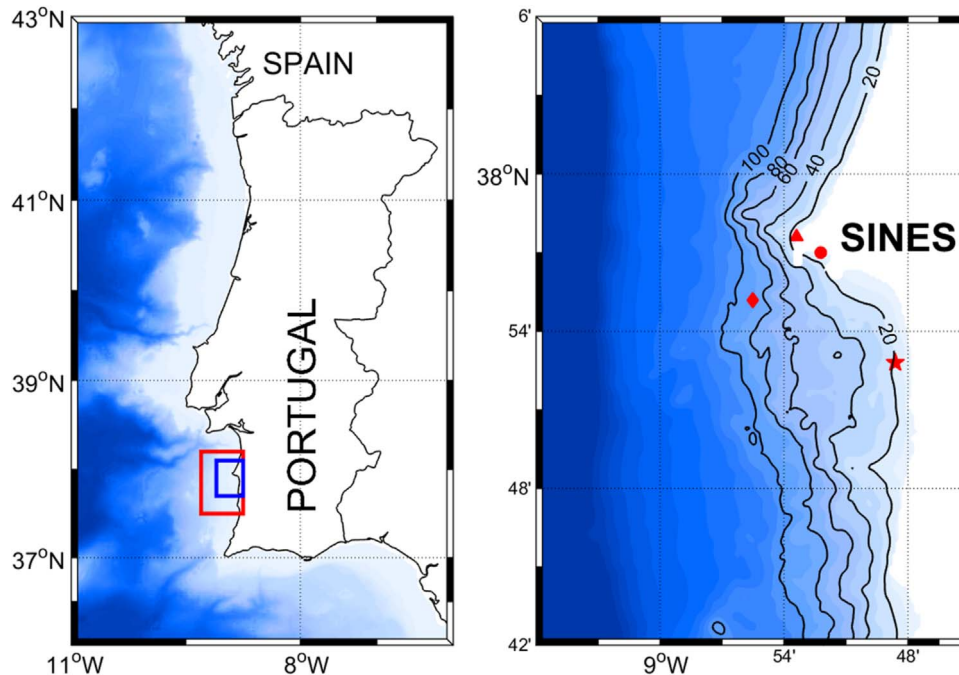
Fig. 1. Left: Study area (blue box) on the southwestern coast of Portugal. Red box shows the numerical model domain. Right: zoom of the study area showing different sites of in-situ data: triangle – Meteorological Station, diamond – Wave-rider buoy, star – ADCP and Thermistors, and circle – Tide gauge. (For interpretation of the references to color in this figure legend, the reader is referred to the web version of this article.)

ments, the major axis orientation was less than 2.4° clockwise from north, and it was roughly aligned with local bathymetry and coastline. The coordinate axis was rotated according to this angle and the velocity profiles are now considered to be in cross-shelf (x) and along-shelf (y) directions, with x negative offshore and y positive along-shelf northwards.

All further analysis was performed with hourly averaged data.

2.3. Model setup

A numerical simulation was conducted using the Regional Ocean Modelling System (ROMS) (Shchepetkin and McWilliams, 2005; Haidvogel et al., 2008), a free-surface, terrain-following (sigma coordinate), primitive equation ocean model largely used for coastal applications.

The model configuration was developed to simulate the period between 20 July and 04 August 2006 in the region focused by this study (around Cape Sines, in the Southwestern coast of Portugal). The configuration consisted of a high resolution (0.22 km) grid in a 50 × 80 km domain around Cape Sines (red square in Fig. 1). 32-σ levels were used with enhanced vertical resolution at surface levels. Topography data compiled in Peliz et al. (2013) was used, with a low-level smoothing and a cut-off depth of 800 m. Radiation conditions are used along the open boundaries for momentum and tracers, together with passive-active nudging open boundary forcing (Marchesiello et al., 2001). A sponge layer of 15 km is placed near the open boundaries to reduce reflections that tend to appear as a consequence of the reduced grid dimension.

The model initially assumes a flat ocean with a vertical density distribution typical of summer time. The same salinity and temperature conditions are preserved near the open boundaries using a relaxation time scale (Marchesiello et al., 2001). Homogeneous surface heat fluxes with a fixed diurnal variability are used to maintain the stratification (more details in Trindade et al. (2016)).

The model was forced with 15 days (between 20 July and 04 August 2006) of winds downscaled from Era-Interim data using the Weather Research and Forecast Model (Fig. 2), with 9 km resolution, to allow

spatial inhomogeneity (Soares et al., 2012; Peliz et al., 2013). Since WRF model seems to systematically overestimate the winds when compared with the observed time series, the WRF wind magnitude was reduced by the time-mean wind magnitude difference between the data and model at the location of the meteorological station.

The focus of this study is to analyse the wind-driven circulation, and therefore tides were not included in the model forcing. A spin-up of 3 days was considered for the model to stabilize and the results from that period were disregarded. To avoid misinterpretations, the model description and analysis will be based on the zonal (x) and meridional (y) oriented axis, with the consideration that away from the cape (including the ADCP site) it is coincident with the along- and cross-shelf coordinate axis.

3. Results

3.1. Observations

3.1.1. Winds

Cross-shelf wind stress ($\tau_s{}^x$) ranged, on average, between values of −0.05 Pa and 0.05 Pa (Fig. 3a) and was mostly positive (onshore) with short periods of offshore winds. Along-shelf winds were dominantly from north (negative values of along-shelf wind stress), with episodic and weaker events of southerly winds (Fig. 3b). Along-shelf wind stress ($\tau_s{}^y$) was overall higher than cross-shelf wind stress, and ranged between −0.1 Pa and 0.05 Pa.

3.1.2. Waves and tides

Throughout the 3 summers the waves had a mean significant wave height of 1.2 m (Fig. 3c) and significant wave heights above 2.5 m were rare during this period. As seen in Lentz et al. (2008) and Fewings et al. (2008), wave-driven cross-shelf currents for waves with Hsig 1.2 m are in the order of 0.01 m s^{-1}, and directed offshore (wave-driven undertow). The tidal components were diagnosed using the tidal gauge data and the T_TIDE package (Pawlowicz et al., 2002). The dominant tidal component was the M2 (lunar semidiurnal tide, with period of 12.42 h) followed by S2,
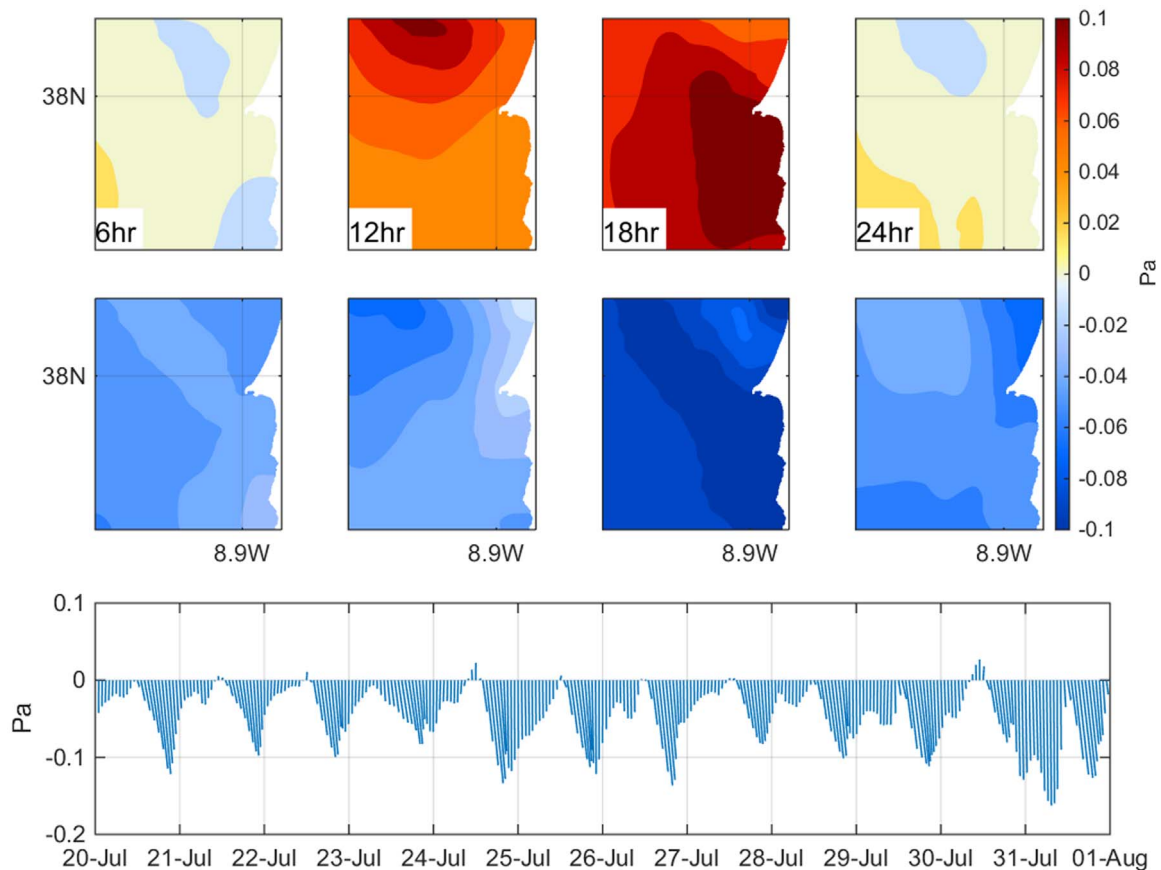
Fig. 2. Wind field from WRF model for the period between 20 July 2006 to 04 August 2006. First row: U-component of wind stress [units: Pa] for different hours of an average day. Second Row. V-Component of wind stress [units: Pa] for different hours of an average day. Bottom Row: Wind vectors for the 15-day run at the ADCP site.

N2 (semidiurnal) and K1 (diurnal tide). The mean tidal amplitude at this site, during these 3 summers, was 1.7 m with maximum of 3.6 m (Fig. 3d). Estimations of the barotropic tidal contribution of the M2 tide resulted in cross-shelf velocities around 2×10^{-3} m s^{-1}.

3.1.3. Stratification

Throughout the period when water temperature was measured, the water column was stratified (Fig. 3e). A mean difference between surface and bottom temperature of 2 °C was observed, which is considered high stratification for a 12-m depth site (Lentz, 2001;
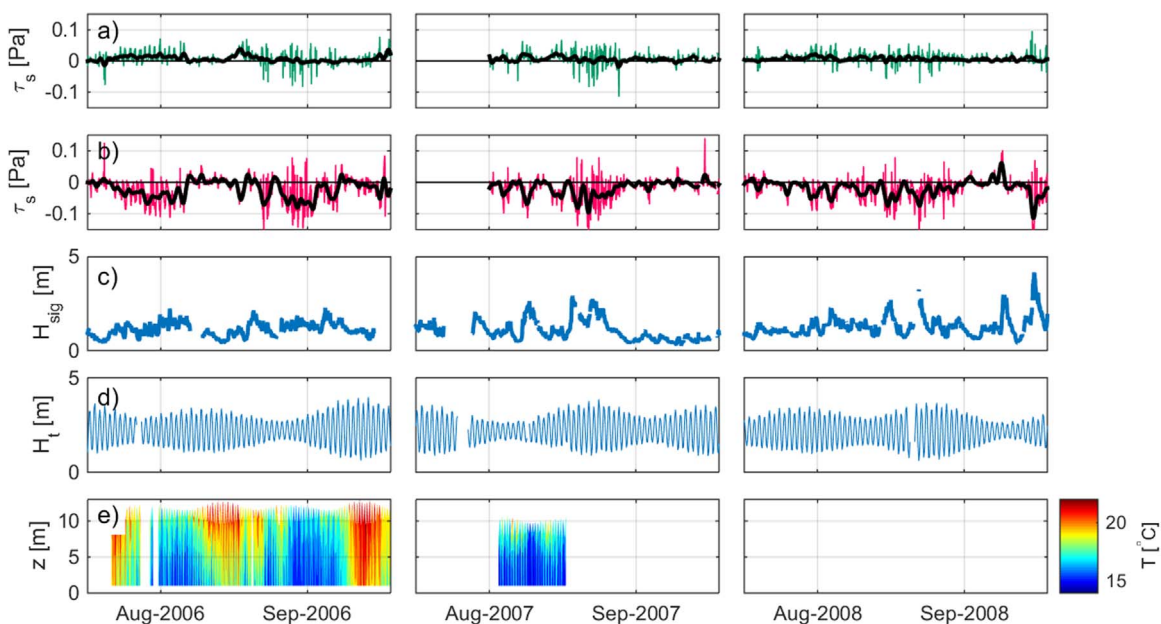
Fig. 3. a) Hourly (green) and subtidal (black) cross-shelf wind stress [Pa]; b) Hourly (red) and subtidal (black) along-shelf wind stress [Pa]; c) Significant Wave Height [m]; d) Tidal Height [m] and e) Temperature [°C], between 15 July and 15 September. Each column indicates a different year, left to right – 2006; 2007 and 2008. (For interpretation of the references to color in this figure legend, the reader is referred to the web version of this article.)
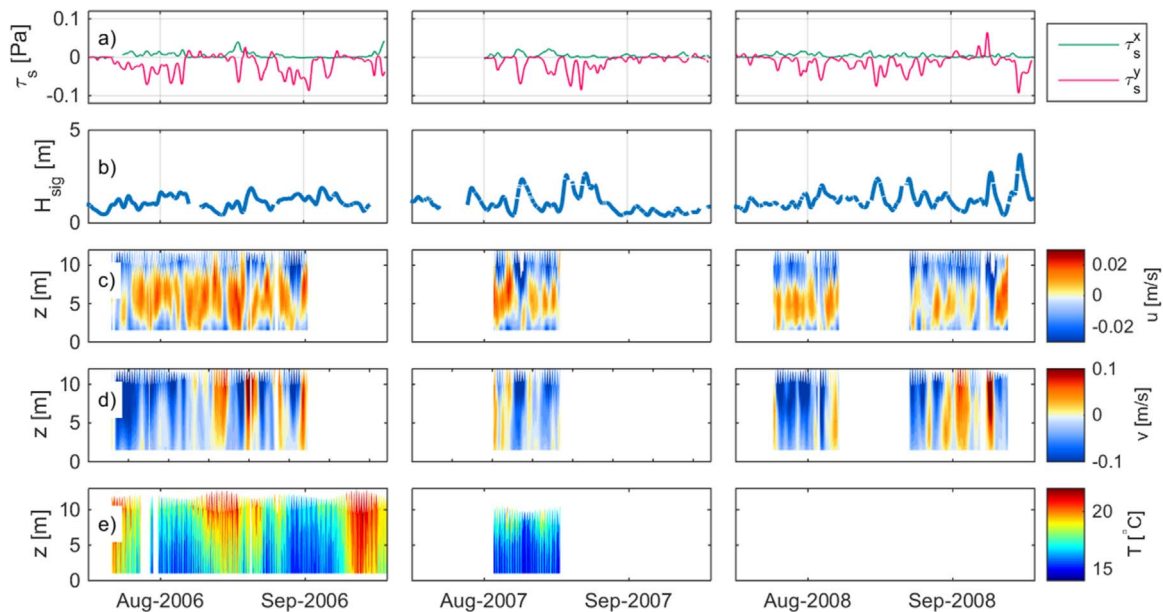
Fig. 4. Subtidal time series of a) cross-shelf ($\tau_s{}^x$) and along-shelf ($\tau_s{}^y$) wind stress [Pa]; b) Significant wave height [m]; c) Cross-shelf velocity profiles [m/s]; d) Along-shelf velocity profiles [m/s]; and e) Temperature profiles [°C]. Each column, left to right – 2006; 2007 and 2008. z = 0 is the bottom.

Durski et al., 2004). Temperature changes are apparently connected with the variability of the along-shelf winds, with higher stratification periods occurring during relaxation of the northerly winds. However, periods of higher surface temperatures are also concurrent with spring tides, meaning that tidal effects on the stratification should not be neglected.

3.1.4. Mean circulation

During the summers of 2006, 2007 and 2008, the subtidal along-shelf velocity (Fig. 4d) was southwards, consistent with a response to northerly, upwelling-favourable winds, which is a typical wind regime in the Western Iberian margin during summer

(Relvas et al., 2007). There were a few events where the upwelling relaxed and the wind rotated northwards. During those events, the along-shelf velocity was northwards. The intensity of the along-shelf velocity was stronger at the surface and decayed with depth. The cross-shelf velocity (Fig. 4c) had a persistent maximum onshore flow at mid-depth, with offshore velocities at surface and bottom. This parabolic profile did not change regarding northerly or southerly winds, except during strong upwelling-favourable wind conditions, when the cross-shelf velocity showed a two-layer vertical structure with offshore velocities at surface and an opposite flow in depth, as should be expected during upwelling conditions.
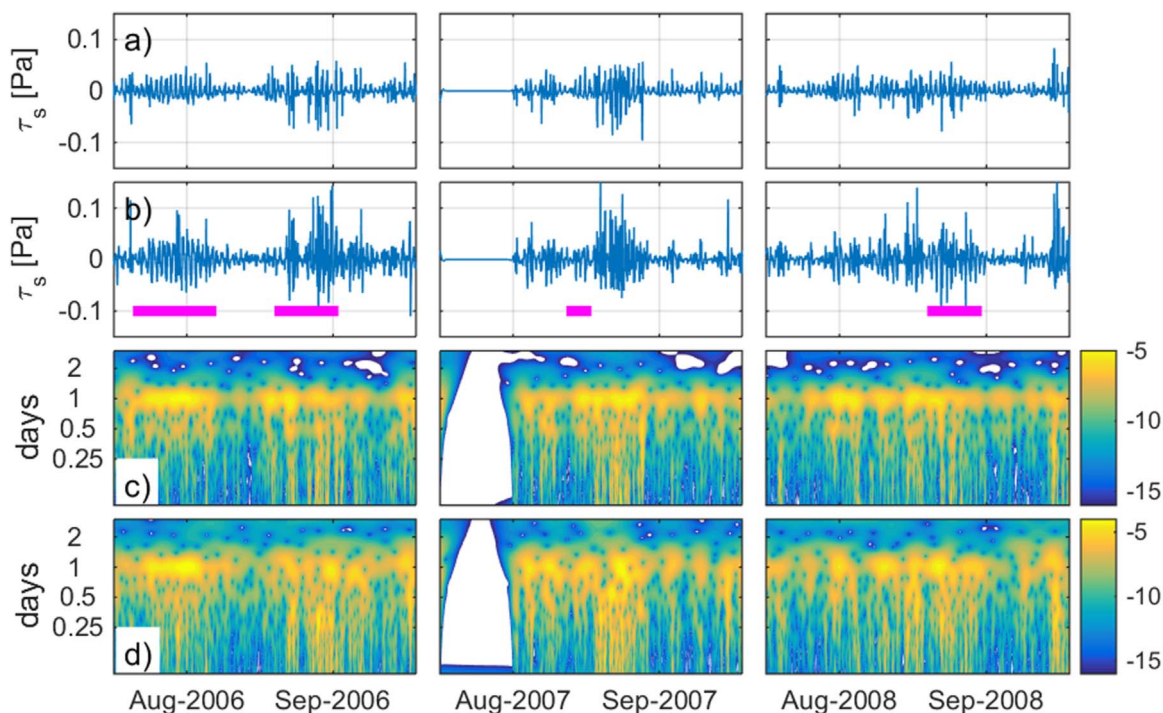
Fig. 5. High passed (<33 h) a) cross-shelf wind stress [Pa] and b) along-shelf wind stress [Pa]. Wavelet power spectrum of the high passed (<33 h) c) cross-shelf and d) along-shelf wind stress. Magenta lines in b) represent the periods of strong diurnal cycle (considering the periods when ADCP data was collected).
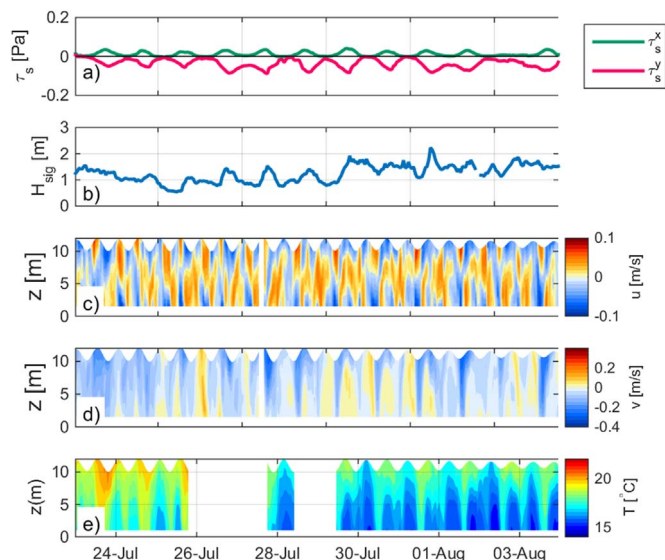
Fig. 6. Time series, between 20 July and 04 August 2006, of a) Wind stress [Pa]; b) Significant wave height [m]; c) Cross-shelf velocity [m/s]; d) Along-shelf velocity [m/s]; and e) Temperature [°C]. z = 0 is the bottom.

3.1.5. Circulation at diurnal timescales

Throughout this study, it was given special attention to the diurnal variability of the circulation. A method defined by Hendrickson and MacMahan (2009) as the '24-h time-averaged' was used. The result consists of an average day (hereinafter clock-hour average day) in which each hour corresponds to a mean of that same hour throughout a chosen period (example: hour 1 is an average of every 1:00 a.m. for a chosen period).

Spectral wavelet analysis (Morlet) at diurnal timescales (<33 h with 95% of confidence level) of the observed wind stress shows that the highest energy is found in the diurnal period (Fig. 5 c and d), and was consistent throughout the summers of 2006, 2007 and 2008. The stronger diurnal signals were found in the following periods: 20 July to 04 August 2006, 18–29 August 2006, 11–14 August 2007 (the strong diurnal signal remained until 23 of August but there is no ADCP data after day 14) and 18–27 August 2008. These periods are marked in Fig. 5b and were the ones selected to compute the clock-hour average day of the current velocity and temperature profiles, wind parameters and wave height.

Emphasis was given to the period between 20 July to 04 August 2006 (hereinafter control period) when both wind and wave forcing maintained similar conditions (Fig. 6). The wind had a very steady pattern of northwesterly wind modulated by a diurnal oscillation of magnitude in both wind components (Fig. 6a). Wave height increased on average throughout this period but had a daily maximum concurrent with the maximum of wind magnitude (Fig. 6b). During this period, the cross- and along-shelf velocity (Fig. 6c and d, respectively) showed a repetitive circulation pattern. The flow in the along-shelf direction was southwards with a daily intensification in the afternoon. There was a daily flow reversal in the cross-shelf circulation at mid-day. Cross-shelf velocities ranged from 0.1 to − 0.1 m s^{-1} while the along-shelf circulation was stronger, reaching − 0.3 m s^{-1}. The water column remained stratified during this period, with a marked diurnal heating and an overall decrease in temperature towards the end of July and beginning of August (Fig. 6e).

Results for the clock-hour average day over the control period are plotted in Fig. 7. The diurnal sea-breeze cycle is clear in the wind stress plots (Fig. 7a). Wind stress was weak in the morning period, but around 11 h there was an increase of both components of the wind stress, with cross-shelf wind stress peaking at 16 h and along-shelf wind stress at 18 h. There was a decrease in H$_{sig}$ throughout the
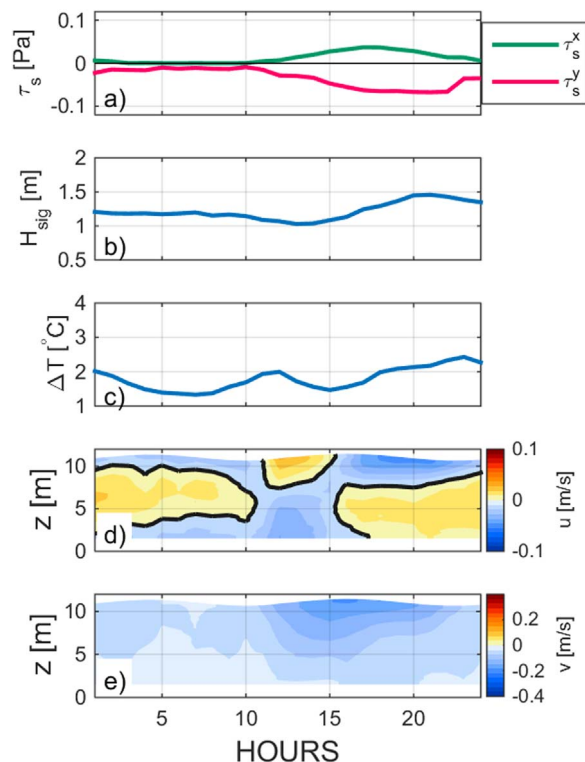
Fig. 7. The clock-hour average day, from July 20 to August 04, 2006, of a) Wind stress [Pa]; b) Significant wave height [m]; c) Difference between temperature at the surface and at the bottom [°C]; d) Cross-shelf velocity [m/s]; e) Along-shelf velocity [m/s]. z = 0 is the bottom. Thick black line marks zero and the contour interval is 0.01 m/s.

morning and mid-day, with minimum height at 13 h. Afterwards, the significant wave height increased, peaking at 20 h (Fig. 7b). A lag between wind and wave maximum was also described in Hendrickson and MacMahan (2009). The stratification (Fig. 7c) was present throughout the day with a semi-diurnal peak and higher values late in the day, related to diurnal heating. In the cross-shelf flow we can clearly identify 3 periods (Fig. 7d). From 00 h to 11 h (morning period) the cross-shelf velocity had a 3-layer structure, with offshore velocities of approximately − 0.01 m s^{-1} at the surface and near the bottom, and an onshore flow at mid-depth. Between 12 h and 15 h (mid-day period), when wave height reached its minimum value and the wind increased in magnitude and rotated onshore, there was a reversal in the cross-shelf flow structure. The cross-shelf velocity profile had a 2-layer structure, with onshore flow in the surface layer, and offshore flow at the bottom (Fig. 7d). After 15 h (evening period), the velocity profile was again reversed, with onshore flow near the bottom and offshore flow at the surface, much stronger than in the morning period. This period corresponds to maximum wave height and strongest wind magnitude with a clear cross-shelf component. Throughout the clock-hour average day the along-shelf velocity was always negative (Fig. 7e) with maximum velocities between 16 h and 18 h, concurrent with the maximum of northerly wind. Overall, the cross-shelf circulation magnitude was around 0.01 m s^{-1}, and the along-shelf circulation was much stronger, reaching up to 0.2 m s^{-1}.

To show consistency of the diurnal variability observed for the control period, we computed the clock-hour average day over four periods when the diurnal cycle of wind in either component was also strong (shown as magenta lines in Fig. 5b). It can be seen in Fig. 8 that the averaged diurnal variability for these periods is much similar to the clock-hour average day of the control period. The cross-shelf circulation (Fig. 8d) also showed a daily three-period variability, although with a weaker magnitude than the clock-hour average day for the control period. The diurnal variability of the along-shelf velocity was
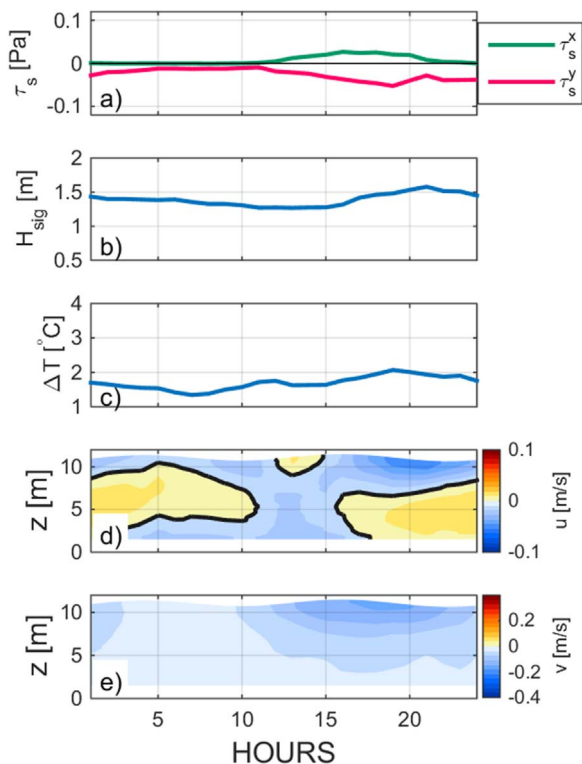
Fig. 8. The clock-hour average day, for the four periods of the three summers with a strong diurnal cycle of the wind marked in 5), of a) Wind stress [Pa]; b) Significant wave height [m]; c) Difference between temperature at the surface and at the bottom [°C]; d) Cross-shelf velocity [m/s]; e) Along-shelf velocity [m/s]. z = 0 is the bottom.

also similar to the control period, with maximum (although slightly weaker) southwards flow near the surface and in the evening, concurrent with maximum wind magnitude.

3.2. Model results

3.2.1. Model-data comparison

Model results for the grid point nearest to the ADCP site are used for comparisons with in-situ data. Overall, the model simulated successfully most features of the circulation and temperature evolution at the ADCP site (Fig. 9). The wind undergoes a diurnal cycle of both magnitude and direction, rotating onshore with increasing magnitude at the end of each day (Fig. 9a). In the cross-shelf direction (Fig. 9b), the circulation shows a permanent two-layer structure, with a repetitive
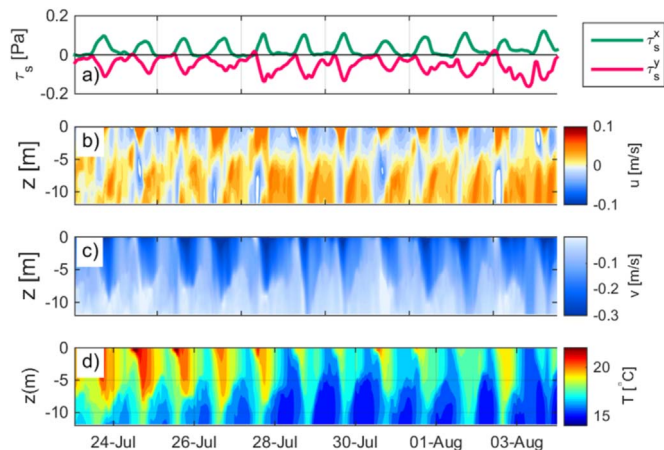
Fig. 9. Modelled time series of a) Wind stress [Pa]; b) Cross-shelf [m/s]; c) Along-shelf velocity [m/s]; d) Temperature profiles [°C], at the ADCP site.
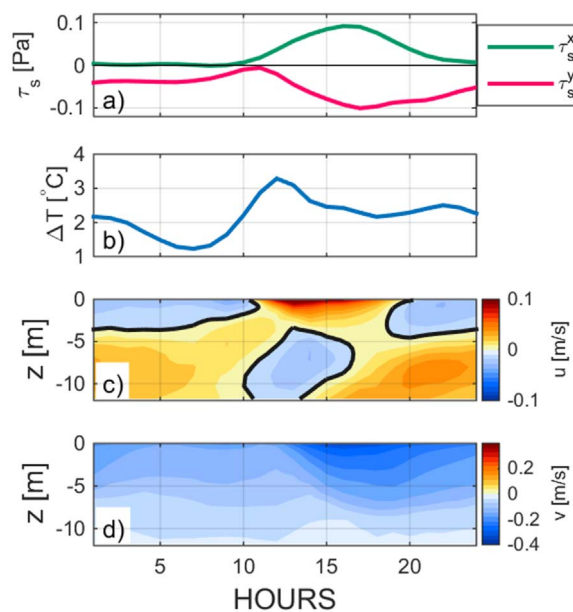
Fig. 10. Modelled clock-hour average day of a) Wind stress [*Pa*]; b) Temperature difference between surface and bottom [°C]; c) Cross-shelf velocity [m/s]; d) Along-shelf velocity [m/s], at the ADCP site. Thick black line marks zero and the contour interval is 0.01 m/s.

daily cycle of flow reversal of the entire water column at mid-day. The along-shelf velocity (Fig. 9c) is always southwards, intensified at the surface, and with a daily increase of magnitude later in the day (concurrent with the daily maximum of wind magnitude). The water column is stratified at all times (Fig. 9d), with stronger stratification in the first 5 days and again in August 02. The 12-day average difference between surface and bottom temperature was 2.2 °C, consistent with the observations.

We then computed the clock-hour average day for the same variables. The results are shown in Fig. 10. The model represents well the observed diurnal cycle of wind and stratification (Fig. 10a and b, respectively) showing the wind variability and the temperature average difference of around 2 °C between the surface and bottom layer. For the cross-shelf circulation (Fig. 10c) the reversal at mid-day is present, with longer duration than in the observations, and the upwelling-type exchange in the evening is also reproduced. The along-shelf velocity (Fig. 10d) has the same structure and variability as the observations, with surface intensified southward velocities and an increase in magnitude in the afternoon.

The model results are about 20–30% stronger than the observations for both velocity components, except for the offshore (cross-shelf negative) values which are about 10% weaker.

3.2.2. Circulation in the vicinity of the Cape

Fig. 11 shows the horizontal fields of surface temperature (top row) and surface elevation (bottom row) with current velocity vectors superimposed (surface temperature and velocity correspond to the average of the first 5 m) for six different hours of the clock-hour average day: 4 h, 8 h, 12 h, 16 h, 20 h and 24 h. The blue vectors represent the wind at the ADCP site for the corresponding hour.

Fig. 11 clearly illustrates the influence of the cape on the temperature and surface elevation fields. The permanence of northerly wind maintains a background upwelling circulation throughout the domain. In the northside of the cape, the largest southward currents, associated with the upwelling-jet, are concentrated from the coast to the 50-m isobath. The presence of the cape causes the deflection of this jet to the west. The upwelling jet is then displaced offshore and follows the 100-m isobath after the cape. As the upwelling-jet is deflected by the cape, it rotates cyclonically. The deviation of the upwelling jet by the cape leads
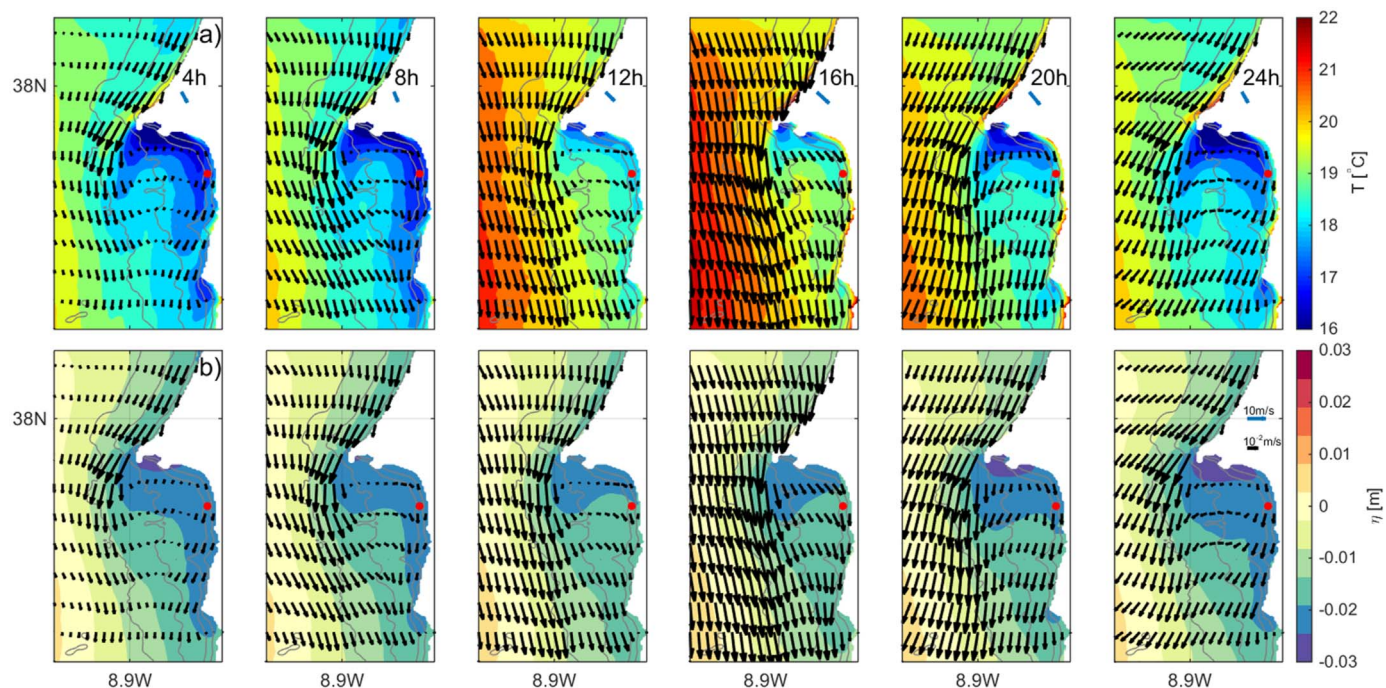
Fig. 11. a) Sea surface temperature [°C] and b) Sea surface height [m], for different hours of the clock-hour average day (each column): 4 h, 8 h, 12 h, 16 h, 20 h and 24 h, with surface current velocity vectors superimposed. The blue arrow represents the wind vector at the ADCP site, for the respective hour. The red dot marks the ADCP location. Scale vectors are represented in the last subfigure. (For interpretation of the references to color in this figure legend, the reader is referred to the web version of this article.)

to lowering the sea surface elevation south of the cape. Similar to the surface elevation, lowest temperatures are seen south of the cape. In a region just below Cape Sines, the circulation is weaker and the cross-shelf component is slightly dominant.

In our case, superimposed to a constant upwelling-favourable wind regime there is also a daily oscillation of the wind magnitude and direction, which will have different impact on the circulation depending on the region considered. Overall the circulation is dominantly to the south, with a weaker zonal component that rotates from west to east and again to west throughout the day.

In the northside of the cape, the upwelling-jet is constrained by the presence of the coast. While most of the flow rotates to the east, the circulation aligns with the bathymetry as we approach the coast, causing a circulation convergence (downwelling), which results in a region of warmer waters near the coast in the afternoon.

In the leeside of the cape the flow becomes meridionally aligned, forming a secondary upwelling-jet within 5 km of the coast. This secondary upwelling flow is dominantly southwards but has a weak zonal component that alternates from westwards in the morning period, to eastwards at mid-day and finally to westwards later in the day. This is consistent with the surface flow reversal observed at the ADCP location (a red dot representing the ADCP location can be seen in Fig. 11 over this secondary upwelling flow). The two upwelling jets are also responsible for the southwards advection of the cooler, newly upwelled waters from the south part of the cape (Fig. 11 top).

3.2.3. Regions with similar diurnal variability

We proceeded to the analysis of whether the circulation observed by the ADCP is local or if it is representative of a region in the leeside of the cape.

The distinct circulation feature identified in the present study is the cross-shelf current reversal at mid-day. For that reason, we analyse how the circulation varies along the domain. We are interested in regions where the velocity at surface and bottom show the flow reversals at the same hours as in the observations, which are in agreement with the wind variability.

To achieve that, we searched for grid points in the model results with

similar characteristics by producing binary maps. These maps were based on the direction of the zonal flow at the surface and bottom layers, and were constructed according to the following rules: i) For each grid point, the signal of the zonal component of the velocity in both layers is compared; ii) In the morning and evening, we searched for regions where the surface velocity was negative (offshore at the ADCP site), and bottom velocity was positive (onshore), for the mid-day period we searched for the opposite - onshore flow in the upper layer and offshore flow in the bottom layer. Whenever these conditions are met, the value on the map is one and for any other situation the value is zero. Note that the 3-layer structure observed in the morning period was not reproduced by the model, and therefore, in the morning period, the circulation pattern considered was the same as the model simulated (2-layer flow).

The binary map for the set of hours: 8 h, 12 h and 24 h, for regions with depth less than 50 m, is shown in Fig. 12, where red represents 1 and white is 0. We show separately the binary maps representing the surface layer (top row), the bottom layer (middle row) and the combination of both (bottom row) for analysis purposes. Thus, the top row of Fig. 12 shows the regions where the surface (top 5 m) cross-shelf velocity was negative (offshore) at 8 h (a), positive (onshore) at 12 h (b) and again negative at 24 h (c). The middle row is analogous for the bottom layer (last 5 m) but with opposite signal: positive cross-shelf velocity at 8 h, negative at 12 h and positive at 24 h. The right column in Fig. 12 (d) shows the product of the previous three (a, b and c). The bottom row is the combination of the surface and bottom layer, showing in red the regions where the cross-shelf flow in both layers has a similar vertical structure as the model at the ADCP site.

In the surface layer, at 8 h (Fig. 12a; top row), only a small region south of Cape Sines has negative velocities at the surface. This zone is limited to a small along-shelf band near the coast where the coast becomes meridionally aligned (consistent with the location of the secondary upwelling jet). On the other hand, at 12 h (Fig. 12b, top row) a great part of the domain is marked in red, showing that most of the domain (considering depths below 50 m) has positive zonal velocities. Lastly, at 24 h (Fig. 12c, top row), most of the shallow part of the domain (<50 m) has negative velocities at the surface, with the exception of a small region south of Cape Sines.

It is clear that, at the surface, eastwards flow at mid-day and westwards
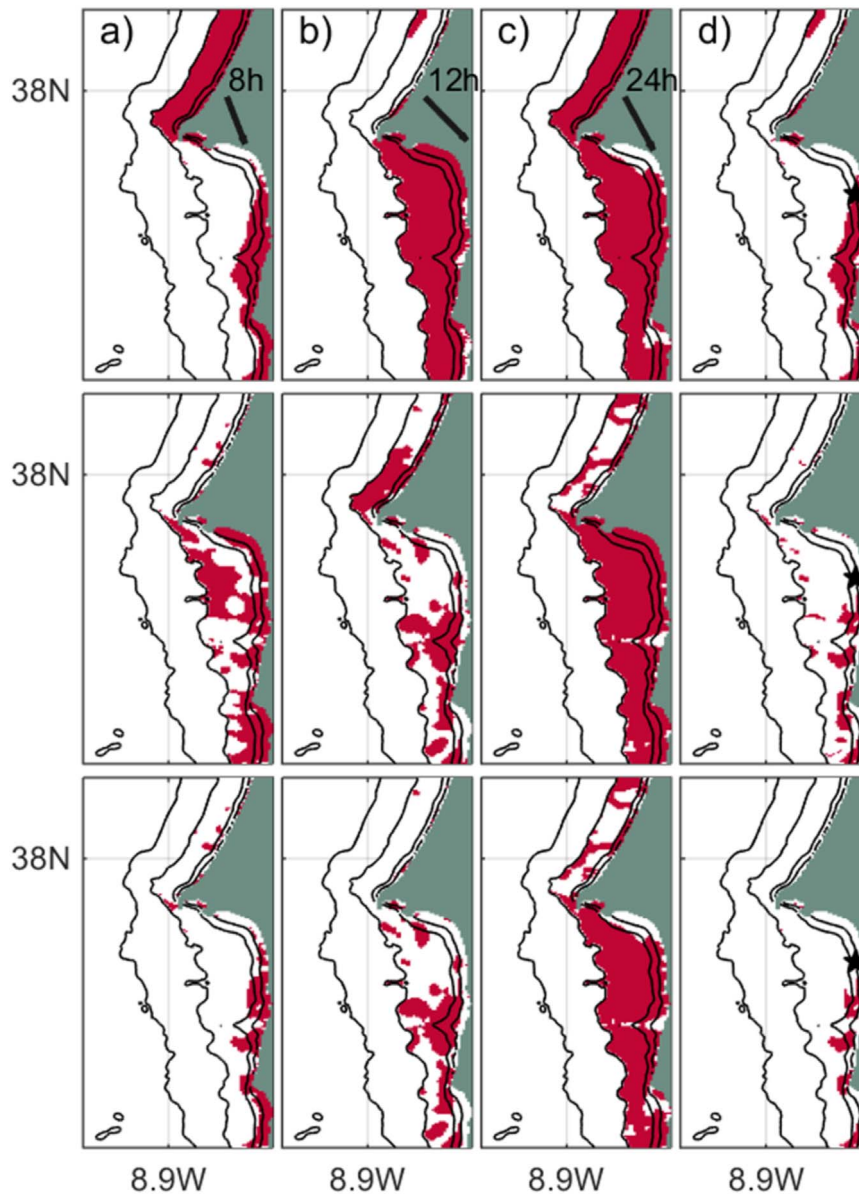
Fig. 12. Binary maps representing the grid points where the modelled cross-shelf velocity had the same structure and evolution as in the ADCP site. Red is 1, white is 0. Top row) Binary map for the surface layer; Middle row) Binary map for the bottom layer; Bottom row) Binary map combining both surface and bottom layers. a) 8 h; b) 12 h; and c) 24 h. d) The regions in red represent the interception between a, b and c. The star represents the ADCP location. (For interpretation of the references to color in this figure legend, the reader is referred to the web version of this article.)

flow in the evening are common circulation features in a large portion of the domain but only a small region, consistent with the location of the secondary upwelling jet, has negative velocities in the morning period. This implies that only the region over the secondary upwelling jet has the same daily evolution of the surface flow as the model at the ADCP site (Fig. 12; top row; map d). It is visible in Fig. 12 that the marked regions in the morning (a) and mid-day (b) hours on the bottom layer (middle row) are sparse and connected with small-scale topographic variations. However, at 24 h (c) most part of the domain (for depths below 50 m) show positive velocities.

Combining the binary maps of both surface and bottom layer (bottom row of Fig. 12) results in few regions with a behaviour synchronous with the observations, mainly due to the small scale variations in the bottom layer. The analysis of the last map indicates that only a few zones fit our criteria and, by definition, the ADCP site is included (marked as a star in Fig. 12). The resulting map shows that these zones are located in the shallow region south of cape Sines, when the coast becomes meridionally aligned, consistent with the location of the secondary upwelling jet.

4. Discussion and conclusions

Nearshore circulation was analysed using ADCP data collected at 12-m in the lee of Cape Sines (Fig. 1), during the summers of 2006, 2007 and 2008. The region is under persistent upwelling-favourable wind conditions modulated by a daily cycle similar to sea breeze. We focused on a 15-day period between 20 July to 04 August of 2006, when the wind maintained similar conditions, to study the diurnal variability of the cross-shelf circulation.

The daily variability of the observed cross-shelf circulation consists of three distinct periods. A morning period with a 3-layer structure with onshore velocities at mid-depth, a mid-day period where the flow is reversed and has a 2-layer structure with onshore velocities at surface and offshore flow at the bottom (downwelling), and, lastly, a 2-layer period, with strong offshore velocities at the surface and onshore flow at the bottom (upwelling).

The observed cross-shelf circulation showed a peculiar vertical shape and diurnal variability different from several other systems

described in literature. Most inner-shelf studies admit that cross-shore wind stress may induce a circulation of similar magnitude as upwelling or downwelling, specifically over stratified waters. Cross-shore wind stress is found to force a circulation of same direction as wind (onshore or offshore) in the surface layer and a compensating opposite flow underneath (Lentz and Fewings, 2012). Although previous works have found that the cross-shelf circulation is strongly modified by sea breeze events, the observed 3-period clock-hour average day described here is different from previous studies (Woodson et al., 2007; Hendrickson and MacMahan, 2009; Xiaoqian Zhang et al., 2010). Hendrickson and MacMahan (2009) described a diurnal circulation forced by sea breeze. In their study, the most clear feature was a wave-driven undertow forced by the sea breeze effect on wave height. They found that a wind stress threshold of 0.5 Pa was needed to modify the background circulation. We do not observe that type of circulation, probably due to lower H_{sig} and wind stress present at this location. Except for the upwelling-type cross-shelf circulation in the evening period, the observed diurnal circulation did not show a simple wind- or wave-driven circulation coherent to previous inner-shelf studies (Tilburg, 2003; Kirincich et al., 2005; Fewings et al., 2008; Lentz et al., 2008; Hendrickson and MacMahan, 2009; Lentz and Fewings, 2012).

A distinctive feature of the circulation at this site appears to be the parabolic cross-shelf profile, with maximum onshore velocity at mid-depth, that also appears in the morning period of the clock-hour average-day. (Lentz and Chapman, 2004) showed that for strong stratification conditions, the onshore return flow (as response to upwelling) can be in the interior of the water column, as a response to increasing momentum flux divergence and small bottom stress in the momentum balance. Mid-shelf studies on the Middle Atlantic Bight (Lentz, 2008) and Oregon coast (McCabe et al., 2015) showed mean cross-shelf profiles with maximum onshore flow at mid-depth which were explained by a combination between wind stress and local along-shelf pressure gradients. In a study around Point Conception, California, Fewings et al. (2015) consistently observed vertical profiles of the same form, which were associated with pressure gradients connected with local wind relaxations. These studies indicate that the along-shelf pressure gradient is likely a key factor in the cross-shelf vertical profile form at this site.

The realistic model was forced exclusively with local winds and simulated most of the current variability seen at the ADCP site, including the mid-day flow reversal and the upwelling-type circulation in the evening. This supports the hypothesis that the observed cross-shelf circulation pattern at diurnal timescales is mostly wind-driven. The observed two-layer pattern in the evening (after 19 h) is consistent with an upwelling circulation (Allen et al., 1995; Austin and Lentz, 2002). Although in shallow waters the circulation tends to align barotropically with the wind (Lentz, 2001; Kirincich et al., 2005), the presence of stratification enables the cross-shelf exchange to penetrate into shallower waters, as suggested in several studies (Lentz, 2001; Austin and Lentz, 2002; Durski et al., 2004; Kirincich et al., 2005). However, the model fails to reproduce the 3-layer structure seen in the morning. This can be due to the fact that other forcing elements may have a stronger impact in this period (like tides and or waves) or larger scale processes described before (Lentz, 2008; McCabe et al., 2015; Fewings et al., 2015) but not reproduced in the model due to the small domain.

Wave data collected at 98-m depth showed significant wave heights of less than 2 m for most part of the time (Fig. 3). At this point we can only speculate that the waves do not affect significantly the circulation since H_{sig} 1.2 m which corresponding wave forcing (cross-shelf velocities below 0.01 m s^{-1}), is most likely not sufficiently energetic to modify the wind-driven circulation (Fewings et al., 2008; Lentz et al., 2008; Hendrickson and MacMahan, 2009).

Tidal forcing may have some significance in the circulation, especially in the morning period. A recent work by Trindade et al. (2016) that used the same model configuration as this study, but included tidal forcing, showed little differences between the modelled circulation during neap and spring tides. In their study, the model also failed to reproduce the 3-layer structure in the morning period. This further indicates that tides probably do not significantly affect the observed circulation.

Studies over different inner-shelves (Lentz et al., 1999; Liu and Weisberg, 2005; Fewings and Lentz, 2010) seem to agree that the circulation is mainly forced by along-shelf pressure gradient (generated by local wind forcing) and wind stress, though other processes can also be important depending on water depth and wave regime.

Several modelling studies (Austin and Lentz, 2002; Cudaback et al., 2005; Estrade et al., 2008; Marchesiello and Estrade, 2010; Tilburg, 2003) and observations (Lentz et al., 1999; Lentz, 2001; Kirincich et al., 2005; Fewings et al., 2008) found that along-shelf wind alone is not an efficient mechanism in driving cross-shelf exchange on inner-shelf. As seen in Gan and Allen (2002) and Kuebel Cervantes and Allen (2006), strong onshore flows in the leeside of the cape result from the interaction between the wind-driven flow and the variations in topography, which are responsible for the setting up of an along-shelf pressure gradient as a response to the decreased surface elevation in the leeside of a cape, which results from the intensification of the along-shelf velocity around the cape. A work by Sanay et al. (2008) over the inner-shelf showed that there is a 3-D circulation response to wind in the presence of a cape. Ganju et al. (2011) pointed out the importance of topographic features in the circulation over the inner-shelf by showing that the dynamical balance was dominated by pressure gradient and horizontal advection terms, which varied with subtle bathymetric changes. Finally, several studies found that non-linear advection is particularly important in the vicinity of topographic features (Doglioli et al., 2004; Meunier et al., 2010; Liu and Gan, 2014). It is expected that Cape Sines will have a similar effect on the circulation, which will promote the generation of localized wind-forced pressure gradients and enhance the cross-shelf exchange in the leeside of the cape.

The upwelling jet deflection and corresponding cyclonic circulation due to the presence of a cape and the intensified upwelling in the leeside of the cape is consistent with several studies (Barth et al., 2000; Gan and Allen, 2002; Doglioli et al., 2004; Kuebel Cervantes and Allen, 2006; Meunier et al., 2010; Perlin et al., 2011; Liu and Gan, 2014). However, most of these studies deal with steady upwelling regimes or with relaxation periods of more than one day, and do not describe the diurnal variability caused by a daily oscillating upwelling regime. In our case, the diurnal variability of the wind is felt differently across the domain and the small-scale spatial alternation of upwelling/downwelling regions can effectively drive cross-shelf exchange, especially in the leeside of Cape Sines.

In summary, in-situ data and the numerical model results helped to characterize the nearshore circulation in the vicinity of Cape Sines. We conclude that the presence of the cape is responsible for the observed cross-shelf circulation pattern but only very few regions show a similar flow evolution as the observations. The persistence of upwelling-favourable winds promoted retention of cold and newly upwelled waters in the leeside of Cape Sines which is significantly relevant for pythoplankton blooms and larvae development (Roughan et al., 2005a, 2005b, Peliz et al., 2007; Oliveira et al., 2009). The fact that the wind diurnally undergoes relaxation and intensification strongly modifies the cross-shelf circulation, promoting superficial onshore flows at mid-day, in the leeside of Cape Sines, that overpower the strong along-shelf currents. The combination of these two wind regimes indicates that the study region has effective mechanisms of onshore transport during this period, as seen in Trindade et al. (2016). The small-scale circulation patterns described here can be particularly helpful to understand the transport and settlement of larvae in this region and in other regions with similar topography and wind characteristics.

Acknowledgements

References

Allen, J.S., Newberger, P.A., Federiuk, J., 1995. Upwelling circulation on the oregon continental shelf. Part I: response to idealized forcing. J. Phys. Oceanogr. 25, 1843–1866.

Austin, J., Lentz, S.J., 2002. The inner-shelf response to wind-driven upwelling and downwelling. J. Phys. Oceanogr. 32, 2171–2193.

Barth, J.A., Pierce, S.D., Smith, R.L., 2000. A separating coastal upwelling jet at Cape Blanco, Oregon and its connection to the California current system. Deep-Sea Res. II 47, 783–810.

Cruz, T., 1999. Settlement patterns of Chthamalus spp. at Praia da Oliveirinha (SW Portugal). Acta Oecol. 20, 285–287.

Cruz, T., Castro, J., Delany, J., McGrath, D., Myers, A., O'Riordan, R., Power, A.M., Rabaa, J., Hawkins, S., 2005. Tidal rates of settlement of the intertidal barnaclesChthamalus stellatus and Chthamalus montagui in western Europe: the influence of the night/day cycle. J. Exp. Mar. Biol. Ecol. 318, 5160.

Cruz, T., Oliveira, P., Fernandes, J., Angélico, M., Castro, J., Lima, N., Quintela, M., 2009. Final Report of project VERY NEAR Departures and Arrivals of Barnacle Larvaeonshore: Very Nearshore Physical Processes and Behaviour in SWPortugal (POCI/MAR/57630/2004).(Unpublished).

Cudaback, C.N.L., Washburn, L., Dever, E., 2005. Subtidal inner-shelf circulation near Point Conception, California. J. Geophys. Res. 110, C10007.

Doglioli, A.M., Griffa, A., Magaldi, M.G., 2004. Numerical study of a coastal current on a steep slope in presence of a cape: the case of the Promontorio di Portofino. J. Geophys. Res. 109, C12033.

Durski, S.M., Glenn, S.M., Haidvogel, D.B., 2004. Vertical mixing schemes in the coastal ocean: comparison of the level 2.5 Mellor-Yamada scheme with an enhanced version of the K profile parameterization. J. Geophys. Res. 109, C01015.

Estrade, P., Marchesiello, P., de Verdière, A.C., Roy, C., 2008. Cross-shelf structure of coastal upwelling: a two-dimensional extension of Ekman's theory and a mechanism for inner-shelf upwelling shut down. J. Mar. Res. 66, 589–616.

Fewings, M., Lentz, S.J., 2010. Momentum balances on the inner continental shelf at Martha's Vineyard coastal observatory. J. Geophys. Res. 115, C12023.

Fewings, M., Lentz, S.J., Fredericks, J., 2008. ADCP site of cross-shelf flow driven by cross-shelf winds on the inner continental shelf. J. Phys. Oceanogr. 38, 2358–2378.

Fewings, M., Washburn, S.L., Ohlmann, J.C., 2015. Coastal water circulation patterns around the Northern Channel Islands and Point Conception, California. Prog. Oceanogr. 138, 283–304.

Gan, J., Allen, J.S., 2002. A modeling study of shelf circulation off northern California in the region of the coastal ocean dynamics experiment: response to relaxation of upwelling winds. J. Geophys. Res. 107, C93123.

Ganju, N.K., Lentz, S.J., Kirincich, A.R., Farrar, J.T., 2011. Complex mean circulation over the inner shelf south of Marthas Vineyard revealed by ADCP site and a high-resolution model. J. Geophys. Res. 116, C10036.

Gutierrez, B.T., Voulgaris, G., Work, P.A., 2006. Cross-shore variation of wind-driven flows on the inner shelf in Long Bay, South Carolina,United States. J. Geophys. Res. 111, C03015.

Haidvogel, D., Arango, H., Budgell, W., Cornuelle, B., Curchitser, E., Di Lorenzo, E., Fennel, K., Geyer, W., Hermann, A., Lanerolle, L., Levin, J., McWilliams, J., Miller, A., Moore, A., Powell, T., Shchepetkin, A., Sherwood, R., Signell, R., Warner, J., Wilkin, J., 2008. Ocean forecasting in terrain-following coordinates: formulation and skill assessment of the regional ocean modelling system. J. Comp. Phys. 227, 3595–3624.

Hendrickson, J., MacMahan, J., 2009. Diurnal sea breeze effects on inner-shelf cross-shelf exchange. Cont. Shelf Res. 29, 2195–2206.

Horwitz, R., Lentz, S.J., 2014. Inner-shelf response to cross-shelf wind stress: the importance of the cross-shelf density gradient in idealized numerical model and Field ADCP site. J. Phys. Oceanogr. 44, 86–103.

Jacinto, D., Cruz, T., 2008. Tidal settlement of the intertidal barnacles Chthamalusspp. in SW portugal: interaction between diel and semi-lunar cycles. Mar. Ecol. Prog. Ser. 366, 129–135.

Kirincich, A.R., Barth, J.A., Grantham, B.A., Menge, B.A., Lubchenco, J., 2005. Wind-driven inner-shelf circulation off central Oregon during summer. J. Geophys. Res. 110, C10S03.

Kuebel Cervantes, A., Allen, J.S., 2006. Numerical model simulations of continental shelf flows off northern California. Deep-Sea Res. II 53, 2956–2984.

Lentz, S.J., 2001. The influence of stratification on the wind-driven cross-shelf circulation over the North Carolina shelf. J. Phys. Oceanogr. 31, 2749–2760.

Lentz, S.J., 2008. ADCP site and a model of the mean circulation over the Middle Atlantic Bight Continental Shelf. J. Phys. Oceanogr. 38, 1203–1221.

Lentz, S.J., Chapman, C., 2004. The importance of Nonlinear Cross-Shelf Momentum Flux during Wind-Driven coastal upwelling. J. Phys. Oceanogr. 34, 2444–2457.

Lentz, S.J., Fewings, M., 2012. Wind- and Wave-driven Inner-shelf Circulation. Annu. Rev. Mar. Sci. 14, 317–343.

Lentz, S.J., Guza, R.T., Fedderson, F., Herbers, T.H.C., 1999. Momentum balances on the North Carolina inner shelf. J. Geophys. Res. 226, 18205–18226.

Lentz, S.J., Fewings, M., Howd, P., Fredericks, J., Hathaway, K., 2008. ADCP site and a model of undertow over the inner continental shelf. J. Phys. Oceanogr. 38, 2341–2357.

Liu, Y., Weisberg, R.H., 2005. Momentum balance diagnoses for the West Florida shelf. Cont. Shelf Res. 25, 2054–2074.

Liu, Z., Gan, J., 2014. Modeling study of variable upwelling circulation in the East China Sea: response to a Coastal Promontory. J. Phys. Oceanogr. 44, 1078–1094.

Lucas, A.J., Pitcher, G.C., Probyn, T.A., Kudela, R.M., 2013. The influence of diurnal winds on phytoplankton dynamics in a coastal upwelling system off southwestern Africa. Deep-Sea Res. II 101, 50–62.

Marchesiello, P., Estrade, P., 2010. Upwelling limitation by geostrophic onshore flow. J. Mar. Res. 68, 37–62.

Marchesiello, P., McWilliams, J., Shchepetkin, A., 2001. Open boundary conditions for long-term integration of regional oceanic models. Ocean Model. 3, 1–20.

Maza, M., Voulgaris, G., Subrahmanyam, B., 2006. Subtidal inner shelf currents off Cartagena de Indias, Caribbean coast of Colombia. Geophys. Res. Lett. 33, L21606.

McCabe, R.M., Hickey, B.M., Dever, E.P., MacCready, P., 2015. Seasonal cross-shelf flow structure, upwelling relaxation, and the alongshelf pressure gradient in thenorthern California current system. J. Phys. Oceanogr. 45, 209227.

Meunier, T., Rossi, V., Morel, Y., Carton, X., 2010. Influence of bottom topography on an upwelling current: generation of long trapped filaments. Ocean Model. 35, 277–303.

Oliveira, P.B., Nolasco, R., Dubert, J., Moita, T., Peliz, A., 2009. Surface temperature, chlorophyll and advection patterns during a summer upwelling event off central Portugal. Cont. Shelf Res. 29, 759–774.

Pawlowicz, R., Beardsley, B., Lentz, S.J., 2002. Classical tidal harmonic analysis including error estimates in MATLABusing T_TIDE. Comput. Geosci. 28, 929–937.

Peliz, A., Marchesiello, P., Dubert, J., Marta-Almeida, M., Roy, C., Queiroga, H.H., 2007. A study of Crab Larvae Dispersal on the Western Iberian Shelf: physical processes. J. Mar. Syst. 68, 215–236.

Peliz, A., Boutov, D., Cardoso, R., Delgado, J., Soares, P., 2013. The Gulf of Cadiz-Alboran sea sub-basin: model setup, exchange and seasonal variability. Oceanogr. Model. 61, 49–67.

Perlin, N., Skyllingstad, E.D., Samelson, R.M., 2011. Coastal atmospheric circulation around a Cape during wind-driven upwelling studied from a coupled ocean atmosphere model. Mon. Weather Rev. 139, 809–829.

Pineda, J., Reyns, N.B., Starczak, V.R., 2009. Complexity and simplification in understanding recruitment in benthic populations. Popul. Ecol. 51, 17–32.

Relvas, P., Barton, E., Dubert, J., Oliveira, P.B., Peliz, A., da Silva, J., 2007. Physical oceanography of the western iberia ecosystem: latest views and challenges. Prog. Ocean 74, 149–173.

Roughan, M., Terrill, E.J., Largier, J.L., Otero, M.P., 2005a. Observations of divergence and upwelling around Point Loma California. J. Geophys. Res. 110, C04011.

Roughan, M., Mace, A., Largier, J., Morgan, S., Fisher, J., 2005b. Sub-surface recirculation and larval retention in the lee of a small headland: a variation on the upwelling shadow theme. J. Geophys. Res. 110, C10027.

Sanay, R., Yankovsky, A., Voulgaris, G., 2008. Inner shelf circulation patterns and nearshore flow reversal underdownwelling and stratified conditions off a curved coastline. J. Geophys. Res. 113, C08050.

Shchepetkin, A.F., McWilliams, J.C., 2005. The regional oceanic modeling system (ROMS): a split-explicit, free-surface, topography-following coordinate oceanic model. Oceangr. Model. 9, 347–404.

Soares, P.M.M., Cardoso, R.M., de Medeiros, J., Miranda, P., Belo-Pereira, M., Espáirito-Santo, F., 2012. WRF high resolution dynamical downscaling of ERA-Interim for Portugal. Clim. Dyn. 39, 2497–2522.

Tilburg, C., 2003. Across-shelf transport on a continental shelf: do across-shelf windsmatter? J. Phys. Oceanogr. 33, 2675–2688.

Trindade, A., Peliz, A., Dias, J., Lamas, L., Oliveira, P.B., Cruz, T., 2016. cross-shelf transport in a daily varying upwelling regime: a case study of barnacle larvae on the southwestern Iberian coast. Cont. Shelf Res. 127, 12–27.

Woodson, C.B., Eerkes-Medrano, D.I., Flores-Morales, A., Foley, M.M., Henkel, S.K., Hessing-Lewis, M., Jacinto, D., Needles, L., Nishizaki, M.T., OLeary, J., Ostrander, C.E., Pespeni, M., Schwager, K.B., Tyburczy, J.A., Weersing, K.A., Kirincich, A.R., Barth, J.A., McManus, M.A., Washburn, L., 2007. Local diurnal upwelling driven by sea breeze in northern Monterey Bay. Cont. Shelf Res. 27, 2289–2302.

Zhang, Xiaoqian, Smith, X.D.C., IV, DiMarco, S.F., Hetland, R.D., 2010. A numerical study of sea-breeze-driven ocean poincare wave propagation and mixing near the critical. J. Phys. Oceanogr. 40, 48–66.

Appendix B

Cross-shore transport in a daily varying upwelling regime: A case study of barnacle larvae on the southwestern Iberian coast

This Appendix is an article published in *Continental Shelf Research*. Because this article is primarily the work of Ana Trindade, it is not part of Luisa Lamas' thesis work but is included here for reference.

Research papers

Cross-shore transport in a daily varying upwelling regime: A case study of barnacle larvae on the southwestern Iberian coast

A. Trindade [a,*], A. Peliz [b], J. Dias [c], L. Lamas [b,c], P.B. Oliveira [d], T. Cruz [e,f]

[a] Institut de Ciències del Mar (ICM-CSIC), Departament Oceanografia Física i Tecnològica, 37-49, 08003, Barcelona, Spain
[b] Instituto Dom Luiz, Faculdade de Ciências da Universidade de Lisboa, Campo Grande, Edifício C8, 1749-016 Lisboa, Portugal
[c] MARE – Marine and Environmental Sciences Centre, Faculdade de Ciências da Universidade de Lisboa, Campo Grande, 1749-016 Lisboa, Portugal
[d] Instituto Português do Mar e Atmosfera, 1449-006 Lisboa, Portugal
[e] MARE – Marine and Environmental Sciences Centre, Laboratório de Ciências do Mar, Universidade de Évora, Apartado 190, 7521-903 Sines, Portugal
[f] Departamento de Biologia, Escola de Ciências e Tecnologia, Universidade de Évora, Portugal

ABSTRACT

With favored offshore and downstream advection, the question of which physical mechanism may promote onshore transport of larvae in upwelling systems is of central interest. We have conducted a semi-realistic high resolution (0.25 km) numerical study of Lagrangian transports across the inner-shelf under upwelling-favorable wind forcing conditions, focusing on the shelf area of the Southwestern Portuguese coast, in the lee of Cape Sines. We add our findings to several years of biological observations of *C. montagui*, a planktonic species with higher recruitment during the upwelling peak timely with the daylight flood. Simulations cover a fifteen days period during the summer of 2006. We focused on Spring and Neap tide periods and observed upfront differences between simulations and the in situ observations. However, the model is capable of representing the main dynamics of the region, namely the repetitive character of the inner-shelf currents. We find that the cross-shore flow varies significantly in the daily cycle, and locally within a scale of a few kilometers in association with local topography and the presence of the cape. We consider the region immediately in the lee of the cape to be an upwelling shadow where the larvae became retained, and found that tidally tied migration proves beneficial for successful recruitment during the spring tides period. Our work suggested that the wind is not the only mechanism responsible for the daily variability of the cross-shore exchange. However, its sharp reversal at midday is critical for the advection of larvae towards the coast.

© 2016 Elsevier Ltd. All rights reserved.

1. Introduction

The inner-shelf dynamical processes of plankton cross-shore transport and dispersion, are critical in several aspects of marine ecology and have motivated many different studies in recent years (Fewings et al., 2008; Lentz et al., 2008; Paris et al., 2013).

Many coastal species have a planktonic phase and larvae must be transported back onshore for settlement. This process is particularly interesting for species inhabiting coastal zones dominated by upwelling regime where average wind conditions favor offshore transport of surface material and onshore transport of the intermediate and bottom waters (dos Santos et al., 2008). This average circulation pattern may require complex adaptive responses in terms of the larval behavior and vertical distribution

(Shanks and Brink, 2005; Marta-Almeida et al., 2006), for larvae to overcome the mean advective tendency, and enable recruit on inshore areas. At the inner shelf, however, the double layer cross-shore circulation may shut down (Lentz et al., 2008) with a blocking of the cross-shore transport. Very close to shore, processes other than wind (e.g., tides and waves) need to be accounted for to explain onshore transport.

In this paper, we contribute to the knowledge of the cross-shore transport processes in upwelling systems. The southwestern Iberian coast is dominated by quasi-steady upwelling winds in summer (May–September) (Lemos and Pires, 2004). This coast is characterized by rocky shores that provide habitat for many benthic species with a planktonic phase. In particular, the case of *Chthamalus montagui* that is the most abundant intertidal barnacle of the Portuguese continental coast (Cruz et al., 2005). From the point of view of cross-shore transport, *C. montagui* has two interesting characteristics. First, its recruitment has been observed to occur from March to October, being highest during summer (O'Riordan et al., 2004) timely with the peak of upwelling activity.

* Corresponding author.
E-mail addresses: atrindade@icm.csic.es (A. Trindade), ajpeliz@fc.ul.pt (A. Peliz), jdias@fc.ul.pt (J. Dias), lalamas@fc.ul.pt (L. Lamas), pboliveira@ipma.pt (P.B. Oliveira), tcruz@uevora.pt (T. Cruz).
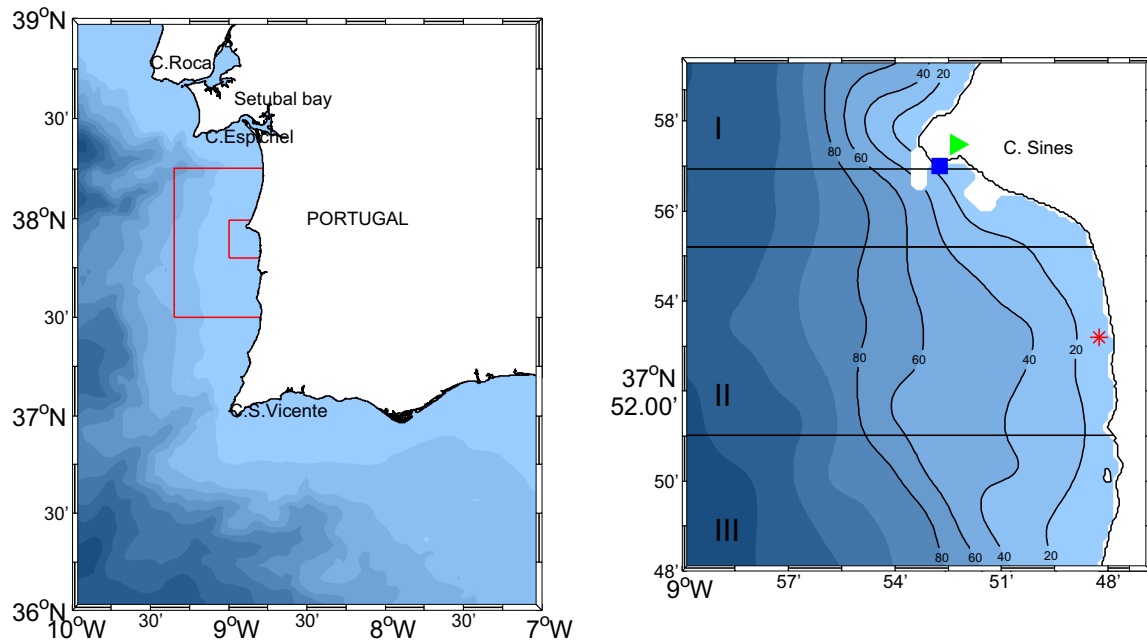
Fig. 1. Map and topography of the study area. The red boxes show the model domain and the study area. The right side figure shows the Port of Sines (P. Sines), the model topography in the study area, the location of the moored ADCP (✱), the Meteorological Station (▶) and the Tide Gauge (■). Markers I, II and III represent regions of recruitment assessment. (For interpretation of the references to color in this figure legend, the reader is referred to the web version of this article.)

On the other hand, variability of tidal recruitment (recruitment within the tidal cycle) of this species has been observed (Cruz, 1999; Cruz et al., 2005; Jacinto and Cruz, 2008). Recently it has been observed that settlement of this species occurs mostly during the day and during the flood (Cruz et al., 2005, 2009) and suggested that cyprids (last larval stage) of this species are mostly neustonic during daylight flood (Cruz et al., 2009).

In this study, we use numerical modeling to simulate the shelf circulation and the cross-shore transport patterns during a typical period of upwelling on the southwestern coast of Portugal (around Cape Sines (Fig. 1)) where the recruitment of *C. montagui* has been studied for several years now (e.g., O'Riordan et al., 2004). The processes of plankton dispersal on larger spatial and time scales, which determine the availability of larvae for settlement, are not addressed here. We assume that larvae are available near the coast, and our central objective is to understand the near shore circulation and the physical mechanisms that promote onshore transport during typical upwelling conditions, as well as explore its relation with the observed larval preference for settling during the daylight flood (Cruz et al., 2009).

Despite the localized nature and species-specific assumptions our conclusions may be applicable to other upwelling areas and to other planktonic species.

In the next sections we describe all the observations and models that were used. After, we make a detailed description of an upwelling event in the selected period with the existing data. We described all the numerical simulations of the shelf circulation and compared them to observations with a focus on the cross-shore circulation. The Lagrangian model results are presented, summarized and discussed with emphasis on the most relevant patterns of the daily cycle.

2. Data and models

2.1. Data

Atmospheric data (air temperature, incoming solar radiation and wind) were collected at the meteorological station of the Port of Sines authority. Tides were measured by a tide gauge located inside the port (Fig. 1 (right)). The above data were collected for three summers (2006–2008). Velocity and temperature profiles of the inner-shelf zone in the lee of Cape Sines (see Fig. 1), were measured with an Acoustic Doppler Current Profiler (ADCP) and a 5 thermistors chain deployed at a nominal depth of about 12 m. Thermistors measured temperature data at 2, 3, and 5 m above the sea floor, at the surface and 2 m depth. ADCP data were also collected for the above mentioned summer periods while thermistors data were only available for the summers of 2006 and 2007. All the data were hourly averaged. We used the observation period between July 20th and August 4th of 2006 to produce the ocean model initialization and forcing, and also to compare with the ocean model simulation outputs.

Satellite derived SST daily maps (∼2 km resolution) are used to illustrate the larger scale context during the study period, for the 20th and 30th of July and the 4th August of 2006. The satellite data were obtained from the Ifremer Cersat website (Medspiration Project).

2.2. Ocean model

Simulations were carried out with the Regional Oceanic Modeling System (ROMS), described in Shchepetkin and McWilliams (2005) and Haidvogel et al. (2008), on a high resolution 0.22×0.22 km grid for a fifteen day period. In the vertical, 32 σ levels are used with significant surface stretching ($\theta_s = 7$), a critical depth ($Hc = 5$ m) and no bottom stretching ($\theta_b = 0$) resulting in enhanced vertical resolution at surface levels. Topography data compiled in Peliz et al. (2013) was used. A low level of topographic smoothing is required because of the high resolution. To avoid large differences of topography around the domain (in particular the canyons on the north), a cutoff depth of 800 m is imposed. The minimum depth is 5 m (see model topography in Fig. 1 right).

Bottom drag quadratic parametrization is used with a variable coefficient $Cd = (k/\log(z_b/z_0)^2)$ with $z_0 = 0.005$, where k is the von Kármáan's constant and z_b is the height of the deepest level (Marta-Almeida and Dubert, 2006) (a test with constant

Table 1
ROMS configuration settings.

Lm	229	Number of points E-W
Mm	382	Number of points N-S
N	32	σ levels
h_{max}	800	Maximum depth [m]
h_{min}	5	Minimum depth [m]
h_c	5	Critical depth [m]
Δx	0.22	Horizontal resolution [km]
θ_s	7	Surface stretching parameter
θ_b	0	Bottom stretching parameter
r	3.0^{-4}	Linear bottom drag coefficient [m s^{-1}]
r2	0.005	Quadratic bottom drag roughness [m]
r_{log}	0.005	Log layer bottom drag parameterization [m]
sponge	15^3	Sponge layer [m]
A_h	200	Maximum horizontal viscosity [m^2/s]
$\rho 0$	1025	Sea water density [kg/m^3]

coefficients for a bottom drag of r2=0.005 showed the model not to be particularly sensitive to the bottom drag). Vertical mixing and diffusion is performed with the Large et al. (1994) K-Profile Parametrization (KPP) scheme.

Radiation conditions are used along the open boundaries for momentum and tracers, together with passive-active nudging open boundary forcing (Marchesiello et al., 2003). A sponge layer of 15 km is placed near the open boundaries, with maximum horizontal viscosity of $A_h = 200$ m^2/s to suppress reflections that tend to appear consequence of the reduced grid dimension. This configuration setting can be seen in Table 1.

2.3. Initialization and atmospheric forcing

The model assumes an initially flat ocean with a vertical density distribution typical of summer time (a sharp thermocline and a simplified linearly decaying salinity profile not shown here). The same temperature and salinity conditions are preserved near the open boundaries using a relaxation time scale (Marchesiello et al., 2001).

Different wind forcing conditions were tested. In a first case, we assume spatially homogeneous wind and use the wind time series of the metro-station to produce the hourly forcing values for the whole domain (here after the MS experiment). In a second case, we used model winds downscaled from Era-Interim data using the Weather Research and Forecast Model (see Soares et al. (2012) and Peliz et al. (2013)). The WRF wind fields show some relevant spatial inhomogeneity (not shown), but seem to systematically overestimate the winds when compared with the observed time series. The time-mean magnitude difference between the MS and the WRF winds at the meteorological station location was calculated and the WRF wind magnitude was reduced by that same quantity (preserving the direction). The experiment using this modified WRF winds will be referred to as WRF in the text.

Between the MS and WRF experiments there is no apriori reason to select one instead of the other. The WRF simulated winds seem to diverge from the observed winds at the meteorological station. They are too strong in the night-morning period and there is a sharper transition in the afternoon (see Fig. 2 (b) and (c)). On the other hand, the model winds capture part of the spatial variability missing if the forcing is based on the MS winds only (this however, cannot be properly checked). In the description of the results we show both simulations. However, for conformity between the lagrangian studies, we will conduct these simulations only for the WRF case.

The atmospheric forcing heat fluxes include shortwave radiation (a diurnal cycle peaking at 1100 W/m^{-2}), latent and sensible fluxes (using averaged data from the meteorological station, and outgoing long-wave heat flux calculated based on the model SST).
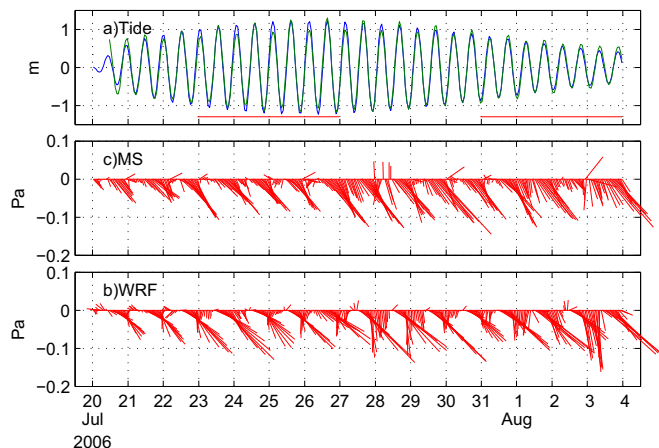
Fig. 2. (a) Observed sea level (green) and model free surface elevation (blue) at the tide gauge location. (b) Stick plots of wind stress vector time series at the meteorological station location for the MS experiment, and in (c) for the WRF experiment. The latter were reduced in magnitude by comparison with the hourly winds from the meteorological station of the Port of Sines authority. In (a) the red lines along the x axis indicate the 4-day averaging periods used in the study: the first will be referred to as spring and the second as neap. (For interpretation of the references to color in this figure legend, the reader is referred to the web version of this article.)

The surface heat fluxes are spatially homogeneous with a fixed daily variability during the 2-week experiment (only the long wave emission is variable because of the internal SST dependence).

The spin-up period ($\sim$3 days) is visible from model outputs and was excluded from the subsequent analyzed periods.

Tidal elevations and 2D momentum fluxes associated with tides were applied along the open boundaries. This tidal elevations and currents are obtained from TPXO 07, a global model of ocean tides that best suits the Laplace tidal equation, (Egbert and Erofeeva, 2002; Marta-Almeida and Dubert, 2006; Sauvaget et al., 2000). Marta-Almeida and Dubert (2006), pointed the M_2 and S_2 as the main harmonic for the western Portuguese coast, which cause clear spring-neap cycles modulated by other constituents. Despite the fact that their cotidal charts for the diurnal tidal components presented very small amplitudes, the forcing implemented includes the main semi-diurnal and diurnal constituents, and the model is set to process 8 tide components, namely M_2, S_2, N_2, K_2, K_1, O_1, P_1 and Q_1.

The grid and the tidal forcing were produce using ROMSTOOLS v2.1 package (Penven et al., 2010).

2.4. Particle models

We conducted plankton transport studies with Ichthyop, an offline particle tracking model configurable for plankton applications (Lett et al., 2008). Also, to account for complex vertical migration patterns and to resolve more accurately the advection scales, we performed online experiments with ROMS using floats, described in Capet et al. (2004) and Peliz et al. (2007).

Onshore transport of larvae is the main focus of this study, therefore, transport to shore was studied under three advection scenarios, in which we differed mainly the vertical movement conditions imposed to the particles advection. Every particle is initiated at the surface level.

We will address the scenarios tested in Ichthyop as Fixed depth mode (Fm) and Passive mode (Pm), the base experiments. In both scenarios particles are released at the surface level, being that the former one concerns simulations where particles drifted horizontally without changing their depth throughout the simulation, and the latter where the particles are advected freely in the water

column, both horizontally and vertically, depending on the model 3D velocity field.

The assumed larval behavior for this species was implemented in ROMS online floats, and is referenced from now on as the daylight flood Vertical Migration (VM) scenario, where floats have a passive behavior in time, with the exception for the periods of daylight flood (tidally tied migration), when they are bound to and only advected on the surface level (the upper sigma).

The purpose of these simulations is to assess the percentage of particles arriving inshore (referred hereafter as recruitment for simplicity), the hours when the recruitment is larger, as well as the source areas of the recruited particles. Shanks et al. (2010), re-inforces the hypothesis that the surf zone is a semi-permeable barrier to shoreward migration. This region is the last body of water that particles must cross before reaching the shoreline. However, the ocean model used here is unable to resolve the physical processes that take place in such proximity to the coast, thus, we consider that for a particle to be counted as recruited, it needs to arrive to a near-shore region within the 24 h frame of the advection.

For the study period, regions in the northern/southern edge of Cape Sines present different current regimes. Therefore, we chose to analyze zone I, which is in the northern edge of the cape, and zones II and III, two adjacent regions in the lee of the cape, which consist of a more cape sheltered and a more wind exposed region. Between zones I and II, there is the Port of Sines which was not considered a study region (see Fig. 1 (right)).

We assessed arrival in coastal zones I, II and III individually to characterize the local recruitment pattern.

Simulations ran for a period in the spring tide (days 23rd to 26th July), and another in the neap tide (31st July to 3rd August), these periods are indicated in Fig. 2(a). The rationale for the choice of these specific periods will be explained in the next sections.

2.4.1. Ichthyop: large release experiment

Initial Ichthyop simulations, where we released particles throughout the shrinked domain (see Table 2), set the base configuration settings for the a posteriori experiments. These configuration settings are summarized in Table 2.

The near shore is defined as the zone within 150 m, which in the ocean model corresponds to a little more than half a cell point (3/5), from any coastal point of the three specific regions, namely

Table 2
Ichthyop large release configuration.

Limits	(lon,lat) degree
(a) Shrinked domain	
NW corner	[−9.00,38.00]
SW corner	[−9.00,37.76]
NE corner	[−8.78,38.00]
SE corner	[−8.78,37.76]

Set Up		
(b) Set up		
Period of simulation	Spring	23–26 July [4 days]
	Neap	31 July to 03 August [4 days]
Duration of transport	1	Days of transport upon release
Daily releases	12	Number of releases
Release schedule	Homogeneous	Every 2 h for a day
Release condition	Homogeneous	Offshore extention of 3 [km]
VP for release event	954	Individuals released every two hours
Vertical migration	NO	Vertical diel
Advection	Horizontal	YES
Recruitment target	< = 0.15	Distance to the coast [km]
Experiments	Fm	Surface Fixed mode
	Pm	Surface Passive mode

zone I, II and III (see Fig. 1 (right)).

Ichthyop was forced by 30 min averaged velocity outputs, for the two simulation periods of the previously generated ROMS record, with particles initialized at an along-shore band, with a homogeneous distribution (every 2 grid cells) and with an offshore extention of 3 km (see Fig. 3 left). Surface releases were homogeneously distributed in time and scheduled to start at midnight on day 1, and continue on a 2 h interval, ending at 22 h of the penultimate day (July 25th and August 2nd). Particles were advected for 24 h because we are interested in understanding the variability of recruitment in a daily scale. The tracking of the particles was limited to their advection period, and comprised to the geographical area between 37.76–38.00°N, and 9.00–8.78°W.

2.4.2. ROMS and Ichthyop: releases per recruitment zone

Due to numerical limitations in ROMS, we redefine a few configuration settings as follows. The near shore distance is broadened to 375 m (about 1.5 cell point), while the spatial coverage of released particles is reduced.

For the ROMS online experiments (VM scenario), the ocean model initializes floats at the most superficial sigma with a homogeneous distribution over each zone. It has the same offshore extension as earlier in Ichthyop, but with less meridional coverage (Fig. 3 (right)). We also apply the same release schedule, advection period, and tracking of floats as in the offline model. Offline per zone releases are conducted in Ichthyop for the base cases (Fm and Pm), with the altered configuration in order to be compared with the VM experiment.

3. Results

3.1. Observations

3.1.1. Inner-shelf conditions during the study period

During the selected study period, the winds had moderate magnitude with steady northwestern direction bearing a conspicuous daily cycle that reaches its maximum towards the late afternoon (Fig. 2(b)). This upwelling favorable wind pattern started by 20 July and remained quasi-steady for about 2 weeks. WRF winds (same figure bottom plot) show a very similar pattern, but are more intense in the morning period and the transition to the afternoon peak is sharper than in the observations.

To analyze the upwelling event in its context, we show three synoptic SST maps (Fig. 4) of the southwestern Portuguese coast (centered on the study area). The images were selected to include a period at the beginning of the event (20 July) and two situations during its fully developed phase (July 30 and 4 August). The first image shows that a previous upwelling event had taken place since the western coast is clearly cooled, but the upwelling front is not as sharp. In particular, it is still visible in the tip of the Southwestern coast (Cape S. Vincent) the remaining of the coastal counter-current (note the warmer water contouring the cape anticyclonically) that usually forms during strong Levantine episodes (Relvas and Barton, 2002; Teles-Machado et al., 2007; Relvas et al., 2007). This current is characterized by the generation of a warm and fast flow that initiates along the southern coast exceeding 0.4 m/s when it turns Cape S. Vincent (Relvas and Barton, 2005). This flow reaches the latitude of Cape Sines, and even northwards in some cases. This current affects the inner-shelf zone by producing a downward movement of the isopycnals and a considerable warming (up to a few degrees) of the coastal waters (Relvas et al., 2007). The following images in Fig. 4 show a fully developed upwelling with a surface structure typical of summer time. A first larger cold filament rooted on the northern zone (Capes Roca and Espichel), progresses southwestward offshore of our study area.
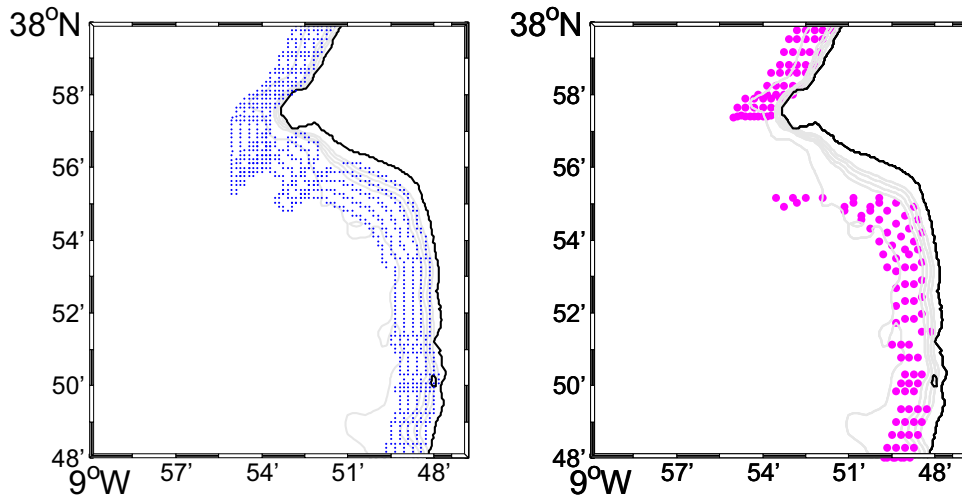
Fig. 3. Map with the release location of the lagrangian particles. Left: blue dots are particles initial positions in the large release experiment with Ichthyop; right: magenta dots are lagrangian floats/particles for releases in the recruitment zones experiment. (For interpretation of the references to color in this figure legend, the reader is referred to the web version of this article.)
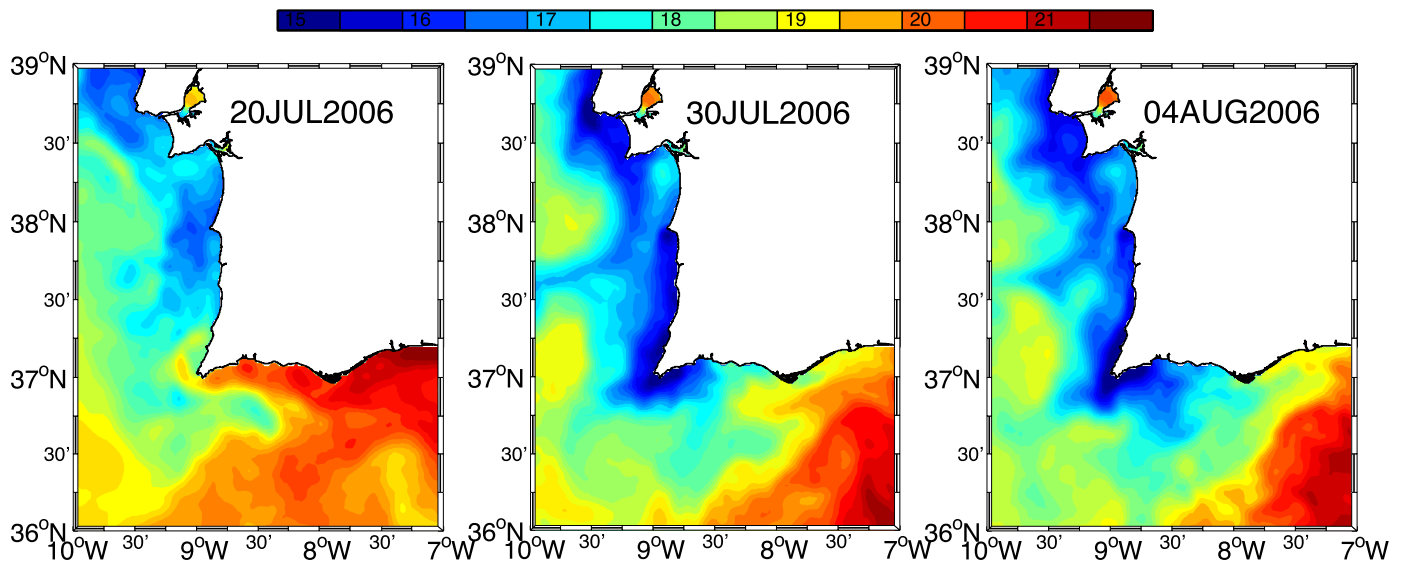
Fig. 4. AVHRR derived SST for 20, 30 July and 4 August.

The Setubal bay is occupied by a warmer water pool indicating the absence of local active upwelling in that site possible as a consequence of a sheltering effect (Oliveira et al., 2009). The surface cooling is much stronger in the lee side of the capes, indicating a topography driven enhancement of the upwelling. Between the last two SST scenes there is little change of the SST field confirming that the ocean has reached a relatively steady state.

3.1.2. Measurements in the inner-shelf

The inner-shelf currents and water column stratification (mostly driven by temperature since fresh water fluxes are reduced in summer time) were observed at a mooring south of Cape Sines (see Fig. 1 right). The water column temperature profile evolution is represented in Fig. 5 (a). The warming effect from the previous counter-current event is visible in the first 3–4 days. After that, the inner-shelf cools up by a few degrees entering a relatively steady phase marked by a pronounced diurnal cycle. Besides the diurnal cycle, the major changes in temperature seem to happen during the transition between flood and ebb periods, specially at the deeper levels, suggesting an association to the semi-diurnal

tide (Fig. 5(d)). Fig. 5(c) and (d), show the time series of in situ temperature (blue line) and model temperature (red line) for the upper and lower thermistors positions. The diurnal cycle is clear in both series and the bottom record also reveals a sub-daily periodicity likely associated with mixing and tidal effects. Despite the cooling trend of the whole water column the stratification is maintained with a top down temperature difference usually above 1°, with a maximum late in the afternoon. In summary, despite the peaks of north winds in the afternoon, and the tidal mixing from below, the buoyancy input prevents the homogenization of the water column even at these shallow depths.

The currents were also profiled by an ADCP at the same place, and the daily evolution of the along-shore and cross-shore components during the study period is plotted in Fig. 6 (a) and (b).

Despite some variations during the 2-week study period, the wind forcing is very regular and the response of the shelf currents is also repetitive. The along-shore flow shows the development of a diurnal coastal jet that intensifies in the afternoon (Fig. 6(a)). In the cross-shore component, the flow takes a sharp reversal at about mid-day (Fig. 6(b)), from offshore (negative) to onshore
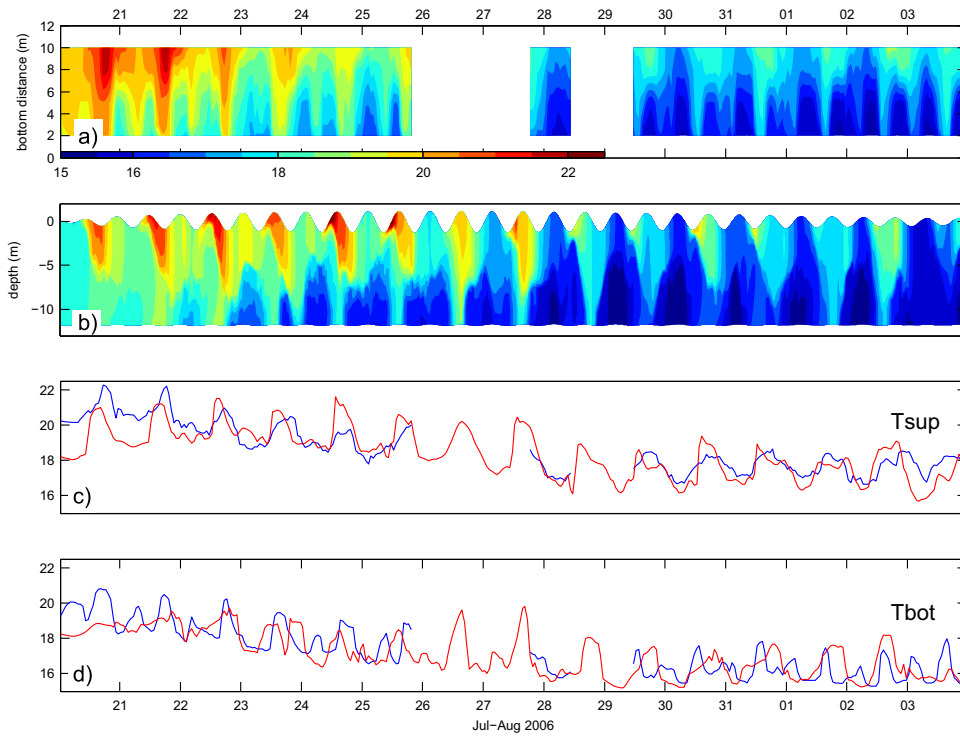
Fig. 5. Time series of temperature profiles. (a) from moored thermistors and (b) from the model output at the mooring site. In (c) and (d), respectively, the time series of near surface (2 m) and near bottom temperature. Thermistors data (blue) and model (red). (For interpretation of the references to color in this figure legend, the reader is referred to the web version of this article.)
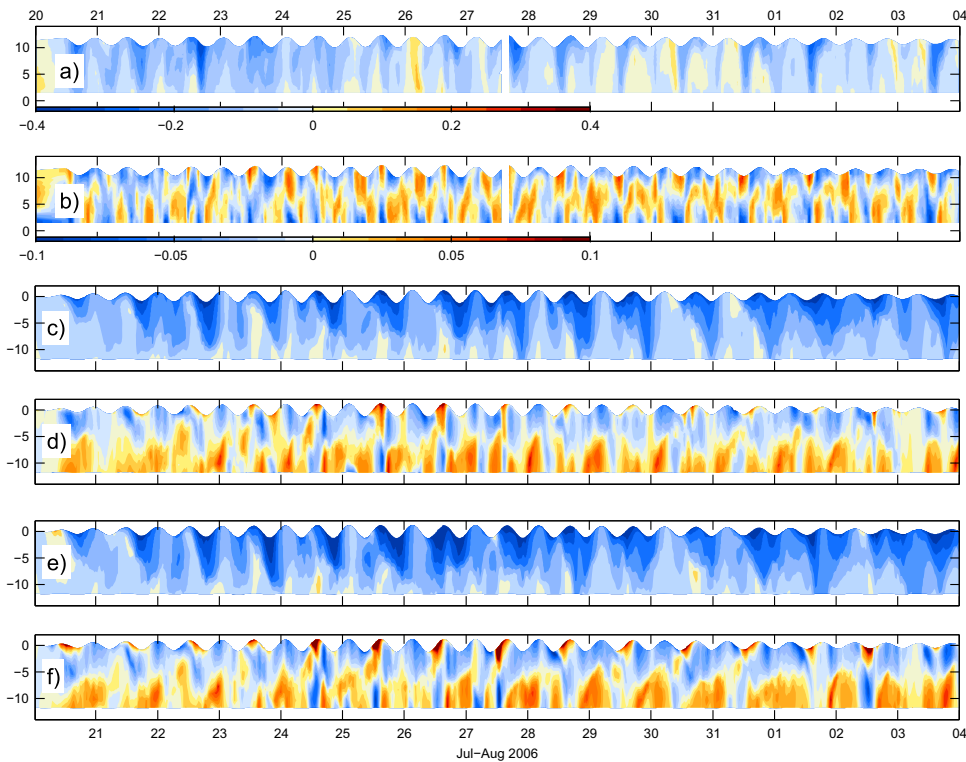
**Fig. 6.** Top two plots show the velocity profiles measured by the ADCP for the (a) along-shore and (b) cross-shore components (m/s). Model results for these components are plotted for the MS, (c) and (d), and WRF (e) and (f) experiments. Model profiles were extracted at the same location of the ADCP data.

(positive) at the surface early in the afternoon (and exactly the reverse bellow), it is a repetitive pattern observed almost every day throughout the fortnight cycle. For most of the days, it seems to be in phase with the tidal transition from daylight ebb to flood in the spring and neap phases of the time series.

Due to the dominant daily variability it makes sense to analyze an average day. This average-day is produced as follows: for a given number of days we average all existing data between 24 h and 1 a.m. to produce the first data point; all data between 1 and 2 a.m. to produce the second, and so on such that a 24 h average cycle is
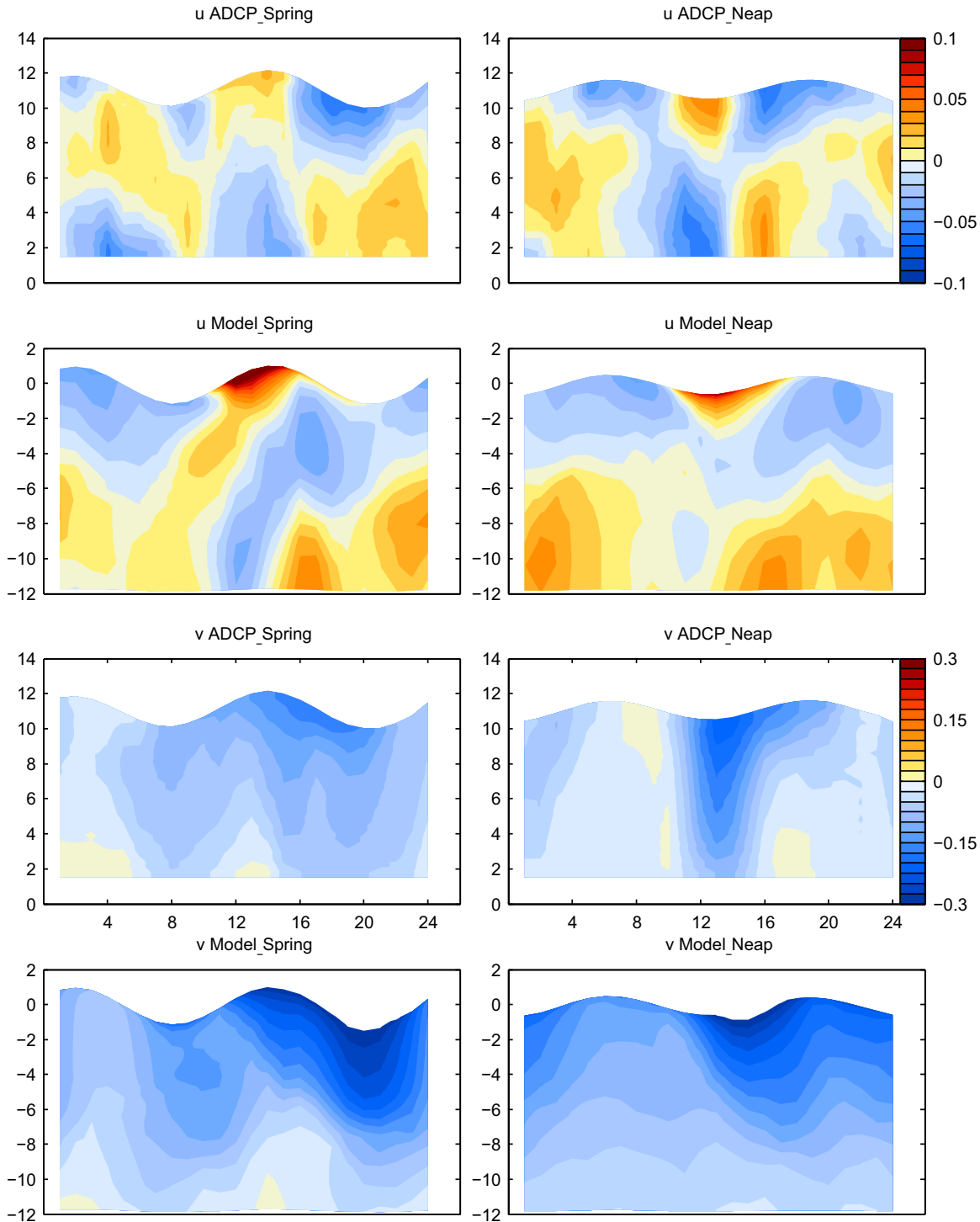
Fig. 7. Averaged-day cross-shore (top four plots) and along-shore (bottom four plots) currents components (m/s), during the spring (left) and neap (right) periods defined in Fig. 2(a). For each component, the average-day is computed from ADCP data (first and third rows) and from model results of the WRF experiment (second and fourth rows).

computed. Since tides are important and their phase changes from day to day, this averaging needs to be done with care to avoid aliasing effects. In principle, averaging over the entire fortnight cycle should filter out significantly the effect of semi-diurnal tides. However, since we want to focus on different periods in what concerns the tidal phase and magnitude, it was decided to conduct 4-day averaging periods so that the phase lag is about 1/4 of the M2 period. For this averaging we selected the periods indicated in Fig. 2(a).

Note that the selected periods are not centered with the

maximal/minimal tide magnitude. The selection was done so that the diurnal high-tide/low tide peak happens around noon for the first/second averaging period. Since the first period mostly covers the spring phase we shall refer to it as spring, and neap for the second one.

Fig. 7 shows the currents for the spring/neap periods. At upper levels, the onshore current during the spring tidal phase (days 23–26 July) occurs mostly during the daylight flood period. Conversely, during the neap period (31 July–3 August), the onshore current period is centered at the low-tide.

The average daily behavior of the cross-shore currents at this site (Fig. 7; second row) indicates that surface waters flow offshore the largest part of the day, but with some exceptions. The early afternoon period when the sharp reversal is observed and the surface transport becomes shoreward is very clear in the average day of both periods. At deeper levels, the cross-shore flow averaged-day pattern is more complex. During the night-morning period the cross-shore flow tends to be characterized by a three-layer flow: return at mid-depth and offshore both at the surface and bottom. In the afternoon, after the reversal, there is an up-welling type double layer circulation with offshore flow at the surface. Note that the water column measured by the ADCP does not reach the very surface (the upper most bin used in this study corresponds to approximately 1 m from the surface). This may partially explain the differences between model and moored measurements in what concerns the shoreward current intensity in the top meter and the phase of the tidal cycle in which surface shoreward transport happens (discussed below).

3.2. Ocean model results

3.2.1. Comparison with the shallow water mooring

The model temperature and velocity profiles were extracted at the model point closest to the mooring site. The time series and average-day profiles were computed for the same periods as provided in the observations. Fig. 5(b) shows the model temperature profile time series at the mooring site. The diurnal heating seems to be more limited to the surface than in the observations. The near surface temperature time series (Fig. 5(b)) indicates that the evolution of the surface temperature is close to that in the observations, but the heating tends to be more rapid in the model. Also, the model temperature decays faster in the afternoon than the observed one. Note for example the period between 30 July and 4 August (Fig. 5(a) and (b)). With the set-up of the diurnal coastal jet there is a general warming of the entire water column probably induce by vertical mixing. Later in the day the upper water column restratifies and a secondary mixing event (probably from below due to tidal mixing) takes place. In the model, the mixing at the beginning of the afternoon is much weaker and prolongs itself during the day. This may be caused by too much mixing in the afternoon, by an underestimation of heat flux later in the day, or by overestimation of the advective effect - the coastal jet bringing colder waters to the south and preventing re-stratification by overturning. Note that the mooring site is in the lee of the cape and it is likely that the real winds may be somewhat damped relative to the winds measured at the cape by the meteorological station. This effect may be underestimated in the model (the available model winds of 9 km resolution are not fine enough to simulate this effect).

Also, it is clear that the model is not able to reproduce accurately the sub-daily temperature fluctuations associated with tides (Fig. 5(d)). The near bottom measurements display a semidiurnal signal associated with tides (most pronounced when the low tide is observed timely with the development of the coastal jet). This latter feature is not consistently reproduced by the model owing to a deficient representation of the coastal jet in the deeper levels: an over-stratified water column is produced and the coastal jet is more vertically sheared than in the observations (see below).

The along-shore and cross-shore velocity components at the mooring site are plotted in Fig. 6((c) and (d) for MS and e and f for WRF experiments). Although some differences are readily clear, the repetitive character of the inner-shelf currents is also evident in the model. The model output currents for the WRF experiment are slightly stronger than the ones for the MS experiment. Besides that, there are no significant and consistent differences between the output currents of the two experiments. The daily behavior

and the model-observations differences are best represented in the averaged-day plots (Fig. 7). The upper four plots in this Figure, compare the ADCP (upper row) and the model (lower row) averaged-day cross-shore flow during the spring (left) and neap (right) days, while the bottom four plots do so for the along-shore flow. The latter, tends to be stronger and shallower in the model than in the observations (Fig. 7 bottom four plots). Besides that, the phase of the along-shore jet is well simulated in the spring period, but not so good in the neap days. In fact, the observed mid-day jet is more temporary (mostly between noon and 16 h), and decays very fast to the end of the day. The model has its maximum at about the same time at the surface, but lags in depth, and is maintained much longer in the day.

Despite the importance of the along-shore component, the cross-shore flow is more relevant for our central objective. As it was mentioned before, the cross-shore component during the second half of the day approximates a double-layer flow. Around mid-day there is a sharp reversal in the current direction, the 3 cm/s offshore flow reverses onshore in less than one hour. At about 16 h (averaged-day time), the pattern reverses and approximately stays so for the rest of the day (sometimes the flow assumes a 3-layer structure). In general, the model represents reasonably well the cross-shore flow structure, both in magnitude and in phase, during this half of the day (especially for the spring days when the flow is shoreward during the diurnal flood). During the night/morning period, the vertical structure of the cross-shore flow is more complex and the difference between the neap and spring phases is more striking. Also, its representation in the model is not as good for the spring period as it is for the neap. The model tends to preserve a 2-layer like flow with offshore flow at the surface, and that is not always true in the spring period although the measured surface flow is generally offshore.

The main transport should be along-shore and southward during the whole event (with very few exceptions), since the along-shore is about 3 times larger in magnitude than the cross-shore flow, as can be seen in Fig. 6. The four lower panels of Fig. 7 show more clearly the structure of this along-shore flow, with a surface-intensified current developing throughout the day and peaking in the afternoon. In the model plots there is an over-estimation of the current in respect to the ADCP panels. Apart from that, the structure of the coastal jet is well reproduced for both periods. For what concerns the cross-shore component, the transport near the surface (first few meters) undergoes a clear daily cycle. The transport is offshore most of the day with a sharp reversal of few hours usually in the early afternoon (the reversal is observable in both periods but it is sharper in during the neap phase (Fig. 7, first row from the top)). On the other hand, model results clearly show a sharper reversal in the spring period, taking place during the diurnal flood period. The pattern seems to be more complex in the interior and bottom levels during the night/morning period, and tends to be the reverse situation (in a 2-layer type flow) in the afternoon. In this context, it can be anticipated that onshore transport of plankton, drifting at the surface, mostly happens from midday to 3 p.m., but that of plankton migrating vertically or randomly distributed in the water column can be much more complex.

3.2.2. Spatial variability

To understand to what extend the flow pattern described above is representative of the domain we now analyze the spatial structure.

Fig. 8 shows the model surface temperature and currents averaged for the spring (top row) and neap (lower row) periods and for different times of the day. We recall that the selected hours of the averaged-day are in opposite phases of the tide in our selected neap and spring periods. The SST changes from one period
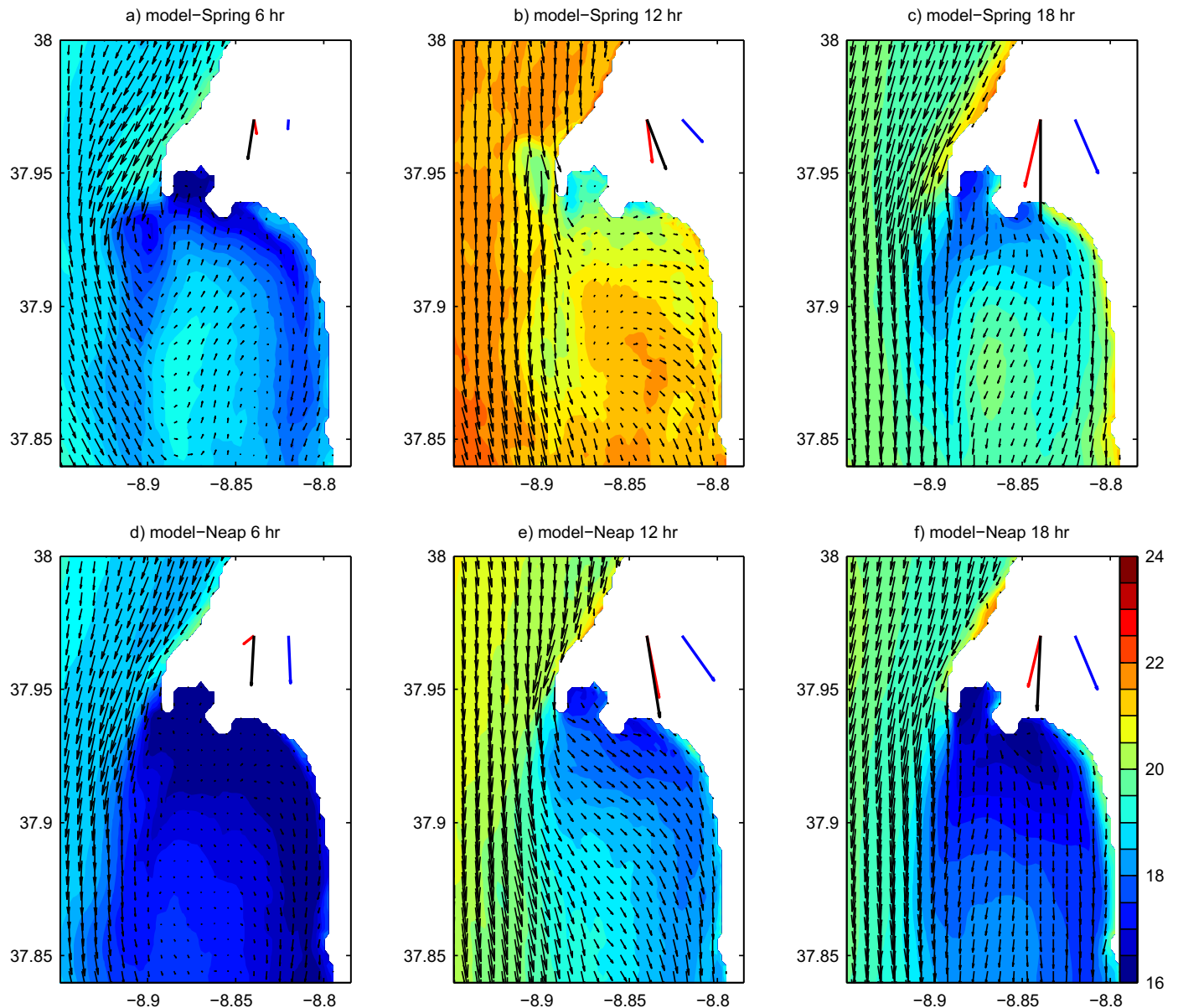
Fig. 8. Modeled surface temperature (°C) and velocity vectors averaged for spring (a)–(c) and neap (d)–(f) periods at 6, 12 and 18 h (average-day hours). The arrows are plotted every 3 grid cells. The arrows over land indicate: (blue) wind (not scaled with currents); (red) ADCP upper bin averaged over the indicated period; (black) model currents at the ADCP site (nearest grid cell). (For interpretation of the references to color in this figure legend, the reader is referred to the web version of this article.)

to the other are associated with the accumulated effect of cooling along the upwelling event. Within the averaged-day the cooling is associated with the heat fluxes and wind strengthening along the day. The most intense upwelling takes place in the lee of the cape (a careful analysis of Fig. 4 also allows the confirmation of this aspect). The currents show that there is an active jet all day long that intensifies in the afternoon. The jet separates in the lee of the cape leaving a zone of weaker currents to the east. North of the cape the currents tend to be along-shore with a convergent component in around mid-day (note that by this time the wind is almost perpendicular to the coast). South of the cape the currents have a clear onshore tendency - with the wind – by 12 h. About 6 h later (by 18 h averaged-day time), the rotation effects begin to overcome friction and despite the maintenance of the wind magnitude (or even increase in the spring period), the surface flow begins to have a meridional orientation to the right of the wind. Note that in the jet zone, these changes are subtle since the interior effects of the water column are also important. The flow

along the coast in the lee of the cape is more convergent around noon and then progressively becomes more along-shore with an offshore component later in the day and south of 37.9 N, where the coast becomes meridionally oriented again.

The comparison between the model and observations at the mooring site (arrows over land) confirm the current overestimation in the morning period (model winds are too strong during this period), and a better agreement in the afternoon period. The phase of transition from convergence to divergence near the coast is also not exactly simulated as was observed in Fig. 7 (upper four plots), the onshore convergence period in the model seems to be 1 or 2 h longer (note however that this happens within a very shallow noisy layer, and thus removed in the ADCP data processing).

3.2.3. Model sensitivity analysis

The reasons for the discrepancies between the model and the observations may be numerous: the initialization and assumption about no larger scale forcing; the spatial homogeneity and
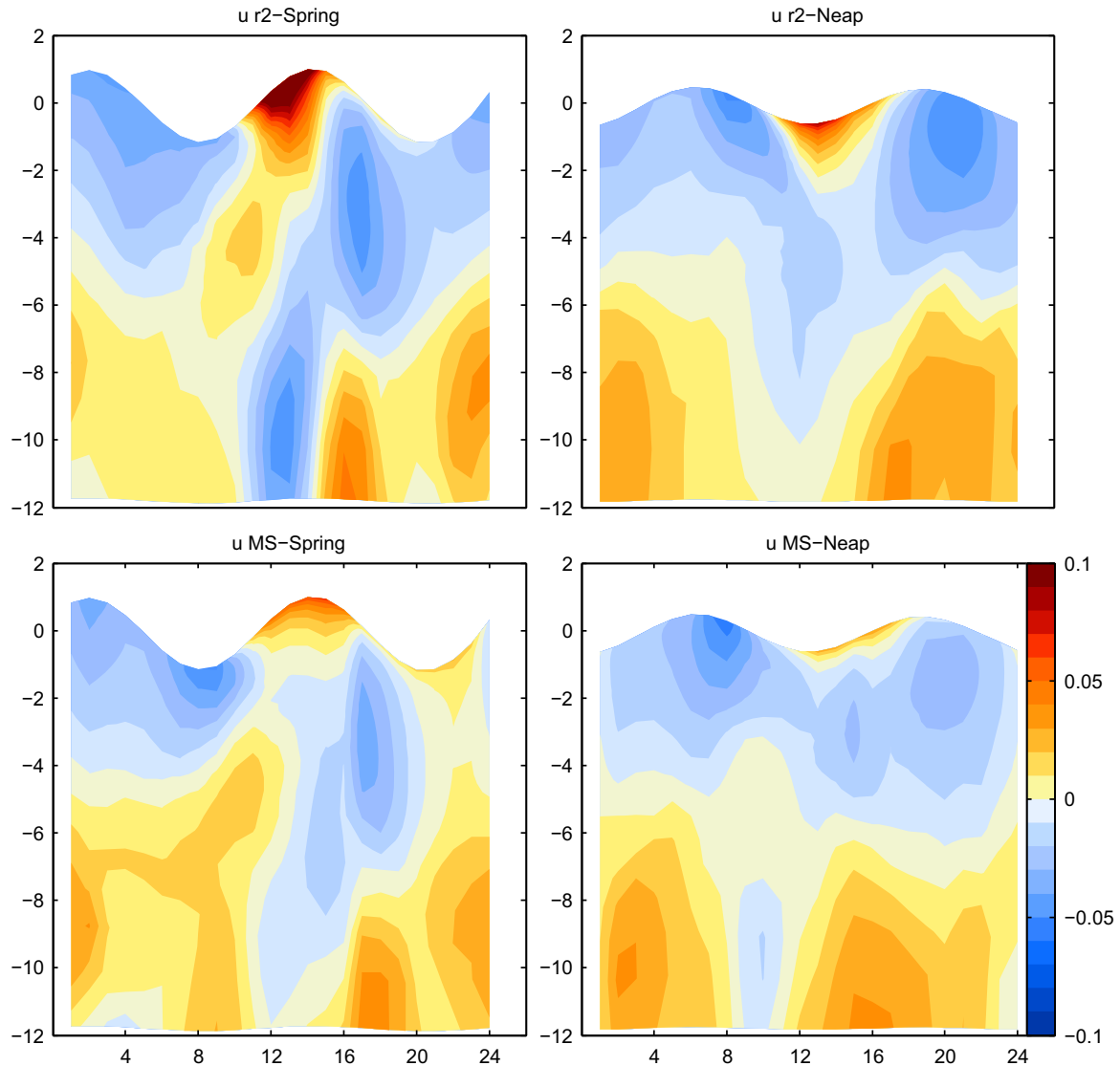
Fig. 9. Cross-shore averaged-day structure (m/s) at the mooring site for different experiments (to be compared with the four upper plots in Fig. 7).

repetition of the atmospheric heat fluxes forcing; the accurate representation of the local winds, the complexity of mixing processes not accounted for in the model (surface waves for example). In the present case, we tested different wind forcing conditions and bottom drag. The analysis, however, indicates that the major features of the surface circulation are maintained and the major changes happen in the timings of the mid-day inversion of the cross-shore flow and of the details of circulation near the bottom. Overall the patterns of the surface flow are not very different. Fig. 9, shows the cross-shore structure for spring and neap periods of different experiments, in the top plots the WRF experiment with a constant bottom drag coefficient (r2) and in the bottom the MS experiment forced with a log layer.

Note that both experiments seem to agree well in the spring period, although the magnitude of the MS in this period shows a better agreement with the observations (see Fig. 7). Yet, the performance for the neap period is not so good. The convergence period is too weak at the surface. Overall, the r2 experiment is not very different from the base case shown in the top row of Fig. 7 (in which a log layer is used).

After a careful evaluation of the average profiles in Figs. 7 and 9, we chose to use the WRF experiment (forced by a log layer varying bottom drag coefficient) in the lagrangian tests because it best

reproduces the ADCP data in the neap period. In the spring period all experiments show similar results, with the MS experiment being marginally better in reproducing the magnitude of the currents.

In summary, to the extent that the mooring data is representative of the inner-shelf cross-shore flow, the WRF experiment represents relatively well the major features of the surface circulation at the ADCP location. It's main weaknesses reside in the model tendency to behave as a double-layer flow, with too strong along-shore flow in the morning. Also, the inshore convergence period seems to be longer and more intense then the observations (although we have not very near surface current data).

3.3. Lagrangian models results

In this section we analyze how each of the chosen advection scenarios (Fm, Pm and VM) affect the amount of particles arriving to the shoreline, in terms of temporal (daily scale) and spatial (coastal zone) variability.

As to the latter, we present only Fig. 10 that shows the distribution maps for particles from source areas to their recruitment location in the large release experiment. This figure is illustrative of the recruitment patterns in the offline simulations, given that
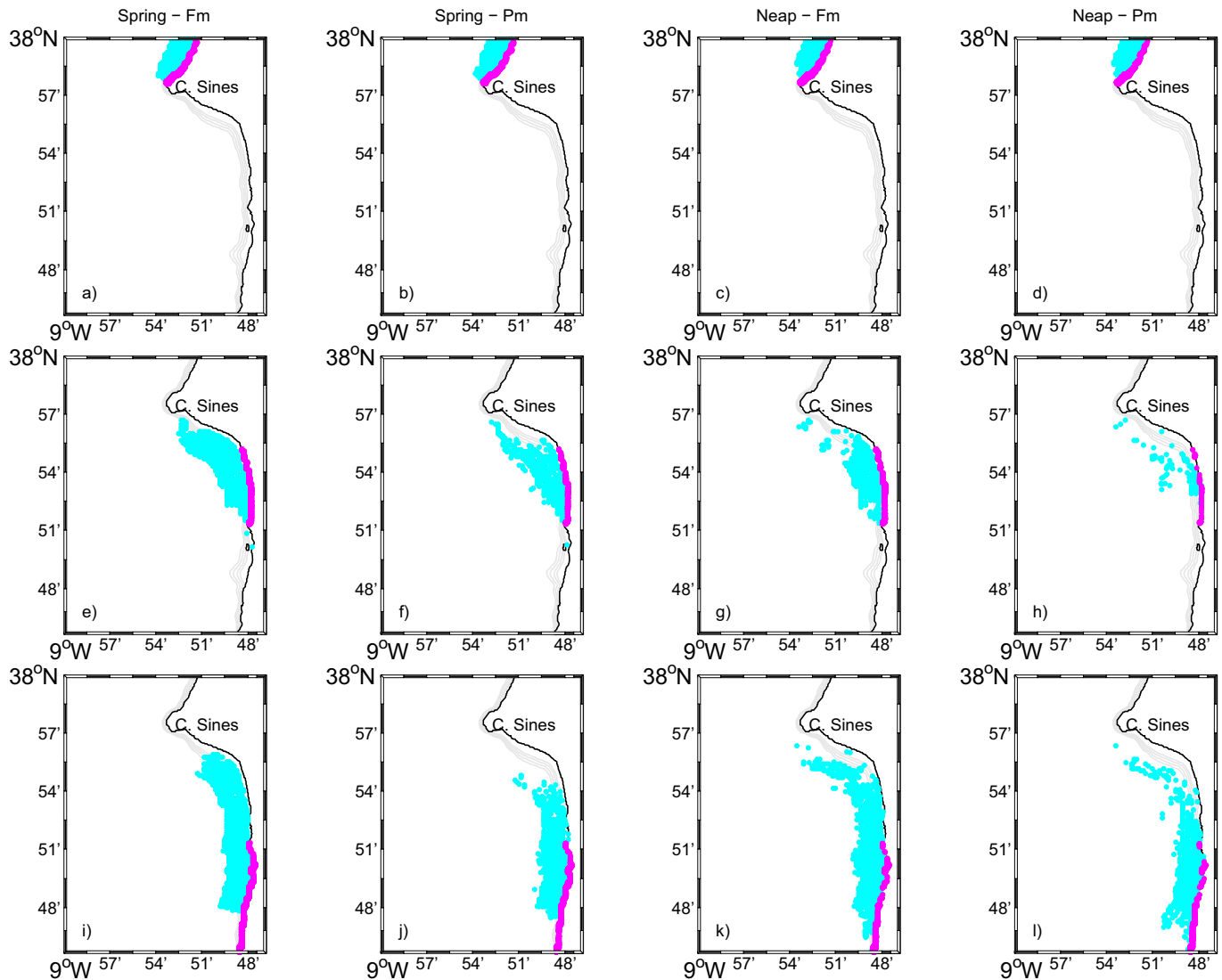
Fig. 10. Recruitment maps for zones I, II and III (first, second and third rows) with the initial positions of the drifters in blue and their recruitment position in magenta, for the large release experiment in Ichthyop. Spring simulations in the two columns to the left, neap simulation in the right columns. Fm particles on plots (a), (c), (e), (g), (i) and (k), Pm particles on the remaining plots. (For interpretation of the references to color in this figure legend, the reader is referred to the web version of this article.)

both experiment (large and per zone release) show the same results. We observed that arrivals on the northern section (Fig. 10 first row) came exclusively from the north of the cape. Recalling Fig. 8 this was to be expected, as described, the surface flow for this region is along-shore and has a convergent component around mid-day. The region immediately in the lee of the cape is somewhat sheltered (Fig. 10 second row), and particles recruiting within this section of coast came mainly from the region south of the Cape and to the east of the upwelling jet. In the southernmost region (Fig. 10 third row), we see recruited particles originate from the entire along-shore region south of the Cape, allowing for those released more offshore to benefit from the predominant meridional surface flow and also recruit, thus explaining why recruitment is larger for this section.

Closer examination of the maps on Fig. 10, reveals that within each recruitment zone, the initial position of arriving particles is invariant with respect to both simulation period and advection scenario. Also, with this figure we intent to establish that weather a particle is successful in recruiting or not, is extremely dependent in its proximity to a recruitment zone at the moment of release, thus sustaining that a release per zone proves a more suitable approach to our study goals.

Also not shown, due to their similarity are the corresponding maps for the ROMS online experiment conducted with floats under the VM scenario.

3.3.1. Advection scenarios

Here we compare results obtained in the per zone experiments. For each four-day simulation, the arrival of recruited particles time-series was condensed into a 24 h cumulative recruitment index, for particles reaching the shoreline in zones I, II and III. Indexes show the percentage of hourly arrivals to a particular zone, relative to the total number of successfully recruiting particles in that zone and per simulation (Figs. 11–13).

In the Fm scenario, the particles were bound to the surface level throughout the simulation for as long as they were active, i.e., as long as they don't reach the coast. On the northern edge, Fig. 11 (left column), recruitment can be observed for the entire day, but the gross arrival takes place in the afternoon, exhibiting arrival peaks between [14,15] h, followed by a fast decay. The same continuous distribution is evident both in the Pm and VM scenarios for this region (Figs. 12 and 13). We speculate that the orientation of the coast here may be responsible for the continuous arrival of particles. In the lee of Cape Sines (zone II), when the coast
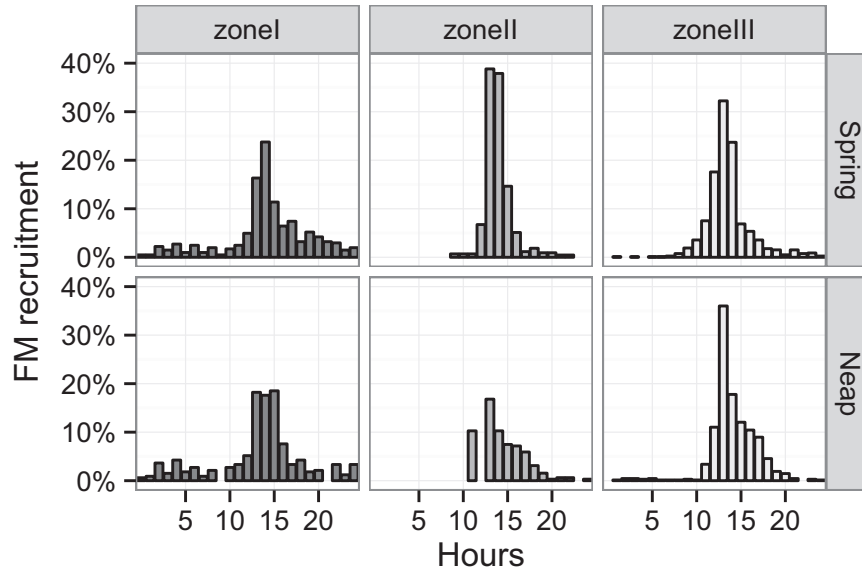
Fig. 11. Cumulative hour arrival of Fm particles in the spring and neap simulation for the three recruitment zones. Upper panels for the spring simulation, lower panels for the neap period. Each column represents the zone of the recruited particles, from left to right, zone I, II and III.

becomes meridionally oriented, the rate at which particles arrive inshore holds a daily pattern, consistent with the diurnal variability of the wind. This pattern shows particles arriving mostly from midday to late afternoon, with abundance peaks around 13 h, which occurs by the middle of the diurnal flood (see Figs. 11–13 (middle columns)). At the southernmost region (zone III), the 24 hrs cumulative indexes in Figs. 11 and 12 (right columns), follow a similar trend has the one described for zone II (middle columns), and spring and neap periods are very alike.

Apart from a forward time displacement of the abundance peak in the neap simulation for zone III, the 24 h cumulative recruitment index in the VM scenario (Fig. 13), has no major differences in its daily structure when compared to the base scenarios.

A comparison between Figs. 11 and 12 shows that the percentage of larvae arriving to the shore in the lee of the cape, is primarily linked to the number of larvae at the surface during the hours of shoreward transport.

Listed in Table 3, is the percentage of successful recruitment,

which corresponds to the percentage of particles that successfully arrive to the near shore, for each zone and scenario, in respect to the total amount released in the experiment. These results suggest that a VM scenario would be beneficial for larvae present in zone II and III, but only in the spring simulations. North of Cape Sines, the three scenarios show less discrepancies among themselves. We would speculate that in this region a tide tied migration (such as the applied in VM) would neither benefit nor prejudice the arrival to the near shore.

3.3.2. Recruitment during the daylight flood

The intensity of recruitment in the daylight flood periods is not dismissible. During the spring simulation, the diurnal flood is from [8–14] h on the first day, starting one hour later in the subsequent days. On the other hand, in the neap simulation, with 14 h of sunlight, days can have two diurnal floods, thus, the following periods were chosen to represent the diurnal flood: on the 31st July from [13–19] h, 1st August from [14–20] h, 2nd August [15–
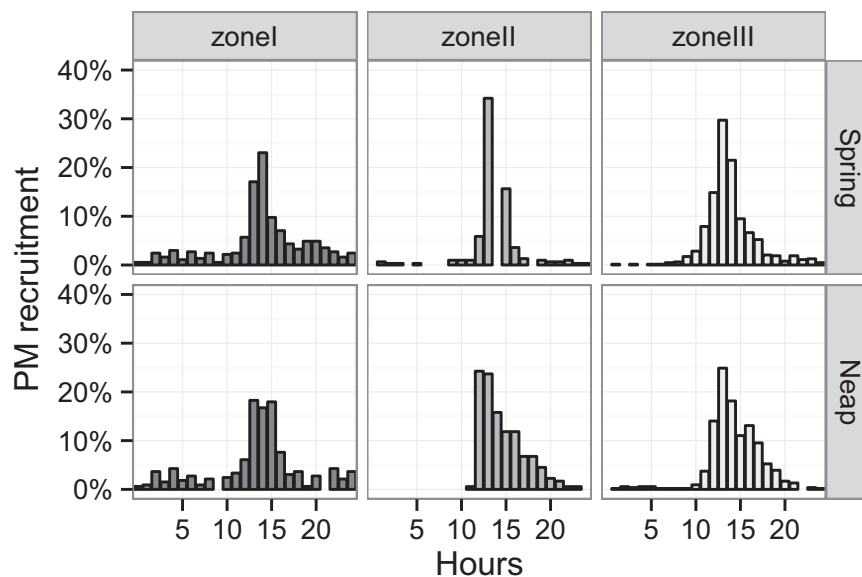

Fig. 12. Cumulative hour arrival of Pm particles in the spring and neap simulation for the three recruitment zones. Upper panels for the spring simulation, lower panels for the neap period. Each column represents the zone of the recruited particles, from left to right, zone I, II and III.
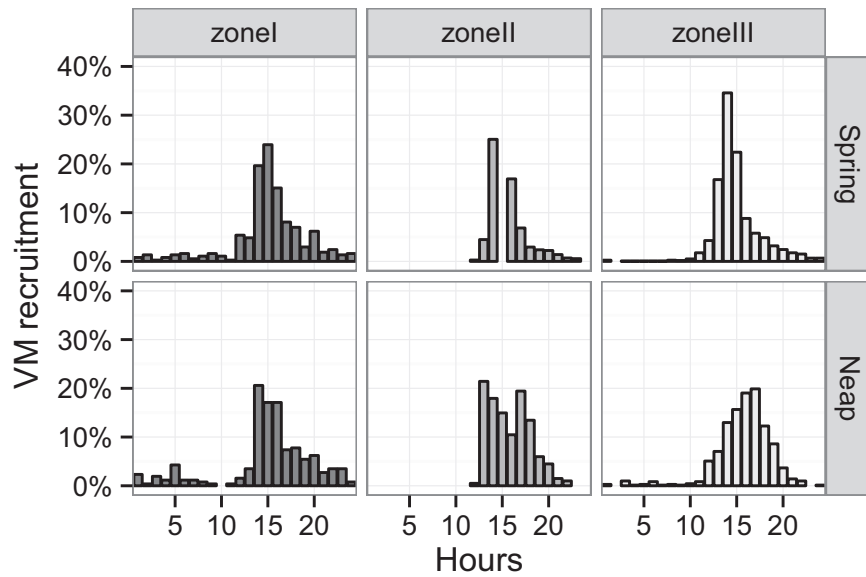
Fig. 13. Cumulative hour arrival of floats in the spring and neap simulation for the three recruitment zones conducted under the VM scenario. Upper panels for the spring simulation, lower panels for the neap period. Each column represents the zone of the recruited floats, from left to right, zone I, II and III.

Table 3
Descriptive statistics: mean and mode of "arrival hour" and percentage of successful recruitment, according to recruitment zone (zone I, II and III), period (spring and neap) and experiment: fixed depth (Fm), passive (Pm) and vertical migration (VM). In red, between brackets, the number of particles/floats released per zone (invariant per period).

	Spring			Neap		
	Fm	*Pm*	*VM*	*Fm*	*Pm*	*VM*
Mean						
Zone I	14.1	14.0	15.1	13.3	13.4	15.0
Zone II	13.9	13.8	15.4	13.4	14.6	15.8
Zone III	13.5	13.8	14.9	14.1	14.3	15.8
Mode						
Zone I	14.0	14.0	15.0	15.0	13.0	14.0
Zone II	13.0	14.0	15.0	12.0	12.0	13.0
Zone III	13.0	13.0	14.0	13.0	13.0	17.0
Success %						
Zone I (2196)	20.45	18.67	18.81	16.67	16.62	13.02
Zone II (2736)	17.47	12.46	29.02	13.05	7.20	8.15
Zone III (3276)	26.62	21.46	40.42	23.08	18.13	24.08

21] h, 3rd August from [6 h30 - 9; 16–21] h. The intensity of the recruitment during those periods in respect to the total amount of recruited particles, in each zone and for each scenario of advection, are summarized in Figs. 14 and 15.

From Figs. 14 and 15 we assess how much of the recruitment takes place during the daylight flood in scenarios without an imposed tidal migration. We see a prevalence of black bars (daylight flood) over grey bars (other tidal phases) in both advection scenarios, that seems to be even greater during spring tides and in zones II and III. The same figures also show that Fm particles have a slightly better rate of arrival to any of the three zones than Pm particles, while showing the same temporal distribution (recall cumulative indexes). Neap simulation in zone II exhibit an erratic behavior (Figs. 14 and 15 middle columns, second rows), with a single significant peak on the third day, which is masked in the cumulative index, and with a prevalence of recruitment taking place outside the daylight flood hours. It is clear that the spring tide simulations consistently produce higher recruitment, probably due to a stronger surface onshore flow in that period (see Table 3 success percentages).

We computed the mean and mode for the variable arrival hour

(time of arrival to the near shore in the time series), which is presented in Table 3. We find in all scenarios an agreement between abundance peaks in recruitment, identified by the mode values, and the immediate response of the upper ocean to the sharp turn to SW of the wind stress. It should be kept in mind that this stronger cross-shore current, favoring onshore transport, exists during a very limited time frame and must compete with the stronger along-shore currents. For that reason, we observed that most of the released particles drifted either offshore or rapidly in the southward direction with the along shore current (releases from the north edge cannot transpose the upwelling jet, neither can those immediately in the lee of the cape). As Cape Sines produces an offshore deflection of the equatorward upwelling jet, particles in the downstream of Cape Sines (zone II) are caught in where we believe an upwelling shadow may be found.

4. Discussion and conclusions

The variability of tidal recruitment of *C. montagui* described by Cruz et al. (2005, 2009) and Jacinto and Cruz (2008), namely the higher recruitment observed during daylight flood, led us to study the inner-shelf circulation in the vicinity of Cape Sines (SW Portuguese coast). We examine the cross-shelf exchange during a typical daily varying upwelling regime, and try to understand the physical mechanisms that may promote larval onshore transport through a series of numerical experiments.

The stratification in the inner-shelf is maintained throughout the day, despite the intensification of the sea breeze in the afternoon and tidal mixing near the bottom. The diurnal cycle is clear in the surface and bottom temperature records, and in the latter a sub-daily periodicity is also present. A clear repetitive response of currents to the regular wind forcing was observed in the ADCP data. It is most striking in the cross-shore velocity component, and is characterized by a midday inversion in the direction of the flow. Further understanding of these fluctuations led us to compute an average-day for the spring and neap phases of the tidal cycle.

Surface flow (Fig. 7) is mostly offshore throughout the averaged-day, turning onshore for a couple of hours in the early afternoon. Comparing average-day results (spring/neap) for the ADCP measurements, with the average-day computed by Lams et al. (Submitted) for the entire 15 day period (July 20th–August
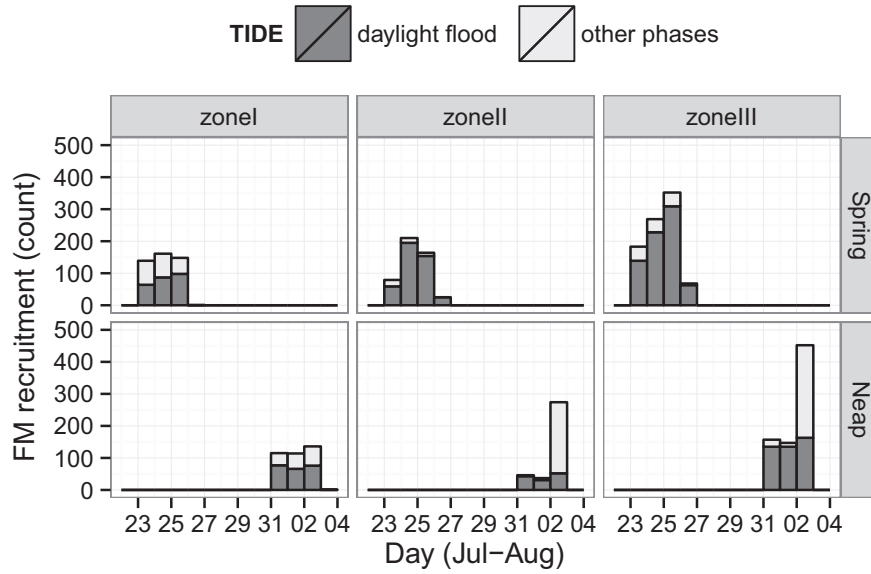
Fig. 14. Daily count of Fm particles arrival during the daylight flood (black bars) and in other tidal phases (grey bars), assessed by zone (columns) and simulation periods (rows).

Fig. 15. Daily count of Pm particles arrival during the daylight flood (black bars) and in other tidal phases (grey bars), assessed by zone (columns) and simulation periods (rows).
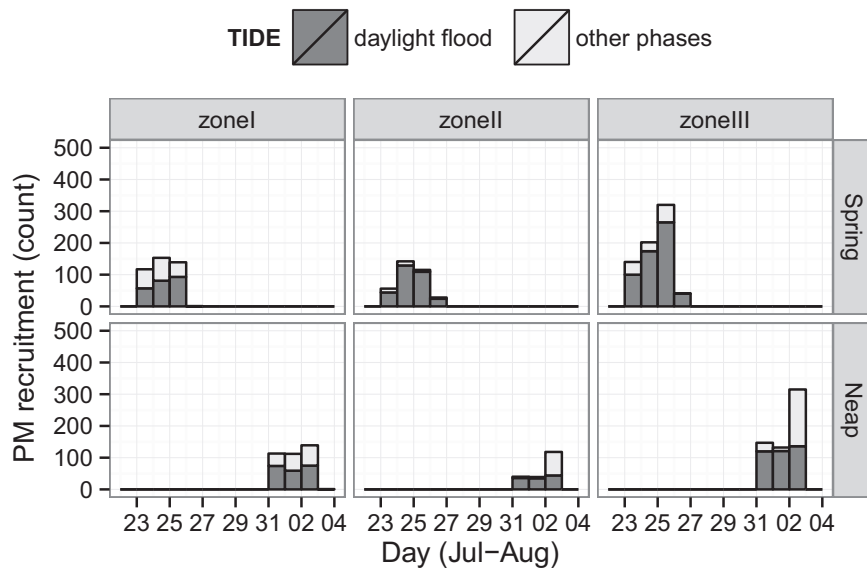
4th, 2006), it is striking that their 3-layer flow during the morning is present in the spring average, and less pronounced in the neap one, thus we assume the bottom flow may be due to additional tide related mixing.

The numerical simulations show some upfront differences to the observations, but the main dynamics are represented. In particular, the repetitive character of the inner-shelf currents is well reproduced. In what respects cross-shore exchange, model profiles do not reproduce quit well observations during the first 6–8 h of the day, specially for the neap period. The modeled flow is approximately a 2-layer type, offshore at surface and reversing below. At mid-day, a sharp reversal of the flow happens, lasting until 3 p.m. (averaged hour), at this period both model and observations exhibit a 2-layer flow, with shoreward intense flow near the surface and the reverse below. During the afternoon, with the establishment of the sea breeze, average profiles show onshore transport at mid-depth, and offshore flow at surface. Along-shore current profiles show a prevailing southward current, stronger and shallower in the model.

These results show that the structure of the flow is not fully represented in the model during the morning, suggesting that other processes may act together with the wind. Processes like tidal mixing and wave effects near the bottom are under-represented. Classic inner-shelf circulation theories, as those in Fewings et al. (2008) and Lentz et al. (2008), are unable to explain the 3-layer morning flow present in the observations. The 2-layer reverse flow at midday resembles the sea-breeze driven circulation described in Hendrickson and MacMahan (2009) that happens when the wind increases in magnitude and rotates onshore. According to Lamas et al. (Submitted) this reversal is an inertial response to the abrupt change of the wind magnitude and direction at mid-day, that can occur in the leeside of a cape. In the afternoon, the circulation pattern is typical for upwelling-favorable wind forcing with fully developed Ekman dynamics. Nonetheless, neither of the daily cycle phases can be fully described by this wave-driven undertow.

Regarding the surface circulation in the domain in Fig. 8, patterns are coherent with the described SST maps in Fig. 4 and agree with other studies like Gan and Allen (2002) and Li and Weisberg (1999), placing the most intense upwelling in the lee of capes.

The model reasonably reproduces the local circulation patterns, including the described cross-shore variability in a daily scale, and we assume that apart from the intensification of the flow, the ADCP location may be representative of the inner-shelf leeside of the cape.

Sensitivity tests showed that differences appeared near the bottom, due to mixing processes and in the timings of the midday inversion, in the cross-shore velocity component. Analysing the results in the MS and WRF experiments, we found no reason to choose one in particular. We suspect that in both cases forcing winds are stronger than real winds in leeside of the cape.

Model recruitment indexes for base experiments (Fm and Pm) support the wind as the main mechanism forcing onshore transport. The observed peaked recruitment in Figs. 11–13, agrees with the idea that larvae transport by advective events produces a peaked recruitment function, as reported in several studies by Shanks (1983) and Pineda (1991, 2000).

However, we also notice that during the diurnal spring flood this flow is intensified, thus recruitment is larger (Figs. 14 and 15). This is in consonance with previous studies by Cruz et al. (2005, 2009) and Jacinto and Cruz (2008).

Through field observations, Cruz et al. (2009) suggest that cyprids of *C. montagui* are mostly neustonic during the daylight flood. Although more studies are needed on the vertical distribution of larvae in the nearshore, a view of the local cross-shelf circulation in Fig. 7 explains how this type of distribution could be beneficial for the larvae onshore transport, since it allows them to avoid offshore flow.

The larvae recruiting in the lee of the cape were trapped between the upwelling front and the shore and never left the inner shelf. We attribute this to the upwelling shadow in the downstream of Cape Sines, this retention is in consonance with reports of identified upwelling shadows in the upwelling system of south of Bodega Bay (Point Reys) and Monterey Bay (Graham et al., 1992; Graham and Largier, 1997; Roughan et al., 2005). Some studies about vertical migration effects on larvae recruitment, also suggest that upwelling can enhance retention on the inner shelf, (Peliz et al., 2007; Marta-Almeida et al., 2006; Domingues et al., 2012). Furthermore, Tapia et al. (2004) proposes that the combination of physical processes like the sea breeze and behavioral mechanisms such as vertical migration might increase local retention of larvae and transport to shore.

In summary, numerical model results were used to understand how a daily varying upwelling regime can promote onshore transport of larvae. In the lee of the cape, results show that the inner-shelf currents and stratification are clearly affected by the local wind fluctuations and the semi-diurnal tide (even though stratification is never broken). These fluctuations produce repetitive daily patterns in the currents, and a surface wind-driven onshore flow with the midday wind shift. We suspect that the wind is not the only mechanism responsible for the daily variability of the cross-shore exchange, however its sharp reversal at midday is critical for the advection of larvae towards the coast. Most of the dispersion studies agree with the proposed larval transport onshore during the daylight flood, by showing higher recruitment rates during this phase of the tidal cycle.

References

Capet, X., Marchesiello, P., McWilliams, J., 2004. Upwelling response to coastal wind profiles. Geophys. Res. Lett. 31. http://dx.doi.org/10.1029/2004GL020123.

Cruz, T., 1999. Settlement patterns of *Chthamalus* spp. at Praia da Oliveirinha (SW Portugal). Acta Oecol. 20, 285–287. http://dx.doi.org/10.1016/S1146-609X(99)00138-1.

Cruz, T., Castro, J., Delany, J., McGrath, D., Myers, A., O'Riordan, R., Power, A.M., Rabaa, J., Hawkins, S., 2005. Tidal rates of settlement of the intertidal barnacles *Chthamalus stellatus* and *Chthamalus montagui* in western Europe: the influence of the night/day cycle. J. Exp. Mar. Biol. Ecol. 318, 51–60. http://dx.doi.org/10.1016/j.jembe.2004.12.005.

Cruz, T., Oliveira, P., Fernandes, J., Anglico, M., Castro, J., Lima, N., Quintela, M., 2009. Final report of project VERY NEAR – departures and arrivals of barnacle larvae onshore: very near shore physical processes and behaviour in SW Portugal (POCI/MAR/57630/2004). (Unpublished).

Domingues, C., Nolasco, R., Dubert, J., Queiroga, H., 2012. Model-derived dispersal pathways from multiple source populations explain variability of invertebrate larval supply. PLoS One 7. http://dx.doi.org/10.1371/journal.pone.0035794.

Egbert, G.D., Erofeeva, S.Y., 2002. Efficient Inverse Modeling of Barotropic Ocean Tides. J. Atmos. Oceanic Technol. 19, 183–204. http://dx.doi.org/10.1175/1520-0426(2002)019 < 0183:EIMOBO > 2.0.CO;2.

Fewings, M., Lentz, S., Fredericks, J., 2008. Observations of cross-shelf flow driven by cross-shelf winds on the inner continental shelf. J. Phys. Oceanogr. 38, 38. http://dx.doi.org/10.1175/2008JPO3990.1.

Gan, J., Allen, J.S., 2002. A modeling study of shelf circulation off northern California in the region of the Coastal Ocean dynamics experiment: response to relaxation of upwelling winds. J. Geophys. Res. 107. http://dx.doi.org/10.1029/2000JC000768.

Graham, W., Largier, J., 1997. Upwelling shadows as nearshore retention sites: the example of northern Monterey Bay. Cont. Shelf Res. 17, 509–532. http://dx.doi.org/10.1016/j.pocean.2015.01.014.

Graham, W., Field, J., Potts, D., 1992. Persistent upwelling shadows and their influence on zooplankton distributions. Mar. Biol. 114, 561–570. http://dx.doi.org/10.1007/BF00357253.

Haidvogel, D., Arango, H., Budgell, W., Cornuelle, B., Curchitser, E., Di Lorenzo, E., Fennel, K., Geyer, W., Hermann, A., Lanerolle, L., Levin, J., McWilliams, J., Miller, A., Moore, A., Powell, T., Shchepetkin, A., Sherwood, C., Signell, R., Warner, J., Wilkin, J., 2008. Ocean forecasting in terrain-following coordinates: formulation and skill assessment of the regional ocean modelling system. J. Comput. Phys. 227, 3595–3624. http://dx.doi.org/10.1016/j.jcp.2007.06.016.

Hendrickson, J., MacMahan, J., 2009. Diurnal sea breeze effects on inner-shelf cross-shore exchange. Cont. Shelf Res. 29, 2195–2206. http://dx.doi.org/10.1016/j.csr.2009.08.011.

Jacinto, D., Cruz, T., 2008. Tidal settlement of the intertidal barnacles *Chthamalus* spp. in sw portugal: interaction between diel and semi-lunar cycles. Mar. Ecol. Prog. Ser. 366, 129–135.

Lamas, L., Peliz, A., Dias, J., Oliveira, P., Angelico, M., Castro, J., Cruz, T., Fernandes, J., and Trindade, A., 2016. Diurnal variability of inner-shelf circulation in the lee of a cape under upwelling conditions. (submitted for publication).

Large, W., McWilliams, J., Doney, S., 1994. Oceanic vertical mixing: a review and model with a nonlocal boundary layer parameterization. Rev. Geophys. 32, 363–403. http://dx.doi.org/10.1029/94RG01872.

Lemos, R., Pires, H., 2004. The upwelling regime off the West Portuguese Coast, 1941–2000. Int. J. Climatol. 24, 511–524. http://dx.doi.org/10.1002/joc.1009.

Lentz, S., Fewings, M., Howd, P., Fredericks, J., Hathaway, K., 2008. Observations and a model of undertow over the inner continental shelf. J. Phys. Oceanogr. 38, 2341–2357. http://dx.doi.org/10.1175/2008JPO3986.1.

Lett, C., Verley, P., Mullon, C., Parada, C., Brochier, T., Penven, P., Blanke, B., 2008. A lagrangian tool for modelling ichthyoplankton dynamics. Environ. Model. Softw. 23, 1210–1214. http://dx.doi.org/10.1016/j.envsoft.2008.02.005.

Li, Z., Weisberg, R.H., 1999. West Florida shelf response to upwelling favorable wind forcing: kinematics. J. Geophys. Res. 104. http://dx.doi.org/10.1029/1999JC900073.

Marchesiello, P., McWilliams, J.C., Shchepetkin, A.F., 2001. Open boundary conditions for long-term integration of regional oceanic models. Ocean Model. 3, 1–20. http://dx.doi.org/10.1016/S1463-5003(00)00013-5.

Marchesiello, P., McWilliams, J., Shchepetkin, A., 2003. Equilibrium structure and dynamics of the California current system. J. Phys. Oceanogr. 33.

Marta-Almeida, M., Dubert, J., 2006. The structure of tides in the Western Iberian region. Cont. Shelf Res. 26, 385–400. http://dx.doi.org/10.1016/j.csr.2005.11.011.

Marta-Almeida, M., Dubert, J., Peliz, A., Queiroga, H., 2006. Influence of vertical migration pattern on retention of crab larvae in the shelf in a seasonal upwelling system. Mar. Ecol. Prog. Ser. 307, 1–19. http://dx.doi.org/10.3354/meps307001.

Oliveira, P., Nolasco, R., Dubert, J., Moita, T., Peliz, A., 2009. Surface temperature, chlorophyll and advection patterns during a summer upwelling event off

central Portugal. Cont. Shelf Res. 29, 759–774. http://dx.doi.org/10.1016/j.csr.2008.08.004.

O'Riordan, R., Arenas, F., Arrontes, J., Castro, J., Cruz, T., Delany, J., Martnez, B., Fernandez, C., Hawkins, S., McGrath, D., Myers, A.A., Oliveros, J., Pannacciulli, F., Power, A.M., Relini, G., Rico, J., Silva, T., 2004. Spatial variation in the recruitment of the intertidal barnacles *Chthamalus montagui* southward and *Chthamalus stellatus* (poli) (crustacea: Cirripedia) over an european scale. J. Exp. Mar. Biol. Ecol. 304, 243–264. http://dx.doi.org/10.1016/j.jembe.2003.12.005.

Paris, C., Helgers, J., Sebille, E., Srinivasan, A., 2013. Connectivity modeling system: a probabilistic modeling tool for the multi-scale tracking of biotic and abiotic variability in the ocean. Environ. Model. Softw. 42, 47–54.

Peliz, A., Boutov, D., Cardoso, R., Delgado, J., Soares, P., 2013. The gulf of Cadiz-Alboran sea sub-basin: model setup, exchange and spatial seasonal variability. Ocean Model. 61, 49–67. http://dx.doi.org/10.1016/j.ocemod.2012.10.007.

Peliz, A., Marchesiello, P., Dubert, J., Marta-Almeida, M., Roy, C., Queiroga, H., 2007. A study of crab larvae dispersal on the Western Iberian Shelf: physical processes. J. Mar. Syst. 68, 215–236. http://dx.doi.org/10.1016/j.jmarsys.2006.11.007.

Penven, P., Cambon, G., Tan, T. Marchesiello, P., Debreu, L., 2010. ROMS_AGRIF/ROMSTOOLS User's Guide. Tech. Rep. IRD. URL: ⟨http://fraise.univ-brest.fr/penven/roms_tools/⟩.

Pineda, J., 1991. Predictable upwelling and the shoreward transport of planktonic larvae by internal tidal bores. Science 253, 548–551. http://dx.doi.org/10.1126/science.253.5019.548.

Pineda, J., 2000. Linking larval settlement to larval transport: assumptions, potentials, and pitfalls. Oceanogr. East. Pac. I, 15–84.

Relvas, P., Barton, E., 2002. Mesoscale patterns in the Cape São Vicente (Iberian Peninsula) upwelling region. J. Geophys. Res. 107, 3164. http://dx.doi.org/10.1029/2000JC000456.

Relvas, P., Barton, E., 2005. A separated jet and coastal counterflow during upwelling relaxation off Cape São Vicente (Iberian Peninsula). Cont. Shelf Res. 25, 29–49. http://dx.doi.org/10.1016/j.csr.2004.09.006.

Relvas, P., Barton, E., Dubert, J., Oliveira, P.B., Álvaro Peliz, da Silva, J., Santos, A.M.P., 2007. Physical oceanography of the western iberia ecosystem: latest views and challenges. Prog. Oceanogr. 74, 149–173. http://dx.doi.org/10.1016/j.pocean.2007.04.021.

Roughan, M., Mace, A., Largier, J., Morgan, S., Fisher, L., Carter, M., 2005. Subsurface recirculation and larval retention in the lee of a small headland: a variation on the upwelling shadow theme. J. Geophys. Res. 110, C10027. http://dx.doi.org/10.1029/2005JC002898.

dos Santos, A., Santos, A., Conway, D., Bartilotti, C., Loureno, P., Queiroga, H., 2008. Diel vertical migration of decapod larvae in the Portuguese coastal upwelling ecosystem: implications for offshore transport. Mar. Ecol. Prog. Ser. 359, 171–183. http://dx.doi.org/10.3354/meps07341.

Sauvaget, P., David, E., Soares, C., 2000. Modelling tidal currents on the coast of portugal. Coast. Eng. 40, 393–409. http://dx.doi.org/10.1016/S0378-3839(00)00020-X.

Shanks, A., 1983. Surface slicks associated with tidally forced internal waves may transport pelagic larvae of benthic invertebrates and fishes shoreward. Mar. Ecol. Prog. Ser. 13, 311–315.

Shanks, A., Brink, L., 2005. Upwelling, downwelling, and cross-shelf transport of bivalve larvae: test of a hypothesis. Mar. Ecol. Prog. Ser. 302, 1–12. http://dx.doi.org/10.3354/meps302001.

Shanks, A., Morgan, S., MacMahan, J., Reniers, A., 2010. Surf zone physical and morphological regime as determinants of temporal and spatial variation in larval recruitment. J. Exp. Mar. Biol. Ecol. 392, 140–150. http://dx.doi.org/10.1016/j.jembe.2010.04.018.

Shchepetkin, A.F., McWilliams, J.C., 2005. The regional oceanic modeling system (ROMS): a split-explicit, free-surface, topography-following-coordinate oceanic model. Ocean Model. 9, 347–404. http://dx.doi.org/10.1016/j.ocemod.2004.08.002.

Soares, P., Cardoso, R., de Medeiros, J., Miranda, P., Belo-Pereira, M., Espirito-Santo, F., 2012. WRF high resolution dynamical downscaling of ERA-Interim for Portugal. Clim. Dyn. 39, 2497–2522. http://dx.doi.org/10.1007/s00382-012-1315-2.

Tapia, F.J., Pineda, J., Ocampo-Torres, F.J., Fuchsa, H.L., Parnellc, P.E., Monterod, P., Ramos, S., 2004. High-frequency observations of wind-forced onshore transport at a coastal site in Baja California. Cont. Shelf Res. 24, 1573–1585. http://dx.doi.org/10.1016/j.csr.2004.03.013.

Teles-Machado, A., Peliz, A., Dubert, J., Sanchez, R., 2007. On the onset of the Gulf of Cadiz coastal countercurrent. Geophys. Res. Lett. 34. http://dx.doi.org/10.1029/2007GL030091.

Bibliography

Aguiar-González, B., Rodríguez-Santana, A., Cisneros-Aguirre, J., Martínez-Marrero, A., 2011. Diurnal-inertial motions and diapycnal mixing on the Portuguese shelf. Continental Shelf Research 31, 1193–1202.

Allen, J. S., Newberger, P. A., Federiuk, J., 1995. Upwelling circulation on the Oregon continental shelf part i: Response to idealized forcing. Journal of Physical Oceanography 25, 1843–1866.

Allen, S. E., 1996. Topographically generated, subinertial flows within a finite length canyon. Journal of Physical Oceanography 27, 1608–1632.

Austin, J., Lentz, S. J., 2002. The inner-shelf response to wind-driven upwelling and downwelling. Journal of Physical Oceanography 32, 2171–2193.

Barth, J. A., Pierce, S. D., Smith, R. L., 2000. A separating coastal upwelling jet at Cape Blanco, Oregon and its connection to the California current system. Deep-Sea Research II 47, 783–810.

Brink, K. H., 2016. Cross-shelf exchange. Annual Review of Marine Science 8, 59–78.

Castelao, R., Barth, J. A., 2006. The relative importance of wind strength and along-shelf bathymetric variations on the separation of a coastal upwelling jet. Journal of Physical Oceanography 36, 412–425.

Crépon, M., Richez, C., Chartier, M., 1984. Effects of coastline geometry on upwellings. Journal of Physical Oceanography 14, 1365–1382.

Cruz, T., 1999. Settlement patterns of *Chthamalus spp.* at Praia da Oliveirinha (SW portugal). Acta Oecologica 20, 285–287.

Cruz, T., Castro, J., Delany, J., McGrath, D., Myers, A., O'Riordan, R., Power, A., Rabaa, J., Hawkins, S., 2005. Tidal rates of settlement of the intertidal barnacles *Chthamalus stellatus* and *Chthamalus montagui* in western Europe: the influence

of the night/day cycle. Journal of Experimental Marine Biology and Ecology 318, 5160.

de Boyer Montégut, C., Mardec, G., Fischer, A. S., Lazar, A., Iudicone, D., 2004. Mixed layer depth over the global ocean: An examination of profile data and a profile based climatology. Journal of Geophysical Research 109, C12003.

Doglioli, A. M., Griffa, A., Magaldi, M. G., 2004. Numerical study of a coastal current on a steep slope in presence of a cape: the case of the Promontorio di Portofino. Journal of Geophysical Research 109, C12033.

Durski, S. M., Glenn, S. M., Haidvogel, D. B., 2004. Vertical mixing schemes in the coastal ocean: Comparison of the level 2.5 Mellor-Yamada scheme with an enhanced version of the K profile parameterization. Journal of Geophysical Research 109, C01015.

Estrade, P., Marchesiello, P., de Verdière, A. C., Roy, C., 2008. Cross-shelf structure of coastal upwelling: a two-dimensional extension of Ekman's theory and a mechanism for inner-shelf upwelling shut down. Journal of Marine Research 66, 589–616.

Fewings, M., Lentz, S. J., 2010. Momentum balances on the inner continental shelf at Martha's Vineyard coastal observatory. Journal of Geophysical Research 115, C12023.

Fewings, M., Lentz, S. J., Fredericks, J., 2008. Observations of cross-shelf flow driven by cross-shelf winds on the inner continental shelf. Journal of Physical Oceanography 38, 2358–2378.

Fewings, M., Washburn, S. L., Ohlmann, J. C., 2015. Coastal water circulation patterns around the Northern Channel Islands and Point Conception, California. Progress in Oceanography 138, 283–304.

Gan, J., Allen, J. S., 2002. A modeling study of shelf circulation off northern California in the region of the Coastal Ocean Dynamics Experiment: Response to relaxation of upwelling winds. Journal of Geophysical Research 107, C93123.

Gan, J., Cheung, A., Guo, X., Li, L., 2009. Intensified upwelling over a widened shelf in the northeastern south China Sea. Journal of Geophysical Research 114, C09019.

Ganju, N. K., Lentz, S. J., Kirincich, A. R., Farrar, J. T., 2011. Complex mean circulation over the inner shelf south of Martha's Vineyard revealed by observations and a high-resolution model. Journal of Geophysical Research 116, C10036.

Haidvogel, D., Arango, H., Budgell, W., Cornuelle, B., Curchitser, E., Lorenzo, E. D., Fennel, K., Geyer, W., Hermann, A., Lanerolle, L., Levin, J., McWilliams, J., Miller, A., Moore, A., Powell, T., Shchepetkin, A., Sherwood, C., Signell, R., Warner, J., Wilkin, J., 2008. Ocean forecasting in terrain-following coordinates: Formulation and skill assessment of the regional ocean modelling system. Journal of Computational Physics 227, 3595–3624.

Hendrickson, J., MacMahan, J., 2009. Diurnal sea breeze effects on inner-shelf cross-shore exchange. Continental Shelf Research 29, 2195–2206.

Horwitz, R., Lentz, S. J., 2014. Inner-shelf response to cross-shelf wind stress: the importance of the cross-shelf density gradient in idealized numerical model and field observations. Journal of Physical Oceanography 44, 86–103.

Jacinto, D., Cruz, T., 2008. Tidal settlement of the intertidal barnacles *Chthamalus spp.* in SW Portugal: interaction between diel and semi-lunar cycles. Marine Ecology Progress Series 366, 129–135.

Kämpf, J., 2012. Lee effects of localized upwelling in a shelf-break canyon. Continental Shelf Research 42, 78–88.

Kim, S. Y., Kosro, P., Kurapov, A., 2014. Evaluation of directly wind-coherent near-inertial surface currents off Oregon using a statistical parametrization and analytical numerical models. Journal of Geophysical Research 119, C010115.

Kirincich, A. R., Barth, J. A., Grantham, B. A., Menge, B. A., Lubchenco, J., 2005. Wind-driven inner-shelf circulation off central Oregon during summer. Journal of Geophysical Research 110, C10S03.

Kirincich, A. R., Lentz, S. J., Barth, J., 2009b. Wave-driven inner-shelf motion on Oregon coast. Journal of Physical Oceanography 39, 2942–2956.

Kuebel Cervantes, B. T., Allen, J. S., 2006. Numerical model simulations of continental shelf flows off northern California. Deep-Sea Research II 53, 2956–2984.

Lamas, L., Peliz, A., Dias, J., Oliveira, P. B., Angélico, M. M., Castro, J. J., Fernandes, J. N., Trindade, A., Cruz, T., 2017. Diurnal variability of inner-shelf

circulation in the lee of a cape under upwelling conditions. Continental Shelf Research 143, 67–77.

Large, W., Pond, S., 1981. Open ocean momentum measurements in moderate to strong winds. Journal of Physical Oceanography 11, 324–336.

Large, W. G., McWilliams, J. C., Doney, S. C., 1994. Oceanic vertical mixing: A review and a model with a nonlocal boundary layer parameterization. Reviews of Geophysics 32(4), 363–403.

Lentz, S. J., 1995. Sensitivity of the inner-shelf circulation to the form of the eddy-viscosity profile. Journal of Physical Oceanography 25, 19–28.

Lentz, S. J., 2001. The influence of stratification on the wind-driven cross-shelf circulation over the North Carolina shelf. Journal of Physical Oceanography 31, 2749–2760.

Lentz, S. J., 2008. ADCP site and a model of the mean circulation over the Middle Atlantic Bight continental shelf. Journal of Physical Oceanography 38, 1203–1221.

Lentz, S. J., Chapman, C., 2004. The importance of nonlinear cross-shelf momentum flux during wind-driven coastal upwelling. Journal of Physical Oceanography 34, 2444–2457.

Lentz, S. J., Fewings, M., 2012. Wind- and wave-driven inner-shelf circulation. Annual Review of Marine Science 14, 317–343.

Lentz, S. J., Fewings, M., Howd, P., Fredericks, J., Hathaway, K., 2008. Observations and a model of undertow over the inner continental shelf. Journal of Physical Oceanography 38, 2341–2357.

Lentz, S. J., Guza, R. T., Fedderson, F., Herbers, T. H. C., 1999. Momentum balances on the North Carolina inner shelf. Journal of Geophysical Research 226, 18205–18226.

Li, Z., Weisberg, R. H., 1999b. West Florida continental shelf response to upwelling favorable wind forcing: 2. dynamics. Journal of Geophysical Research 104 (C10), 23427–23442.

Liu, Y., Weisberg, R. H., 2005. Momentum balance diagnoses for the West Florida shelf. Continental Shelf Research 25, 2054–2074.

Liu, Z., Gan, J., 2014. Modeling study of variable upwelling circulation in the east china sea: Response to a coastal promontory. Journal of Physical Oceanography 44, 1078–1094.

Longuet-Higgins, M. S., Stewart, R. W., 1964. Radiation stresses in water waves; a physical discussion, with applications. Deep-Sea Research II 11, 529–562.

Lucas, A. J., Pitcher, G. C., Probyn, T. A., Kudela, R. M., 2013. The influence of diurnal winds on phytoplankton dynamics in a coastal upwelling system off southwestern Africa. Deep-Sea Research II 101, 50–62.

Marchesiello, P., Debreu, L., Couvelard, X., 2009. Spurious diapycnal mixing in terrain-following coordinate models: the problem and a solution. Ocean Modelling 26, 156–169.

Marchesiello, P., Estrade, P., 2010. Upwelling limitation by geostrophic onshore flow. Journal of Marine Research 68, 37–62.

Marchesiello, P., McWilliams, J., Shchepetkin, A., 2001. Open boundary conditions for long-term integration of regional oceanic models. Ocean Modelling 3, 1–20.

Marchesiello, P., McWilliams, J., Shchepetkin, A., 2003. Equilibrium structure and dynamics of the California current system. Journal of Physical Oceanography 33, 753–783.

Marta-Almeida, M., Dubert, J., 2006. The structure of tides in the Western Iberian region. Continental Shelf Research 36, 385–400.

McCabe, R., Hickey, B. M., Dever, E. P., MacCready, P., 2015. Seasonal cross-shelf flow structure, upwelling relaxation, and the alongshelf pressure gradient in the northern California current system. Journal of Physical Oceanography 45, 209227.

Meunier, T., Rossi, V., Morel, Y., Carton, X., 2010. Influence of bottom topography on an upwelling current: Generation of long trapped filaments. Ocean Modelling 35, 277–303.

Oliveira, P., Nolasco, R., Dubert, J., Moita, T., Peliz, A., 2009. Surface temperature, chlorophyll and advection patterns during a summer upwelling event off central Portugal. Continental Shelf Research 29, 759–774.

Pawlowicz, R., Beardsley, B., Lentz, S. J., 2002. Classical tidal harmonic analysis including error estimates in MATLAB using T_TIDE. Computers and Geosciences 28, 929–937.

Pedlosky, J., 1978. An inertial model of steady coastal upwelling. Journal of Physical Oceanography 8, 171–177.

Peliz, A., Boutov, D., Cardoso, R., Delgado, J., Soares, P., 2013. The Gulf of Cadiz-Alboran sea sub-basin: Model setup, exchange and seasonal variability. Ocean Modelling 61, 49–67.

Peliz, A., Dubert, J., Haidvogel, D. B., Cann, B. L., 2003. Generation and unstable evolution of a density-driven eastern poleward current: The Iberian Poleward current. Journal of Geophysical Research 108, C83268.

Peliz, A., Marchesiello, P., Dubert, J., Roy, P., Marta-Almeida, M., Queiroga, H., 2007. A study of crab larvae dispersal off western Iberia: Physical processes. Journal of Marine Research 68, 215–236.

Perlin, N., Skyllingstad, E. D., Samelson, R. M., 2011. Coastal atmospheric circulation around an idealized cape during wind-driven upwelling studied from a coupled ocean-atmosphere model. Monthly Weather Review 139, 809–829.

Pineda, J., Reyns, N. B., Starczak, V. R., 2009. Complexity and simplification in understandig recruitment in benthic populations. Population Ecology 51, 17–32.

Relvas, P., Barton, E., Dubert, J., Oliveira, P. B., Peliz, A., da Silva, J., 2007. Physical oceanography of the western Iberia ecosystem: Latest views and challenges. Progress in Oceanography 74, 149–173.

Roughan, M., Garfield, N., Largier, J., Dever, E., Dorman, C., Peterson, D., Dorman, J., 2006. Transport and retention in an upwelling region: the role of across-shelf structure. Deep-Sea Research II 53, 2931–2955.

Roughan, M., Mace, A., Largier, J., Morgan, S., Fisher, J., 2005a. Sub-surface recirculation and larval retention in the lee of a small headland: a variation on the upwelling shadow theme. Journal of Geophysical Research 110, C10027.

Roughan, M., Terrill, E. J., Largier, J. L., Otero, M. P., 2005b. Observations of divergence and upwelling around Point Loma California. Journal of Geophysical Research 110, C04011.

Sanay, R., Yankovsky, A., Voulgaris, G., 2008. Inner shelf circulation patterns and nearshore flow reversal under downwelling and stratified conditions off a curved coastline. Journal of Geophysical Research 113, C08050.

Shchepetkin, A. F., McWilliams, J. C., 2005. The regional oceanic modeling system (ROMS): a split-explicit, free-surface, topography-following coordinate oceanic model. Ocean Modelling 9, 347–404.

Simpson, J. H., Hyder, P., Rippeth, T. P., 2002. Forced oscillations near the critical latitude for diurnal-inertial response. Journal of Physical Oceanography 32, 177–187.

Smith, R. L., 1988. Coefficients for sea surface wind stress, heat flux, and wind profiles as function of wind speed and temperature. Journal of Geophysical Research 93, 15467–15472.

Soares, P. M. M., Cardoso, R. M., de Medeiros, J., Miranda, P., Belo-Pereira, M., Espírito-Santo, F., 2012. WRF high resolution dynamical downscaling of ERA-Interim for Portugal. Climate Dynamics 39, 2497–2522.

Sobarzo, M., Bravo, L., Moffat, C., 2010. Diurnal-period, wind-forced ocean variability on the inner shelf off Concepción, Chile. Continental Shelf Research 30, 2043–2056.

Stokes, G. G., 1847. On the theory of oscillatory waves. Transactions of the Cambridge Philosophical Society 8, 441–455.

Tilburg, C., 2003. Across-shelf transport on a continental shelf: do across-shelf winds matter? Journal of Physical Oceanography 33, 2675–2688.

Trindade, A., Peliz, A., Dias, J., Lamas, L., Oliveira, P. B., Cruz, T., 2016. Cross-shore transport in a daily varying upwelling regime: a case study of barnacle larvae on the southwestern Iberian coast. Continental Shelf Research 127, 12–27.

Woodson, C., Eerkes-Medrano, D., Flores-Morales, A., Foley, M., Henkel, S., Hessing-Lewis, M., Jacinto, D., Needles, L., Nishizaki, M., O'Leary, J., Ostrander,

C., Pespeni, M., Schwager, K., Tyburczy, J., Weersing, K., Kirincich, A., Barth, J., McManus, M., Washburn, L., 2007. Local diurnal upwelling driven by sea breeze in northern Monterey Bay. Continental Shelf Research 27, 2289–2302.

Xu, J., Lowe, R. J., Ivey, G. N., Pattiaratchi, C., Jones, N. L., Brinkman, R., 2013. Dynamics of the summer shelf circulation and transient upwelling off Ningaloo Reef, western Australia. Journal of Geophysical Research 118, 1–27.

Zhang, X., IV, D. C. S., DiMarco, S., Hetland, R., 2010. A numerical study of sea-breeze-driven ocean Poincare wave propagation and mixing near the critical. Journal of Physical Oceanography 40, 48–66.